

**The Sae two-component system of *Staphylococcus aureus*: sensing mechanism and impact on bacteria-phagocyte interaction**

**Dissertation**

der Mathematisch-Naturwissenschaftlichen Fakultät  
der Eberhard Karls Universität Tübingen  
zur Erlangung des Grades eines  
Doktors der Naturwissenschaften  
(Dr. rer. nat.)

vorgelegt von

**Lisa Bleul**

aus Ostfildern

Tübingen

2019

Gedruckt mit Genehmigung der Mathematisch-Naturwissenschaftlichen Fakultät der  
Eberhard Karls Universität Tübingen.

Tag der mündlichen Qualifikation: 19.08.2019

Dekan: Prof. Dr. Wolfgang Rosenstiel

1. Berichterstatter: Prof. Dr. Christiane Wolz

2. Berichterstatter: Prof. Dr. Friedrich Götz

**Für meine Familie**

# Contents

---

## Table of contents

<b>Summary</b>	<b>1</b>
<b>Zusammenfassung</b>	<b>2</b>
<b>List of publications</b>	<b>4</b>
<b>Personal contribution to publications</b>	<b>6</b>
<b>Introduction</b>	<b>7</b>
<b>Objectives of the thesis</b>	<b>22</b>
<b>Results</b>	<b>23</b>
Part I SaeS sensing mechanism	24
Part II Sae impact on phagocyte interaction	31
<b>Discussion</b>	<b>38</b>
<b>References</b>	<b>42</b>
<b>Appendix</b>	<b>52</b>
Accepted publications	53
Manuscripts ready for submission	97
<b>Eidesstattliche Erklärung</b>	<b>121</b>
<b>Curriculum vitae</b>	<b>122</b>
<b>Acknowledgements</b>	<b>123</b>



### Summary

In the human pathogen *Staphylococcus aureus* (*S. aureus*), two-component systems (TCS) enable the bacteria to respond to different environmental stimuli. The core genome of *S. aureus* encodes 16 TCSs of which only *walKR* is essential. Recent studies showed that all TCSs can act functionally autonomous allowing the bacteria to sense, respond and adapt to environmental changes. For most TCSs the mechanism leading to activation remains unclear. The SaePQRS System regulates the expression of various secreted and cell bound virulence factors which were shown to be important for the interaction with our immune system. It was shown that the Sae system is activated by phagocytosis-related signals, specifically human neutrophil peptides (HNP1-3). Promotor activities and target genes are well studied whereas the mechanism of signal sensing is unknown. Here I show, that the D-alanylation of wall teichoic acids (WTA) is important for HNP1-3 sensing. Studies on the regulation of *dltABCD* as well as a gene complementation approach could not explain strain specificity. Thereby I hypothesize, that strain differences in the content of teichoic acids and their alanylation is the reason for strain specificity and that this distinct composition is not imitable in an experimental setup. Furthermore, I could confirm sodium hypochlorite as another activator of the Sae-System which interestingly is not a strain specific activator. *S. aureus* is able to survive and even escape from professional phagocytes. Whereas lysis of neutrophils by *S. aureus* is well studied, factor(s) required for the escape from human macrophages are less clear. I could show that the Agr-regulated PSMs are responsible for the escape of *S. aureus* from the phagosome into the cytoplasm whereas the Sae-regulated two-component toxins LukAB and PVL are mainly involved in cell death and subsequent escape of the bacteria from within the cells. Complete escape could only be enabled with the combined action of Agr- and Sae-regulated virulence factors. Altogether, my results shed light on the sensing mechanism of the important virulence regulator Sae. It is the first study, showing that WTA is involved in the signal sensing of a two-component system. Furthermore, I could show that the Sae-system plays a major role in the interaction with human macrophages after phagocytosis. Concerning the role of the intracellular lifestyle of *S. aureus* for bacterial dissemination in the human body, a deeper understanding of post-phagocytosis events is of great interest.

### Zusammenfassung

Im humanpathogenen Erreger *Staphylococcus aureus* (*S. aureus*) ermöglichen Zwei-Komponenten Systeme (TCS) den Bakterien, auf unterschiedliche Umweltreize zu reagieren. Das Kerngenom von *S. aureus* kodiert 16 TCSs, von denen nur walKR essentiell ist. Neuere Studien zeigen, dass alle TCSs funktional autonom agieren können, so dass die Bakterien in der Lage sind, Umweltveränderungen wahrzunehmen, darauf zu reagieren und sich diesen anzupassen. Für die meisten TCS bleibt der Mechanismus, der zur Aktivierung führt, unklar. Das SaePQRS-System reguliert die Expression verschiedener sekretierter und zellgebundener Virulenzfaktoren, die sich als wichtig für die Interaktion mit unserem Immunsystem erwiesen haben. Es wurde gezeigt, dass das Sae-System durch phagozytose-ähnliche Signale, speziell von humanen  $\alpha$ -Defensinen (HNP1-3), aktiviert werden kann. Die Aktivität der Promotoren und die Ziel Gene sind weitreichend untersucht, wohingegen der Mechanismus der Signalwahrnehmung unbekannt ist. In dieser Arbeit zeige ich, dass die D-Alanylierung von Wand-Teichonsäuren (WTA) für die Wahrnehmung von HNP1-3 wichtig ist. Studien zur Regulation von *dltABCD* sowie ein Genkomplementierungsansatz konnten die Stammspezifität nicht erklären. Deshalb ist meine Hypothese, dass Stammunterschiede in der Menge von Teichonsäuren und deren Alanylierung der Grund für die Stammspezifität sind und dass diese individuelle Zusammensetzung in einem Versuchsaufbau nicht imitierbar ist. Weiterhin konnte ich Natriumhypochlorit als weiteren Aktivator des Sae-Systems bestätigen, der interessanterweise kein Stamm-spezifischer Aktivator ist. *S. aureus* ist in der Lage intrazellulär zu überleben und sogar aus professionellen Phagozyten auszubrechen. Während die Lyse von Neutrophilen durch *S. aureus* gut untersucht ist, sind die, für den Ausbruch aus humanen Makrophagen erforderlichen Faktoren weniger klar. Ich konnte zeigen, dass die Agr-regulierten PSMs für die Freisetzung von *S. aureus* aus dem Phagosom in das Zytoplasma verantwortlich sind, während die Sae-regulierten Zwei-Komponenten Toxine LukAB und PVL hauptsächlich am Zelltod und der anschließenden Freisetzung der Bakterien aus den Zellen verantwortlich sind. Ein vollständiger Ausbruch konnte nur durch die kombinierte Wirkung von Agr- und Sae-regulierten Virulenzfaktoren ermöglicht werden. Insgesamt beleuchten meine Ergebnisse den Sensormechanismus, des wichtigen

## Zusammenfassung

---

Virulenzregulators Sae, näher. Es ist die erste Studie die zeigt, dass WTA an der Signalwahrnehmung eines Zwei-Komponenten Systems beteiligt ist. Darüber hinaus konnte ich zeigen, dass das Sae- System eine entscheidende Rolle bei der Interaktion mit humanen Makrophagen nach Phagozytose spielt. Hinsichtlich der Rolle des intrazellulären Lebensstils von *S. aureus* für die Ausbreitung im menschlichen Körper ist ein tieferes Verständnis der Ereignisse, die sich nach der Phagozytose abspielen, von großem Interesse.

## List of publications

### Accepted publications

1. **Influence of Sae-regulated and Agr-regulated factors on the escape of *Staphylococcus aureus* from human macrophages**

Lisa Münzenmayer, Tobias Geiger, Ellen Daiber, Berit Schulte, Stella E. Autenrieth, Martin Fraunholz and Christiane Wolz

**Cellular Microbiology (2016) 18(8): 1172–1183**

2. **Human NACHT, LRR, and PYD domain–containing protein 3 (NLRP3) inflammasome activity is regulated by and potentially targetable through Bruton tyrosine kinase**

Xiao Liu, Tica Pichulik, Olaf-Oliver Wolz, Truong-Minh Dang, Andrea Stutz, Carly Dillen, Magno Delmiro Garcia, Helene Kraus, Sabine Dickhöfer, Ellen Daiber, Lisa Münzenmayer, Silke Wahl, Nikolaus Rieber, Jasmin Kümmerle-Deschner, Amir Yazdi, Mirita Franz-Wachtel, Boris Macek, Markus Radsak, Sebastian Vogel, Berit Schulte, Juliane Sarah Walz, Dominik Hartl, Eicke Latz, Stephan Stilgenbauer, Bodo Grimbacher, Lloyd Miller, Cornelia Brunner, Christiane Wolz and Alexander N. R. Weber

**J Allergy Clin Immunol (2017) Oct 140(4): 1054-1067**

3. **Cyanobacterial antimetabolite 7-deoxysedoheptulose blocks the shikimate pathway to inhibit the growth of prototrophic organisms**

Klaus Brilisauer, Johanna Rapp, Pascal Rath, Anna Schöllhorn, Lisa Bleul, Elisabeth Weiß, Mark Stahl, Stephanie Grond & Karl Forchhammer

**Nature Communications (2019) Feb 1;10(1): 545**

### Submitted Manuscripts

1. **Oxygen-dependent PSM toxicity drives the selection of quorum sensing mutants in the *Staphylococcus aureus* population**

Shilpa Elizabeth George, Jennifer Hrubesch, Inga Breuing, Katja Hennemann, Lisa Bleul, Natalya Korn, Matthias Willmann, Patrick Ebner, Friedrich Götz, Christiane Wolz

## List of publications

---

### Manuscripts ready for submission

1. **Two-component systems of *Staphylococcus aureus*: signals and sensing mechanisms**

Lisa Bleul and Christiane Wolz

2. **Strain dependent activation of the sensor kinase SaeS of *Staphylococcus aureus* by human neutrophil peptides 1-3 (HNP 1-3) is influenced by the D-alanylation of wall teichoic acids**

Lisa Bleul, Jana-Julia Götz, Jessica Ziemann, Andres Lamsfus-Calle, Hubert Kalbacher and Christiane Wolz

## Personal contribution to publications

### Accepted publications

**1. Influence of Sae-regulated and Agr-regulated factors on the escape of *Staphylococcus aureus* from human macrophages**

I performed all but the following experiments: Flow cytometry and multispectral imaging flow cytometry was performed with the help of Stella E. Autenrieth. Manuscript writing and figure design was done by me and Christiane Wolz.

**2. Human NACHT, LRR, and PYD domain-containing protein 3 (NLRP3) inflammasome activity is regulated by and potentially targetable through Bruton tyrosine kinase**

For this work I performed LukAB and PVL toxin purification.

**3. Cyanobacterial antimetabolite 7-deoxysedoheptulose blocks the shikimate pathway to inhibit the growth of prototrophic organisms**

I performed cell cytotoxicity experiments and microscopy with THP1 macrophages.

### Submitted Manuscripts

**1. Oxygen-dependent PSM toxicity drives the selection of quorum sensing mutants in the *Staphylococcus aureus* population**

I performed cell cytotoxicity experiments and I constructed the RNAIII mutagenesis plasmid.

### Manuscripts ready for submission

**1. Two-component systems of *Staphylococcus aureus*: signals and sensing mechanisms**

For this review article, I wrote main parts of the manuscript and performed figure design.

**2. Strain dependent activation of the sensor kinase SaeS of *Staphylococcus aureus* by human neutrophil peptides 1-3 (HNP 1-3) is influenced by the D-alanylation of wall teichoic acids**

I performed all but the following experiments: isolation of human neutrophil peptides was done by Hubert Kalbacher. Figure design and manuscript writing was done by me and Christiane Wolz.

### Introduction

#### **Lifestyle of *Staphylococcus aureus***

*Staphylococcus aureus* (*S. aureus*) is a human commensal primarily colonizing the anterior nares of healthy individuals where it was shown to interact with other members of the nasal microbiota (Krismer *et al.*, 2017). On the other hand *S. aureus* is a major human pathogen which can cause a variety of diseases, including soft skin and tissue infections but also invasive and life-threatening infections (Lowy, 1998). This dual lifestyle is enabled by the complex regulation of virulence determinants. Although *S. aureus* is not a classical intracellular bacterium it is able to survive inside human phagocytes. Due to its ability to escape from within the cells after phagocytosis it is thought that *S. aureus* exploits phagocytes for dissemination in the human body (Lehar *et al.*, 2015). In this context the interaction of *S. aureus* and phagocytes may be critical for disease outcome.

#### **Regulation of Virulence factors**

Intracellular survival and phagocytic escape require precise control of accessory gene expression in response to phagocytosis-related signals. The Sae two-component system was shown to be activated in response to human neutrophil peptides (Geiger *et al.*, 2008) whereas the quorum sensing system Agr is activated by an auto inducer (AIP) (Ji *et al.*, 1995).

**The Sae-system** regulates different surface bound and secreted virulence factors (Giraud *et al.*, 1994, Rogasch *et al.*, 2006) of which the bi-component leucocidins LukAB and PVL were shown to play a role in the lysis of neutrophils (Ventura *et al.*, 2010). The Sae operon encodes for SaeP, SaeQ, the response regulator SaeR and the histidine kinase SaeS (Steinhuber *et al.*, 2003, Geiger *et al.*, 2008). The P1 Promotor is strongly auto regulated whereas the P3 Promotor is constitutive active. The expression of target genes (e.g. *eap*, *lukAB*) is highly dependent on the level of phosphorylated SaeR. In strain Newman the system is hyperactive due to a single amino acid substitution in the first transmembrane helix (L18P) (Mainiero *et al.*, 2010). It has been shown that the Sae system of some strains (e.g. COL) does not respond to HNP1-3 although there is no difference in the Sae sequence compared to responder strains (Geiger *et al.*, 2008). This indicates that other factors are involved

## Introduction

---

in the HNP1-3 dependent activation of SaeS. The sensor kinase SaeS consists of two transmembrane regions and a small extracellular linker and was therefore classified as intramembrane-sensing histidine kinase (IM-HK) (Mascher, 2006). The overall confirmation of the N-terminal domain (Liu *et al.*, 2015) and the composition of the linker peptide were shown to be important for the kinase activity (Flack *et al.*, 2014, Liu *et al.*, 2015). For Sae and other two-component systems, sensing mechanisms are largely unknown as summarized in the following review article (Bleul *et al.*, ready for submission). Therefore a major aim of this thesis was the investigation of the Sae sensing mechanism.

**The Agr-system** globally regulates the expression of virulence factors via its effector molecule RNAIII (Novick *et al.*, 1993) which is under the control of the P3 Promotor. The P2 Promotor regulates transcription of a two-component system and the auto inducing peptide. In addition to P2 and P3, the response regulator AgrA can directly activate the expression of Phenol-soluble modulins (PSMs). PSMs are small cytolytic peptides with diverse function in *S. aureus* pathogenesis (Li *et al.*, 2014).

### **Interaction of *S. aureus* with human macrophages**

Invading pathogens first encounter tissue resident cells like dermal, alveolar or liver macrophages (Green & Kass, 1964, Zeng *et al.*, 2016, Feuerstein *et al.*, 2017). Thereby these cells display an important line of defense. *S. aureus* can survive, replicate and escape from within human macrophages (Kubica *et al.*, 2008, Grosz *et al.*, 2013, Flannagan *et al.*, 2015, Jubrail *et al.*, 2015, Tranchemontagne *et al.*, 2015). The fate of the bacteria and host cells is strongly dependent on the *S. aureus* strain and the macrophage cell type. In this context it is also important to consider the species dependency of *S. aureus* two-component leukotoxins towards their human receptors counterparts (Loffler *et al.*, 2010, Malachowa *et al.*, 2012). The Sae-regulated two-component toxin LukAB was proposed to be involved in the killing of human monocytes from the interior and exterior of the host cell (Melehani *et al.*, 2015). Extracellular LukAB toxin was shown to kill THP1 monocytes by activating the NLRP3 inflammasome thereby eliciting a highly pro inflammatory host response. However, cell death induced by intracellular LukAB was independent of NLRP3. It is likely that phagocytic escape from within human macrophages requires additional factors. The Agr-regulated PSM peptides were shown to mediate escape from the phagosome into the cytoplasm of non-professional as well as professional



## Introduction

---

phagocytes (Grosz *et al.*, 2014). It is not clear if different factors act in concert to mediate escape of *S. aureus* from within macrophages how these factors are regulated intracellularly or if these factors even influence each other. Furthermore, it is unclear if the bacteria exploit programmed cell death mechanisms to mediate phagocytic escape.

Different studies describe the activation of apoptosis (Martinez *et al.*, 2017), pyroptosis (Mariathasan *et al.*, 2006, Shimada *et al.*, 2010) or necroptosis (Gonzalez-Juarbe *et al.*, 2015, Kitur *et al.*, 2015) pathways when macrophages encounter *S. aureus*. Experiments with an alveolar macrophage cell line from mice showed upregulation of different cell death and apoptosis related pathways after intracellular infection with *S. aureus* strain Newman (Martinez *et al.*, 2017). Shimada *et al.* describe that peptidoglycan activates the NLRP3 inflammasome and IL1 $\beta$  secretion and this is inhibited by the O-acetylation of peptidoglycan. On the other hand it was described that Caspase-1 and NLRP3 activity positively regulate the acidification of phagosomes thereby functioning in host defence (Sokolovska *et al.*, 2013). Activation of necroptosis was shown to be mediated by the pore-forming capacity of different toxins, as it could be blocked by the addition of extracellular K<sup>+</sup> (Kitur *et al.*, 2015). Interestingly the production of the caspase-1 derived IL-1 $\beta$  in macrophages infected with *S. aureus* could be decreased through the inhibition of necroptosis. This indicates interplay between different cell death pathways. Therefore, the second aim of this thesis was the investigation of the fate of bacteria and cells after phagocytosis of *S. aureus* by human macrophages.

## Introduction

---

The following manuscript serves as part of the Introduction:

### **Two-component systems of *Staphylococcus aureus*: signals and sensing mechanisms**

Lisa Bleul and Christiane Wolz\*

Interfaculty Institute of Microbiology and Infection Medicine, University of Tübingen,  
Elfriede-Aulhorn-Str. 6, D-72076 Tübingen, Germany

\* Corresponding author: Phone: +49 7071 2980187. Fax: +49 7071 295165.

E-mail: [christiane.wolz@med.uni-tuebingen.de](mailto:christiane.wolz@med.uni-tuebingen.de)

Manuscript ready for submission

## Introduction

---

### Abstract

In *Staphylococcus aureus* (*S. aureus*) 16 two-component systems (TCSs) enable the bacteria to sense and respond to changing environmental conditions. Considering their function in survival and virulence and their potential role as drug targets it is of great importance to understand the exact mechanisms of signal perception. The differences between sensing of the appropriate signal and the transcriptional activation of the TCS system are often not well described but are mandatory for a deeper understanding of the molecular mechanism of signalling. This review presents an overview of known TCS signals in *S. aureus* and their proposed mechanism of sensing.

### Key words

*Staphylococcus aureus*, Two-component systems, histidine kinase, signal sensing, ligand

### Introduction

*Staphylococcus aureus* (*S. aureus*) encodes 16 two-component systems (TCSs) in the core genome to sense and respond to environmental changes. One additional TCS is encoded on a SCC-mec island (Kuroda *et al.*, 2001). It was recently shown that under constant environmental conditions despite of WalkR all other TCSs are dispensable for bacterial growth and although there is some level of cross-regulation, for its appropriate environmental signal each TCS is autonomous and self-sufficient to sense and respond (Villanueva & Garcia, 2018). A canonical two-component system consists of a histidine kinase (HK) which auto phosphorylates at a conserved histidine residue and then transfers the phosphoryl group to the aspartate residue of the cognate response regulator (RR) (Stock *et al.*, 2000). Most HKs are membrane-bound homodimers receiving external signals either with transmembrane, extracellular or intracellular sensing domains (Mascher *et al.*, 2006, Abriata *et al.*, 2017). The former ones are also called intramembrane-sensing histidine kinases (IM-HK) and are characterised by the lack of an extra cytoplasmic domain. In *S. aureus* four HKs are classified as IM-HKs namely SaeS, VraS, GraS and BraS (Mascher, 2006, Kolar *et al.*, 2011). One *S. aureus* HK, namely AgrB is a quorum sensor enabling the bacteria to monitor cell density (Novick *et al.*, 1993). PhoR and WalkR

## Introduction

---

are the only HKs in *S. aureus* harbouring a Per-ARNT-Sim (PAS) domain as potential ligand interaction site (Ulrich & Zhulin, 2007). PAS domains are widely distributed signal sensor domains with conserved protein architecture and a wide range of ligands (Mascher *et al.*, 2006, Henry & Crosson, 2011). Two *S. aureus* HKs represent Iron-sulfur (Fe-S) cluster containing proteins, namely AirS and NreB. TCS-2 and TCS-7 are until now uncharacterized. Most TCS gene clusters contain additional proteins (e.g. WalHI, SaePQ) of which some are known to interact with the HKs of the respective TCS. We only described these additional proteins in more detail when they are known to be involved in the sensing mechanism, as this was the aim of this review. In general operon architecture and overall functions of the TCSs are well studied and reviewed in several articles whereas the dedicated signals and the mechanism of sensing by the HKs are largely unknown. Furthermore, the discrimination between transcriptional activation and sensing of the TCSs are not always pointed out clearly but are necessary to understand its mode of action and to find possible sites for inference. Here we focus on signal molecules for the activation of *S. aureus* TCSs and their proposed sensing mechanism known to date.

### WalKR

The WalKR (also called YycGF) system was first described in *Bacillus subtilis* (Fabret & Hoch, 1998) and is highly conserved in low G+C gram positive bacteria. In *S. aureus* WalKR regulates genes involved in cell wall metabolism and virulence (Dubrac & Msadek, 2004) thereby controlling autolysis, biofilm formation and pathogenesis (Dubrac *et al.*, 2007, Delaune *et al.*, 2012). The sensor kinase Walk from *S. aureus* harbours an intracellular and an extracellular PAS domain presumably involved in sensing (Kim *et al.*, 2016). Structural analysis suggests that the core  $\beta$ -sheet of the extracellular PAS domain contains a conserved ligand binding pocket but a potential ligand could not be identified. It was speculated that Walk senses the level of Lipid II or more precisely the D-Ala-D-Ala moiety of Lipid II as a signal for active cell wall synthesis (Dubrac *et al.*, 2008). This is mainly based on the observation that different cell wall acting antibiotics affect the WalKR regulon in *B. subtilis*. More recent studies show that lipid II interacts with the membrane bound serine/threonine kinase PknB stimulating its kinase activity which in turn phosphorylates the response regulator WalR (Hardt *et al.*, 2017). This data suggest that lipid II is not a direct ligand of Walk. Thus although the WalKR system is one of

## Introduction

---

the most studied TCS, potential ligands and sensing mechanisms of the histidine kinase Walk are still unclear.

### HptSRA

The HptSRA (hexose phosphate transport) system regulates the Glucose-6-phosphate (G6P) uptake by activating the hexose phosphate antiporter UhpT (Park *et al.*, 2015). It is important for intracellular survival because in the cytoplasm of host cells carbon source is limited to hexose phosphate which is sensed by the Hpt system to activate the expression of *uhpT*. Transcriptional studies also revealed that the Hpt system is not auto regulated. Signal sensing is likely to be mediated by HptA, a putative secreted protein which binds G6P directly and then transfers the signal to the membrane bound HK HptS by a yet unknown mechanism. It has to be further investigated if there is a direct interaction of HptA and HptS to mediate this signal transfer. Additionally G6P can probably bind directly to HptS because a strain lacking HptA is not completely abolished in G6P sensing (Yang *et al.*, 2016).

### LytSR

The LytSR system was identified in 1996 as a two-component regulator affecting autolysis in *S. aureus* (Brunskill & Bayles, 1996) through activation of the *IrgAB* operon (Brunskill & Bayles, 1996). Decreases in the membrane potential lead to expression of *IrgAB* in a LytS dependent manner which controls programmed cell death and lysis (Patton *et al.*, 2006, Sharma-Kuinkel *et al.*, 2009, Yang *et al.*, 2013). The sensor kinase LytS harbours five transmembrane regions which are likely involved to sense alteration in the membrane potential and thereby acting as a “voltmeter”. Cationic antimicrobial peptides (CAMP) usually alter membrane potential and thereby LytS might function as a universal CAMP sensor and responder. In line with this assumption *lytSR* mutants were shown to be more CAMP sensitive (Yang *et al.*, 2013). This makes the system very important for in vivo survival because it enables a rapid and general response to CAMPs in contrast to the rather selective response of the other CAMP sensing TCSs, namely GraRS and SaeRS.

### GraRS

The GraRS (glycopeptide resistance associated) system (Meehl *et al.*, 2007) also called ApsSR (antimicrobial peptide sensor) (Li *et al.*, 2007) is required for the

## Introduction

---

resistance to several CAMPs and vancomycin via regulation of *vraFG*, *mprF* and *dltABCD* (Li *et al.*, 2007, Meehl *et al.*, 2007). The major difference to the LytSR system which also senses CAMPs is that GraRS responds only to specific CAMPs. Induction was so far shown for indolicidin, mellitin, nisin, LL-37 (Li *et al.*, 2007), colistin (Falord *et al.*, 2011), RP-1 and polymyxin B (PMB) but not hNP-1, vancomycin, gentamycin or daptomycin (Yang *et al.*, 2012). In the homologous system in *S. epidermidis*, the sensor ApsS was shown to bind CAMPs directly via its 9-amino-acid extracellular loop which harbors a high density of negative charges (Li *et al.*, 2007) and the same was proposed for GraS of *S. aureus* (Li *et al.*, 2007). However, loop composition differs between the strains resulting in different selectivity towards CAMPs (Li *et al.*, 2007). Other studies propose that GraX, a cytoplasmic protein and VraFG, an ABC transporter play an important role in signal sensing by forming a five component system (Falord *et al.*, 2012). Indeed the extracellular loop of GraS and more precisely the proline at position 39 and the two aspartic acid residues at positions 37 and 41 was shown to mediate GraS sensing (Cheung *et al.*, 2014) and also interdependency of GraRS and VraFG was shown for induction of GraRS target genes by PMB (Yang *et al.*, 2012). Thus, CAMPs seem to activate GraS via binding to its extracellular loop and/or the VraF transporter. Recent studies could show that GraS is mandatory for *S. aureus* growth inside macrophage phagolysosomes and that this is dependent on the acidic pH (Flannagan *et al.*, 2018).

### SaeRS

The SaeRS (*S. aureus* exoprotein expression) system (Giraudou *et al.*, 1994) regulates numerous virulence factors in *S. aureus* including surface bound as well as secreted proteins (Giraudou *et al.*, 1994, Rogasch *et al.*, 2006). The Sae system was shown to be induced by phagocytosis related signals of which human neutrophil peptides 1-3 (HNP1-3) show the most pronounced effect (Geiger *et al.*, 2008). A summary of signals and target genes can be found in the review of Liu *et al.* 2016. The sensor kinase SaeS is predicted to harbour two transmembrane domains and a nine amino-acid extracellular linker (Adhikari & Novick, 2008). It was shown, that the overall confirmation of the N-terminal domain (Liu *et al.*, 2015) and the linker peptide composition are important for the kinase activity (Flack *et al.*, 2014, Liu *et al.*, 2015). However, the linker peptide is postulated to be too small for direct binding of ligands,

## Introduction

---

therefor SaeS is classified as intramembrane sensing histidine kinase (Mascher, 2006). The sensing mechanism of SaeS is unknown.

### **ArIRS**

The ArIRS (autolysis-related locus) system (Fournier & Hooper, 2000) regulates the expression of several virulence factors including Protein A (*spa*) and the secreted proteins  $\alpha$ -toxin,  $\beta$ -hemolysin, serine protease, coagulase and lipase (Fournier *et al.*, 2001). Of note the ArIRS system downregulates the expression of those virulence genes and most effects are mediated through the *sarA* and/or *agr* regulatory pathways. The expression of capsule is positively regulated by Arl (Luong & Lee, 2006). Recent studies show that also the *ica* operon is regulated by Arl and that the Arl system is a key regulator in catheter colonization (Burgui *et al.*, 2018). Microarray data show that Arl positively and negatively regulated genes involved in many different functions (Liang *et al.*, 2005). DNA relaxing conditions (high osmolality or DNA gyrase inhibitors) enhance *spa* expression in an Arl dependent manner (Fournier & Klier, 2004) but this is due to the regulatory effect of Arl on DNA supercoiling. Nothing is known about a potential activating signal of the histidine kinase ArlS. There is no special motif in the sensor domain predicted but the 118 amino acid extracellular region between the two membrane spanning domains (InterPro prediction) could be a potential ligand interaction site.

### **SrrAB**

The SrrAB (Staphylococcal respiratory response) system (Yarwood *et al.*, 2001) was originally shown to regulate virulence genes including RNAIII and Protein A under micro aerobic conditions. This was not reproducible by a later study (Kinkel *et al.*, 2013) where they could show that SrrAB regulates genes involved in anaerobic metabolism, nitrosative stress and cytochrome biosynthesis. Furthermore SrrAB plays a role in biofilm formation (Mashruwala & Guchte, 2017). The HK SrrB is predicted to harbour two transmembrane domains and a hydrophilic extracellular region (Pragman *et al.*, 2004). SrrAB is activated by hypoxia and nitric oxide (NO) possibly through sensing of reduced menaquinone as a result of impaired electron flow in the electron transport chain (Kinkel *et al.*, 2013) but the exact sensing mechanism is not known.

## Introduction

---

### PhoPR

The PhoPR system is important for phosphate homeostasis in *S. aureus* by sensing phosphate limitation and regulating the expression of three phosphate transporters, namely PstSCAB, NptA and PitA (Kelliher *et al.*, 2018). Besides phosphate transporter expression PhoPR controls factors contributing to virulence. In the homologous system in *E. coli* the PhoR kinase interacts through its PAS domain with the negative regulator PhoU which monitors the activity of the Pi-specific ATP-binding cassette transporter PstSCAB (Gardner *et al.*, 2014). Low activity of the Pst transporter then leads to high activity of PhoR. Signal sensing is mediated through conformational changes of PstB in response to Pi availability (Vuppada *et al.*, 2018). In *Bacillus subtilis* no homolog to PhoU is present and PhoR activity is responsive to biosynthetic intermediates of wall teichoic acid (WTA) metabolism (Devine, 2018). Considering that the respective WTA intermediate is not present in *S. aureus* and that PhoU is not needed for growth of *S. aureus* in Pi depleted medium, Pi sensing in *S. aureus* is likely to be fundamentally different from that in *E. coli* and *B. subtilis* (Kelliher *et al.*, 2018). Nevertheless, the intracellular PAS domain can be assumed to be important for ligand interaction.

### AirSR

The AirSR (anaerobic iron-sulfur cluster-containing redox sensor regulator) system (Sun *et al.*, 2012) also called YhcSR (Sun *et al.*, 2005) responds to oxidation signals. The N-terminal sensor domain of the histidine kinase AirS contains a Fe-S cluster essential for its kinase activity (Sun *et al.*, 2012). Under anaerobic conditions or in the absence of ROS the Fe-S cluster is reduced leading to low phosphorylation of AirS and thereby low kinase activity. When exposed to oxygen  $[2\text{Fe-2S}]^+$  is oxidized to  $[2\text{Fe-2S}]^{2+}$  and this leads to full kinase activity of AirS. Overoxidation and exposure to  $\text{H}_2\text{O}_2$  or NO stress results in protein inactivation. Surprisingly a regulatory effect on gene expression could only be observed under anaerobic conditions indicating that non-phosphorylated AirR represses target genes including the global virulence regulators Sae and Agr. This would mean that under aerobic conditions when AirS is phosphorylated and exhibits full kinase activity the system has no influence on target genes. Considering that other studies describe upregulation of Agr under anaerobic conditions (Wilde *et al.*, 2015) and that AirSR is important for *S. aureus* survival in



## Introduction

---

human blood (Hall *et al.*, 2015) - indicating positive regulation of virulence factors - these finding need to be revisited.

### VraSR

The VraSR (vancomycin resistance associated) system facilitates resistance to cell-wall antibiotics via regulation of cell-wall biosynthesis and antibiotic resistance genes (Kuroda *et al.*, 2003). Activation of VraSR target genes including the auto regulated *vraSR* operon is triggered by cell wall synthesis inhibitors like glycopeptide or  $\beta$ -lactam antibiotics. Perturbations of cell wall synthesis caused by interruption of *pbpB* (Penicillin binding protein 2) transcription triggers the transcription of *vraSR* (Gardete *et al.*, 2006). VraS belongs to the family of intramembrane-sensing histidine kinases because it has no extracellular sensing domain (Mascher, 2006). A deletion of the putative membrane protein VraT leads to similar *vra* operon expression under inducing and uninducing conditions (Boyle-Vavra *et al.*, 2013). It is suggested that cell wall damage or by-products of cell wall damage modifies VraT which interacts with VraS to influence its auto phosphorylation.

### AgrCA

The AgrCA (accessory gene regulator) system (Novick *et al.*, 1993) senses population density through the production of an auto inducing peptide (AIP) and serves as a global virulence regulator via its effector molecule RNAlII. There are several reviews about Agr function, operon architecture, regulation and target genes (Novick, 2003, Bronner *et al.*, 2004, Novick & Geisinger, 2008, Kavanaugh & Horswill, 2016). The AIP is a modified 8- to 9-aa peptide which is processed by AgrB from the AgrD encoded propeptide (Ji *et al.*, 1995). The thiolactone ring of the AIP is necessary for binding whereas the tail is critical for activation thereby deletion of the tail converts the AIP from an agonist into an antagonist (Lyon *et al.*, 2000). The ligand binding site of the HK AgrC is in the N-terminal transmembrane domain, presumably in the third extracellular loop (Lina *et al.*, 1998). Binding of the AIP changes the conformation of the cytoplasmic signalling helix of AgrC (Wang *et al.*, 2014) and this disrupts the hydrogen bonding interaction between the dimerization and histidine phosphotransfer (DHp) domain and the catalytic and ATP binding (CA)

## Introduction

---

domain (Xie *et al.*, 2019). Disruption of this homodimeric interface makes the histidine residue accessible for phosphorylation. Recent publications have shown that the putative metalloprotease MroQ influences Agr activity but the proposed mechanisms are contradictory. It was shown that members of the fengycin cyclic lipopeptide family produced by *Bacillus* strains act as competitive inhibitors of the Agr system because of their structural similarity to AIPs (Piewngam *et al.*, 2018).

### KdpDE

The KdpDE system was first characterised in *E.coli* where it is activated by K<sup>+</sup> limitation and salt stress (Ballal *et al.*, 2007). In *S. aureus* the KdpDE system activates the expression of the high-affinity potassium uptake system KdpFABC under salt stress (Price-Whelan *et al.*, 2013). The KdpDE system is activated by osmotic stress caused by NaCl or sucrose but not by KCl. Another study could show that KCl inhibits the expression of the sensor kinase KdpD but this was not an auto regulatory effect since it was independent of the response regulator KdpE (Xue *et al.*, 2011). The KdpD kinase can directly bind the second messenger molecule c-di-AMP through its intracellular universal stress protein (USP) domain (Moscoso *et al.*, 2016). This binding inhibits KdpDE signalling. It is possible that under salt stress c-di-AMP inhibition is relieved leading to activation of the KdpDE system and expression of *kdpFABC* transporter genes.

### HssRS

The HssRS (heme sensor) system senses the level of extracellular heme and alters the expression of the heme-regulated transporter efflux pump (HrtAB) thereby sustaining heme homeostasis in *S. aureus* (Stauff *et al.*, 2007, Torres *et al.*, 2007). The ligand and sensing mechanism of the histidine kinase HssS is not understood but there are speculations in the review of Stauff and Skaar. Because HssS is missing a putative heme binding site the authors suggest that it is either an indirect sensing mechanism of heme or HssS senses one of the toxic effects of heme (Stauff & Skaar, 2009).

## Introduction

---

### NreBC

The NreBC (nitrogen regulation) system is the only TCS in *S. aureus* with a cytoplasmic sensor kinase and was first discovered in *Staphylococcus carnosus* (Kamps *et al.*, 2004). The Sensor kinase NreB is an oxygen sensing protein in staphylococci containing a Fe-S cluster at the N-terminus and its activity influences nitrate and nitrite reductases (Schlag *et al.*, 2008). Under anoxic conditions NreB contains an oxygen-sensitive  $[4\text{Fe-4S}]^{2+}$  cluster and is phosphorylated at the conserved histidine residue. Disassembly of the  $[4\text{Fe-4S}]^{2+}$  cluster to a  $[2\text{Fe-2S}]^{2+}$  cluster upon exposure to oxygen leads to decreased auto phosphorylation of NreB. The system was also studied in *S. aureus* where it was shown to be important under anaerobic conditions and therefore could play a role in infection. Because this study showed that also in *S. aureus* genes for nitrate and nitrite reduction and transport are upregulated under anaerobic conditions in a NreBC dependent manner it is very likely that function of NreBC is conserved in Staphylococci.

### BraRS

The BraRS (bacitracin resistance associated) system (Hiron *et al.*, 2011) also called NsaRS (nisin susceptibility associated) (Blake *et al.*, 2011) is essential for bacitracin and nisin resistance in *S. aureus*. The sensor kinase BraS is classified as IM-HK harbouring an extremely short extracellular loop of only three amino-acids (Hiron *et al.*, 2011). The ABC transporters BraDE and VraDE are involved in bacitracin resistance and their operon expression is in turn induced by bacitracin and nisin through BraRS. BraDE is important for the detection of antibiotics whereas VraDE confers resistance. Although the system is only involved in bacitracin and nisin resistance, other antimicrobials targeting the cell wall also activate NsaRS expression (Kolar *et al.*, 2011). This shows that NsaRS plays an important role in sensing perturbations of the cell envelope of *S. aureus*.

## Introduction

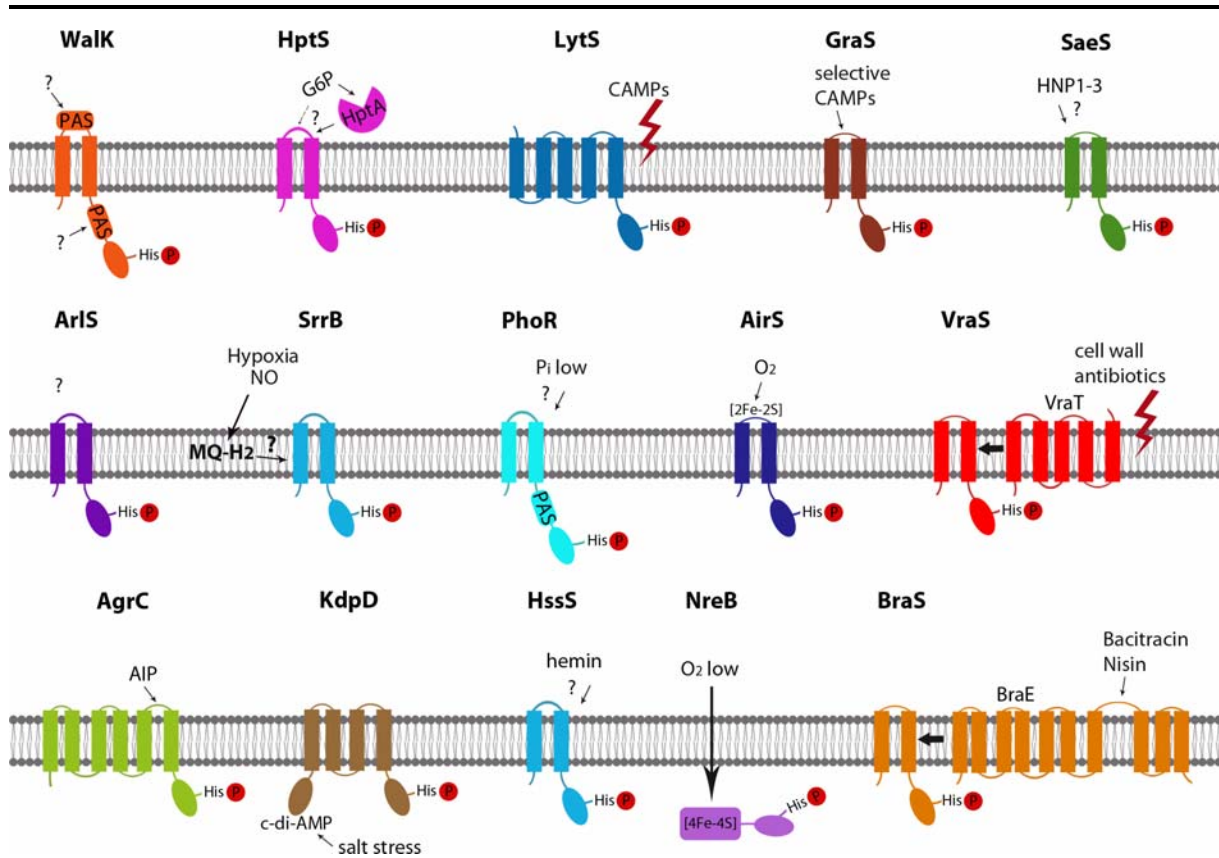


Figure 1: schematic illustration of sensor kinases in *S. aureus*, their proposed signals and sensing mechanisms. PAS: Per-Arnt-Sim domain; His: histidine; P: phosphate; G6P: Glucose 6 phosphate; CAMPs: cationic antimicrobial peptides; Pi: inorganic phosphate; MQ: menaquinone (Pragman *et al.*, 2004, Li *et al.*, 2007, Belcheva & Golemi-Kotra, 2008, Dubrac *et al.*, 2008, Sun *et al.*, 2012, Walker *et al.*, 2013, Cheung *et al.*, 2014, Liu *et al.*, 2015, Park *et al.*, 2015, Patel & Golemi-Kotra, 2015, Yang *et al.*, 2016, Kelliher *et al.*, 2018) (Torres *et al.*, 2007, Schlag *et al.*, 2008, Hiron *et al.*, 2011, Boyle-Vavra *et al.*, 2013, Grundling, 2013, Wang *et al.*, 2014) and InterPro prediction.

## Introduction

Table 1: sensor kinases of *S. aureus* and their proposed signals and sensing mechanisms

HK	Annotation	stimuli	Direct interaction with HK	mechanism	References
WalK	SAUSA300_0021	unknown			
HptS	SAUSA300_0218	G6P	yes/no	binding to sensor protein hptA and signal transfer	(Park <i>et al.</i> , 2015, Yang <i>et al.</i> , 2016)
LytS	SAUSA300_0254	altered membrane potential (CM $\Delta\psi$ )	no	unknown	(Patton <i>et al.</i> , 2006)
GraS	SAUSA300_0646	indolicidin, mellitin, nisin, LL-37, colistin, RP-1 and polymyxin B	proposed		(Li <i>et al.</i> , 2007, Falord <i>et al.</i> , 2011, Yang <i>et al.</i> , 2012)
SaeS	SAUSA300_0690	HNP1-3		unknown	(Geiger <i>et al.</i> , 2008)
ArlS	SAUSA300_1307	unknown			
SrrB	SAUSA300_1441	Reduced menaquinone (MQ-H <sub>2</sub> )	no	unknown	(Kinkel <i>et al.</i> , 2013)
PhoR	SAUSA300_1638	Low P <sub>i</sub>	no	unknown	(Kelliher <i>et al.</i> , 2018)
AirS	SAUSA300_1799	oxygen	no	oxidation of Fe-S cluster	(Sun <i>et al.</i> , 2012)
VraS	SAUSA300_1866	cell wall damage	no	signal transfer through VraT (proposed)	(Gardete <i>et al.</i> , 2006, Boyle-Vavra <i>et al.</i> , 2013)
AgrC	SAUSA300_1991	AIP	yes	binding to extracellular loop of AgrC changes conformation of the cytoplasmic signaling helix thereby disrupting the homodimeric interface	(Ji <i>et al.</i> , 1995, Lina <i>et al.</i> , 1998, Wang <i>et al.</i> , 2014, Xie <i>et al.</i> , 2019)
KdpD	SAUSA300_2035	ci-d-AMP	yes	binding to USP-domain	(Moscoso <i>et al.</i> , 2016)
HssS	SAUSA300_2309	hemin level		unknown	(Stauff <i>et al.</i> , 2007)
NreB	SAUSA300_2338	Low oxygen		Oxygen leads to disassembly of the Fe-S cluster and thereby decreased autophosphorylation	(Schlag <i>et al.</i> , 2008)
BraS	SAUSA300_2558	class I bacteriocins Bacitracin, Nisin	no	unknown	(Hiron <i>et al.</i> , 2011)

### Objectives of the thesis

#### **Objective 1: Elucidate factors involved in the strain specific, HNP1-3 dependent SaeS activation in *Staphylococcus aureus***

The histidine kinase SaeS of *S. aureus* was shown to be induced by phagocytosis-related signals, namely HNP1-3. This induction was shown to be specific for certain *S. aureus* strains. Interestingly responder as well as non-responder strains show sequence identity of their *saePQRS* operon making it likely that other strain features are responsible for the sensing of HNP1-3. I aimed to elucidate factors involved in the HNP1-3 dependent activation of SaeS and the reason for strain specific differences in the response to HNP1-3.

#### **Objective 2: Investigate the impact of the virulence regulator Sae on bacteria-phagocyte interaction after phagocytosis**

*S. aureus* was shown to be able to survive inside professional phagocytes and even escape from within the cells. However, it was not clear which bacterial factors account for the escape after phagocytosis. I aimed to analyze the role of virulence regulatory systems, especially the Sae-system, on the interaction of *S. aureus* with human macrophages after phagocytosis. Furthermore, I aimed to identify the specific Sae target genes responsible for the observed phenotype and their intracellular regulation.

### Results

The results are part of the following manuscripts:

#### Manuscript ready for submission

2. **Strain dependent activation of the sensor kinase SaeS of *Staphylococcus aureus* by human neutrophil peptides 1-3 (HNP 1-3) is influenced by the D-alanylation of wall teichoic acids**

Lisa Bleul, Jana-Julia Götz, Jessica Ziemann, Andres Lamsfus-Calle, Hubert Kalbacher and Christiane Wolz

#### Accepted publication

1. **Influence of Sae-regulated and Agr-regulated factors on the escape of *Staphylococcus aureus* from human macrophages**

Lisa Münzenmayer, Tobias Geiger, Ellen Daiber, Berit Schulte, Stella E. Autenrieth, Martin Fraunholz and Christiane Wolz

**Cellular Microbiology (2016) 18(8): 1172–1183**

### Part I: SaeS sensing mechanism

#### Strain-specific activation of SaeS by HNP1-3

The Sae two-component system was shown to be activated by human neutrophil peptides (HNP1-3) in a strain dependent manner (Geiger *et al.*, 2008). We first performed transcriptional analysis of *saePQRS* (autoregulated) and its target gene *eap*, to confirm strain dependency of this mechanism. We analysed strain USA300 representing a known responder strain and HG001 and Col as non-responders. Additionally, we included strain Newman which is constitutively active due to a single amino acid substitution in SaeS (L18P). We wondered if repair of this mutation in strain Newman (Newman HG (P18L)) renders this strain responsive.

As shown in Fig. 1B, USA300 and Newman HG respond to HNP1-3 with elevated levels of *sae* and *eap* transcripts whereas strains HG001 and Col show the expected non-responsive phenotype. Strain Newman was confirmed to be hyperactive.

Interestingly, sequence of the *saePQRS* operon of responder and non-responder strains is identical. We therefore concluded that other strain features are responsible for the strain specific sensing of HNP1-3.

Strain specific differences in the interference with the P1 Promotor (transcriptional regulation) might be responsible for the different expression of *saePQRS* and *eap*. We therefore constructed complementation plasmids missing the auto regulated P1 Promotor and SaePQ to distinguish between SaeS activation by HNP1-3 and transcriptional regulation. These plasmids, harbouring *saeRS<sup>L</sup>* (native SaeS) or *saeRS<sup>P</sup>* (SaeS with L18P) were integrated into the *sae* mutant of USA300. As a control we also integrated *saePQRS<sup>L</sup>* in this strain. SaeS was fused with C-terminal 3x-FLAG because we planned to perform protein analysis.

When we complemented the *saePQRS* mutant with the short constructs (pRS<sup>L</sup> or pRS<sup>P</sup>), *saeRS* expression was very weak (Fig. 1C). However, HNP1-3 still activated *eap* expression similar to the full length construct. We therefore conclude that HNP1-3 dependent activation of SaeS is independent of the P1 Promotor activity. The auxiliary proteins SaeP and SaeQ were shown to form a protein complex with SaeS thereby activating its phosphatase activity (Jeong *et al.*, 2012). However, our results show that the auxiliary proteins SaeP and SaeQ are dispensable for sensing.



## Results Part I

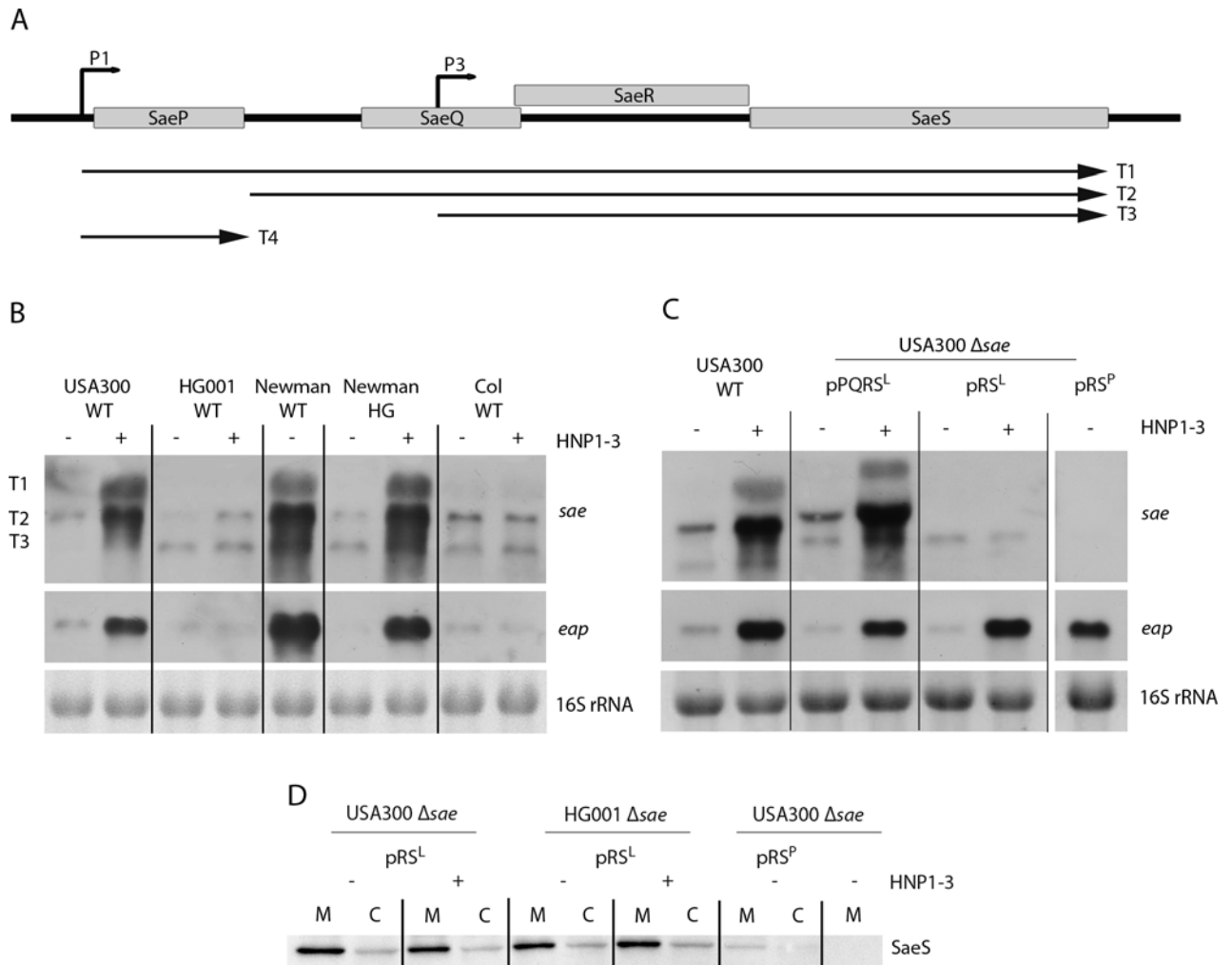


Fig. 1 from Bleul *et al.* (manuscript ready for submission)

HNP1-3 dependent SaeS activation. (A) SaePQRS operon architecture indicating the transcriptional units (T1-T4) starting from promoter P1 or P3 respectively. (B and C) *S. aureus* strains were grown to an OD600 of 1 and aliquots were treated without or with human neutrophil peptides (5  $\mu$ g/ml HNP1-3) for 1 h. 2  $\mu$ g of total RNA was hybridized with DIG-labelled probes for detection of *sae* and *eap* transcripts. 16S rRNA was used as loading control. T1, T2 and T3 indicate the different *sae* transcripts. (D) *S. aureus* strains were grown as described above and harvested for Western Blot analyses. SaeS was detected using anti-Flag antibody. (C and D) pPQRS<sup>L</sup>: integrative *sae* full-length complementation, pRS<sup>L</sup>: integrative complementation with *saeRS*<sup>L</sup> (native SaeS), pRS<sup>P</sup>: integrative complementation with *saeRS*<sup>P</sup> (SaeS with L18P).

Previous studies show, that SaeS<sup>P</sup> is more susceptible to proteolytic cleavage by FtsH and therefore less stable than SaeS<sup>L</sup> (Jeong *et al.*, 2011, Liu *et al.*, 2017). We wondered if FtsH cleavage correlates with the activation of SaeS and thereby would also have an impact on SaeS<sup>L</sup> upon HNP1-3 challenge. We analysed a responder and non-responder strain complemented with the SaeRS-3xFlag fusions for protein abundance and localisation of SaeS. We could confirm that SaeS<sup>P</sup> was less abundant compared to SaeS<sup>L</sup> (Fig. 1D). However, SaeS abundance and localisation

## Results Part I

was not different between the strains and did not change after HNP1-3 treatment and thus is not explaining strain difference.

### Hypochlorite activates the Sae system independent of the strain background

In other two-component systems signals are sensed through alterations in physiological parameters. We wondered if alternative signals for SaeS activation share common features with HNP1-3 and thereby would give us a hint on the sensing mechanism. We tested Melittin, the main component of the honeybee venom because of its structural similarities to HNP1-3 and the antimicrobial peptide LL37 of the human cathelicidin family which was previously shown not to activate the Sae system (Geiger *et al.*, 2008). Melittin as well as LL37 did not show any effects on *sae* or *eap* expression under the same conditions used for HNP1-3.

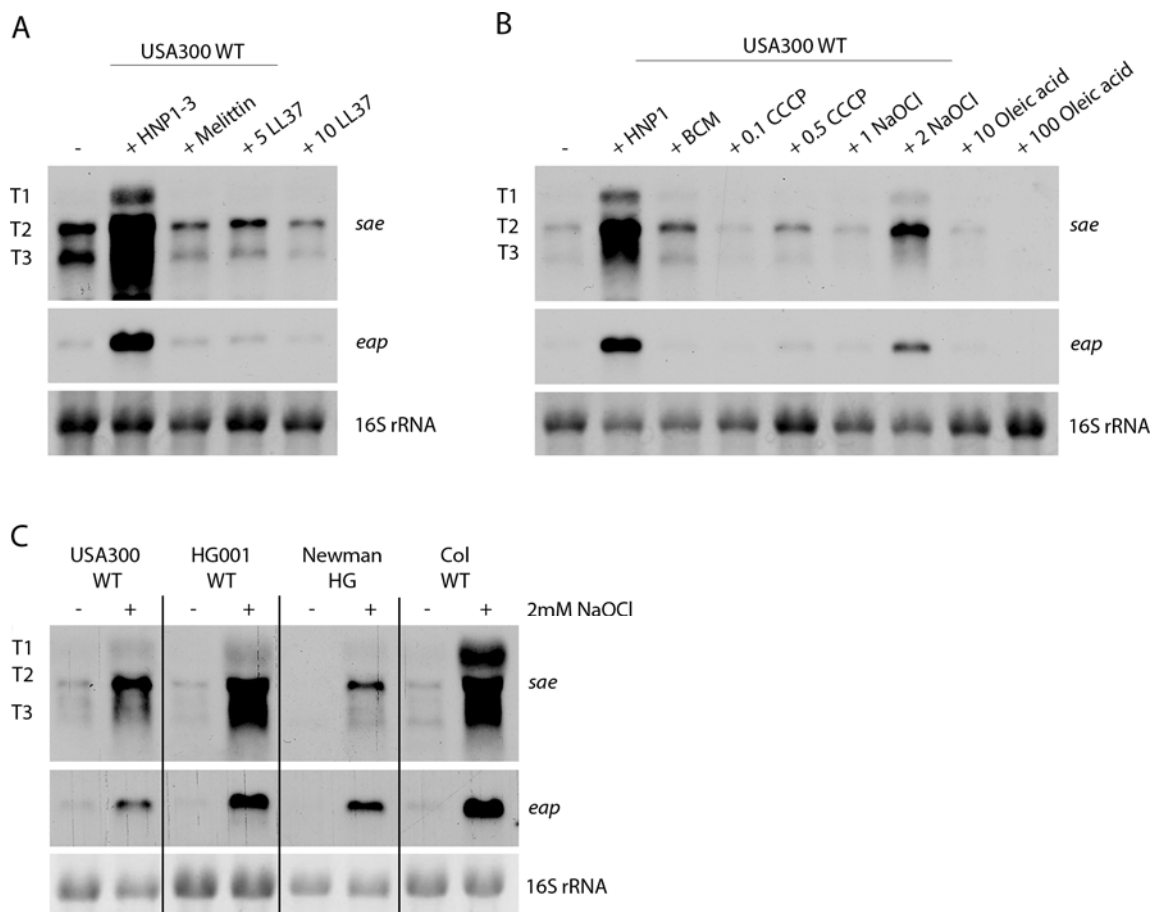


Fig. 2 from Bleul *et al.* (manuscript ready for submission)

Sodium hypochlorite dependent SaeS activation. (A and B) *S. aureus* strain USA300 was treated with HNP1-3 (5 μg/ml), Melittin (0.05 μM), LL-37 (5 μM and 10 μM) (A), synthetic HNP1 (5 μg/ml), Bicyclomycin (BCM, 80 μg/ml), Carbonyl cyanide 3-chlorophenylhydrazone (CCCP, 0.1 and 0.5 μM), sodium hypochlorite (NaOCl, 1 mM and 2 mM) or oleic acid (10 μM and 100 μM) (B) and strains USA300, HG001, Newman HG and Col were treated with 2 mM NaOCl (C) for 1 h. Northern Blot analyses was performed as described above.

## Results Part I

---

There are several other substances described in the literature with potential effects on the Sae regulon. Bicyclomycin (BCM) was recently shown to upregulate genes of the SaeR regulon (Nagel *et al.*, 2018). The proton ionophor CCCP was shown to upregulate the expression of *saeR* and *saeS* but not *saeP* or *saeQ* (Muthaiyan *et al.*, 2008) which already indicates a transcriptional regulation. In contrast exogenous fatty acids were shown to inhibit Sae (Neumann *et al.*, 2015). All compounds showed only weak or no effect under our experimental conditions. We next tested sodium hypochlorite (NaOCl). Hypochlorite is produced by the Myeloperoxidase in neutrophils thereby displaying another phagocytosis-related signal. In line with previous studies (Loi *et al.*, 2018) we could activate *sae* as well as *eap* with 2mM of NaOCl. Activation of Sae by NaOCl turned out to be independent of the strain background (Fig. 2C).

### **The GraRS regulon influences HNP1-3 dependent SaeS activation**

The GraRS two-component system interacts with other antimicrobial peptides to activate the expression of *mprF* and *dltABCD* (Li *et al.*, 2007). Lysinylation of phosphatidylglycerol through *mprF* (Oku *et al.*, 2004, Staubitz *et al.*, 2004) and D-alanylation of teichoic acids through *dltABCD* (Peschel *et al.*, 1999) in turn present natural defence mechanisms by increasing the cell surface charge. We observed that a *graRS* mutant is also impaired in HNP1-3 dependent activation of SaeS (Fig. 3A). We wondered if this effect is mediated by *mprF* and/or *dltABCD*. The mutation in *mprF* had no impact on SaeS activation. However, a *dltABCD* mutant was impaired in sensing. Since a *graRS* mutant shows decreased D-alanylation of WTA (Herbert *et al.*, 2007) the phenotype of the *graRS* mutant might be mainly due to D-Ala deficiency (Fig. 3BC). Interestingly deletion of WTA as substrate of D-alanylation also abrogates sensing. We next wanted to exclude, that abrogated sensing of the *tagO* mutant is due to glycosylation of WTA. Therefore, we tested a *tarS/tarM* double mutant which is deficient in glycosylation of the WTA. We can clearly show that D-alanylation but not glycosylation of WTA influences HNP1-3 dependent activation of SaeS. We could successfully complement the *tagO* mutant as well as the mutation in the *dltABCD* operon (Fig. 3DE).

## Results Part I

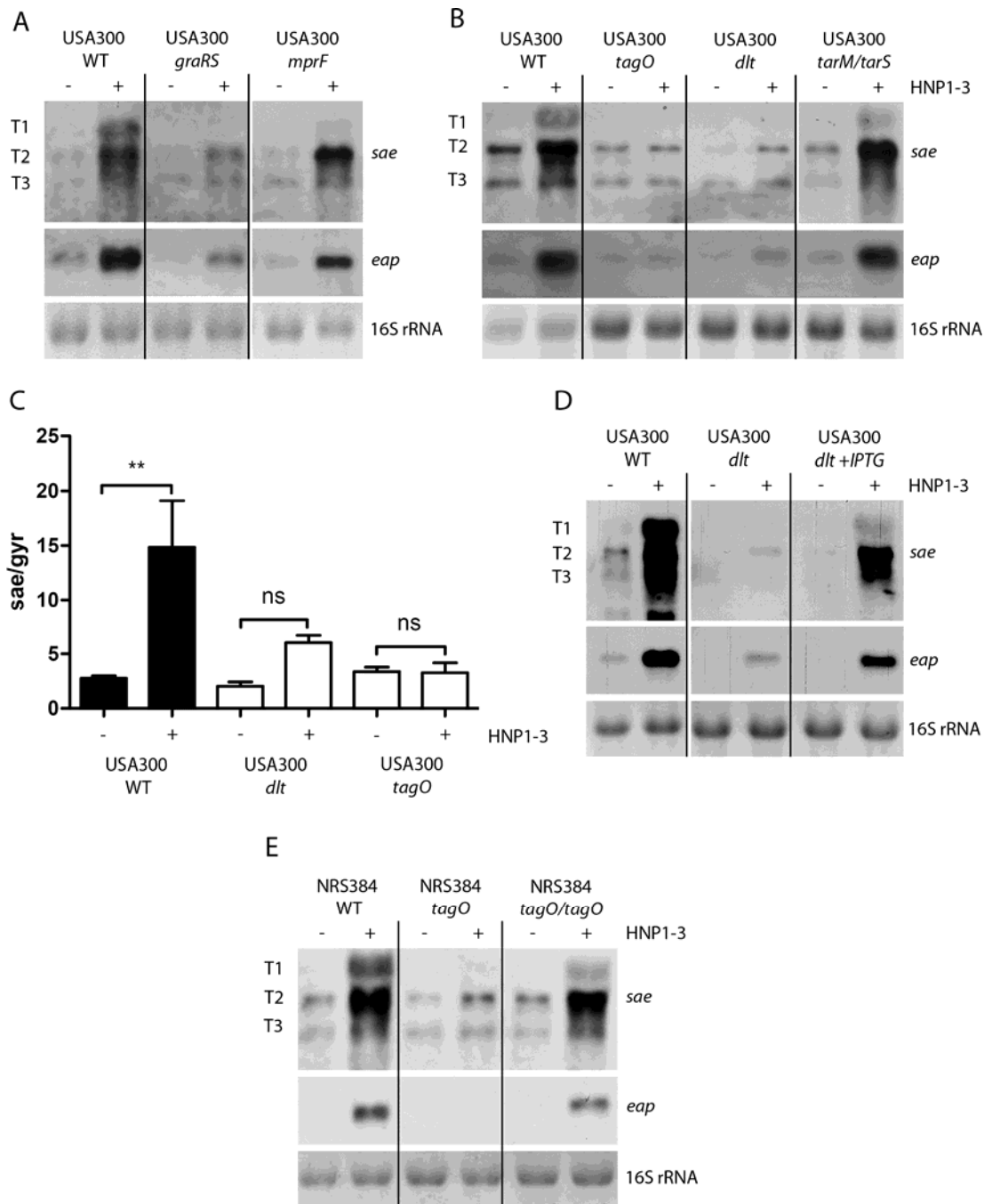


Fig. 3 from Bleul *et al.* (manuscript ready for submission)

D-Alanylation of the WTA influences HNP1-3 dependent SaeS activation.

*S. aureus* strains were grown with HNP1-3 (5µg/ml) for 1h. Northern Blot analyses (A, B, D and E) were performed as described above (C) qRT-PCR with RNA of USA300 and its isogenic *dlt* and *tagO* mutants. Relative quantification of *sae* was expressed in relation to the expression of the constitutive reference gene *gyrB*. Significance was determined by one-way analysis of variance with Tukey's multiple comparison post-test. The data represent the mean of three independent experiments. \*\*P < 0.01, ns, not significant.

## Results Part I

### Strain specificity does not correlate with *dltABCD* operon sequence, *dltA* expression or defensine sensitivity

When we compared the *dltABCD* operon of USA300 and HG001, we found one amino acid in the *dltD* gene to be different. Exchanging the *dltD* gene of USA300 with *dltD* of HG001 and vice versa did not influence the sensing ability of the strains (Fig 4A). Therefore the single amino acid substitution in *dltD* is not the reason for the strain specific sensing mechanism of SaeS.

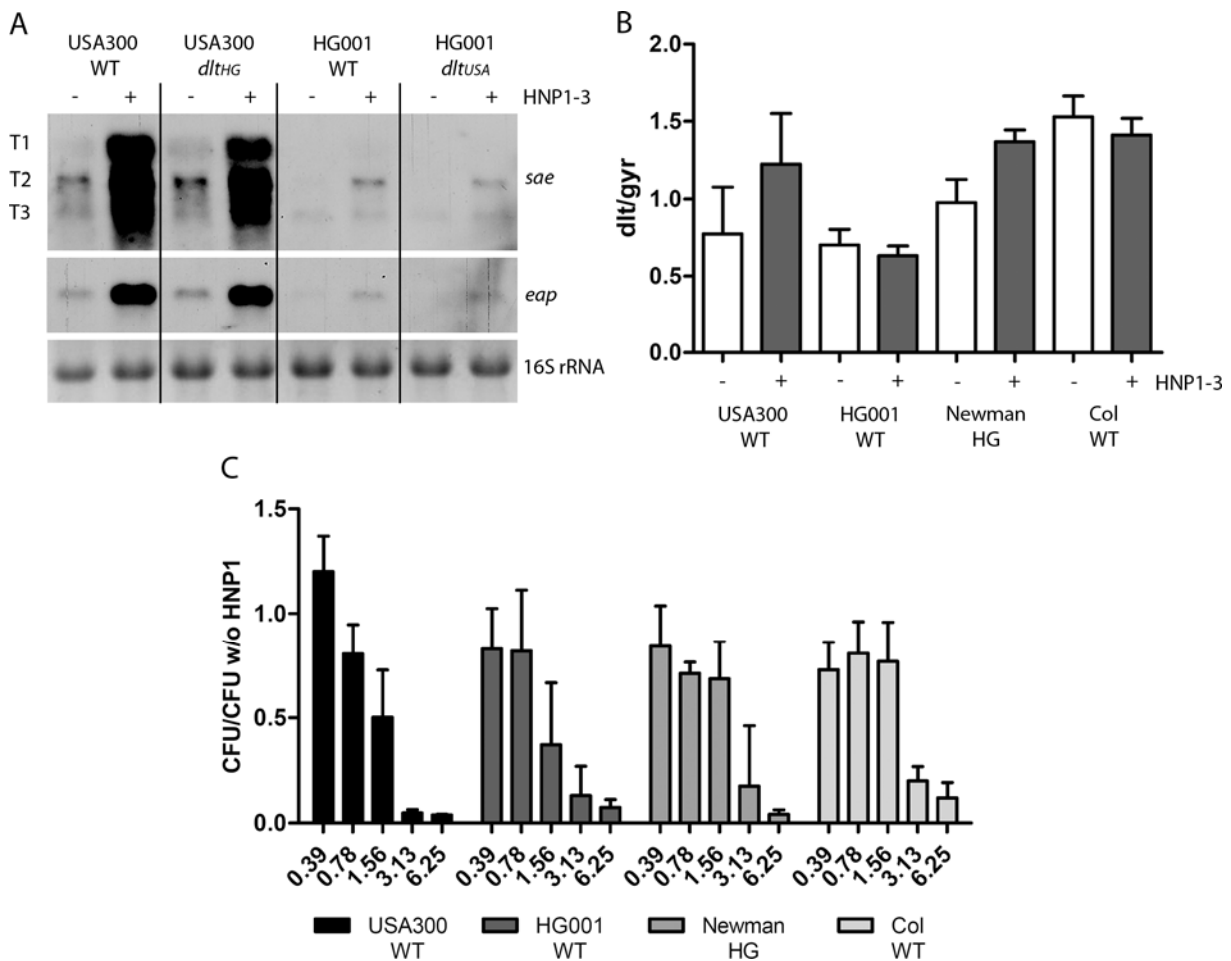


Fig. 4 from Bleul *et al.* (manuscript ready for submission)

*DltA* expression and sensitivity towards HNP1-3. *S. aureus* strains were grown with HNP1-3 (5 µg/ml) for 1h. (A) Northern Blot analysis was performed as described above (B) qRT-PCR with RNA of strains USA300, HG001, Newman HG and Col. Relative quantification of *sae* was expressed in relation to the expression of the constitutive reference gene *gyrB*. (C) *S. aureus* strains USA300, HG001, NewmanHG and Col were incubated with HNP1 concentrations ranging from 0.39 to 6.25 µg/ml (in a final volume of 100 µl) for 2h at 37°C and colony counts enumerated. Bacterial counts after HNP1 treatment are expressed in relation to untreated control.

We then thought that the expression of the *dlt* operon might differ between the strains, therefore explaining the strain specificity in HNP1-3 sensing. We performed

## Results Part I

---

qRT-PCR of responder and non-responder strains, to compare the expression of *dltA*. The tested strains did not show significant differences in *dltA* expression (Fig. 4B). We next tested the sensitivity of responder and non-responder strains against different concentrations of HNP1-3. The results do not correlate with HNP1-3 responsiveness (Fig. 4C).

### Part II: Sae impact on phagocyte interaction

#### Impact of the Sae regulatory system for the escape of *S. aureus* from within THP-1 macrophages

Because Sae-regulated toxins were previously shown to be involved in neutrophil lysis from within the cells (Ventura *et al.*, 2010, DuMont *et al.*, 2013) we aimed to identify the components required for escape from macrophages. We determined the survival of *S. aureus* strain JE2 (Nuxoll *et al.*, 2012) and mutants of the important virulence regulatory systems Agr and Sae after uptake by differentiated THP-1 macrophages. To obtain a reference value of phagocytosed bacteria, the extracellular/escaped bacteria were killed by lysostaphin/gentamicin treatment after 1h. This time point is indicated as t0. The following incubation times were performed with gentamycin to kill all escaping bacteria, whereas intracellular bacteria are protected. As shown in Fig. 1B wild type bacteria were hardly detectable after 24h, indicating escape of the bacteria from within the cells. Likewise, a mutant in the regulatory system *agr* also escaped from within the macrophages, although to a lesser extent than the wild type. On the other hand, in macrophages infected with *sae* and *agr/sae* mutants high numbers of intracellular bacteria could be detected after 24h. One may argue that decrease of bacteria is due to intracellular killing by macrophages. Therefore, we performed a cell toxicity assay to confirm escape of bacteria. Membrane damage of macrophages was reversely proportional to the viable intracellular bacteria thereby correlating with escape (Fig. 1C). It must be pointed out that there was a significant difference between the *sae* single mutant compared to the *agr/sae* double mutant demonstrating the importance of both regulators. To visualize the escape of *S. aureus* we used THP1-macrophages expressing YFP-CWT (recognising peptidoglycan). This recruitment marker binds to cytosolic bacteria (Grosz *et al.*, 2013) forming a yellow ring. Consistent with the protection and cytotoxicity assays we could observe cell damage and condensed nuclei in cells inoculated with WT and *agr* mutants (Fig. 1D). Cells containing the *sae* or *agr/sae* mutants were still viable and packed with bacteria even after 24h. Escape from the phagosome into the cytoplasm could only be observed in cells infected with WT and *sae* mutant at the 3 h time point (Fig. 1D, white arrow) indicating that Agr-regulated factors play a role in this mechanism. Similar results could be obtained with human monocyte derived macrophages (hMDMs).

## Results Part II

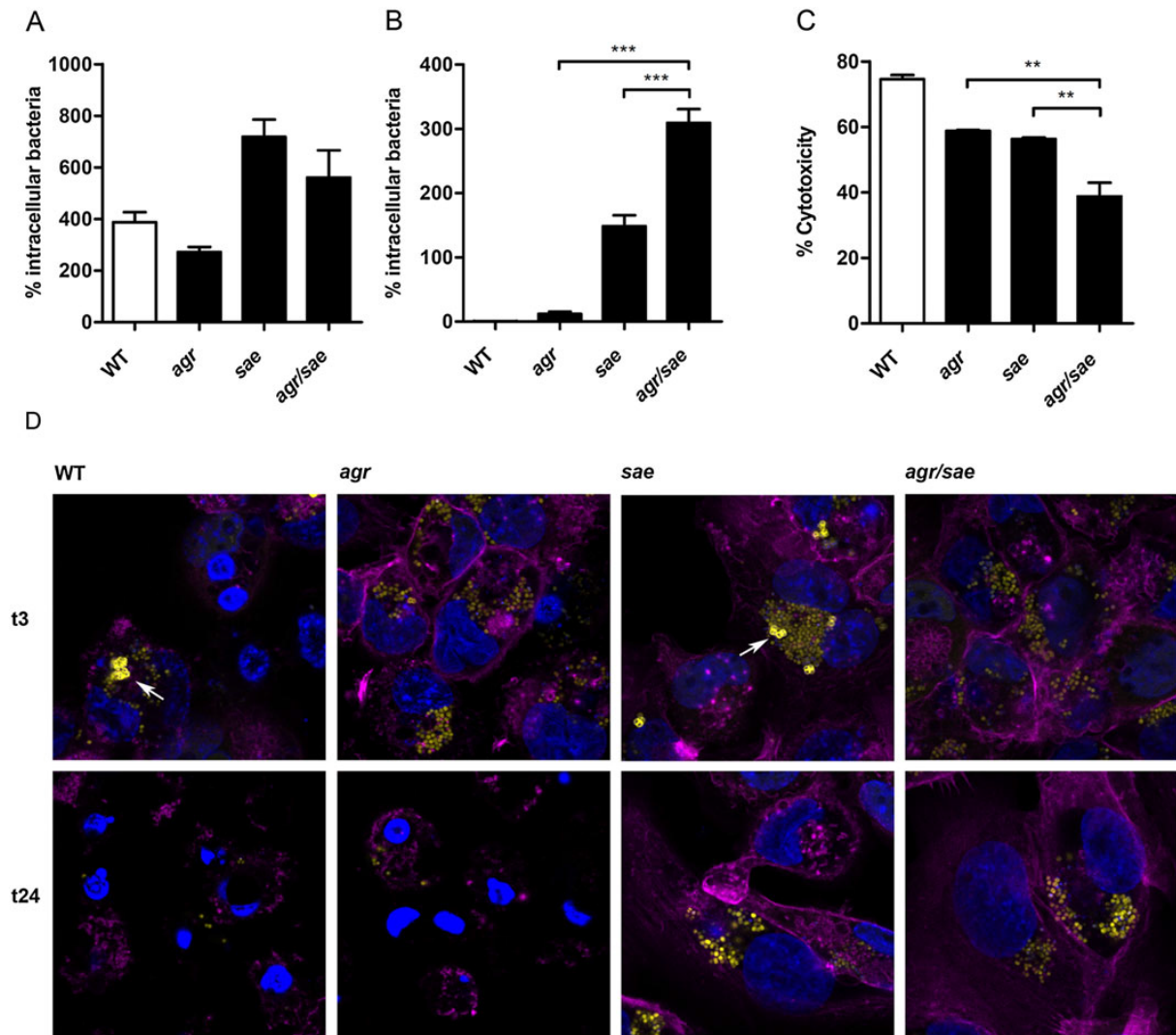


Fig. 1 from Münzenmayer *et al.* 2016

A and B. Intracellular survival (protection) assay with differentiated THP-1 macrophages and *S. aureus* strain JE2 and its isogenic *agr*, *sae* and *agr/sae* double mutants at (A) 3 h or (B) 24h. Intracellular bacteria are expressed as the ratio of cfu at t3 or t24 to cfu at t0.

C. Membrane integrity of the THP-1 cells after 24 h assessed by SYTOX green assay. Significance was determined by one-way analysis of variance with Tukey's multiple comparison post-test. The data represent the mean of three independent experiments. \*\* $P < 0.01$ ; \*\*\* $P < 0.001$ .

D. Cells were stained with phalloidin (pink: actin filaments) and DAPI (blue: DNA). Bacteria express *yfp* (faint yellow). YFP-CWT recruitment marker (yellow ring: bacterial localization in the cytosol, white arrow).

### Agr- and Sae-regulated factors are responsible for the escape of *S. aureus* from within human macrophages

We next analysed the Agr- and Sae-regulated factors, responsible for the above described effects (Fig. 2). Hla had no significant effect on the escape or cell cytotoxicity (Fig. 2A and B). However, mutants in the Sae-regulated two-component toxins PVL and LukAB and the Agr-regulated Psm $\alpha$  escaped less efficient. The effect was more pronounced when *pvl* and *lukAB* were both mutated. Additional mutation of *psma* resulted in further increase in persistence. Interestingly the *pvl/lukAB* double



## Results Part II

mutant was detectable in the cytosol after 3 h (Fig. 2C) similar to the *sae* mutant strain. The *psma* mutant did not show phagosomal escape into the cytoplasm similar to the *agr* mutant.

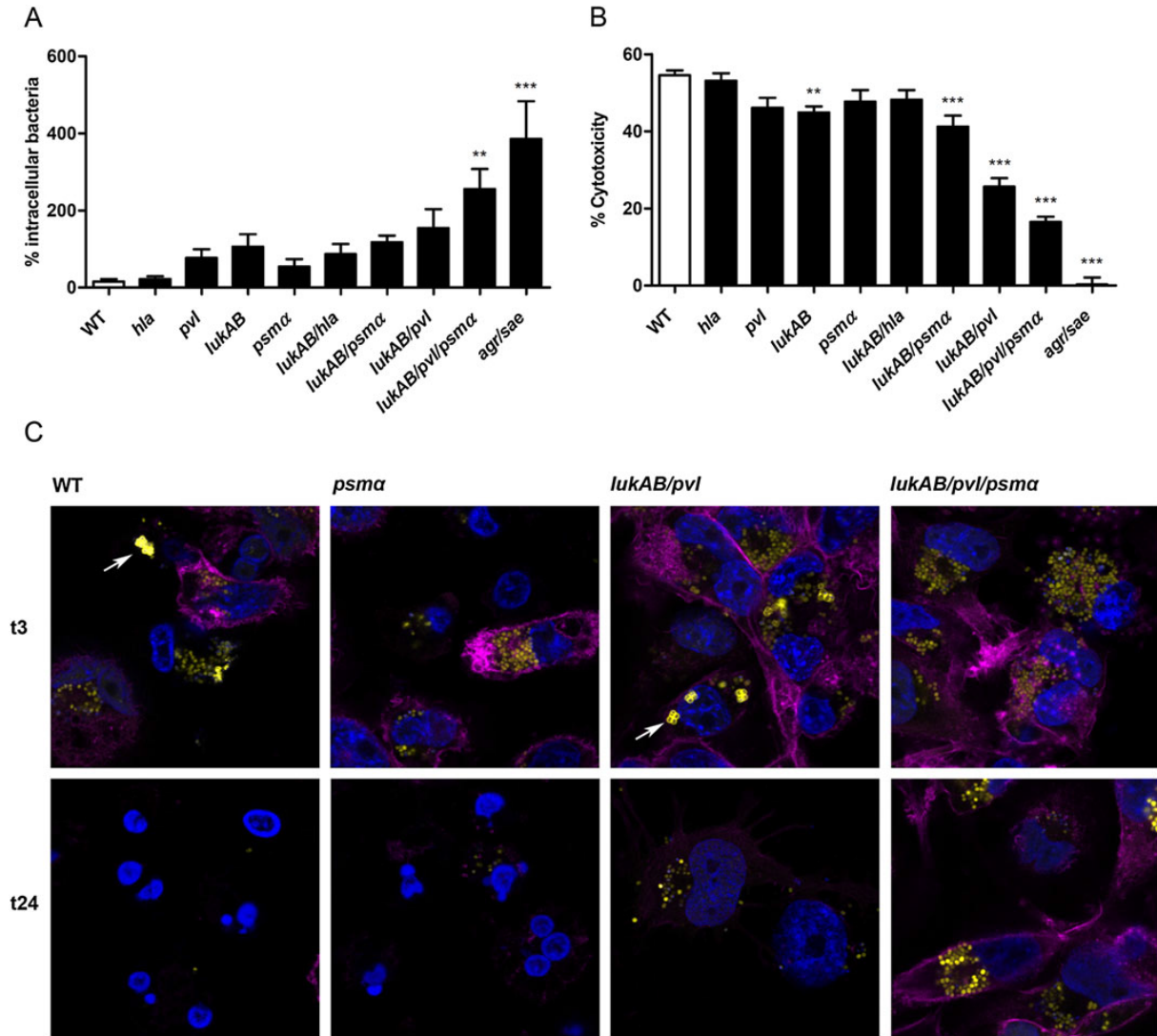


Fig. 2 from Münzenmayer *et al.* 2016

A. Intracellular survival (protection) assay with differentiated THP-1 macrophages and *S. aureus* strain JE2 and its isogenic toxin mutants. After phagocytosis and lysostaphin/gentamicin treatment, the THP-1 cells were further incubated for 24 h in RPMI medium containing gentamicin (200  $\mu$ g/ml) to kill extracellular/escaped bacteria. At indicated time points, the cells were lysed and bacterial cfu determined. Intracellular bacteria are expressed as the ratio of cfu at t24 to cfu at t0.

B. Membrane integrity of the THP-1 cells after 24 h assessed by SYTOX green assay. Significance was determined by one-way analysis of variance with Dunnett's post-test with reference to wild type. The data represent the mean of three to seven independent experiments. \*\*P < 0.01; \*\*\*P < 0.001.

C. Experiment performed as described earlier using chamber slides. Cells were stained with phalloidin (pink: actin filaments) and DAPI (blue: DNA). Bacteria express *yfp* (faint yellow). YFP-CWT recruitment marker (yellow ring: bacterial localization in the cytosol, white arrow).

## Results Part II

### Expression of *pvl*, *lukAB* and *psma* in vitro and within macrophages

To specify further the impact of the virulence regulators Agr and Sae on the expression of the relevant toxins we performed qRT-PCR of regulatory mutants grown in the inoculation medium (Fig. 3A-C). Because of the described influence of *psma* on the expression of *hla* we included a *psma* mutant in the analysis (Berube *et al.*, 2014). As expected the expression of *psma* was regulated by Agr whereas *lukAB* and *pvl* expression was predominantly regulated by Sae. In contrast to the described influence of PSMs on *hla* expression (Berube *et al.*, 2014), we could even observe an

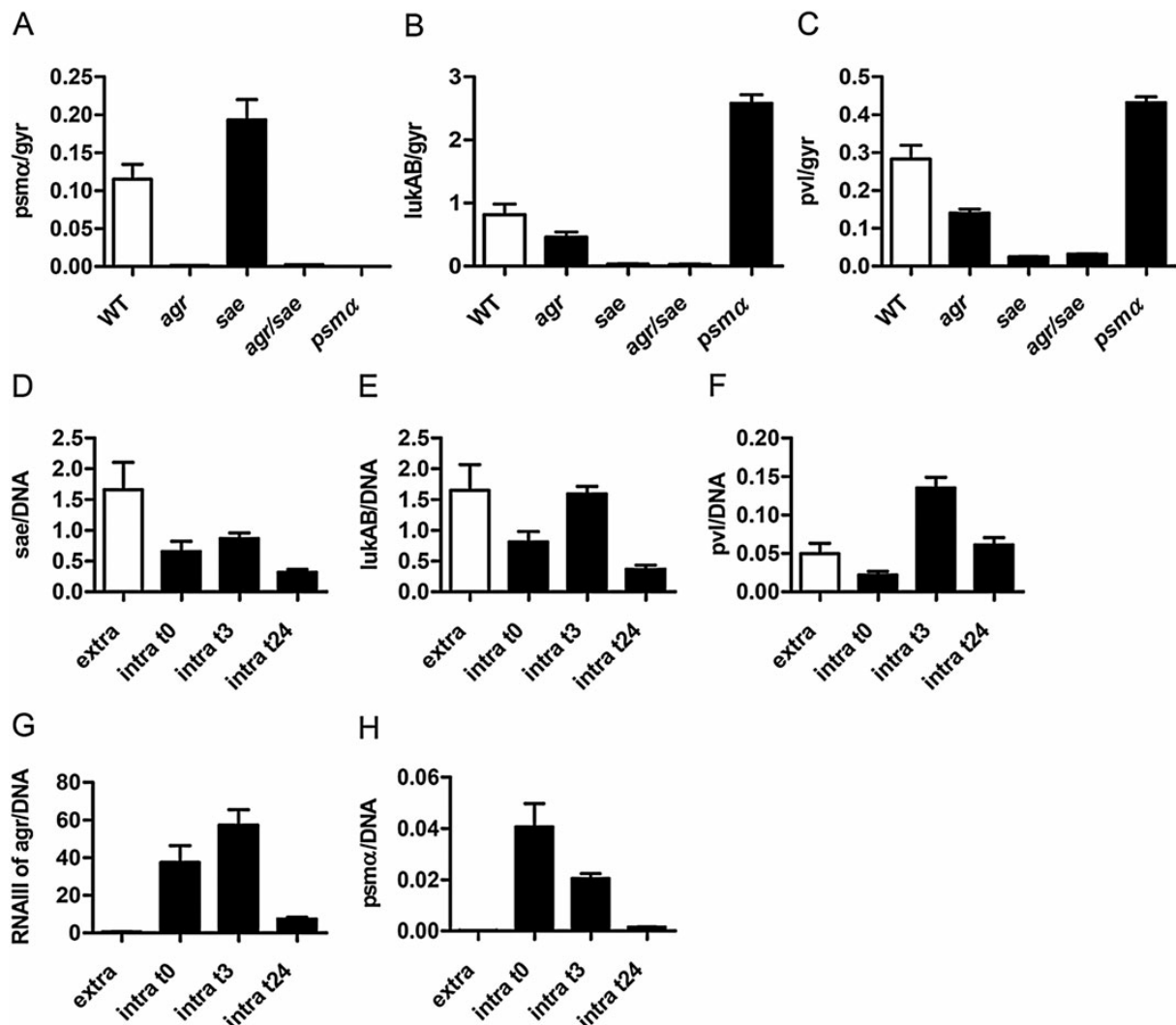


Fig. 3 from Münzenmayer *et al.* 2016

A–C. RNA from bacteria grown in inoculation medium was analysed for gene expression of *psma* (A), *lukAB* (B) and *pvl* (C) by quantitative reverse transcription PCR in relation to *gyr* expression.

D–H. RNA from intracellular bacteria were harvested at t0, t3 and t24 (intra) and from the supernatant (extra) 1 h after inoculation and gene expression of *sae* (D), *lukAB* (E), *pvl* (F), *RNAIII* of *agr* (G) and *psma* $\alpha$  (H) analysed by qRT-PCR. Gene expression is shown in relation to quantified *lukAB* DNA.

Results are presented as the mean of three independent experiments.

## Results Part II

increase in the *lukAB* and *pvl* expression in the *psma* mutant. As already described in the first part of the results, the Sae system of some *S. aureus* strain is known to be activated in response to phagocytosis-related signals (Geiger *et al.*, 2008). Although macrophages do not produce human neutrophil peptides, we aimed to analyse if the expression of Sae and Agr and their corresponding target genes changes after phagocytosis (Fig. 3 D-H). The *sae* activity only slightly changed after phagocytosis and no activation was observed as it was published for neutrophils (Voyich *et al.*, 2008). RNAIII of the *agr* operon and *psma* were highly induced after phagocytosis. Irrespective of that, the expression of all genes decreased 24h after infection, which might be due to host cell damage.

### Role of apoptosis and NLRP3 inflammasome activation on damage of macrophages after phagocytosis

The pore-forming toxins LukAB and PVL led to severe damage of macrophages with condensed nuclei. To analyse whether the toxins may lead to induction of apoptosis we measured caspase 3, 7 and 8 activities in cells harbouring the wild type and mutant bacteria. Uptake of *S. aureus* did not result in significant changes in caspase activity (Fig. 4 A, B) at t3 irrespective of which strain was inoculated. Next we analysed whether intracellular expression of *lukAB* and *pvl* might result in activation of the NLRP3 inflammasome resulting in pyroptosis. MCC950 was shown to block NLRP3-ASC assembly at nanomolar concentrations (Coll *et al.*, 2015).

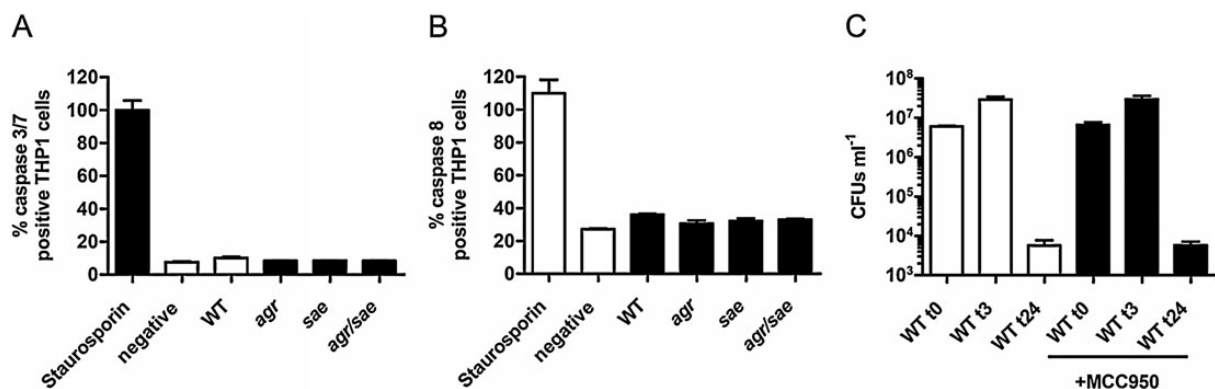


Fig. 4 from Münzenmayer *et al.* 2016

A and B. Activity of caspase 3/7 (A) and caspase 8 (B) was determined at t3. Staurosporine was used as a positive control (100%). Infection was performed as described in Fig. 1.

C. Intracellular survival (protection) assay with differentiated THP-1 macrophages and *S. aureus* strain JE2 with and without MCC950. After phagocytosis and lysostaphin/gentamicin treatment, the THP-1 cells were further incubated for 3 and 24 h in RPMI medium containing gentamicin (200 µg/ml) to kill extracellular/escaped bacteria. At indicated time points, the cells were lysed and bacterial cfu determined.

## Results Part II

Treatment of THP-1 cells with MCC950 did not protect cells from bacterial induced damage and bacteria were not hampered in their escape efficiency (Fig. 4C). Thus, NLRP3 activation by intracellular expressed toxins is not a major pathway leading to the observed escape phenotype of wild type bacteria.

### PSMs are the major factors in non-professional phagocytes

We wondered if the sea-regulated factors also contribute to the escape from epithelial cells. As expected, mutation of *sae* or its target gene *lukAB* had no significant effect in the human epithelial cell line HeLa, because of the missing toxin receptor. We confirmed that the CD11b receptor integrin is not expressed on HeLa cells (Fig. 5B) (Ho & Springer, 1982, Giese *et al.*, 2011, DuMont *et al.*, 2013). In contrast to professional phagocytes, in epithelial cells the Agr-regulated PSMa

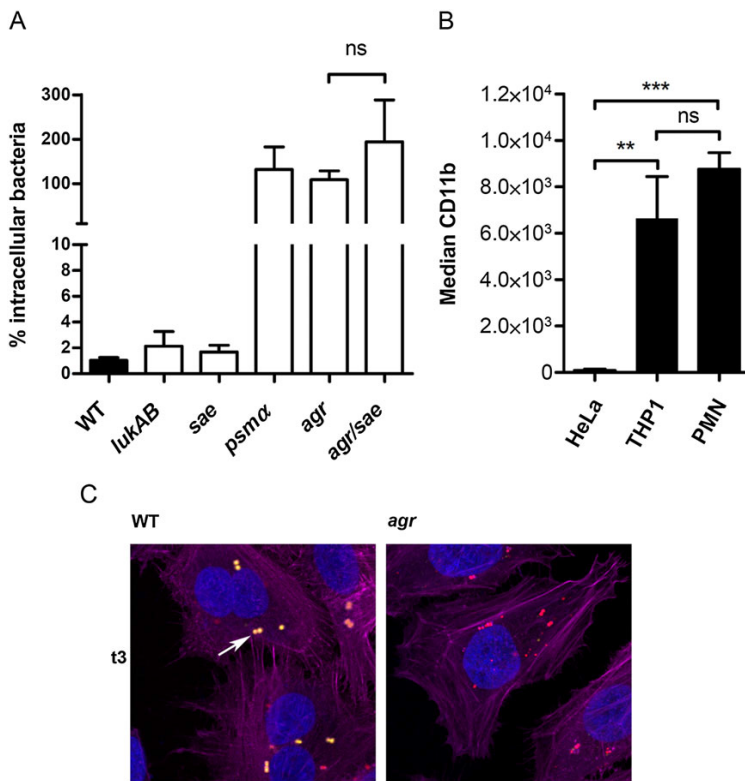


Fig. 5 from Münzenmayer *et al.* 2016

A. Intracellular survival (protection) assay with HeLa epithelial cells and *S. aureus* strain JE and its isogenic *lukAB*, *sae*, *psmA*, *agr* and *agr/sae* double mutants. After phagocytosis and lysostaphin/gentamicin treatment, the HeLa cells were incubated 24 h in RPMI medium containing 200 µg/ml gentamicin to kill extracellular/escaped bacteria. Data represent mean of three independent experiments. Significances were determined by one-way analysis of variance with Tukey's multiple comparison post-test. ns, not significant.

B. Median of CD11b expression on HeLa cells, THP-1 macrophages and neutrophils. Cells were stained with anti-CD11b for 20 min. \*\*P < 0.01, \*\*\*P < 0.001, ns, not significant.

C. Cells were stained with phalloidin (pink: actin filaments) and DAPI (blue: DNA). Bacteria were stained with TritC (red: bacteria in phagosome); YFP-Fc recruitment marker (yellow: bacterial localization in the cytosol, white arrow).

## Results Part II

---

peptides are mainly responsible for escape. The HeLa cells contain the escape marker YFP-F<sub>C</sub>, which recognizes cytosolic bacteria. Wild type bacteria were detectable in the cytosol indicated by YFP-staining (Fig. 5C). However, the *agr* mutant remained YFP-negative indicating that Agr regulated factors are required to escape from the phagosome into the cytosol. Thus, mutation of *agr* is sufficient to abrogate the escape phenotype in HeLa cells, which is in contrast to the results obtained after macrophage phagocytosis, where Sae-regulated factors are essential for escape.

### Discussion

Phagocytic cells are on the one hand important to capture circulating *S. aureus* (Zeng *et al.*, 2016), thereby preventing spread of bacteria, but might be also exploited as “Trojan horses” for dissemination in the human body (Lehar *et al.*, 2015). This shows, that understanding bacterial interaction with macrophages and especially the regulation of virulence factors and their contribution to the escape from within is of high interest concerning spread of the bacteria and possible disease outcome.

In this thesis, I show that the important virulence regulator Sae of *S. aureus* is not only activated by HNP1-3 but also by another phagocytosis related signal, namely sodium hypochlorite. This emphasises the importance of Sae in the interaction with phagocytic cells. Nevertheless, the mechanism of activation by both factors seems to be distinct, as only HNP1-3 sensing is restricted to specific strains. Furthermore, I could identify D-alanylation of WTA as an important factor in the HNP1-3 dependent activation of the histidine kinase SaeS. Mutants in either the *dltABCD* operon or the *tagO* gene, did not show upregulation of the auto regulated *saePQRS* operon or its target gene *eap*. The HNP1-3 induced upregulation of *eap* was highly dependent on SaeS phosphorylation, since I could also observe it in a strain were I deleted the auto regulated P1 Promotor, *saeP* and *saeQ*. Hereby I also exclude that transcriptional regulation or the auxiliary proteins SaeP and SaeQ play a role in sensing of HNP1-3. The WTA is located in the peptidoglycan and thus has no physical contact to SaeS. Therefore, I think that D-alanylation of WTA enables HNP1-3 to access its interaction partner, which might be either SaeS or another factor with closer contact to SaeS. It is suggested that intramembrane-sensing histidine kinases do not directly interact with their cognate signals, instead the signals interact with a another factor displaying the “true sensor” (Mascher, 2014). For SaeS it was suggested that the interaction with this sensor might then change the overall conformation of its N-terminal domain thereby transducing the signal (Liu *et al.*, 2015). D-alanylation of WTA might enable the interaction of HNP1-3 with its “true sensor”. One may think, that in general changes in the cell envelope charge might influence SaeS activity or that sensing of HNP1-3 is dependent on the cell envelope charge. In my opinion, HNP1-3 dependent activation of SaeS is a rather specific mechanism, due to different reasons. First,

## Discussion

---

deletion of *mprF* had no effect on the HNP1-3 dependent activation of SaeS, although influencing membrane charge. Second, a charge dependent mechanism might also enable other cationic antimicrobial peptides to activate SaeS. To get an idea about the strain specificity of the HNP1-3 sensing I next wanted to figure out if there are strain differences in the *dlt* operon sequence or its expression which might explain strain specificity. Indeed, I found one amino acid difference in the *dltD* gene of USA300 compared to HG001. Exchanging this substitution between the two strain by mutagenesis did not influence the responsiveness of both strains. Thereby, *dlt* operon sequence is not the reason for the strain specific sensing of HNP1-3. Comparing the expression of the *dlt* operon of two responder and two non-responder strains was also not informative concerning the strain specificity. I hypothesise that, the level of D-alanylation in the strains is distinct and might be not only dependent on the expression of the *dlt* operon itself but also on the amount of WTA or on post transcriptional events. In my view, one might not be able to mimic the complex composition of the cell envelope to render a non-responder strain responsive.

The Sae system was previously shown to be involved in neutrophil lysis. Here I analysed the role of virulence regulatory systems, especially the Sae system in the interaction with human macrophages after phagocytosis. I show that in human macrophages the Agr-regulated pore-forming toxin PSM $\alpha$  mediates escape of *S. aureus* from the phagosome into the cytoplasm. For the induction of cell death and subsequent escape of the bacteria from within the cells the Sae-regulated toxins LukAB and PVL are the major factors. Taken together it seems that different virulence factors act in concert to mediate the escape of *S. aureus* from within human macrophages. PSMs are small cytolytic peptides with  $\alpha$ -helical structure (Peschel & Otto, 2013). They are receptor independent thereby acting irrespective of the host cell type. We show that PSMs mediate the escape from the phagosome into the cytoplasm but are not required to induce cell damage. The Sae-regulated leukotoxins LukAB and PVL are dependent on their respective receptors, CD11b and the complement receptors (C5aR, C5L2) (DuMont *et al.*, 2013, Dumont & Torres, 2014). We show that CD11b expression level is comparable in neutrophils and macrophages. Different studies describe receptor dependent inflammasome activation and pyroptotic cell death induced by extracellular applied LukAB or PVL toxin (Holzinger *et al.*, 2012, Melehani *et al.*, 2015). This is probably dependent on

## Discussion

---

potassium efflux mediated by the pore forming capacity of the toxins. It was shown that the CD11b receptor is also located on the inside of the phagosomal membrane (DuMont *et al.*, 2013), which can be explained by the invagination of the cytoplasmic membrane. However, it is not clear how interaction of the toxins with the intracellular receptor mediates host cell damage. We observed cell damage and condensed nuclei in cells infected with WT or *agr* mutant bacteria. We hypothesized that this is due to programmed cell death pathways activated by LukAB and PVL toxins. Therefore, we tested activation of the apoptosis-related caspases 3, 7 and 8 and inhibited NLRP3 inflammasome action by the known inhibitor MCC950. In line with other data (Jubrail *et al.*, 2015, Melehani *et al.*, 2015), we could show that LukAB/PVL mediated cell death was not linked to these pathways. It is possible that the mechanisms leading to cell damage present a complex network, in which inhibition of one pathway might be compensated by redundant pathways. One could also consider alternative mechanisms leading to cell damage but this has to be elucidated. Furthermore, I investigated the intracellular expression of virulence factors. As described above, the Sae regulatory system is activated by phagocytosis related signals, like HNP1-3 (Geiger *et al.*, 2008). However, macrophages do not produce HNP1-3 (Agerberth *et al.*, 2000), thus we do not see Sae activation. I confirmed regulation of the two component toxins *lukAB* and *pvl* by the Sae system (Voyich *et al.*, 2005, Wirtz *et al.*, 2009, Mainiero *et al.*, 2010), and their expression was sufficient for the observed phenotype. PSMs were previously shown to enhance the expression of *hla* (Berube *et al.*, 2014). I could even observe the adverse effect of PSMs on the expression of *lukAB* and *pvl*. On the one hand this emphasizes the role of PSMs on the regulation of other toxins, but also shows, that the observed phenotype of the *psm* mutant was not due to downregulation of *lukAB* or *pvl*. In contrast to Sae, Agr was previously found not to be upregulated inside neutrophils (Voyich *et al.*, 2005, Geiger *et al.*, 2012). I found strong upregulation of Agr after uptake by human macrophages and the essentiality of Agr in the expression of *psma* (Queck *et al.*, 2008) could be confirmed. Signals for intracellular Agr activation are less clear. Previous studies showed upregulation of Agr after uptake of *S. aureus* in macrophages or non-professional phagocytes. In this studies, diffusion sensing (Shompole *et al.*, 2003) or acidification (Tranchemontagne *et al.*, 2015) were discussed as reason for Agr activation.



## Discussion

---

TCS are important for adaptation, resistance and virulence, therefore understanding their activation is of high interest. I could show that the D-alanylation of the WTA influences the HNP1-3 dependent activation of the sensor kinase SaeS. The involvement of WTA in a TCS sensing mechanism was never described before (see manuscript Bleul *et al.*), and therefore might be unique. *S. aureus* can exploit professional phagocytes on the one hand as a protective niche and on the other hand to spread among different sites in the human body. Therefore, the intracellular lifestyle of *S. aureus* is currently in the focus of research. I could show that Agr- and Sae-regulated factors act in concert to enable escape of *S. aureus* from within human macrophages. Altogether, this thesis contributes to our knowledge about post-phagocytosis events in the interaction of *S. aureus* with professional phagocytes.

### References

- Abriata LA, Albanesi D, Dal Peraro M & de Mendoza D (2017) Signal Sensing and Transduction by Histidine Kinases as Unveiled through Studies on a Temperature Sensor. *50*: 1359-1366.
- Adhikari RP & Novick RP (2008) Regulatory organization of the staphylococcal *sae* locus. *Microbiology* **154**: 949-959.
- Agerberth B, Charo J, Werr J, Olsson B, Idali F, Lindbom L, Kiessling R, Jornvall H, Wigzell H & Gudmundsson GH (2000) The human antimicrobial and chemotactic peptides LL-37 and alpha-defensins are expressed by specific lymphocyte and monocyte populations. *Blood* **96**: 3086-3093.
- Ballal A, Basu B & Apte SK (2007) The Kdp-ATPase system and its regulation. *J Biosci* **32**: 559-568.
- Belcheva A & Golemi-Kotra D (2008) A close-up view of the VraSR two-component system. A mediator of *Staphylococcus aureus* response to cell wall damage. *J Biol Chem* **283**: 12354-12364.
- Berube BJ, Sampedro GR, Otto M & Bubeck-Wardenburg J (2014) The *psm*alpha locus regulates production of *Staphylococcus aureus* alpha-toxin during infection. *Infect Immun* **82**: 3350-3358.
- Blake KL, Randall CP & O'Neill AJ (2011) In vitro studies indicate a high resistance potential for the lantibiotic nisin in *Staphylococcus aureus* and define a genetic basis for nisin resistance. *Antimicrob Agents Chemother* **55**: 2362-2368.
- Boyle-Vavra S, Yin S, Jo DS, Montgomery CP & Daum RS (2013) VraT/YvqF is required for methicillin resistance and activation of the VraSR regulon in *Staphylococcus aureus*. *Antimicrob Agents Chemother* **57**: 83-95.
- Bronner S, Monteil H & Prevost G (2004) Regulation of virulence determinants in *Staphylococcus aureus*: complexity and applications. *FEMS Microbiol Rev* **28**: 183-200.
- Brunskill EW & Bayles KW (1996) Identification and molecular characterization of a putative regulatory locus that affects autolysis in *Staphylococcus aureus*. *J Bacteriol* **178**: 611-618.
- Brunskill EW & Bayles KW (1996) Identification of LytSR-regulated genes from *Staphylococcus aureus*. *J Bacteriol* **178**: 5810-5812.
- Burgui S, Gil C, Solano C, Lasa I & Valle J (2018) A Systematic Evaluation of the Two-Component Systems Network Reveals That ArlRS Is a Key Regulator of Catheter Colonization by *Staphylococcus aureus*. *Front Microbiol* **9**: 342.
- Cheung AL, Bayer AS, Yeaman MR, Xiong YQ, Waring AJ, Memmi G, Donegan N, Chaili S & Yang SJ (2014) Site-specific mutation of the sensor kinase GraS in *Staphylococcus aureus*

## References

---

alters the adaptive response to distinct cationic antimicrobial peptides. *Infect Immun* **82**: 5336-5345.

Coll RC, Robertson AA, Chae JJ, *et al.* (2015) A small-molecule inhibitor of the NLRP3 inflammasome for the treatment of inflammatory diseases. *Cell* **161**: 248-255.

Delaune A, Dubrac S, Blanchet C, *et al.* (2012) The WalKR system controls major staphylococcal virulence genes and is involved in triggering the host inflammatory response. *Infect Immun* **80**: 3438-3453.

Devine KM (2018) Activation of the PhoPR-Mediated Response to Phosphate Limitation Is Regulated by Wall Teichoic Acid Metabolism in *Bacillus subtilis*. *Front Microbiol* **9**: 2678.

Dubrac S & Msadek T (2004) Identification of genes controlled by the essential YycG/YycF two-component system of *Staphylococcus aureus*. *J Bacteriol* **186**: 1175-1181.

Dubrac S, Boneca IG, Poupel O & Msadek T (2007) New insights into the WalK/WalR (YycG/YycF) essential signal transduction pathway reveal a major role in controlling cell wall metabolism and biofilm formation in *Staphylococcus aureus*. *Journal of bacteriology* **189**: 8257-8269.

Dubrac S, Bisicchia P, Devine KM & Msadek T (2008) A matter of life and death: cell wall homeostasis and the WalKR (YycGF) essential signal transduction pathway. *Mol Microbiol* **70**: 1307-1322.

Dumont AL & Torres VJ (2014) Cell targeting by the *Staphylococcus aureus* pore-forming toxins: it's not just about lipids. *Trends Microbiol* **22**: 21-27.

DuMont AL, Yoong P, Day CJ, Alonzo F, 3rd, McDonald WH, Jennings MP & Torres VJ (2013) *Staphylococcus aureus* LukAB cytotoxin kills human neutrophils by targeting the CD11b subunit of the integrin Mac-1. *Proc Natl Acad Sci U S A* **110**: 10794-10799.

DuMont AL, Yoong P, Surewaard BG, Benson MA, Nijland R, van Strijp JA & Torres VJ (2013) *Staphylococcus aureus* elaborates leukocidin AB to mediate escape from within human neutrophils. *Infect Immun* **81**: 1830-1841.

Fabret C & Hoch JA (1998) A two-component signal transduction system essential for growth of *Bacillus subtilis*: implications for anti-infective therapy. *J Bacteriol* **180**: 6375-6383.

Falord M, Karimova G, Hiron A & Msadek T (2012) GraXSR proteins interact with the VraFG ABC transporter to form a five-component system required for cationic antimicrobial peptide sensing and resistance in *Staphylococcus aureus*. *Antimicrob Agents Chemother* **56**: 1047-1058.

Falord M, Mader U, Hiron A, Debarbouille M & Msadek T (2011) Investigation of the *Staphylococcus aureus* GraSR regulon reveals novel links to virulence, stress response and cell wall signal transduction pathways. *PLoS One* **6**: e21323.

Feuerstein R, Kolter J & Henneke P (2017) Dynamic interactions between dermal macrophages and *Staphylococcus aureus*. *J Leukoc Biol* **101**: 99-106.

## References

---

- Flannagan RS, Heit B & Heinrichs DE (2015) Intracellular replication of *Staphylococcus aureus* in mature phagolysosomes in macrophages precedes host cell death, and bacterial escape and dissemination. *Cell Microbiol.*
- Flannagan RS, Kuiack RC, McGavin MJ & Heinrichs DE (2018) *Staphylococcus aureus* Uses the GraXRS Regulatory System To Sense and Adapt to the Acidified Phagolysosome in Macrophages. **9**.
- Fournier B & Hooper DC (2000) A new two-component regulatory system involved in adhesion, autolysis, and extracellular proteolytic activity of *Staphylococcus aureus*. *J Bacteriol* **182**: 3955-3964.
- Fournier B & Klier A (2004) Protein A gene expression is regulated by DNA supercoiling which is modified by the ArlS-ArlR two-component system of *Staphylococcus aureus*. *Microbiology* **150**: 3807-3819.
- Fournier B, Klier A & Rapoport G (2001) The two-component system ArlS-ArlR is a regulator of virulence gene expression in *Staphylococcus aureus*. *Mol Microbiol* **41**: 247-261.
- Gardete S, Wu SW, Gill S & Tomasz A (2006) Role of VraSR in antibiotic resistance and antibiotic-induced stress response in *Staphylococcus aureus*. *Antimicrob Agents Chemother* **50**: 3424-3434.
- Gardner SG, Johns KD, Tanner R & McCleary WR (2014) The PhoU protein from *Escherichia coli* interacts with PhoR, PstB, and metals to form a phosphate-signaling complex at the membrane. *J Bacteriol* **196**: 1741-1752.
- Geiger T, Goerke C, Mainiero M, Kraus D & Wolz C (2008) The virulence regulator Sae of *Staphylococcus aureus*: promoter activities and response to phagocytosis-related signals. *J Bacteriol* **190**: 3419-3428.
- Giese B, Glowinski F, Paprotka K, Dittmann S, Steiner T, Sinha B & Fraunholz MJ (2011) Expression of delta-toxin by *Staphylococcus aureus* mediates escape from phago-endosomes of human epithelial and endothelial cells in the presence of beta-toxin. *Cell Microbiol* **13**: 316-329.
- Giraud AT, Raspanti CG, Calzolari A & Nagel R (1994) Characterization of a Tn551-mutant of *Staphylococcus aureus* defective in the production of several exoproteins. *Can J Microbiol* **40**: 677-681.
- Gonzalez-Juarbe N, Gilley RP, Hinojosa CA, Bradley KM, Kamei A, Gao G, Dube PH, Bergman MA & Orihuela CJ (2015) Pore-Forming Toxins Induce Macrophage Necroptosis during Acute Bacterial Pneumonia. *PLoS Pathog* **11**: e1005337.
- Green GM & Kass EH (1964) THE ROLE OF THE ALVEOLAR MACROPHAGE IN THE CLEARANCE OF BACTERIA FROM THE LUNG. *J Exp Med* **119**: 167-176.
- Grosz M, Kolter J, Paprotka K, *et al.* (2013) Cytoplasmic replication of *Staphylococcus aureus* upon phagosomal escape triggered by phenol-soluble modulins. *Cell Microbiol* **DOI: 10.1111/cmi.12233**.

## References

---

- Grosz M, Kolter J, Paprotka K, *et al.* (2014) Cytoplasmic replication of *Staphylococcus aureus* upon phagosomal escape triggered by phenol-soluble modulins. *Cell Microbiol* **16**: 451-465.
- Grundling A (2013) Potassium uptake systems in *Staphylococcus aureus*: new stories about ancient systems. *mBio* **4**: e00784-00713.
- Hall JW, Yang J, Guo H & Ji Y (2015) The AirSR two-component system contributes to *Staphylococcus aureus* survival in human blood and transcriptionally regulates *sspABC* operon. *Front Microbiol* **6**: 682.
- Hardt P, Engels I, Rausch M, *et al.* (2017) The cell wall precursor lipid II acts as a molecular signal for the Ser/Thr kinase PknB of *Staphylococcus aureus*. *Int J Med Microbiol* **307**: 1-10.
- Henry JT & Crosson S (2011) Ligand-binding PAS domains in a genomic, cellular, and structural context. *Annu Rev Microbiol* **65**: 261-286.
- Hiron A, Falord M, Valle J, Debarbouille M & Msadek T (2011) Bacitracin and nisin resistance in *Staphylococcus aureus*: a novel pathway involving the BraS/BraR two-component system (SA2417/SA2418) and both the BraD/BraE and VraD/VraE ABC transporters. *Mol Microbiol* **81**: 602-622.
- Ho MK & Springer TA (1982) Mac-1 antigen: quantitative expression in macrophage populations and tissues, and immunofluorescent localization in spleen. *J Immunol* **128**: 2281-2286.
- Holzinger D, Geldon L, Mysore V, *et al.* (2012) *Staphylococcus aureus* Panton-Valentine leukocidin induces an inflammatory response in human phagocytes via the NLRP3 inflammasome. *J Leukoc Biol* **92**: 1069-1081.
- Ji G, Beavis RC & Novick RP (1995) Cell density control of staphylococcal virulence mediated by an octapeptide pheromone. *Proc Natl Acad Sci U S A* **92**: 12055-12059.
- Jubrail J, Morris P, Bewley MA, Stoneham S, Johnston SA, Foster SJ, Peden AA, Read RC, Marriott HM & Dockrell DH (2015) Inability to sustain intraphagolysosomal killing of *Staphylococcus aureus* predisposes to bacterial persistence in macrophages. *Cell Microbiol*.
- Kamps A, Achebach S, Fedtke I, Uden G & Gotz F (2004) Staphylococcal NreB: an O(2)-sensing histidine protein kinase with an O(2)-labile iron-sulphur cluster of the FNR type. *Mol Microbiol* **52**: 713-723.
- Kavanaugh JS & Horswill AR (2016) Impact of Environmental Cues on Staphylococcal Quorum Sensing and Biofilm Development. *J Biol Chem* **291**: 12556-12564.
- Kelliher JL, Radin JN & Kehl-Fie TE (2018) PhoPR Contributes to *Staphylococcus aureus* Growth during Phosphate Starvation and Pathogenesis in an Environment-Specific Manner. *Infect Immun* **86**.
- Kim T, Choi J, Lee S, Yeo KJ, Cheong HK & Kim KK (2016) Structural Studies on the Extracellular Domain of Sensor Histidine Kinase YycG from *Staphylococcus aureus* and Its Functional Implications. *J Mol Biol* **428**: 3074-3089.

## References

---

- Kinkel TL, Roux CM, Dunman PM & Fang FC (2013) The *Staphylococcus aureus* SrrAB two-component system promotes resistance to nitrosative stress and hypoxia. *MBio* **4**: e00696-00613.
- Kitur K, Parker D, Nieto P, Ahn DS, Cohen TS, Chung S, Wachtel S, Bueno S & Prince A (2015) Toxin-induced necroptosis is a major mechanism of *Staphylococcus aureus* lung damage. *PLoS Pathog* **11**: e1004820.
- Kolar SL, Nagarajan V, Oszmiana A, *et al.* (2011) NsaRS is a cell-envelope-stress-sensing two-component system of *Staphylococcus aureus*. *Microbiology* **157**: 2206-2219.
- Krismer B, Weidenmaier C, Zipperer A & Peschel A (2017) The commensal lifestyle of *Staphylococcus aureus* and its interactions with the nasal microbiota. *Nat Rev Microbiol* **15**: 675-687.
- Kubica M, Guzik K, Koziel J, *et al.* (2008) A potential new pathway for *Staphylococcus aureus* dissemination: the silent survival of *S. aureus* phagocytosed by human monocyte-derived macrophages. *PLoS One* **3**: e1409.
- Kuroda M, Kuroda H, Oshima T, Takeuchi F, Mori H & Hiramatsu K (2003) Two-component system VraSR positively modulates the regulation of cell-wall biosynthesis pathway in *Staphylococcus aureus*. *Mol Microbiol* **49**: 807-821.
- Kuroda M, Ohta T, Uchiyama I, *et al.* (2001) Whole genome sequencing of methicillin-resistant *Staphylococcus aureus*. *Lancet* **357**: 1225-1240.
- Lehar SM, Pillow T, Xu M, *et al.* (2015) Novel antibody-antibiotic conjugate eliminates intracellular *S. aureus*. *Nature* **527**: 323-328.
- Li M, Lai Y, Villaruz AE, Cha DJ, Sturdevant DE & Otto M (2007) Gram-positive three-component antimicrobial peptide-sensing system. *Proc Natl Acad Sci U S A* **104**: 9469-9474.
- Li M, Cha DJ, Lai Y, Villaruz AE, Sturdevant DE & Otto M (2007) The antimicrobial peptide-sensing system *aps* of *Staphylococcus aureus*. *Mol Microbiol* **66**: 1136-1147.
- Li S, Huang H, Rao X, Chen W, Wang Z & Hu X (2014) Phenol-soluble modulins: novel virulence-associated peptides of staphylococci. *Future microbiology* **9**: 203-216.
- Liang X, Zheng L, Landwehr C, Lunsford D, Holmes D & Ji Y (2005) Global regulation of gene expression by ArlRS, a two-component signal transduction regulatory system of *Staphylococcus aureus*. *J Bacteriol* **187**: 5486-5492.
- Lina G, Jarraud S, Ji G, Greenland T, Pedraza A, Etienne J, Novick RP & Vandenesch F (1998) Transmembrane topology and histidine protein kinase activity of AgrC, the agr signal receptor in *Staphylococcus aureus*. *Mol Microbiol* **28**: 655-662.
- Liu Q, Cho H, Yeo WS & Bae T (2015) The extracytoplasmic linker peptide of the sensor protein SaeS tunes the kinase activity required for staphylococcal virulence in response to host signals. *PLoS Pathog* **11**: e1004799.
- Loffler B, Hussain M, Grundmeier M, Bruck M, Holzinger D, Varga G, Roth J, Kahl BC, Proctor RA & Peters G (2010) *Staphylococcus aureus* panton-valentine leukocidin is a very potent cytotoxic factor for human neutrophils. *PLoS Pathog* **6**: e1000715.

## References

---

- Loi VV, Busche T, Tedin K, *et al.* (2018) Redox-Sensing Under Hypochlorite Stress and Infection Conditions by the Rrf2-Family Repressor HypR in *Staphylococcus aureus*. *Antioxid Redox Signal* **29**: 615-636.
- Lowy FD (1998) *Staphylococcus aureus* infections. *N Engl J Med* **339**: 520-532.
- Luong TT & Lee CY (2006) The *arl* locus positively regulates *Staphylococcus aureus* type 5 capsule via an *mgrA*-dependent pathway. *Microbiology* **152**: 3123-3131.
- Lyon GJ, Mayville P, Muir TW & Novick RP (2000) Rational design of a global inhibitor of the virulence response in *Staphylococcus aureus*, based in part on localization of the site of inhibition to the receptor-histidine kinase, AgrC. *Proc Natl Acad Sci U S A* **97**: 13330-13335.
- Mainiero M, Goerke C, Geiger T, Gonser C, Herbert S & Wolz C (2010) Differential target gene activation by the *Staphylococcus aureus* two-component system *saeRS*. *J Bacteriol* **192**: 613-623.
- Malachowa N, Kobayashi SD, Braughton KR, Whitney AR, Parnell MJ, Gardner DJ & Deleo FR (2012) *Staphylococcus aureus* leukotoxin GH promotes inflammation. *J Infect Dis* **206**: 1185-1193.
- Mariathasan S, Weiss DS, Newton K, McBride J, O'Rourke K, Roose-Girma M, Lee WP, Weinrauch Y, Monack DM & Dixit VM (2006) Cryopyrin activates the inflammasome in response to toxins and ATP. *Nature* **440**: 228-232.
- Martinez I, Oliveros JC, Cuesta I, *et al.* (2017) Apoptosis, Toll-like, RIG-I-like and NOD-like Receptors Are Pathways Jointly Induced by Diverse Respiratory Bacterial and Viral Pathogens. *Front Microbiol* **8**: 276.
- Mascher T (2006) Intramembrane-sensing histidine kinases: a new family of cell envelope stress sensors in Firmicutes bacteria. *FEMS Microbiol Lett* **264**: 133-144.
- Mascher T (2014) Bacterial (intramembrane-sensing) histidine kinases: signal transfer rather than stimulus perception. *Trends Microbiol* **22**: 559-565.
- Mascher T, Helmann JD & Udden G (2006) Stimulus perception in bacterial signal-transducing histidine kinases. *Microbiol Mol Biol Rev* **70**: 910-938.
- Mashruwala AA & Guchte AV (2017) Impaired respiration elicits SrrAB-dependent programmed cell lysis and biofilm formation in *Staphylococcus aureus*. **6**.
- Meehl M, Herbert S, Gotz F & Cheung A (2007) Interaction of the GraRS two-component system with the VraFG ABC transporter to support vancomycin-intermediate resistance in *Staphylococcus aureus*. *Antimicrob Agents Chemother* **51**: 2679-2689.
- Melehani JH, James DB, DuMont AL, Torres VJ & Duncan JA (2015) *Staphylococcus aureus* Leukocidin A/B (LukAB) Kills Human Monocytes via Host NLRP3 and ASC when Extracellular, but Not Intracellular. *PLoS Pathog* **11**: e1004970.
- Moscoso JA, Schramke H & Zhang Y (2016) Binding of Cyclic Di-AMP to the *Staphylococcus aureus* Sensor Kinase KdpD Occurs via the Universal Stress Protein Domain and Downregulates the Expression of the Kdp Potassium Transporter. **198**: 98-110.

## References

---

- Muthaiyan A, Silverman JA, Jayaswal RK & Wilkinson BJ (2008) Transcriptional profiling reveals that daptomycin induces the *Staphylococcus aureus* cell wall stress stimulon and genes responsive to membrane depolarization. *Antimicrob Agents Chemother* **52**: 980-990.
- Nagel A, Michalik S, Debarbouille M, *et al.* (2018) Inhibition of Rho Activity Increases Expression of SaeRS-Dependent Virulence Factor Genes in *Staphylococcus aureus*, Showing a Link between Transcription Termination, Antibiotic Action, and Virulence. **9**.
- Neumann Y, Ohlsen K, Donat S, Engelmann S, Kusch H, Albrecht D, Cartron M, Hurd A & Foster SJ (2015) The effect of skin fatty acids on *Staphylococcus aureus*. *Arch Microbiol* **197**: 245-267.
- Novick RP (2003) Autoinduction and signal transduction in the regulation of staphylococcal virulence. *Mol Microbiol* **48**: 1429-1449.
- Novick RP & Geisinger E (2008) Quorum sensing in staphylococci. *Annu Rev Genet* **42**: 541-564.
- Novick RP, Ross HF, Projan SJ, Kornblum J, Kreiswirth B & Moghazeh S (1993) Synthesis of staphylococcal virulence factors is controlled by a regulatory RNA molecule. *EMBO J* **12**: 3967-3975.
- Nuxoll AS, Halouska SM, Sadykov MR, Hanke ML, Bayles KW, Kielian T, Powers R & Fey PD (2012) CcpA regulates arginine biosynthesis in *Staphylococcus aureus* through repression of proline catabolism. *PLoS Pathog* **8**: e1003033.
- Park JY, Kim JW, Moon BY, Lee J, Fortin YJ, Austin FW, Yang SJ & Seo KS (2015) Characterization of a novel two-component regulatory system, HptRS, the regulator for the hexose phosphate transport system in *Staphylococcus aureus*. **83**: 1620-1628.
- Patel K & Golemi-Kotra D (2015) Signaling mechanism by the *Staphylococcus aureus* two-component system LytSR: role of acetyl phosphate in bypassing the cell membrane electrical potential sensor LytS. *F1000Res* **4**: 79.
- Patton TG, Yang SJ & Bayles KW (2006) The role of proton motive force in expression of the *Staphylococcus aureus* cid and lrg operons. *Mol Microbiol* **59**: 1395-1404.
- Peschel A & Otto M (2013) Phenol-soluble modulins and staphylococcal infection. *Nat Rev Microbiol* **11**: 667-673.
- Piewngam P, Zheng Y, Nguyen TH, *et al.* (2018) Pathogen elimination by probiotic *Bacillus* via signalling interference. *Nature* **562**: 532-537.
- Pragman AA, Yarwood JM, Tripp TJ & Schlievert PM (2004) Characterization of virulence factor regulation by SrrAB, a two-component system in *Staphylococcus aureus*. *J Bacteriol* **186**: 2430-2438.
- Price-Whelan A, Poon CK, Benson MA, Eidem TT, Roux CM, Boyd JM, Dunman PM, Torres VJ & Krulwich TA (2013) Transcriptional profiling of *Staphylococcus aureus* during growth in 2 M NaCl leads to clarification of physiological roles for Kdp and Ktr K<sup>+</sup> uptake systems. *MBio* **4**.



## References

---

- Queck SY, Jameson-Lee M, Villaruz AE, Bach TH, Khan BA, Sturdevant DE, Ricklefs SM, Li M & Otto M (2008) RNAIII-independent target gene control by the *agr* quorum-sensing system: insight into the evolution of virulence regulation in *Staphylococcus aureus*. *Mol Cell* **32**: 150-158.
- Rogasch K, Ruhmling V, Pane-Farre J, *et al.* (2006) Influence of the two-component system SaeRS on global gene expression in two different *Staphylococcus aureus* strains. *J Bacteriol* **188**: 7742-7758.
- Schlag S, Fuchs S, Nerz C, Gaupp R, Engelmann S, Liebeke M, Lalk M, Hecker M & Gotz F (2008) Characterization of the oxygen-responsive NreABC regulon of *Staphylococcus aureus*. *J Bacteriol* **190**: 7847-7858.
- Sharma-Kuinkel BK, Mann EE, Ahn JS, Kuechenmeister LJ, Dunman PM & Bayles KW (2009) The *Staphylococcus aureus* LytSR two-component regulatory system affects biofilm formation. *J Bacteriol* **191**: 4767-4775.
- Shimada T, Park BG, Wolf AJ, *et al.* (2010) *Staphylococcus aureus* evades lysozyme-based peptidoglycan digestion that links phagocytosis, inflammasome activation, and IL-1beta secretion. *Cell Host Microbe* **7**: 38-49.
- Shompole S, Henon KT, Liou LE, Dziewanowska K, Bohach GA & Bayles KW (2003) Biphasic intracellular expression of *Staphylococcus aureus* virulence factors and evidence for Agr-mediated diffusion sensing. *Mol Microbiol* **49**: 919-927.
- Sokolovska A, Becker CE, Ip WK, *et al.* (2013) Activation of caspase-1 by the NLRP3 inflammasome regulates the NADPH oxidase NOX2 to control phagosome function. *Nat Immunol* **14**: 543-553.
- Stauff DL & Skaar EP (2009) The heme sensor system of *Staphylococcus aureus*. *Contrib Microbiol* **16**: 120-135.
- Stauff DL, Torres VJ & Skaar EP (2007) Signaling and DNA-binding activities of the *Staphylococcus aureus* HssR-HssS two-component system required for heme sensing. *J Biol Chem* **282**: 26111-26121.
- Stock AM, Robinson VL & Goudreau PN (2000) Two-component signal transduction. *Annu Rev Biochem* **69**: 183-215.
- Sun F, Ji Q, Jones MB, Deng X, Liang H, Frank B, Telser J, Peterson SN, Bae T & He C (2012) AirSR, a [2Fe-2S] cluster-containing two-component system, mediates global oxygen sensing and redox signaling in *Staphylococcus aureus*. *J Am Chem Soc* **134**: 305-314.
- Sun J, Zheng L, Landwehr C, Yang J & Ji Y (2005) Identification of a novel essential two-component signal transduction system, YhcSR, in *Staphylococcus aureus*. *J Bacteriol* **187**: 7876-7880.
- Torres VJ, Stauff DL, Pishchany G, Bezbradica JS, Gordy LE, Iturregui J, Anderson KL, Dunman PM, Joyce S & Skaar EP (2007) A *Staphylococcus aureus* regulatory system that responds to host heme and modulates virulence. *Cell Host Microbe* **1**: 109-119.

## References

---

- Tranchemontagne ZR, Camire RB, O'Donnell VJ, Baugh J & Burkholder KM (2015) *Staphylococcus aureus* Strain USA300 Perturbs Acquisition of Lysosomal Enzymes and Requires Phagosomal Acidification for Survival inside Macrophages. *Infect Immun* **84**: 241-253.
- Ulrich LE & Zhulin IB (2007) MiST: a microbial signal transduction database. *Nucleic Acids Res* **35**: D386-390.
- Ventura CL, Malachowa N, Hammer CH, Nardone GA, Robinson MA, Kobayashi SD & DeLeo FR (2010) Identification of a novel *Staphylococcus aureus* two-component leukotoxin using cell surface proteomics. *PLoS One* **5**: e11634.
- Villanueva M & Garcia B (2018) Sensory deprivation in *Staphylococcus aureus*. **9**: 523.
- Voyich JM, Sturdevant DE & DeLeo FR (2008) Analysis of *Staphylococcus aureus* gene expression during PMN phagocytosis. *Methods Mol Biol* **431**: 109-122.
- Voyich JM, Braughton KR, Sturdevant DE, *et al.* (2005) Insights into mechanisms used by *Staphylococcus aureus* to avoid destruction by human neutrophils. *J Immunol* **175**: 3907-3919.
- Vuppada RK, Hansen CR, Strickland KAP, Kelly KM & McCleary WR (2018) Phosphate signaling through alternate conformations of the PstSCAB phosphate transporter. *BMC Microbiol* **18**: 8.
- Walker JN, Crosby HA, Spaulding AR, Salgado-Pabon W, Malone CL, Rosenthal CB, Schlievert PM, Boyd JM & Horswill AR (2013) The *Staphylococcus aureus* ArlRS two-component system is a novel regulator of agglutination and pathogenesis. *PLoS pathogens* **9**: e1003819.
- Wang B, Zhao A, Novick RP & Muir TW (2014) Activation and inhibition of the receptor histidine kinase AgrC occurs through opposite helical transduction motions. *Mol Cell* **53**: 929-940.
- Wilde AD, Snyder DJ, Putnam NE, *et al.* (2015) Bacterial Hypoxic Responses Revealed as Critical Determinants of the Host-Pathogen Outcome by TnSeq Analysis of *Staphylococcus aureus* Invasive Infection. *PLoS Pathog* **11**: e1005341.
- Wirtz C, Witte W, Wolz C & Goerke C (2009) Transcription of the phage-encoded Panton-Valentine leukocidin of *Staphylococcus aureus* is dependent on the phage life-cycle and on the host background. *Microbiology* **155**: 3491-3499.
- Xie Q, Zhao A, Jeffrey PD, Kim MK, Bassler BL, Stone HA, Novick RP & Muir TW (2019) Identification of a Molecular Latch that Regulates Staphylococcal Virulence. *Cell Chem Biol*.
- Xue T, You Y, Hong D, Sun H & Sun B (2011) The *Staphylococcus aureus* KdpDE two-component system couples extracellular K<sup>+</sup> sensing and Agr signaling to infection programming. *Infect Immun* **79**: 2154-2167.
- Yang SJ, Xiong YQ, Yeaman MR, Bayles KW, Abdelhady W & Bayer AS (2013) Role of the LytSR two-component regulatory system in adaptation to cationic antimicrobial peptides in *Staphylococcus aureus*. *Antimicrob Agents Chemother* **57**: 3875-3882.

## References

---

Yang SJ, Bayer AS, Mishra NN, Meehl M, Ledala N, Yeaman MR, Xiong YQ & Cheung AL (2012) The *Staphylococcus aureus* two-component regulatory system, GraRS, senses and confers resistance to selected cationic antimicrobial peptides. *Infect Immun* **80**: 74-81.

Yang Y, Sun H, Liu X, Wang M, Xue T & Sun B (2016) Regulatory mechanism of the three-component system HptRSA in glucose-6-phosphate uptake in *Staphylococcus aureus*. *Med Microbiol Immunol* **205**: 241-253.

Yarwood JM, McCormick JK & Schlievert PM (2001) Identification of a novel two-component regulatory system that acts in global regulation of virulence factors of *Staphylococcus aureus*. *J Bacteriol* **183**: 1113-1123.

Zeng Z, Surewaard BG, Wong CH, Geoghegan JA, Jenne CN & Kubes P (2016) CR1g Functions as a Macrophage Pattern Recognition Receptor to Directly Bind and Capture Blood-Borne Gram-Positive Bacteria. *Cell Host Microbe* **20**: 99-106.

**Appendix**

- a) Accepted publication 1 (page 49-61)  
Accepted publication 2 (page 62-80)  
Accepted publication 3 (page 81-92)
  
- b) Manuscripts ready for submission (page 93-117)  
and page 10-21 as part of the introduction

Accepted publication 1

**Influence of Sae-regulated and Agr-regulated factors on the escape of  
*Staphylococcus aureus* from human macrophages**

Lisa Münzenmayer, Tobias Geiger, Ellen Daiber, Berit Schulte, Stella E. Autenrieth,  
Martin Fraunholz and Christiane Wolz

**Cellular Microbiology (2016) 18(8): 1172–118**

# Influence of Sae-regulated and Agr-regulated factors on the escape of *Staphylococcus aureus* from human macrophages

Lisa Münzenmayer,<sup>1</sup> Tobias Geiger,<sup>1,4</sup> Ellen Daiber,<sup>1</sup> Berit Schulte,<sup>1</sup> Stella E. Autenrieth,<sup>2</sup> Martin Fraunholz<sup>3</sup> and Christiane Wolz<sup>1\*</sup>

<sup>1</sup>Interfaculty Institute of Microbiology and Infection Medicine, University of Tübingen, Tübingen, Germany.

<sup>2</sup>Department of Internal Medicine II, University of Tübingen, Tübingen, Germany.

<sup>3</sup>Department of Microbiology, Biocenter, University of Würzburg, Würzburg, Germany.

<sup>4</sup>School of Medicine, Section of Microbial Pathogenesis Boyer Center for Molecular Medicine Yale University, New Haven, CT, 06536, USA.

## Summary

Although *Staphylococcus aureus* is not a classical intracellular pathogen, it can survive within phagocytes and many other cell types. However, the pathogen is also able to escape from cells by mechanisms that are only partially understood. We analysed a series of isogenic *S. aureus* mutants of the USA300 derivative JE2 for their capacity to destroy human macrophages from within. Intracellular *S. aureus* JE2 caused severe cell damage in human macrophages and could efficiently escape from within the cells. To obtain this full escape phenotype including an intermittent residency in the cytoplasm, the combined action of the regulatory systems Sae and Agr is required. Mutants in Sae or mutants deficient in the Sae target genes *lukAB* and *pvl* remained in high numbers within the macrophages causing reduced cell damage. Mutants in the regulatory system Agr or in the Agr target gene *psm $\alpha$*  were largely similar to wild-type bacteria concerning cell damage and escape efficiency. However, these strains were rarely detectable in the cytoplasm, emphasizing the role of phenol-soluble modulins (PSMs) for phagosomal escape. Thus, Sae-regulated toxins largely determine damage and escape from within macrophages, whereas PSMs are mainly responsible for

the escape from the phagosome into the cytoplasm. Damage of macrophages induced by intracellular bacteria was linked neither to activation of apoptosis-related caspase 3, 7 or 8 nor to NLRP3-dependent inflammasome activation.

## Introduction

*Staphylococcus aureus* primarily colonizes the noses of healthy human individuals (Weidenmaier *et al.*, 2012). In addition to its commensal characteristics, *S. aureus* is a major human pathogen that causes a variety of human diseases such as skin infections, sepsis, endocarditis, pneumonia and toxic shock syndrome (Lowy, 1998). The appearance and spread of community-associated methicillin-resistant *S. aureus* (CA-MRSA) led to increasing public health costs as well as increased morbidity and mortality for patients. Pulsed field-type USA300 strains are the most common CA-MRSA strain in the USA. Strains of this lineage are highly virulent, which is thought to be at least partially due to the high level of toxin expression (Otto, 2012). The enhanced virulence phenotype includes the capacity to efficiently cope with the human immune system. Professional phagocytes play a key role in the host defence against bacterial pathogens by recognizing, engulfing and eradicating invading bacteria. *S. aureus* has developed a variety of mechanisms to avoid being killed by phagocytes, including the inhibition of chemotaxis and the destruction of immune cells from the exterior and interior of the host cells (Rigby and DeLeo, 2012; Spaan *et al.*, 2013; van Kessel *et al.*, 2014). The mechanisms for escape from within the phagocytes have not been fully elucidated. Recently, mutants deficient in the production of either the phenol-soluble modulins PSM $\alpha$ 1–4 (Geiger *et al.*, 2012; Surewaard *et al.*, 2013) or the bicomponent leucocidin LukAB (Ventura *et al.*, 2010; DuMont *et al.*, 2013b) were found to be less able to lyse neutrophils from within.

The intracellular expression of putative toxins required for survival/escape is driven by a complex interactive regulatory network. The SaePQRS system appears to be a central downstream regulator that controls the expression of many virulence genes via the binding of the response regulator SaeR to a consensus sequence

Received 16 April, 2015; revised 12 January, 2016; accepted 26 January, 2016. \*For correspondence. E-mail christiane.wolz@med.uni-tuebingen.de; Tel. (+49) 7071 2980187; Fax (+49) 7071 295165.

preceding the genes encoding pore-forming toxins such as Hla, HlgABC, PVL and LukAB (Geiger *et al.*, 2008; Nygaard *et al.*, 2010; Cho *et al.*, 2012). Furthermore, the Sae system is activated by phagocytosis-related signals such as  $\alpha$ -defensins (Geiger *et al.*, 2008; Zurek *et al.*, 2014). The quorum sensing system AgrBCDA also contributes to the intracellular activation of toxin genes via the regulatory RNAlII (Boisset *et al.*, 2007) or by direct activation of the *psmA* genes through the response regulator AgrA (Queck *et al.*, 2008). Intracellular *psmA* expression in neutrophils was shown to require at least basal levels of AgrA activity as well as the intracellular induction of the stringent response with its effector molecule (p)ppGpp (Geiger *et al.*, 2012).

Bacterial and host factors important for the escape from human macrophages are less clear. *S. aureus* are avidly phagocytosed by macrophages by different mechanisms but are not efficiently killed (Kneidl *et al.*, 2012; Cole *et al.*, 2014; Flannagan *et al.*, 2015; Jubrail *et al.*, 2016; Tranchemontagne *et al.*, 2015). Depending on the *S. aureus* strain and/or macrophage cell type, the bacteria may either escape from the macrophages or persist in these cells for a prolonged time (Kubica *et al.*, 2008; Koziel *et al.*, 2009; Grosz *et al.*, 2013; Flannagan *et al.*, 2015; Jubrail *et al.*, 2016). It is unclear whether similar mechanisms are employed by *S. aureus* to escape from different cell types, whether different factors/toxins act in concert to help the bacteria to escape phagocytosis and how the intracellular expression of the relevant genes is regulated. Recently, the Sae-regulated toxin LukAB was proposed to be involved in THP-1 killing. However, there is also strong evidence for the contribution of other factors (Melehani *et al.*, 2015).

We aimed to analyse *S. aureus* factors that determine bacterial fate after macrophage phagocytosis. We show that several factors contribute to the escape. The Sae-regulated pore-forming toxins LukAB and PVL are the major factors inducing cell death and bacterial escape in macrophages. However, these toxins are not required for the escape from HeLa epithelial cells. The Agr-regulated PSMs are mainly responsible for phagosomal escape into the cytoplasm irrespective of cell type.

## Results

### *The importance of the Sae regulatory system for the escape of S. aureus from within THP-1 macrophages*

To gain insight into the components and regulatory systems required for escape from macrophages, we determined the survival of *S. aureus* strain JE2 (a plasmid-cured derivative of strain LAC of the USA300 lineage) (Nuxoll *et al.*, 2012) and regulatory mutants after uptake by differentiated THP-1 macrophages. We first focused on Agr and Sae because most immunomodulatory

molecules or toxins are controlled by one or both of these regulators. After 1 h of incubation, all of the extracellular/escaped bacteria were killed by lysostaphin/gentamicin treatment for 1 h. This time point [indicated as time point 0 (t<sub>0</sub>)] was chosen as reference for further analysis. At t<sub>0</sub>, >99% of all cells contained *S. aureus* bacteria as determined by image stream analysis (Fig. S1D), and ~30–50% of the inoculated bacteria were found within macrophages. Interestingly, the mutation in *sae* resulted in a twofold decrease of intracellular bacteria, indicating slightly reduced uptake efficiency in *sae* deletion strains. The fate of the intracellular bacteria was then followed for 3 and 24 h with gentamicin used to kill all escaping, extracellular bacteria. After 3 h, replication of the intracellular bacteria is indicated by an increase in bacterial numbers. This effect was more prominent in *sae* mutants (Fig. 1A). After 24 h, wild-type bacteria were difficult to detect within the host cells. This indicates that the bacteria escaped from within the cells and were killed by the extracellular gentamicin. An *agr* mutant was also able to escape from the macrophages, although to a lesser extent than the wild type (Fig. 1B). However, intracellular *sae* and the *sae/agr* bacteria were detectable in high numbers after 24 h. To confirm that the decrease of viable wild-type bacteria within cells is due to escape, cell toxicity was measured. Macrophage membrane damage was clearly detectable after incubation with the wild-type and *agr* mutant strains (Fig. 1C). There was significantly less membrane damage in macrophages incubated with the *sae* or *agr/sae* mutant wherein high intracellular bacterial numbers were found. Altogether bacterial escape correlated with cytotoxicity. Notably, the escape was dependent on both Agr and Sae as indicated by the significant difference between the *agr/sae* double mutant compared with the single mutants.

We next monitored *S. aureus* escape by use of a recruitment marker, YFP-CWT (recognizing peptidoglycan) expressed in the THP-CWT cell line. The marker cannot enter into phagosomes and thus recognizes only cytosolic bacteria (Grosz *et al.*, 2013). After phagocytosis, significant differences between the bacterial strains were observed (Fig. 1D). Cells inoculated with the wild type and *agr* mutant exhibited significant cell damage and condensed nuclei. However, no obvious cell damage was seen in cells containing the *sae* mutants even after 24 h, at which time the cells were filled with bacteria. Interestingly, phagosomal escape into the cytosol could only be observed in cells infected with WT and *sae* mutant at the 3 h time point (Fig. 1D, white arrow), indicating a contribution of Agr-regulated factors in this mechanism.

Next, the bacterial survival after uptake by human monocyte-derived macrophages (hMDMs) was analysed. Similar to the results obtained with THP-1 cells, bacteria

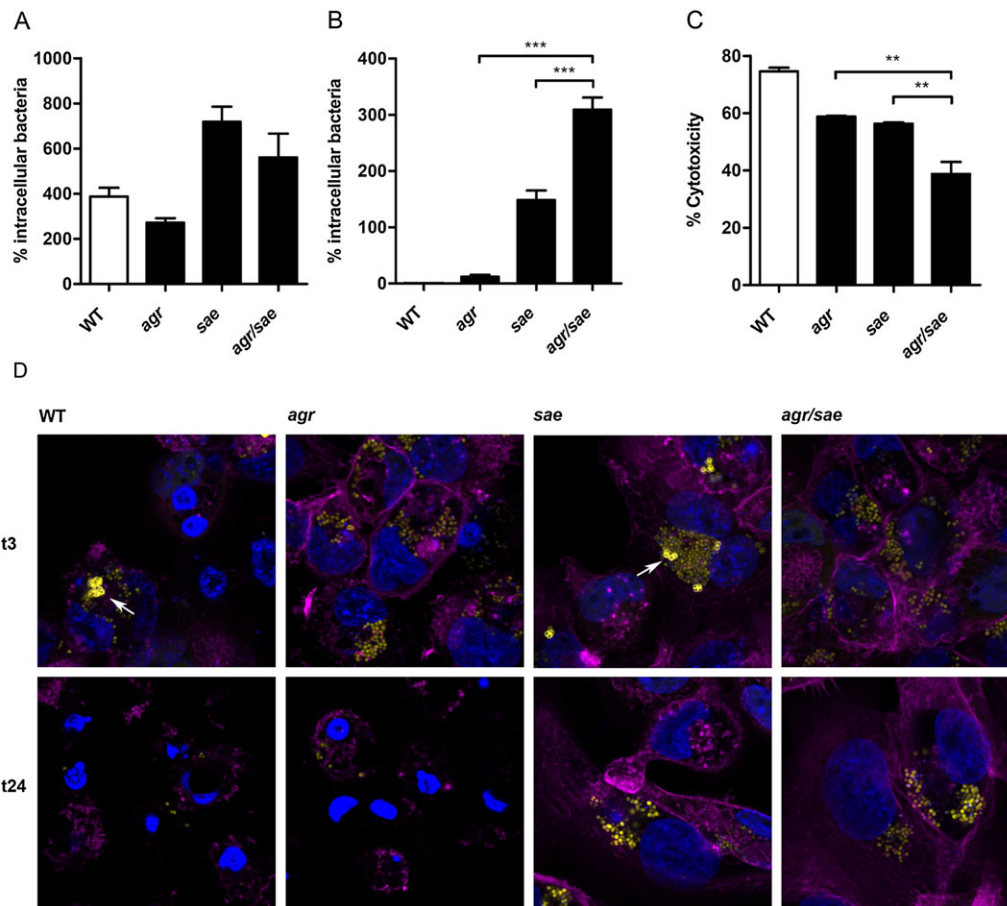


**Fig. 1.** Influence of Agr and Sae on the escape from within macrophages. Intracellular survival (protection) assay with differentiated THP-1 macrophages and *S. aureus* strain JE2 and its isogenic *agr*, *sae* and *agr/sae* double mutants. A and B. After phagocytosis and lysostaphin/gentamicin treatment, the THP-1 cells were further incubated for (A) 3 h or (B) 24 h in RPMI medium containing gentamicin ( $200 \mu\text{g ml}^{-1}$ ) to kill extracellular/escaped bacteria. At indicated time points, the cells were lysed and bacterial cfu determined. Intracellular bacteria are expressed as the ratio of cfu at t3 or t24 to cfu at t0. C. Membrane integrity of the THP-1 cells after 24 h assessed by SYTOX green assay. Significance was determined by one-way analysis of variance with Tukey's multiple comparison post-test. The data represent the mean of three independent experiments. \*\* $P < 0.01$ ; \*\*\* $P < 0.001$ . D. Experiment performed as described earlier using chamber slides. Cells were stained with phalloidin (pink: actin filaments) and DAPI (blue: DNA). Bacteria express *yfp* (faint yellow). YFP-CWT recruitment marker (yellow ring: bacterial localization in the cytosol, white arrow).

replicated within 3 h after uptake by hMDMs. After 24 h, again significantly more *agr/sae* bacteria were found within the hMDMs (Fig. S2) when compared with the wild-type or *agr* mutant strain. However, the percentage of intracellular bacteria for the *agr/sae* mutant after 24 h was significantly lower compared with that at the 3 h time point. This might be due to bacterial killing, additional factors not regulated by Agr/Sae or the high bacterial load (Flannagan *et al.*, 2015). Nevertheless, cells infected with wild type or the *agr* mutant showed severe damage with condensed nuclei, whereas cell infected with *agr/sae* mutant appeared healthier (Fig. S2C).

In summary, these results indicate that Sae-regulated factor(s) are mainly responsible for bacterial escape and cell damage observed after infection with wild-type bacteria. Agr partially contributes to the escape and at

least one *agr*-regulated factor confers temporal escape of the bacteria into the cytoplasm as illustrated by the comparison of *sae* versus *agr/sae* mutant.

#### *LukAB and PVL are mainly responsible for the escape of S. aureus from within human macrophages*

In search for the proposed Agr-regulated and Sae-regulated factor(s), we analysed the role of pore-forming toxins known to be tightly regulated via Sae or Agr (Fig. 2). Analysis of a set of mutant strains revealed that Hla had no significant impact on the escape phenotype or cell cytotoxicity. PVL and LukAB showed an additive effect: mutation of both genes resulted in prolonged persistence in macrophages (Fig. 2A) and less cell damage (Fig. 2B). The effect of the single mutants was less pronounced. Of note, the *pvl/lukAB* double mutant was detectable in the



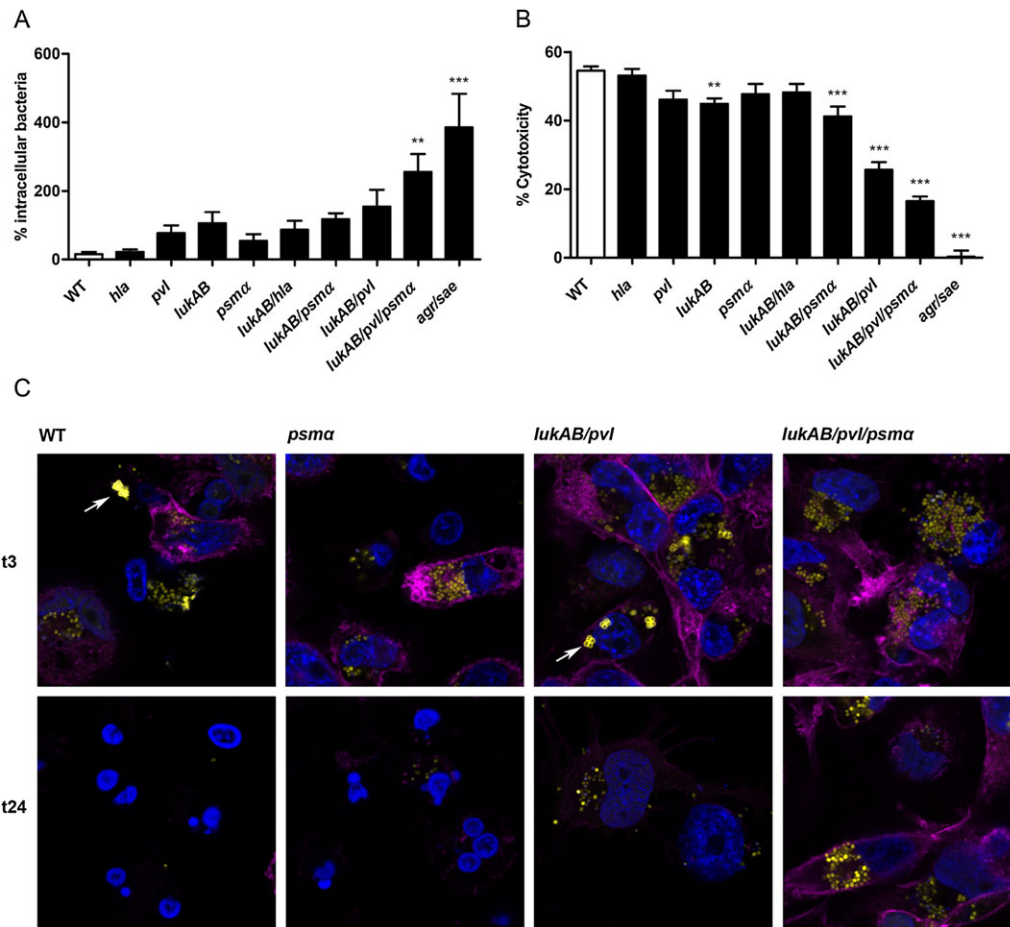


**Fig. 2.** LukAB and PVL are mainly responsible for the escape of *S. aureus* from within human macrophages.

A. Intracellular survival (protection) assay with differentiated THP-1 macrophages and *S. aureus* strain JE2 and its isogenic toxin mutants. After phagocytosis and lysostaphin/gentamicin treatment, the THP-1 cells were further incubated for 24 h in RPMI medium containing gentamicin ( $200 \mu\text{g ml}^{-1}$ ) to kill extracellular/escaped bacteria. At indicated time points, the cells were lysed and bacterial cfu determined. Intracellular bacteria are expressed as the ratio of cfu at t24 to cfu at t0.

B. Membrane integrity of the THP-1 cells after 24 h assessed by SYTOX green assay. Significance was determined by one-way analysis of variance with Dunnett's post-test with reference to wild type. The data represent the mean of three to seven independent experiments. \*\* $P < 0.01$ ; \*\*\* $P < 0.001$ .

C. Experiment performed as described earlier using chamber slides. Cells were stained with phalloidin (pink: actin filaments) and DAPI (blue: DNA). Bacteria express yfp (faint yellow). YFP-CWT recruitment marker (yellow ring: bacterial localization in the cytosol, white arrow).

cytosol after 3 h (Fig. 2C), showing a similar phenotype to the *sae* mutant strain. Additional mutation of *psm $\alpha$*  resulted in a further increase in persistence, and no phagosomal escape into the cytoplasm was detectable similar to the *agr/sae* double mutant.

#### Expression of pvl, lukAB and psm $\alpha$ in vitro and within macrophages

To analyse whether and to what extent the expression of the toxins is determined by the Agr or Sae system, toxin gene expression of the regulatory mutants grown in inoculation medium was assessed (Fig. 3A–C). We also included a *psm $\alpha$*  mutant in the analysis, because it was recently shown that a *psm $\alpha$*  mutant exhibits a transcriptional delay in *hla* expression (Berube *et al.*, 2014). In the *agr* mutant strain, the expression of *psm $\alpha$*  was severely

repressed. However, only a slight decrease of *lukAB* and *pvl* expression was observed in the *agr* mutant strain. These toxin genes are predominantly regulated by Sae because mutation in *sae* resulted in severe inhibition of *lukAB* and *pvl*. *psm $\alpha$*  expression is clearly not dependent on *sae*. The *sae* mutant even showed a slight increase in *psm $\alpha$*  expression. Interestingly, in the *psm $\alpha$*  mutant, an increased expression of *lukAB* and *pvl* was detected. This is contrary to the described effect of PSMs on *hla* expression (Berube *et al.*, 2014) but also emphasizes that PSMs exert some regulatory effect on other toxin genes.

Next, we analysed the activity of the Agr and Sae systems after phagocytosis (Fig. 3D–H). Both Agr target genes, RNAlII of the *agr* operon and *psm $\alpha$* , were highly induced directly after bacterial uptake. Only slight changes in *sae* activity were observed upon macrophage infection

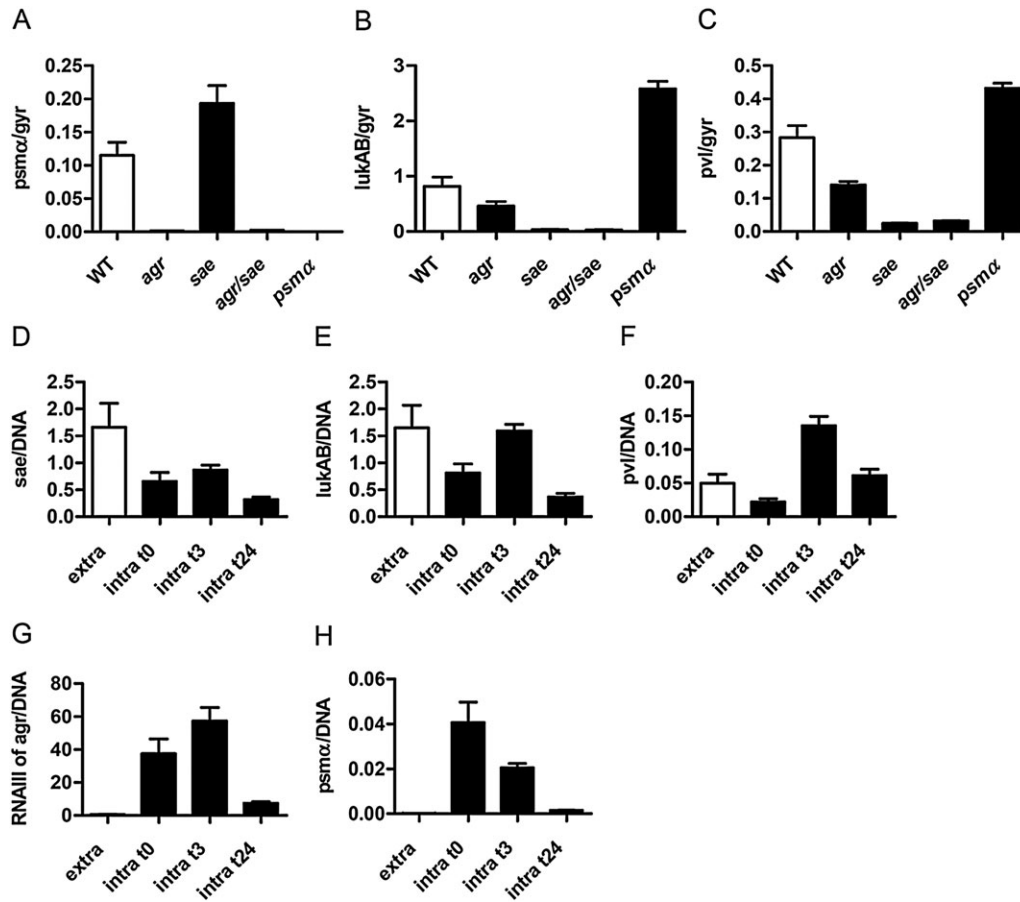


**Fig. 3.** Expression of *pvl*, *lukAB* and *psm $\alpha$*  *in vitro* and within macrophages.

A–C. RNA from bacteria grown in inoculation medium was analysed for gene expression of *psm $\alpha$*  (A), *lukAB* (B) and *pvl* (C) by quantitative reverse transcription PCR in relation to *gyr* expression.

D–H. RNA from intracellular bacteria were harvested at t0, t3 and t24 (intra) and from the supernatant (extra) 1 h after inoculation and gene expression of *sae* (D), *lukAB* (E), *pvl* (F), RNAIII of *agr* (G) and *psm $\alpha$*  (H) analysed by qRT-PCR. Gene expression is shown in relation to quantified *lukAB* DNA. Results are presented as the mean of three independent experiments.

with no indication of specific activation after phagocytosis. For all genes, a decrease of expression was found 24 h after infection, which might be due to the severe damage of the host cells.

*Damage of macrophages after phagocytosis is not linked to caspase 3, 7 and 8 or NLRP3-dependent inflammasome activation*

We observed severe damage of macrophages mainly due to expression of the pore-forming toxins LukAB and PVL. To analyse whether the toxins may lead to induction of apoptosis, we measured caspase 3, 7 and 8 activity in cells harbouring the wild-type and mutant bacteria. Uptake of *S. aureus* did not result in significant changes in caspase activity (Fig. 4A, B) at t3, irrespective of which strain was inoculated. Next, we analysed whether intracellular expression of *lukAB/pvl* might result in activation of the NLRP3 inflammasome resulting in pyroptosis. The inhibitor MCC950 was shown to block

NLRP3-ASC assembly at nanomolar concentrations (Coll *et al.*, 2015). Treatment of THP-1 cells with MCC950 did not protect cells from bacteria-induced damage, and bacteria were not hampered in their escape efficiency (Fig. 4C). Thus, NLRP3 activation by intracellularly expressed toxins is not a major pathway leading to the observed escape phenotype of wild-type bacteria.

*PSMs are mainly responsible for escape from non-professional phagocyte*

Next we analysed whether similar factors are involved in the escape from epithelial cells. Intracellular protection assays using human epithelial cells HeLa-YFP-F<sub>C</sub> were performed (Fig. 5A). In these cells, mutations of *sae* showed no significant effect. This is presumably due to the lack of toxin receptors in HeLa cells. We confirmed that these cells do not express the CD11b receptor integrin (Fig. 5B) (Ho and Springer, 1982; Giese *et al.*, 2011; DuMont *et al.*, 2013a). CD11b acts as receptor for LukAB,

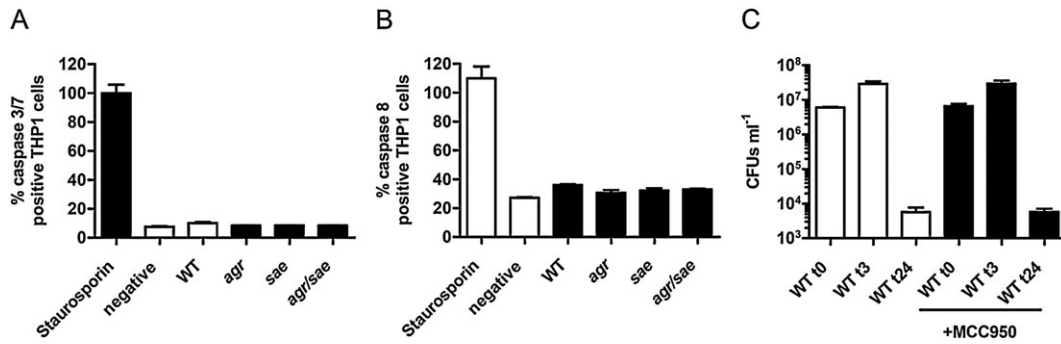


**Fig. 4.** Caspase activity and NLRP3 inhibition.

A and B. Activity of caspase 3/7 (A) and caspase 8 (B) was determined at t3. Staurosporine was used as a positive control (100%). Infection was performed as described in Fig. 1.

C. Intracellular survival (protection) assay with differentiated THP-1 macrophages and *S. aureus* strain JE2 with and without MCC950. After phagocytosis and lysostaphin/gentamicin treatment, the THP-1 cells were further incubated for 3 and 24 h in RPMI medium containing gentamicin (200 µg ml<sup>-1</sup>) to kill extracellular/escaped bacteria. At indicated time points, the cells were lysed and bacterial cfu determined.

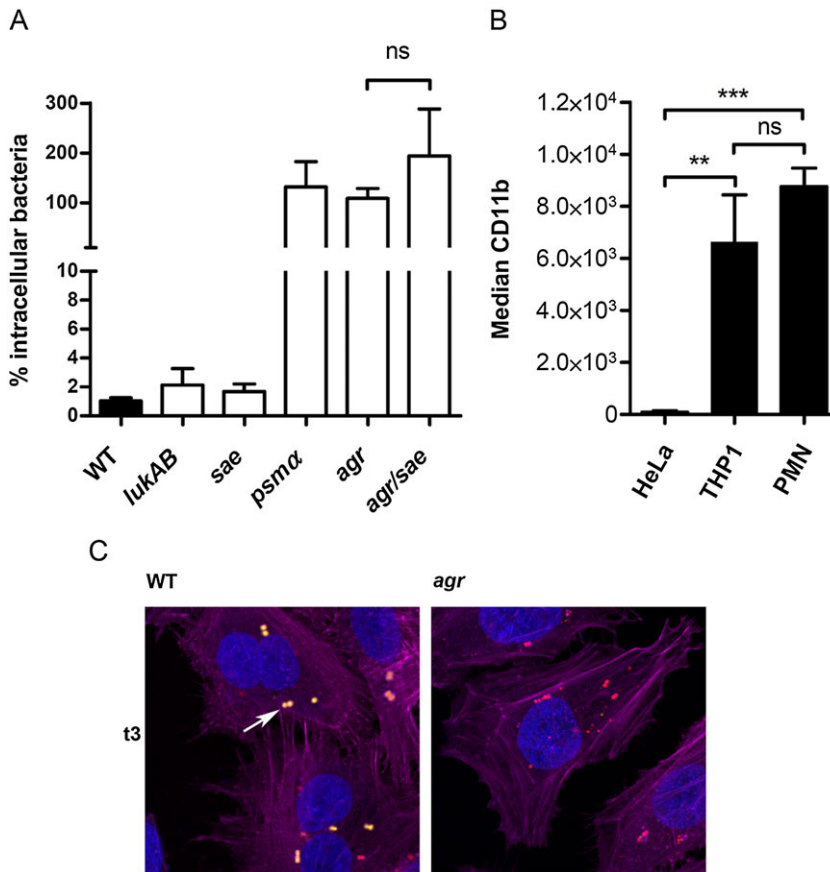


**Fig. 5.** CD11b expression and escape from HeLa epithelial cells.

A. Intracellular survival (protection) assay with HeLa epithelial cells and *S. aureus* strain JE and its isogenic *lukAB*, *sae*, *psmα*, *agr* and *agr/sae* double mutants. After phagocytosis and lysostaphin/gentamicin treatment, the HeLa cells were incubated 24 h in RPMI medium containing 200 µg ml<sup>-1</sup> gentamicin to kill extracellular/escaped bacteria. Data represent mean of three independent experiments. Significances were determined by one-way analysis of variance with Tukey's multiple comparison post-test. ns, not significant.

B. Median of CD11b expression on HeLa cells, THP-1 macrophages and neutrophils. Cells were stained with anti-CD11b for 20 min. \*\**P* < 0.01, \*\*\**P* < 0.001, ns, not significant.

C. Cells were stained with phalloidin (pink: actin filaments) and DAPI (blue: DNA). Bacteria were stained with TritC (red: bacteria in phagosome); YFP-Fc recruitment marker (yellow: bacterial localization in the cytosol, white arrow).

and consequently, *lukAB* mutation also showed no impact on the escape in HeLa cells (Fig. 5B). Deletion of *agr* or the target gene *psmα* is sufficient to prevent the escape from within HeLa cells. Additional deletion of *sae* had no effect on the escape. The HeLa cells contain the escape marker YFP-Fc, which recognizes cytosolic bacteria. Wild-type bacteria were detectable in the cytosol indicated by

YFP staining (Fig. 5C). However, the *agr* mutant remained YFP negative, indicating that Agr-regulated factors are required to escape from the phagosome into the cytosol. Thus, mutation of *agr* is sufficient to abrogate the escape phenotype in HeLa cells, which is in contrast to the results obtained after macrophage phagocytosis, where Sae-regulated factors are essential for escape.

## Discussion

The human immune system and its professional phagocytes provide an effective line of defence against staphylococcal infections (Rigby and DeLeo, 2012). However, *S. aureus* possesses a large number of virulence factors that contribute to its ability to circumvent the immune system (Spaan *et al.*, 2013). There is now evidence that *S. aureus* exploit phagocytic cells as 'Trojan horses' for dissemination (Lehar *et al.*, 2015), and thus, the mechanism leading to bacterial escape after phagocytosis is highly relevant. We aimed to decipher the factors that are required for the pathogen to escape from macrophages. Here, we show that after phagocytosis by human macrophages, the Sae-regulated pore-forming toxins LukAB and PVL are the major factor(s) required for induction of cell death leading to the release of the bacteria. PSMs facilitated phagosomal escape probably because of their lytic activity. Altogether, escape seems to be not exclusively facilitated by one toxin but an additive effect of different virulence factors.

### *LukAB/PVL induced cell damage and bacterial escape from macrophages*

The receptor-dependent bicomponent leucocidins LukAB and PVL display host cell specificity because they are dependent on the cognate human receptors CD11b or complement receptors (C5aR and C5L2) respectively (DuMont *et al.*, 2013a, 2014; Baur *et al.*, 2014). CD11b is expressed at comparable amounts on neutrophils and macrophages (Fig. 5B) and was shown to be located in the phagosomal membrane, which originates from the invaginated host membrane (DuMont *et al.*, 2013b). Localization of the PVL receptor at the phagosomal membrane can also be assumed. However, it remains unclear how the intracellular interaction of the toxins with the receptors finally led to cell damage. When applied from the outside, the toxins can induce the NLRP3 inflammasome and pyroptosis presumably as a result of the accompanied potassium efflux (Holzinger *et al.*, 2012; Alonzo and Torres, 2014; Melehani *et al.*, 2015).

When acting from inside, changes in cell morphology, for example, condensed nuclei, were readily observed preceding bacterial escape. Cells infected with the wild-type or *agr* mutant strain showed condensed nuclei already at t0. However, bacteria replicated in the cells at least until t3, at which time cells were still packed with bacteria as shown by protection assay and image stream analysis (Figs 1 and S1D). The mechanism resulting in LukAB/PVL-mediated cell damage from inside was linked neither to activation of apoptosis via caspase 3, 7 or 8 nor to NLRP3 inflammasome activation (Fig. 4). These findings are in line with recently published data from others (Jubrail *et al.*, 2016; Melehani *et al.*, 2015).

Alternatively, toxin-induced potassium efflux was proposed to activate necroptosis in alveolar macrophages (Gonzalez-Juarbe *et al.*, 2015; Kitur *et al.*, 2015). One may assume that a similar cell death pathway is activated upon intracellular expression of LukAB/PVL. However, it is not obvious how these toxins should result in potassium efflux when expressed intracellularly. Moreover, adding high potassium (80 mM) to the infection medium did not inhibit bacterial escape or cell death (data not shown). Therefore, alternative mechanisms leading to cell damage have to be considered.

### *PSM-dependent phagosomal escape from macrophages*

Phenol-soluble modulins with their  $\alpha$ -helical structure are described to function as detergents and are receptor independent. They have no host cell type specificity and primarily act by disrupting the hydrophobic cell membranes (Peschel and Otto, 2013). We show that PSMs were not required to induce cell damage but facilitated phagosomal escape. Only PSM-expressing bacteria were detected in the cytosol (Figs 1D and 2C). Low concentration of PSMs is usually not sufficient for cell lysis (Löffler *et al.*, 2010), but the intracellular activation of *psm* $\alpha$  expression seems to be sufficient to disrupt the phagosomal membrane.

### *Intracellular regulation of toxin genes*

We could confirm that *lukAB* and *pvl* are tightly regulated by the Sae system (Voyich *et al.*, 2005; Wirtz *et al.*, 2009; Geiger *et al.*, 2008).  $\alpha$ -Defensins are the major signals leading to activation of the histidine kinase SaeS, which is in line with the immediate activation of Sae target genes after neutrophil phagocytosis (Voyich *et al.*, 2005; Geiger *et al.*, 2008). Macrophages are deficient in production of  $\alpha$ -defensins (Agerberth *et al.*, 2000), and thus, the Sae system is not activated after phagocytosis. SaeS activity within macrophages was similar to that found in the inoculation medium, which seems to be sufficient to mediate cell damage and escape. The Agr system was confirmed to be essential for *psm* $\alpha$  expression (Queck *et al.*, 2008) but showed little effect on *lukAB* and *pvl*. Agr activity was immediately induced after phagocytosis. The signals involved in this strong intracellular activation are not yet clear. Intracellular Agr activation was previously shown after uptake in non-professional phagocytes and macrophages and described in the context of diffusion sensing (Shompole *et al.*, 2003) or acidification (Tranchemontagne *et al.*, 2015) respectively. Of note, Agr was found not to be specifically activated after uptake into neutrophils (Voyich *et al.*, 2005; Geiger *et al.*, 2012).

### *Predominant role of PSMs for escape in HeLa cells*

Agr and PSMs were essential for escape after bacterial uptake in HeLa cells, whereas the role of LukAB or other



Sae-regulated factors was negligible. Agr/PSM-positive bacteria were detectable in the cytosol, whereas the *agr* mutant was retained in the phagosome. The requirement of PSMs for escape in HeLa cells was shown previously by analysis of a variety of non-professional phagocytes (Giese *et al.*, 2011; Fraunholz and Sinha, 2012; Grosz *et al.*, 2013). However, these results also demonstrated that PSMs alone are not sufficient for the escape from epithelial and endothelial cells (Grosz *et al.*, 2013). Other factors acting in concert with PSMs in non-professional phagocytes remain to be identified. Our results indicate that these proposed factors are not Sae regulated.

### Conclusion

*Staphylococcus aureus* is taken up by professional phagocytes and numerous other cells but can efficiently escape from the inside (Fraunholz and Sinha, 2012). The escape is determined by Agr-regulated and Sae-regulated toxins. In non-professional phagocytes, the expression of Agr-regulated PSMs is responsible for the escape into the cytosol, where bacteria can replicate and finally exit into the extracellular milieu (Fraunholz and Sinha, 2012). In human macrophages, the bacteria mainly replicate in the phagosome, and the Sae-regulated pore-forming toxins LukAB/PVL are most important for the bacteria to escape from the cells, but there is also an additive effect of PSMs, which seem to be responsible for the escape into the cytosol. The escape processes are accompanied by cell damage, which is probably initiated by different, so far ill-defined, mechanisms. Canonical apoptosis or pyroptosis pathways involving caspase 3, 7 and 8 or NLRP3 could be excluded. The roles of other mechanisms leading to cell damage have to be elucidated.

## Experimental procedures

### Bacterial strains and growth conditions

*Staphylococcus aureus* strains (Table S1) were grown in tryptic soy broth. For strains carrying resistance genes, antibiotics were used only in precultures (5 µg ml<sup>-1</sup> of tetracycline and 10 µg ml<sup>-1</sup> of erythromycin or chloramphenicol). Bacteria from an overnight culture were diluted to an initial optical density (OD<sub>600</sub>) of 0.05 and grown (37°C) to the desired OD.

### Generation of isogenic mutants in strain JE2

The markerless *lukAB*, *saePQRS* and *agrBCDA* deletion mutants were obtained using the mutagenesis vector pBASE6 (Geiger *et al.*, 2012). Flanking regions were amplified, and total deletions were introduced by overlapping polymerase chain reaction (PCR) employing primers listed in Table S2. The amplicons were cloned into pBASE6 using the BglIII/Sall restriction sites for *lukAB* and *sae* deletion and by using Gibson assembly for *agr* deletion. The resulting plasmids for *lukAB* (pCG367), *sae* (pCG335) and *agr* (pCG391) mutagenesis were transformed into RN4220 followed

by transduction into *S. aureus* strain JE2. Mutagenesis was performed as described (Bae and Schneewind, 2006). The deletions were verified by PCR with oligonucleotides spanning the deletion region. The *agr/sae* double mutant was obtained by transducing the *sae::Tn917* insertion of strain AS2 (Geiger *et al.*, 2012) into the markerless *agr* mutant. Single, double and triple mutants of toxin genes were obtained by transduction using donor strains listed in Table S1. All mutants were verified by PCR using oligonucleotides flanking the mutated genes and phenotypically on blood agar plates to confirm the expected haemolytic pattern. For imaging, strains were transduced with plasmid pJL94 carrying constitutively expressed *yfp*.

### Cell culture and growth conditions

THP-1-CWT cells containing the recruitment marker YFP-CWT (recognizing Gram-positive peptidoglycan) (Grosz *et al.*, 2013) and HeLa cells containing the recruitment marker YFP-F<sub>C</sub> (recognizing staphylococcal protein A) (Giese *et al.*, 2011) were grown in RPMI 1640 medium (Biochrom) with 2 mM glutamine, 10% heat-inactivated foetal bovine serum (Sigma), 2% HEPES (Biochrom) and 1% penicillin/streptomycin (Gibco). The media for THP-1 cells also contained 1 mM sodium pyruvate (Sigma-Aldrich). Cell viability was determined by trypan blue staining and was at least 90% before all experiments. For experiments that included bacteria, the antibiotics were omitted. To induce differentiation, 1 × 10<sup>5</sup> ml<sup>-1</sup> THP-1 cells were treated with 160 nM phorbol-12-myristate-13-acetate (PMA) for 48 h. The differentiated cells were then washed twice with Hank's Balanced Salt Solution (HBSS) and further incubated for 24 h in RPMI medium without PMA. After differentiation, the cells became adherent to the culture dishes. Cellular proliferation markedly decreased, and morphological changes consistent with differentiation were observed (macrophage-like appearance with a diffused and enlarged shape). Differentiation was also accompanied by susceptibility to purified LukAB. Undifferentiated cells appeared resistant because of a lack of the specific receptor CD11b.

### Preparation of human monocyte-derived macrophages

Monocytes were isolated from the peripheral blood by Ficoll/Histopaque gradient centrifugation. Cells were washed once in phosphate-buffered saline (PBS) and adjusted to a cell number of 2 × 10<sup>6</sup> ml<sup>-1</sup> in RPMI 1640 medium (Biochrom) with 2 mM glutamine, 10% heat-inactivated foetal calf serum (FCS, Sigma), 2% HEPES (Biochrom), 1% penicillin/streptomycin (Gibco) and 1 mM sodium pyruvate (Sigma-Aldrich). Seven hundred microlitres or 300 µl was seeded into each well of 12-well tissue culture plates or 8-well tissue culture µ-slides (Ibidi) respectively. After 1 h of incubation, cells were washed twice with PBS to remove non-adherent cells. Cells were further incubated with medium containing 25 nM granulocyte macrophage colony-stimulating factor (PeproTech), which was additionally added every second day. After 7 days of incubation, cells were used for experiments.

### Cytotoxicity assay

Cells were seeded in 24-well tissue culture plates at  $5 \times 10^5$  per well in a final volume of 500  $\mu\text{l}$  of RPMI medium. Cells were infected for 24 h at 37°C and 5% CO<sub>2</sub> with different *S. aureus* strains at a multiplicity of infection of 50:1. To determine the membrane integrity of the THP-1 cells after 24 h, a SYTOX green assay (Invitrogen) was employed. Each well was mixed with 500  $\mu\text{l}$  of PBS + SYTOX green (0.5  $\mu\text{M}$ ) and incubated at room temperature for 10 min. Fluorescence was measured using a Tecan InfinitePro200 Reader (excitation 485 nm, emission 535 nm). Activity of caspases 3, 7 and 8 was determined at t3 according to the instruction of the manufacturer (Promega).

### Intracellular survival (protection) in macrophages and HeLa cells

The intracellular protection assays were performed in 6-well tissue culture plates (2 ml per well for THP-1 and HeLa cells), in 12-well tissue culture plates (1 ml per well for hMDMs) or in 8-well tissue culture  $\mu$ -slides (Ibidi). Bacterial cultures grown to an OD<sub>600</sub> = 1 were washed twice with sterile PBS and adjusted to reach a multiplicity of infection of 50:1. Phagocytosis was performed in RPMI medium (Biolyz) containing 10% human serum (Sigma) and 10% FCS (Sigma). For experiments with MCC950, cells were incubated prior to infection with 0.1  $\mu\text{M}$  MCC950 (Biomol) for 30 min. The incubation time for the uptake of the bacteria was 60 min. The cells were then washed twice with HBSS, and the remaining extracellular bacteria were killed by incubation with lysostaphin (10  $\mu\text{g ml}^{-1}$ ) and gentamicin (200  $\mu\text{g ml}^{-1}$ ) for 60 min (t0). The cells were washed twice with HBSS and then incubated in RPMI containing gentamicin (200  $\mu\text{g ml}^{-1}$ ) for 3 h (t3) or 24 h (t24). At the indicated time points, the cells grown on  $\mu$ -slides were processed for imaging. Cells grown on 6-well or 12-well plates were washed twice with HBSS and incubated in 0.1% TritonX-100 for 5 min to disrupt the host cells. Appropriate dilutions were plated on tryptic soy agar plates and incubated at 37°C for the enumeration of colony-forming units (cfu) on the following day. The ratio of intracellular surviving bacteria was expressed as cfu at t24/cfu at t0 or cfu at t3/cfu at t0.

### Microscopy

For infections of HeLa cells, the bacteria were grown to OD<sub>600</sub> = 1 and stained with tetramethylrhodamine (TritC, Thermo Fisher) for 30 min at 37°C. For THP-1 cells, bacteria constitutively expressing YFP were used. After infection on  $\mu$ -slides, cells were washed twice with HBSS and fixed with 150  $\mu\text{l}$  of ice-cold PBS containing 3.7% formaldehyde for 30 min. Wells were washed three times with HBSS and incubated with 2.5  $\mu\text{l}$  of Alexa Fluor 647 Phalloidin (Thermo Fisher) in 100  $\mu\text{l}$  of PBS containing 1% bovine serum albumin for 30 min. After three washes with HBSS, cells were covered with 100  $\mu\text{l}$  of PBS and stained with one drop of NucBlue® Fixed Cell ReadyProbes® reagent [4,6-diamidino-2-phenylindole (DAPI), Thermo Fisher]. After three more washes

with HBSS, cells were mounted using fluorescence mounting medium (DAKO).

Image acquisition was performed in the confocal mode of an inverted Zeiss LSM 710 NLO microscope equipped with a spectral detector and employing a Zeiss Plan-Apochromat 63x/1.40 oil DIC M27 objective. The following excitation wavelengths were used for the immunofluorescence experiments: DAPI, 405 nm; Phalloidin, 633 nm; gpYFP, 514 nm; TritC, 561 nm. Images were exported in the different channels or overlays as 16-bit tagged image files for further analysis. Overlays were batch processed for intensity and colour balance.

### Flow cytometry and multispectral imaging flow cytometry

Adherent THP-1 and HeLa cells were detached from culture plates using Accutase. Neutrophils were isolated from the peripheral blood by Ficoll/Histopaque gradient centrifugation as described previously (Geiger *et al.*, 2012). For flow cytometry, cells were incubated for 20 min at 4°C with 10  $\mu\text{g ml}^{-1}$  of IgGs from human serum (Sigma-Aldrich). Cells were stained with anti-CD11b-APC-eFluor780 (M1/70, eBioscience) for 20 min at 4°C. To exclude dead cells, Aqua LIVE/DEAD (Invitrogen) was used according to the manufacturer's instruction. Samples were acquired using a Canto-II flow cytometer (BD Biosciences) with DIVA software (BD Biosciences) and further analysed using FlowJo v10 OSX software (TreeStar Inc.). A total of  $1\text{--}2 \times 10^5$  cells were acquired.

For multispectral imaging, flow cytometry cells were inoculated with YFP-expressing bacteria as described for the protection assay. At t0 and t3, cells were detached and blocked with human IgG (Sigma), fixed and permeabilized using the Foxp3 staining buffer set (eBioscience). Then cells were stained with anti-CD107a-APC (LAMP1, H4A3, BD Biosciences) for 30 min on ice. After 15 min, DAPI (Sigma) was added. Images of 30 000 THP-1 cells were acquired with multispectral imaging flow cytometry using the ImageStreamx Mark II with the INSPIRE instrument controller software. The data were analysed using the IDEAS analysis software (Amnis, EMD Millipore), which allows an objective and unbiased analysis of thousands of images per sample on the single-cell level. The following masks were used: a spot mask was defined to extract only bright areas within the image of *S. aureus* YFP. The spot-to-cell background ratio was set at 4, and the radius was at 1, which implies a spot thickness of  $2x + 1$ . In order to quantify phagocytosis of *S. aureus* by THP-1 cells, an intracellular mask (erode mask) was created by subtracting 4 pixels from all edges of the bright-field mask.

### RNA isolation and quantitative reverse transcription PCR

For *in vitro* expression studies, bacteria from an overnight culture were diluted to an initial optical density (OD<sub>600</sub>) of 0.05 in RPMI containing 10% human serum and 10% FCS and incubated for 4 h (37°C, 200 r.p.m.). RNA was isolated as described (Geiger *et al.*, 2012). Briefly, bacteria were lysed in 1 ml of TRIzol reagent (Invitrogen Life Technologies, Karlsruhe, Germany) with 0.5 ml of zirconia-silica beads (0.1-mm diameter) in a high-speed

homogenizer (Savant Instruments, Farmingdale, NY). RNA was isolated as described in the instructions provided by the manufacturer of TRIzol, and DNA was removed using DNase I (recombinant, Roche).

To determine intracellular expression, bacterial RNA was isolated from culture supernatants (extracellular bacteria) just before addition of lysostaphin/gentamicin. Intracellular bacteria were harvested after lysostaphin/gentamicin treatment (t0), after 3 h (t3) or after 24 h (t24) post-phagocytosis. RNA isolation was performed as described including additional RNA purification after TRIzol treatment (Geiger *et al.*, 2012). Because *gyr* was not suitable as reference gene for intracellular bacteria, DNA was simultaneously isolated from all specimens following the instructions provided by the manufacturer of TRIzol. RNA was diluted (1:10), reverse transcribed and quantified via real-time PCR using the QuantiFast SYBR Green RNA Kit (Qiagen) (oligonucleotides listed in Table S2). Relative transcript abundance was calculated with the aid of the LightCycler software (Roche, Mannheim, Germany) using a logarithmic dilution series of one sample (JE2 grown to post-exponential growth phase) to generate a standard curve for each gene and to control for comparable efficiency. For *in vitro* specimens, relative quantification of the genes of interest was expressed in relation to the expression of the constitutive reference gene *gyrB* ( $\Delta\Delta C_t$  method). For intracellular expression analysis, DNA was quantified via real-time PCR using the QuantiFast SYBR Green PCR Kit (Qiagen). Relative quantification of genes was expressed in relation to *lukAB* DNA ( $\Delta\Delta C_t$  method). The means were calculated from at least three biological replicates.

### Ethics

Blood was taken from healthy donors in strict accordance with the institutional guidelines, according to the Declaration of Helsinki principles. The protocol was approved by the Institutional Review Board of the University of Tübingen. Written informed consent was received from all participants.

### Acknowledgements

The work was supported by grants from the Deutsche Forschungsgemeinschaft (TR34, project B1, and TR156, project A2) to C.W. and (TR34, project C11) to M.F., from the Landesgraduiertenförderung BW to L.M. and from the Medical Faculty of the University of Tübingen (Fortüne Program, 2068-0-0) to T.G. We thank Simone Poeschel, Natalya Korn and Vittoria Bisanzio for excellent technical assistance. The work was also supported by a grant from the Ministry of Science, Research and Arts of Baden Württemberg (Az.: SI-BW 01222-91) and the Deutsche Forschungsgemeinschaft DFG (German Research Foundation) (Az.: INST 2388/33-1).

### References

Agerberth, B., Charo, J., Werr, J., Olsson, B., Idali, F., Lindbom, L., *et al.* (2000) The human antimicrobial and chemotactic peptides LL-37 and alpha-defensins are expressed by specific lymphocyte and monocyte populations. *Blood* **96**: 3086–3093.

- Alonzo, F., 3rd, and Torres, V.J. (2014) The bicomponent pore-forming leucocidins of *Staphylococcus aureus*. *Microbiol Mol Biol Rev* **78**: 199–230.
- Bae, T., and Schneewind, O. (2006) Allelic replacement in *Staphylococcus aureus* with inducible counter-selection. *Plasmid* **55**: 58–63.
- Baur, S., Rautenberg, M., Faulstich, M., Grau, T., Severin, Y., Unger, C., *et al.* (2014) A nasal epithelial receptor for *Staphylococcus aureus* WTA governs adhesion to epithelial cells and modulates nasal colonization. *PLoS Pathog* **10**: e1004089.
- Berube, B.J., Sampedro, G.R., Otto, M., and Bubeck-Wardenburg, J. (2014) The psmalpha locus regulates production of *Staphylococcus aureus* alpha-toxin during infection. *Infect Immun* **82**: 3350–3358.
- Boisset, S., Geissmann, T., Huntzinger, E., Fechter, P., Bendridi, N., Possedko, M., *et al.* (2007) *Staphylococcus aureus* RNAIII coordinately represses the synthesis of virulence factors and the transcription regulator Rot by an antisense mechanism. *Genes Dev* **21**: 1353–1366.
- Cho, H., Jeong, D.W., Li, C., and Bae, T. (2012) Organizational requirements of the SaeR binding sites for a functional P1 promoter of the sae operon in *Staphylococcus aureus*. *J Bacteriol* **194**: 2865–2876.
- Cole, J., Aberdein, J., Jubrail, J., and Dockrell, D.H. (2014) The role of macrophages in the innate immune response to *Streptococcus pneumoniae* and *Staphylococcus aureus*: mechanisms and contrasts. *Adv Microb Physiol* **65**: 125–202.
- Coll, R.C., Robertson, A.A., Chae, J.J., Higgins, S.C., Munoz-Planillo, R., Inserra, M.C., *et al.* (2015) A small-molecule inhibitor of the NLRP3 inflammasome for the treatment of inflammatory diseases. **21**: 248–255.
- DuMont, A.L., Yoong, P., Day, C.J., Alonzo, F., 3rd, McDonald, W.H., Jennings, M.P., and Torres, V.J. (2013a) *Staphylococcus aureus* LukAB cytotoxin kills human neutrophils by targeting the CD11b subunit of the integrin Mac-1. *Proc Natl Acad Sci U S A* **110**: 10794–10799.
- DuMont, A.L., Yoong, P., Surewaard, B.G., Benson, M.A., Nijland, R., van Strijp, J.A., and Torres, V.J. (2013b) *Staphylococcus aureus* elaborates leukocidin AB to mediate escape from within human neutrophils. *Infect Immun* **81**: 1830–1841.
- DuMont, A.L., Yoong, P., Liu, X., Day, C.J., Chumbler, N.M., James, D.B., *et al.* (2014) Identification of a crucial residue required for *Staphylococcus aureus* LukAB cytotoxicity and receptor recognition. *Infect Immun* **82**: 1268–1276.
- Flannagan, R.S., Heit, B., and Heinrichs, D.E. (2015) Intracellular replication of *Staphylococcus aureus* in mature phagolysosomes in macrophages precedes host cell death, and bacterial escape and dissemination. *Cell Microbiol*. doi:http://dx.doi.org/10.1111/cmi.12527
- Fraunholz, M., and Sinha, B. (2012) Intracellular *Staphylococcus aureus*: live-in and let die. *Front Cell Infect Microbiol* **2**: 43.
- Geiger, T., Goerke, C., Mainiero, M., Kraus, D., and Wolz, C. (2008) The virulence regulator Sae of *Staphylococcus aureus*: promoter activities and response to phagocytosis-related signals. *J Bacteriol* **190**: 3419–3428.
- Geiger, T., Francois, P., Liebeke, M., Fraunholz, M., Goerke, C., Krismer, B., *et al.* (2012) The stringent response of



- Staphylococcus aureus* and its impact on survival after phagocytosis through the induction of intracellular PSMs expression. *PLoS Pathog* **8**: e1003016.
- Giese, B., Glowinski, F., Paprotka, K., Dittmann, S., Steiner, T., Sinha, B., and Fraunholz, M.J. (2011) Expression of delta-toxin by *Staphylococcus aureus* mediates escape from phago-endosomes of human epithelial and endothelial cells in the presence of beta-toxin. *Cell Microbiol* **13**: 316–329.
- Gonzalez-Juarbe, N., Gilley, R.P., Hinojosa, C.A., Bradley, K. M., Kamei, A., Gao, G., et al. (2015) Pore-forming toxins induce macrophage necroptosis during acute bacterial pneumonia. *PLoS Pathog* **11**: e1005337.
- Grosz, M., Kolter, J., Paprotka, K., Winkler, A.C., Schafer, D., Chatterjee, S.S., et al. (2013) Cytoplasmic replication of *Staphylococcus aureus* upon phagosomal escape triggered by phenol-soluble modulins alpha. *Cell Microbiol*. DOI: <http://dx.doi.org/10.1111/cmi.12233>.
- Ho, M.K., and Springer, T.A. (1982) Mac-1 antigen: quantitative expression in macrophage populations and tissues, and immunofluorescent localization in spleen. *J Immunol* **128**: 2281–2286.
- Holzinger, D., Gieldon, L., Mysore, V., Nippe, N., Taxman, D. J., Duncan, J.A., et al. (2012) *Staphylococcus aureus* Panton-Valentine leukocidin induces an inflammatory response in human phagocytes via the NLRP3 inflammasome. *J Leukoc Biol* **92**: 1069–1081.
- Jubrail, J., Morris, P., Bewley, M.A., Stoneham, S., Johnston, S.A., Foster, S.J., et al. (2016) Inability to sustain intraphagolysosomal killing of *Staphylococcus aureus* predisposes to bacterial persistence in macrophages. *Cell Microbiol* **18**(1): 80–96.
- Kitur, K., Parker, D., Nieto, P., Ahn, D.S., Cohen, T.S., Chung, S., et al. (2015) Toxin-induced necroptosis is a major mechanism of *Staphylococcus aureus* lung damage. *PLoS Pathog* **11**: e1004820.
- Kneidl, J., Löffler, B., Erat, M.C., Kalinka, J., Peters, G., Roth, J., and Barczyk, K. (2012) Soluble CD163 promotes recognition, phagocytosis and killing of *Staphylococcus aureus* via binding of specific fibronectin peptides. *Cell Microbiol* **14**: 914–936.
- Koziel, J., Maciag-Gudowska, A., Mikolajczyk, T., Bzowska, M., Sturdevant, D.E., Whitney, A.R., et al. (2009) Phagocytosis of *Staphylococcus aureus* by macrophages exerts cytoprotective effects manifested by the upregulation of antiapoptotic factors. *PLoS One* **4**: e5210.
- Kubica, M., Guzik, K., Koziel, J., Zarebski, M., Richter, W., Gajkowska, B., et al. (2008) A potential new pathway for *Staphylococcus aureus* dissemination: the silent survival of *S. aureus* phagocytosed by human monocyte-derived macrophages. *PLoS One* **3**: e1409.
- Lehar, S.M., Pillow, T., Xu, M., Staben, L., Kajihara, K.K., Vandlen, R., et al. (2015) Novel antibody–antibiotic conjugate eliminates intracellular *S. aureus*. *Nature* **527**: 323–328.
- Löffler, B., Hussain, M., Grundmeier, M., Bruck, M., Holzinger, D., Varga, G., et al. (2010) *Staphylococcus aureus* Panton-Valentine leukocidin is a very potent cytotoxic factor for human neutrophils. *PLoS Pathog* **6**: e1000715.
- Lowy, F.D. (1998) *Staphylococcus aureus* infections. *N Engl J Med* **339**: 520–532.
- Melehani, J.H., James, D.B., DuMont, A.L., Torres, V.J., and Duncan, J.A. (2015) *Staphylococcus aureus* leukocidin A/B (LukAB) kills human monocytes via host NLRP3 and ASC when extracellular, but not intracellular. *PLoS Pathog* **11**: e1004970.
- Nuxoll, A.S., Halouska, S.M., Sadykov, M.R., Hanke, M.L., Bayles, K.W., Kielian, T., et al. (2012) CcpA regulates arginine biosynthesis in *Staphylococcus aureus* through repression of proline catabolism. *PLoS Pathog* **8**: e1003033.
- Nygaard, T.K., Pallister, K.B., Ruzevich, P., Griffith, S., Vuong, C., and Voyich, J.M. (2010) SaeR binds a consensus sequence within virulence gene promoters to advance USA300 pathogenesis. *J Infect Dis* **201**: 241–254.
- Otto, M. (2012) MRSA virulence and spread. *Cell Microbiol* **14**: 1513–1521.
- Peschel, A., and Otto, M. (2013) Phenol-soluble modulins and staphylococcal infection. *Nat Rev Microbiol* **11**: 667–673.
- Queck, S.Y., Jameson-Lee, M., Villaruz, A.E., Bach, T.H., Khan, B.A., Sturdevant, D.E., et al. (2008) RNAlII-independent target gene control by the *agr* quorum-sensing system: insight into the evolution of virulence regulation in *Staphylococcus aureus*. *Mol Cell* **32**: 150–158.
- Rigby, K.M., and DeLeo, F.R. (2012) Neutrophils in innate host defense against *Staphylococcus aureus* infections. *Semin Immunopathol* **34**: 237–259.
- Shompole, S., Henon, K.T., Liou, L.E., Dziewanowska, K., Bohach, G.A., and Bayles, K.W. (2003) Biphasic intracellular expression of *Staphylococcus aureus* virulence factors and evidence for Agr-mediated diffusion sensing. *Mol Microbiol* **49**: 919–927.
- Spaan, A.N., Surewaard, B.G., Nijland, R., and van Strijp, J.A. (2013) Neutrophils versus *Staphylococcus aureus*: a biological tug of war. *Annu Rev Microbiol* **67**: 629–650.
- Surewaard, B.G., de Haas, C.J., Vervoort, F., Rigby, K.M., DeLeo, F.R., Otto, M., et al. (2013) Staphylococcal alpha-phenol soluble modulins contribute to neutrophil lysis after phagocytosis. *Cell Microbiol* **15**: 1427–1437.
- Tranchemontagne, Z.R., Camire, R.B., O'Donnell, V.J., Baugh, J., and Burkholder, K.M. (2015) *Staphylococcus aureus* strain USA300 perturbs acquisition of lysosomal enzymes and requires phagosomal acidification for survival inside macrophages. *Infect Immun* **84**: 241–253.
- van Kessel, K.P., Bestebroer, J., and van Strijp, J.A. (2014) Neutrophil-mediated phagocytosis of *Staphylococcus aureus*. *Front Immunol* **5**: 467.
- Ventura, C.L., Malachowa, N., Hammer, C.H., Nardone, G.A., Robinson, M.A., Kobayashi, S.D., and DeLeo, F.R. (2010) Identification of a novel *Staphylococcus aureus* two-component leukotoxin using cell surface proteomics. *PLoS One* **5**: e11634.
- Voyich, J.M., Braughton, K.R., Sturdevant, D.E., Whitney, A. R., Said-Salim, B., Porcella, S.F., et al. (2005) Insights into mechanisms used by *Staphylococcus aureus* to avoid destruction by human neutrophils. *J Immunol* **175**: 3907–3919.
- Weidenmaier, C., Goerke, C., and Wolz, C. (2012) *Staphylococcus aureus* determinants for nasal colonization. *Trends Microbiol* **20**: 243–250.



Wirtz, C., Witte, W., Wolz, C., and Goerke, C. (2009) Transcription of the phage-encoded Panton-Valentine leukocidin of *Staphylococcus aureus* is dependent on the phage life-cycle and on the host background. *Microbiology* **155**: 3491–3499.

Zurek, O.W., Nygaard, T.K., Watkins, R.L., Pallister, K.B., Torres, V.J., Horswill, A.R., and Voyich, J.M. (2014) The role of innate immunity in promoting SaeR/S-mediated virulence in *Staphylococcus aureus*. *J Innate Immun* **6**: 21–30.

### Supporting information

Additional Supporting Information may be found in the online version of this article at the publisher's web-site:

**Fig. S1.** Protection assay. THP1 cells inoculated with an MOI 50:1. CFU (A) cytotoxicity (B) and imaging (C) at time point T0.(D) Image stream analysis of intracellular bacteria at t0 and t3.

**Fig. S2.** Protection assay. hMDMs were inoculated with an MOI 50:1. Surviving bacteria were determined at time point t3 (A) and t24 (B). Bacterial numbers are expressed in relation to intracellular bacteria at t0. Cytotoxicity of hMDMs at t24 (C). Results are the mean of three experiments with macrophages from three independent donors. (D) Imaging of hMDMs infected with an MOI 50:1.

**Fig. S3.** Protection assay. Hela cells were inoculated with an MOI 50:1. CFU (A) determined at time point T0.

**Table S1.** Strains and plasmids.

**Table S2.** Oligonucleotides.

Accepted publication 2

**Human NACHT, LRR, and PYD domain–containing protein 3 (NLRP3)  
inflammasome activity is regulated by and potentially targetable through  
Bruton tyrosine kinase**

Xiao Liu, Tica Pichulik, Olaf-Oliver Wolz, Truong-Minh Dang, Andrea Stutz, Carly Dillen, Magno Delmiro Garcia, Helene Kraus, Sabine Dickhöfer, Ellen Daiber, Lisa Münzenmayer, Silke Wahl, Nikolaus Rieber, Jasmin Kümmerle-Deschner, Amir Yazdi, Mirita Franz-Wachtel, Boris Macek, Markus Radsak, Sebastian Vogel, Berit Schulte, Juliane Sarah Walz, Dominik Hartl, Eicke Latz, Stephan Stilgenbauer, Bodo Grimbacher, Lloyd Miller, Cornelia Brunner, Christiane Wolz and Alexander N. R. Weber

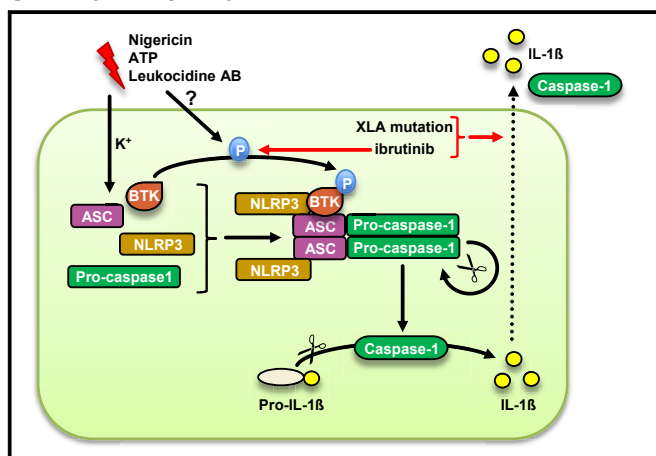
**J Allergy Clin Immunol (2017) Oct 140(4): 1054-1067**

# Human NACHT, LRR, and PYD domain-containing protein 3 (NLRP3) inflammasome activity is regulated by and potentially targetable through Bruton tyrosine kinase



Xiao Liu, MSc,<sup>a</sup> Tica Pichulik, MSc, PhD,<sup>a</sup> Olaf-Oliver Wolz, MSc, PhD,<sup>a</sup> Truong-Minh Dang, MSc, PhD,<sup>a</sup> Andrea Stutz, MSc,<sup>b</sup> Carly Dillen, MSc, PhD,<sup>c</sup> Magno Delmiro Garcia, MSc,<sup>a</sup> Helene Kraus, MD,<sup>d</sup> Sabine Dickhöfer, MTA,<sup>a</sup> Ellen Daiber, MSc,<sup>e</sup> Lisa Münzenmayer, MSc,<sup>e</sup> Silke Wahl, MSc, PhD,<sup>f</sup> Nikolaus Rieber, MD,<sup>g</sup> Jasmin Kümmerle-Deschner, MD,<sup>g</sup> Amir Yazdi, MD,<sup>h</sup> Mirita Franz-Wachtel, MSc, PhD,<sup>f</sup> Boris Macek, MSc, PhD,<sup>f</sup> Markus Radsak, MD,<sup>i</sup> Sebastian Vogel, MD,<sup>j</sup> Berit Schulte, MD,<sup>e</sup> Juliane Sarah Walz, MD,<sup>k</sup> Dominik Hartl, MD, PhD,<sup>g</sup> Eicke Latz, MD, PhD,<sup>b,l</sup> Stephan Stilgenbauer, MD, PhD,<sup>m</sup> Bodo Grimbacher, MD, PhD,<sup>d</sup> Lloyd Miller, MD, PhD,<sup>c</sup> Cornelia Brunner, MSc, PhD,<sup>n</sup> Christiane Wolz, MSc, PhD,<sup>e</sup> and Alexander N. R. Weber, MPhil, PhD<sup>a</sup> *Tübingen, Bonn, Freiburg, Mainz, and Ulm, Germany; Baltimore, Md; and Worcester, Mass*

## GRAPHICAL ABSTRACT



**Background:** The Nod-like receptor NACHT, LRR, and PYD domain-containing protein 3 (NLRP3) and Bruton tyrosine kinase (BTK) are protagonists in innate and adaptive immunity, respectively. NLRP3 senses exogenous and endogenous insults, leading to inflammasome activation, which occurs spontaneously in patients with Muckle-Wells syndrome; *BTK* mutations cause the genetic immunodeficiency X-linked agammaglobulinemia (XLA). However, to date, few proteins that regulate NLRP3 inflammasome activity in human primary immune cells have been identified, and clinically promising pharmacologic targeting strategies remain elusive. **Objective:** We sought to identify novel regulators of the NLRP3 inflammasome in human cells with a view to exploring interference with inflammasome activity at the level of such regulators.

From <sup>a</sup>the Interfaculty Institute for Cell Biology, Department of Immunology, <sup>c</sup>the Interfaculty Institute of Microbiology and Infection Medicine, and <sup>d</sup>Proteome Center Tübingen, University of Tübingen; <sup>b</sup>the Institute of Innate Immunity, University Hospital Bonn; <sup>e</sup>the Department of Dermatology, Johns Hopkins University, Baltimore; <sup>f</sup>the Centre of Chronic Immunodeficiency, University Hospital Freiburg; <sup>g</sup>the Department of Pediatrics I, <sup>h</sup>the Department of Dermatology, <sup>i</sup>the Department of Cardiology and Cardiovascular Diseases, and <sup>k</sup>Medical Hospital II (Department of Hematology and Oncology), University Hospital Tübingen; <sup>j</sup>Medical Hospital III, University Hospital Mainz; <sup>l</sup>the Division of Infectious Diseases & Immunology, University of Massachusetts, Worcester; <sup>m</sup>the Department of Internal Medicine III, Ulm University Hospital; <sup>n</sup>the Department of Otorhinolaryngology, Ulm University Medical Center. Supported by the Else-Kröner-Fresenius Stiftung (to A.N.R.W.), the University of Tübingen, and the University Hospital Tübingen (Fortüne Grant 2310-0-0 to X.L. and A.N.R.W.).

Disclosure of potential conflict of interest: X. Liu has received a PhD stipend from the China Scholarship Council. T. Pichulik is employed by Merck Serono GmbH. A. Stutz has received grants from the European Research Council and the German Research Council, is employed by IFM Therapeutics GmbH, and has received stock/stock options from IFM Therapeutics GmbH. E. Daiber, L. Münzenmayer, B. Schulte, and C. Wolz have received grants from Deutsche Forschungsgemeinschaft. J. Kümmerle-Deschner is a board member for Novartis, has consultant arrangements with and has received travel support from Novartis and Sobi, has received a grant from Novartis, and has received payment for lectures and development of educational presentations from Novartis. M. Radsak has received a grant from Deutsche Forschungsgemeinschaft

(CRC156/1 Project A05). E. Latz has consultant arrangements with IFM Therapeutics and Pfizer and has stock/stock options with IFM Therapeutics. S. Stilgenbauer has consultant arrangements with and has received payment for lectures and development of educational presentations from Janssen and Pharmacyclics. B. Grimbacher has received grants from BMBF, the European Union, Helmholtz, DFG, DLR, and DZIF; is employed by University College London and University Medical Center Freiburg; and has received payment for lectures from CSL Behring, Baxalta, and Biotest. L. Miller has consultant arrangements with Nantworks; has received grants from MedImmune, Regeneron Pharmaceuticals, Pfizer, and Nantworks; and has received stock/stock options from Noveome Biotherapeutics. A. N. R. Weber has received grants from Else-Kröner-Fresenius-Stiftung and Tübingen University Fortune Program and is employed by the University of Tübingen. The rest of the authors declare that they have no relevant conflicts of interest.

Received for publication April 8, 2016; revised December 23, 2016; accepted for publication January 11, 2017.

Available online February 16, 2017.

Corresponding author: Alexander N. R. Weber, MPhil, PhD, Interfaculty Institute for Cell Biology, Department of Immunology, University of Tübingen, Auf der Morgenstelle 15, 72076 Tübingen, Germany. E-mail: alexander.weber@uni.tuebingen.de.

The CrossMark symbol notifies online readers when updates have been made to the article such as errata or minor corrections

0091-6749/\$36.00

© 2017 American Academy of Allergy, Asthma & Immunology

<http://dx.doi.org/10.1016/j.jaci.2017.01.017>

**Methods:** After proteome-wide phosphoproteomics, the identified novel regulator BTK was studied in human and murine cells by using pharmacologic and genetic BTK ablation. **Results:** Here we show that BTK is a critical regulator of NLRP3 inflammasome activation: pharmacologic (using the US Food and Drug Administration–approved inhibitor ibrutinib) and genetic (in patients with XLA and *Btk* knockout mice) BTK ablation in primary immune cells led to reduced IL-1 $\beta$  processing and secretion in response to nigericin and the *Staphylococcus aureus* toxin leukocidin AB (LukAB). BTK affected apoptosis-associated speck-like protein containing a CARD (ASC) speck formation and caspase-1 cleavage and interacted with NLRP3 and ASC. *S aureus* infection control *in vivo* and IL-1 $\beta$  release from cells of patients with Muckle-Wells syndrome were impaired by ibrutinib. Notably, IL-1 $\beta$  processing and release from immune cells isolated from patients with cancer receiving ibrutinib therapy were reduced. **Conclusion:** Our data suggest that XLA might result in part from genetic inflammasome deficiency and that NLRP3 inflammasome–linked inflammation could potentially be targeted pharmacologically through BTK. (J Allergy Clin Immunol 2017;140:1054-67.)

**Key words:** *IL-1*, ibrutinib, Bruton tyrosine kinase, NLRP3, inflammasome, macrophage, X-linked agammaglobulinemia, *Staphylococcus aureus*, Muckle-Wells syndrome, inflammation

The human immune system relies on both innate and adaptive mechanisms to defend the host against infections (eg, from pathogenic bacteria, such as *Staphylococcus aureus*). Initial pathogen sensing by the innate immune system uses so-called pattern recognition receptors, such as Toll-like receptors (TLR) and Nod-like receptors (NLRs). Their activation by microbe-associated molecular patterns or invader-induced cellular insults leads to production of proinflammatory cytokines, which establish an inflammatory state and are critical in activating adaptive immunity.<sup>1</sup> Conversely to other cytokines, the important proinflammatory cytokine IL-1 $\beta$  is induced (“primed”) at the mRNA level but requires processing and secretion initiated by NLR activation.<sup>2</sup> NACHT, LRR, and PYD domain–containing protein 3 (NLRP3), the most prominent NLR member, is activated by various pathogenic, environmental, and endogenous stress-related insults and thus plays a role in both microbe-elicited and sterile inflammation.<sup>3,4</sup> On activation, NLRP3 assembles a so-called inflammasome complex, with the adaptor apoptosis-associated speck-like protein containing a CARD (ASC) and caspase-1 leading to caspase autoactivation and consequent proteolytic cleavage of pro-IL-1 $\beta$  into bioactive IL-1 $\beta$  for subsequent secretion.<sup>2</sup> The latter is a vital step in host defense against infectious agents, such as *S aureus*.<sup>5</sup> Interestingly, the IL-1 axis also has pathophysiologic significance, as exemplified by autoinflammatory periodic fever syndromes, such as Muckle-Wells syndrome (MWS), in which rare gain-of-function polymorphisms in NLRP3 lead to spontaneous inflammasome activation.<sup>4,6</sup> Furthermore, NLRP3 inflammasome activity has been implicated in a diverse range of complex human diseases, including gout, rheumatoid arthritis, type 2 diabetes, atherosclerosis, and neurodegeneration.<sup>4</sup> Thus the NLRP3 inflammasome can be considered an attractive therapeutic target, but efforts to develop inflammasome inhibitors have been hampered by incomplete knowledge regarding the identity and role of the molecular

#### Abbreviations used

APC:	Allophycocyanin
ASC:	Apoptosis-associated speck-like protein containing a CARD
BMDM:	Bone marrow–derived macrophage
BTK:	Bruton tyrosine kinase
CFU:	Colony-forming unit
DMSO:	Dimethyl sulfoxide
DSS:	Disuccinimidylyl suberate
FDA:	US Food and Drug Administration
FITC:	Fluorescein isothiocyanate
GFP:	Green fluorescent protein
HEK:	Human embryonic kidney
IVIG:	Intravenous immunoglobulin
KO:	Knockout
LukAB:	Leukocidin AB
M-CSF:	Macrophage colony-stimulating factor
MoMac:	Monocyte-derived macrophage
MWS:	Muckle-Wells syndrome
Ni-NTA:	Nitrilotriacetic acid
NLR:	Nod-like receptor
NLRP3:	NACHT, LRR, and PYD domain–containing protein 3
PE:	Phycocerythrin
PIP <sub>3</sub> :	Phosphatidylinositol (3,4,5)-trisphosphate
PMA:	Phorbol 12-myristate 13-acetate
PVL:	Panton Valentine Leukocidin
SCX:	Strong cation exchange
SH:	Src homology
shRNA:	Short hairpin RNA
TBP:	TATAA-box binding protein
TH:	Tec homology
TLR:	Toll-like receptor
Xid:	X-linked immunodeficiency
XLA:	X-linked agammaglobulinemia

steps involved in activating and regulating the inflammasome. Additionally, how the thus far proposed experimental inhibitors work is unclear. Thus identification of well-defined and therapeutically tractable regulatory proteins would be highly desirable.

Bruton tyrosine kinase (BTK) has long been regarded as a protagonist in adaptive antimicrobial defense because in the 1990s *BTK* mutations were discovered to be the cause for X-linked agammaglobulinemia (XLA),<sup>7</sup> the first described primary immunodeficiency.<sup>8</sup> XLA, also termed Bruton disease, is characterized by the almost complete absence of B cells and, consequently, antibodies, leading to severe immunodeficiency. More recently, BTK has also become appreciated as an important therapeutic target, such as in patients with B-cell malignancies, which are characterized by continuous B-cell receptor signaling through BTK.<sup>9</sup> Promising results have been obtained by using US Food and Drug Administration (FDA)–approved ibrutinib (PCI-32765), an orally administered, selective, and covalent BTK inhibitor, in patients with mantle cell lymphoma and chronic lymphocytic leukemia trials. Ibrutinib was both efficacious and well tolerated.<sup>10,11</sup>

*BTK* encodes a cytoplasmic protein tyrosine kinase expressed at high levels in B cells, controlling development, survival, differentiation, and activity from very early stages of development.<sup>12,13</sup> Additionally, *BTK* is also expressed in cells of the myeloid lineage, including macrophages, neutrophils, mast cells, and dendritic cells,<sup>1,2</sup> so that a contribution of the myeloid compartment to the overall phenotype of XLA cannot

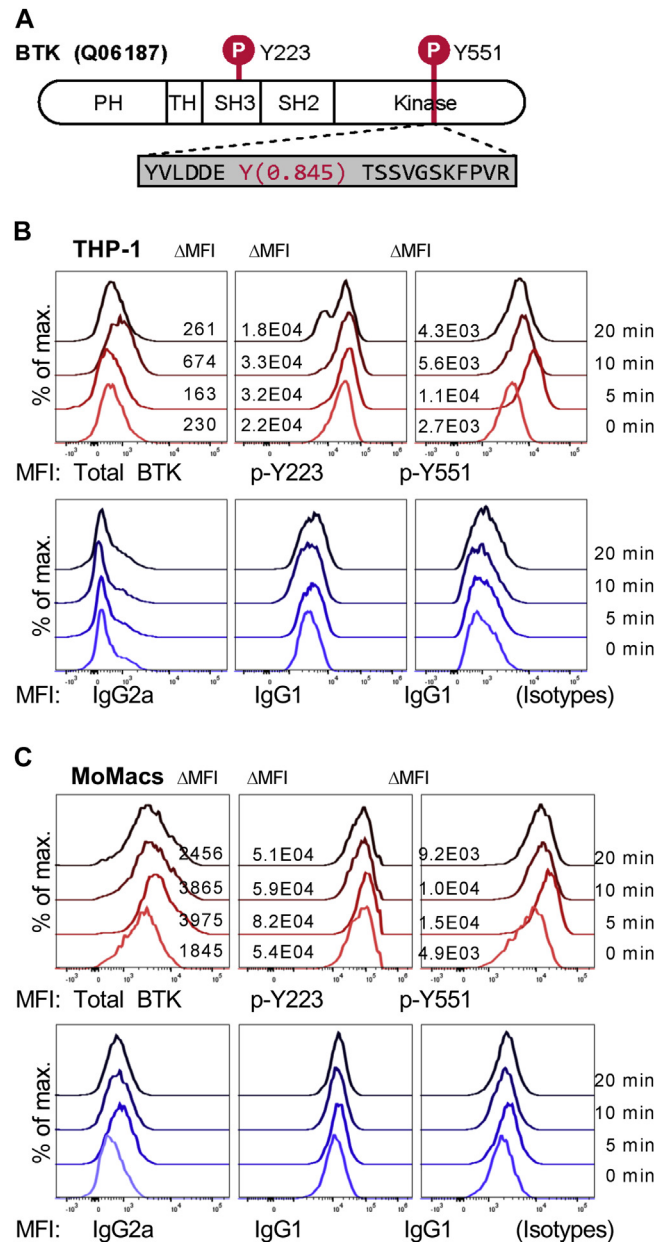


**FIG 1.** BTK is rapidly phosphorylated in myeloid cells on NLRP3 inflammasome triggering. **A**, Domains, phosphosites (red), and the regulated phosphopeptide (gray) in BTK. **B** and **C**, PMA-primed THP-1 cells (Fig 1, *B*) or LPS-primed human primary MoMacs (Fig 1, *C*) were stimulated with nigericin, stained, and analyzed by means of flow cytometry.  $\Delta$ MFI differences for each antibody-isotype pair are given. One representative of 3 experiments each is shown.

be excluded. BTK contains several functional domains (Fig 1, *A*): an N-terminal pleckstrin homology domain that binds phosphatidylinositol (3,4,5)-trisphosphate (PIP<sub>3</sub>), toward which BTK can translocate from the cytoplasm to PIP<sub>3</sub>-containing membranes; this property is abrogated in X-linked immunodeficiency (*Xid*) mutant mice (R28C mutation), which exhibit, like *Btk*-deficient (*Btk*<sup>-/-</sup>) mice, characteristics similar to the human XLA phenotype, although the phenotype is less severe.<sup>14</sup> Furthermore, BTK features central Tec homology (TH) and Src homology (SH) 3 and SH2 domains involved in protein-protein interactions and a C-terminal catalytically active kinase domain.

Two critical tyrosine phosphorylation sites, Y223 and Y551, play a pivotal role in BTK activation. Y551 is first transphosphorylated by upstream Syk or Lyn kinases, which promotes the catalytic activity of BTK with subsequent autophosphorylation at position Y223. A known downstream target of BTK is phospholipase C, but additional signaling pathways regulating cell proliferation, differentiation, and apoptosis have been shown to at least partially depend on BTK function.<sup>12,15</sup> Because XLA can be adequately managed clinically by means of regular administration of intravenous immunoglobulin (IVIG) and antimicrobial therapy,<sup>14</sup> a BTK-related defect in the humoral arm of the adaptive immune system has been taken as the primary immunologic explanation for the observed severe susceptibility of patients with XLA for pyogenic bacteria, including *S aureus*. However, it is known that immunity against these bacteria also strongly depends on innate immunity exerted by macrophages and neutrophils,<sup>16,17</sup> posing the question of whether XLA might also encompass BTK-related defects in the innate immune system.

We show here that BTK is a critical NLRP3 inflammasome regulator in both human subjects and mice and thus functions in a key innate immune process. Inflammasome activity was found to be impaired in *Btk*-deficient mice and patients with XLA, suggesting that the XLA phenotype might indeed encompass the first known primary genetic inflammasome deficiency. Furthermore, we demonstrated that pharmacologic BTK inhibition is able to block IL-1 $\beta$  release in a murine *in vivo* model, as well as human primary cells from healthy donors, patients with MWS, and ibrutinib-treated patients.

## METHODS

### Reagents

Nigericin, LPS, phorbol 12-myristate 13-acetate (PMA), and ionomycin were purchased from InvivoGen (San Diego, Calif), ATP from Sigma (St Louis, Mo), ibrutinib and CGI1746 were purchased from Selleckchem (Houston, Tex), recombinant GM-CSF or macrophage colony-stimulating factor (M-CSF) were purchased from PeproTech (Rocky Hill, NJ), and Ficoll was purchased from Merck Millipore (Temecula, Calif). Antibodies are listed in the [Methods](#) section in this article's Online Repository at [www.jacionline.org](http://www.jacionline.org).

### Study subjects and sample acquisition

All human subjects provided written informed consent in accordance with the Declaration of Helsinki, and the study was approved by local ethics committees. Detailed information regarding buffy coats and blood samples from healthy donors, patients with XLA, patients with MWS, and ibrutinib-treated patients is provided in the [Methods](#) section in this article's Online Repository.

### Isolation and stimulation of primary immune cells

PBMCs from healthy donors and patients with XLA were isolated from whole blood by using Ficoll density gradient purification, primed with 10 ng/mL LPS for 3 hours, and stimulated with 15  $\mu$ mol/L nigericin for 1 hour or instead with 50 ng/mL PMA and 1  $\mu$ mol/L ionomycin for 4 hours. PBMCs from patients with MWS were treated with 10 ng/mL LPS and 1 mmol/L ATP concomitantly with the indicated doses of ibrutinib or a dimethyl sulfoxide (DMSO) control for 4 hours. For macrophage differentiation, monocytes were purified by means of positive selection from PBMCs (from buffy coats using Ficoll purification) by using anti-CD14 magnetic beads (>90% purity; Miltenyi Biotec, Bergisch Gladbach, Germany) differentiated into macrophages (GM-CSF for 5 days). The resulting monocyte-derived macrophages (MoMacs) were primed with 300 ng/mL LPS for 3 hours and pretreated with



ibrutinib at 20 or 60  $\mu\text{mol/L}$  for 10 minutes before stimulation with 15  $\mu\text{mol/L}$  nigericin or the indicated amounts of leukocidin AB (LukAB) or Panton Valentine Leukocidin (PVL) for 1 hour. Further details are provided in the [Methods](#) section in this article's Online Repository.

### Plasmid constructs

ASC, NLRP3, and BTK coding sequences in pENTR clones were generated, as described by Wang et al<sup>18</sup> and in the [Methods](#) section in this article's Online Repository.

### Cell culture

All cells were cultured at 37°C and 5% CO<sub>2</sub> in Dulbecco modified Eagle medium or RPMI supplemented with 10% FCS, L-glutamine (2 mmol/L), penicillin (100 U/mL), and streptomycin (100  $\mu\text{g/mL}$ ); all from Life Technologies, Grand Island, NY), unless described otherwise in the [Methods](#) section in this article's Online Repository. THP-1-null cells (InvivoGen) stably express a nontargeting short hairpin RNA (shRNA) and are referred to throughout as THP-1 cells, unless otherwise stated. NLRP3-deficient THP-1 cells express an NLRP3-targeting shRNA (InvivoGen). iGluc THP-1<sup>19</sup> and THP-1 cells with stable BTK knockdown and corresponding mock cells<sup>20</sup> were kind gifts of V. Hornung, Gene Center, Munich, Germany, and R. Morita, Keio University School of Medicine, Tokyo, Japan, respectively. ASC-mCerulean expressing immortalized macrophages or THP-1 cells were described previously.<sup>21,22</sup>

### Mice and generation of bone marrow-derived macrophages

Bone marrow cells were isolated from femurs and tibiae of 8- to 12-week-old *Btk* knockout (KO)<sup>23</sup> mice and wild-type littermates (all on a C57BL/6 background) grown and differentiated with GM-CSF (M1 polarization) or M-CSF (M2 polarization). Cells were always counted and reseeded before *in vitro* assays to ensure equal cell numbers. For *in vivo* infections, 8-week-old C57BL/6 female mice (Jackson Laboratory, Bar Harbor, Me) were used. All mouse colonies were maintained in specific pathogen-free conditions. All animal experiments were approved by local authorities and done in accordance with local institutional guidelines and animal protection laws, as detailed in the [Methods](#) section in this article's Online Repository.

### Mass spectrometry

THP-1-null cells (InvivoGen) labeled to 97% with "light," "medium-heavy," and "heavy" SILAC medium were primed with 300 ng/mL PMA for 3 hours and left to rest overnight. The next day, the cells were detached and either left unstimulated (light) or stimulated with 15  $\mu\text{mol/L}$  nigericin for 5 (medium) or 10 (heavy) minutes. After washing with ice-cold PBS (containing phosphatase and protease inhibitors; Roche, Mannheim, Germany), cell pellets were snap-frozen and stored at -80°C before analysis. Further details on phosphopeptide enrichment, liquid chromatography-tandem mass spectrometry, and peptide identification are described in the [Methods](#) section in this article's Online Repository.

### ELISA

IL-1 $\beta$ , IL-2, TNF, and IFN- $\gamma$  levels in supernatants were determined by using half-area plates by ELISA (BioLegend, San Diego, Calif) with triplicate points on a standard plate reader.

### Quantitative RT-PCR

mRNA was isolated with the RNeasy Mini Kit on a Qiacube robot (both from Qiagen, Hilden, Germany) and transcribed to cDNA (High Capacity RNA-to-cDNA Kit; Life Technologies), and *Il1b*, *Nlrp3*, *IL1B*, and *NLRP3* mRNA expression was quantified in triplicates relative to TATAA-box binding protein (*Tbp/TBP*) by using TaqMan primers (Life Technologies) on a real-time cyclor (7500 fast; Applied Biosystems, Foster City, Calif), as described

by Wang et al.<sup>18</sup> Comparable cycle threshold values for *TBP* (data not shown) in all treatment groups confirmed equal cell numbers.

### ASC speck formation assay and confocal microscopy

Human embryonic kidney (HEK) 293T cells ( $4 \times 10^4$ ) were plated, transiently transfected, fixed with 100% methanol, and stained for nucleic acids (To-pro-3; Thermo Fisher, Waltham, Mass) and BTK-HA (anti-HA-Alexa Fluor 594). Immortalized *Nlrp3* KO macrophages overexpressing NLRP3-FLAG and ASC-mCerulean were pretreated with ibrutinib or CGI1745 (and a solvent control) for 10 or 60 minutes, respectively, before stimulation with either 5  $\mu\text{mol/L}$  nigericin (Life Technologies) for 60 minutes or 1 mmol/L Leu-Leu-OMe•HCl (Chem-Impex, Wood Dale, Ill) for 90 minutes and then fixed (4% formaldehyde), and nucleic acids were stained (DRAQ5; eBioscience, San Diego, Calif). Details regarding analysis with a Zeiss confocal microscope (Zeiss, Oberkochen, Germany) and image quantification with ImageJ (National Institutes of Health, Bethesda, Md) or CellProfiler software are described in the [Methods](#) section in this article's Online Repository.

### Pro-IL-1 $\beta$ and caspase-1 cleavage

Equal amounts of cells were primed and then stimulated in Opti-MEM medium (Gibco, Grand Island, NY). Proteins in supernatants were precipitated with methanol (VWR International, Radnor, Pa) and chloroform (Sigma, St Louis, Mo). Cells were lysed in RIPA buffer with protease inhibitors (Sigma). Where applicable, recombinant Protein A was added before precipitation to control for equal precipitation. Fifteen percent and 12% SDS-PAGE gels were used for protein from supernatants and whole-cell lysates, respectively, and probed with the indicated antibodies.

### Co-immunoprecipitation

HEK293T cells were transfected with CaPO<sub>4</sub> and lysed 48 hours later in buffer (50 mmol/L Tris [pH 8], 280 mmol/L NaCl, 0.5% NP-40, 0.2 mmol/L EDTA, 2 mmol/L EGTA, 10% glycerol, and 1 mmol/L dithiothreitol) with protease/phosphatase inhibitors (Roche). Cleared lysates were subjected to immunoprecipitation of the BTK-Protein A fusion protein with Dynabeads (M-280 Sheep Anti-Mouse IgG, Thermo Fisher Scientific). Washed beads were boiled in loading buffer and applied to SDS-PAGE and immunoblots (see the [Methods](#) section in this article's Online Repository).

### Crosslinking of ASC oligomers

THP-1 ASC-mCerulean cells ( $2 \times 10^6$ ) were primed with 300 ng/mL LPS for 2 hours and then treated with 60  $\mu\text{mol/L}$  ibrutinib for 1 hour and then 15  $\mu\text{mol/L}$  nigericin for 1 hour. After washing with PBS, cells were lysed, and lysates and pellets were cross-linked with disuccinimyl suberate (DSS; Thermo Scientific) and analyzed as described by de Almeida et al<sup>24</sup> and in the [Methods](#) section in this article's Online Repository.

### Flow cytometry and phospho-flow

Whole blood from healthy donors and patients with XLA was subjected to standard cell-surface staining and flow cytometry by using anti-CD3-fluorescein isothiocyanate (FITC), anti-CD19-Pacific Blue, anti-CD14-phycoerythrin (PE), and anti-CD11b-allophycocyanin (APC) by using a standardized protocol and identical flow cytometer settings for all donors. For phospho-flow analysis, the indicated primed cells were treated, fixed (Lyse/Fix Buffer; BD Biosciences, San Jose, Calif), and permeabilized with 1 mL of cold methanol; Fc receptors were blocked (Human AB serum); and cells were stained with anti-Btk (pY551) PE, anti-Btk (pY223) BV421, and anti-total BTK Alexa Fluor 647 antibodies (all from BD Biosciences). Corresponding isotype controls were from ImmunoTools (Friesoythe, Germany). For further details, see the [Methods](#) section in this article's Online Repository.

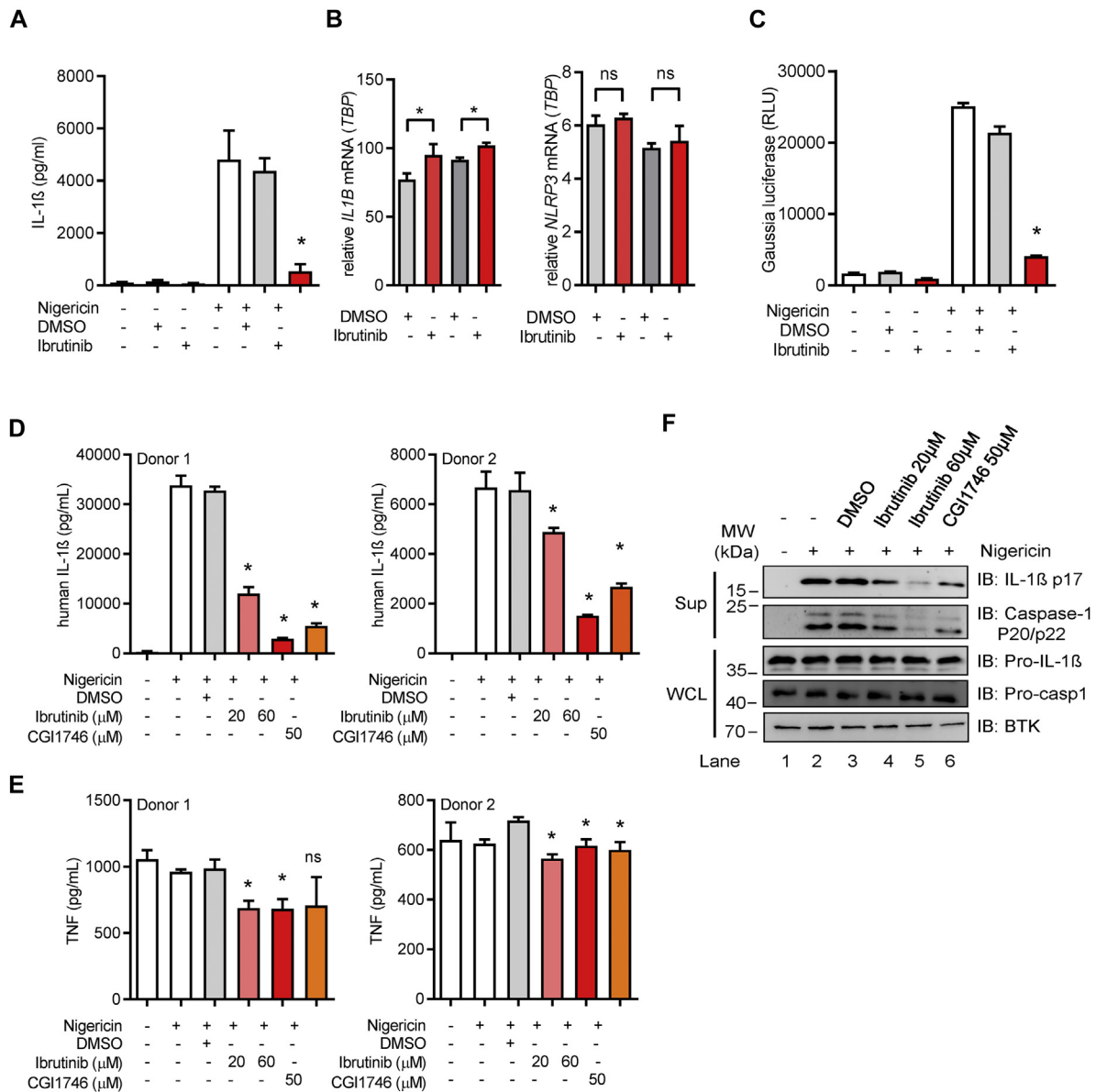


**FIG 2.** Ablation of BTK impairs NLRP3 inflammasome activity. **A**, IL-1 $\beta$  release from PMA-differentiated and nigericin-treated THP-1 cells preincubated with ibrutinib (60  $\mu$ mol/L). **B**, mRNA levels before nigericin addition. **C**, IL-1 $\beta$ -Gaussia levels assessed as in Bartok et al.<sup>19</sup> **D-F**, Cleaved IL-1 $\beta$  (Fig 2, **D** and **F**), caspase-1 (Fig 2, **F**), and TNF (Fig 2, **E**) from primed and nigericin-treated human primary MoMacs pretreated with DMSO (mock), ibrutinib, or CGI-1746 for 10 minutes. Numbers of experiments shown are as follows: 1 of 2 in Fig 2, **A**; 1 of 3 in Fig 2, **B**; and 1 of 3 in Fig 2, **C**. In Fig 2, **D** and **E**, 2 of 5 and in Fig 2, **F**, 1 of 3 donors are shown. Means + SDs are shown, and 2-sided Student *t* tests were used. Comparison with the DMSO control is shown in the gray bar. \**P* < .05. ns, Not significant.

### **S aureus strains**

The community-acquired methicillin-resistant *S aureus* strain USA300 bioluminescent derivative LAC::Lux was grown according to standard microbiological practice and used as indicated (see the [Methods](#) section in this article's Online Repository).

### **In vivo infection model**

Ibrutinib (6 mg/kg) in 3% DMSO and 5% corn oil in PBS or vehicle control was injected intravenously through the retro-orbital vein in anesthetized mice on days -1, 0, and 1 and topically on day 2 (6 mg/kg ibrutinib in 10  $\mu$ L of DMSO or vehicle control). On day 0, the dorsal backs of anesthetized mice (2% isoflurane) were shaved and injected intradermally with  $3 \times 10^7$  colony-forming units (CFU) of *S aureus* LAC::Lux; digitally imaged

on 1, 3, 7, 10, and 14, and total lesion size (in square centimeters) was analyzed by using ImageJ software with a millimeter ruler as a reference.

### **In vivo S aureus bioluminescent imaging**

Mice were anesthetized (2% isoflurane), *in vivo* bioluminescent imaging was performed (Lumina III IVIS; PerkinElmer, Waltham, Mass), and total flux (photons per seconds) within a circular region of interest measuring  $1 \times 10^3$  pixels was measured with Living Image software (PerkinElmer; limit of detection,  $2 \times 10^4$  photons/s).

### **Purification of LukAB and PVL**

The pQE30 vector (Qiagen) was used to produce recombinant His-tagged LukS-PV, LukF-PV, LukA, and LukB, as described in the [Methods](#) section in

this article's Online Repository, by using nitrilotriacetic acid (Ni-NTA) affinity chromatography. Protein stock solutions were dialyzed against PBS/50% glycerol, checked for endotoxin contamination (<0.25 EU/mL; Lonza, Basel, Switzerland), and stored at  $-20^{\circ}\text{C}$  until use. Single components were mixed in an equal molar ratio (IL-1 $\beta$  secretion was not detectable in stimulations using single components, data not shown).

### Data analysis and statistics

Data were analyzed with GraphPad Prism software (version 5.0; GraphPad Software, La Jolla, Calif) by using Student *t* tests and nonparametric Mann-Whitney *U* or Wilcoxon matched-pairs signed-rank tests, as indicated. All tests were 2-tailed unless stated otherwise. A *P* value of less than .05 was generally considered statistically significant and, even if considerably lower, is marked with an asterisk throughout the figures.

## RESULTS

### BTK is rapidly phosphorylated on NLRP3 inflammasome activation

To identify novel NLRP3 regulators of the NLRP3 inflammasome, we used unbiased triple SILAC phosphoproteomics<sup>25</sup> in primed THP-1 macrophages activated by the microbial potassium ionophore and NLRP3 agonist nigericin (see the [Methods](#) section). Differences in the phosphoproteome of unstimulated cells versus cells stimulated for 5 or 10 minutes to capture early NLRP3-proximal events included a phosphopeptide harboring the well-known BTK regulatory site tyrosine 551 (Y551; [Fig 1, A](#)), which was significantly upregulated 2.6-fold within 5 minutes of stimulation. Phospho-flow cytometric analysis in primed THP-1 cells ([Fig 1, B](#)) and primary human MoMacs ([Fig 1, C](#)) confirmed that although Y223 showed only subtle phosphorylation, Y551 was rapidly and robustly phosphorylated, peaking at 5 minutes after nigericin addition, indicating a rapid activation of BTK by an NLRP3 inflammasome trigger.

### Pharmacologic inhibition of BTK impairs inflammasome activation

To assess whether such BTK activation translated to an effect on inflammasome function, we investigated NLRP3-dependent IL-1 $\beta$  release. THP-1 cells pretreated with the FDA-approved inhibitor ibrutinib (PCI-32765) responded with reduced IL-1 $\beta$  release ([Fig 2, A](#)),<sup>19</sup> despite comparable *IL1B* and *NLRP3* mRNA levels ([Fig 2, B](#)). This was confirmed in so-called iGluc THP-1 cells, in which IL-1 $\beta$  release can be quantified in the form of a Gaussia Luciferase assay ([Fig 2, C](#)).<sup>19</sup> Importantly, in primary MoMacs pharmacologic BTK inhibition strongly decreased IL-1 $\beta$  levels ([Fig 2, D](#)), whereas the effect on TNF release was minor ([Fig 2, E](#)). Similar results were obtained with an additional specific BTK inhibitor, CGI1746 ([Fig 2, D and E](#)).<sup>26</sup> Generally, ibrutinib and CGI1746 did not show cytotoxicity at the concentrations used here, as assessed by means of simultaneous CCK8 viability testing (data not shown). Minor effects of BTK inhibition at the level of *IL1B* and *NLRP3* mRNA ([Fig 2, B](#)) or secreted TNF ([Fig 2, E](#)) suggest that the observed effect related directly to IL-1 $\beta$  processing rather than priming. Indeed, pro-IL-1 $\beta$  and caspase-1 processing in primary MoMacs was strongly reduced by both ibrutinib and CGI1746 ([Fig 2, F](#)). Collectively, this pharmacologic approach implicated BTK in NLRP3 inflammasome function.

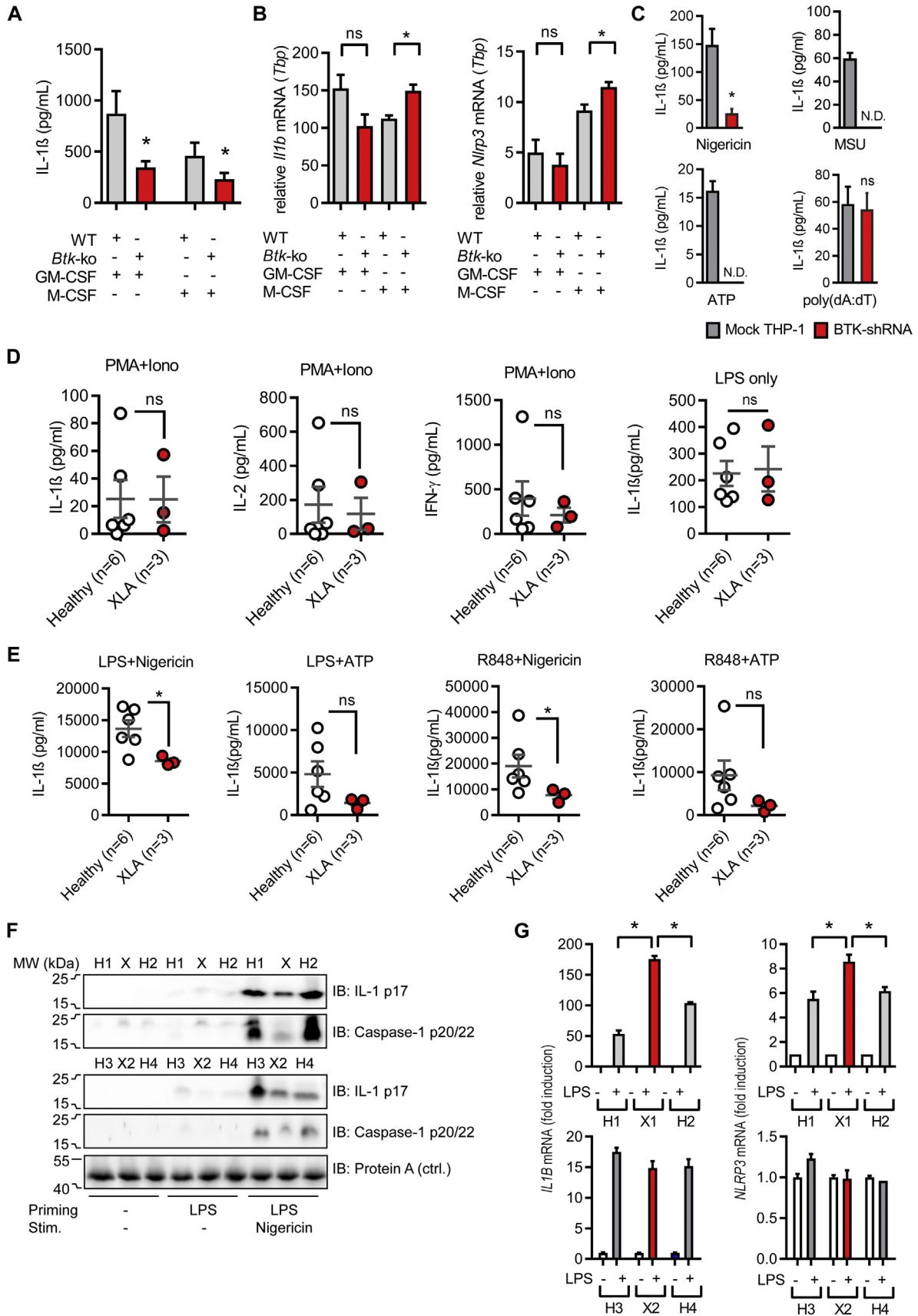
### Genetic ablation of BTK confirms a role in inflammasome activation

To rule out off-target effects and further confirm a role of BTK in NLRP3 inflammasome function, we used genetic ablation of BTK and first analyzed IL-1 $\beta$  release from bone marrow-derived macrophages (BMDMs) from *Btk* KO mice. Evidently, IL-1 $\beta$  release ([Fig 3, A](#)), but not *Il1b* or *Nlrp3* mRNA synthesis ([Fig 3, B](#)), was strongly reduced in BMDMs from GM-CSF- and M-CSF-differentiated *Btk* KO versus WT mice. THP-1 cells, in which BTK was constitutively downregulated by shRNA, showed reduced IL-1 release compared with the corresponding mock THP-1 cells in response to the NLRP3-dependent inflammasome stimuli nigericin, monosodium urate, and ATP but not the AIM2 inflammasome stimulus poly(dA:dT), see [Fig 3, C](#). More importantly, we were able to compare PBMCs from healthy donors and matched patients with XLA with genetically and cytometrically confirmed BTK deficiency (see the [Methods](#) section and [Fig E1](#) in this article's Online Repository at [www.jacionline.org](http://www.jacionline.org)). PMA plus ionomycin, a non-NLRP3-dependent<sup>27</sup> and poorly IL-1 $\beta$ -inducing stimulus, prompted IL-2 and IFN- $\gamma$  release from T cells, in which BTK is not expressed and thus is functionally irrelevant ([Fig 3, D](#)),<sup>28</sup> thus indicating similar overall cellular viability in PBMC preparations from healthy donors and those with XLA. However, IL-1 $\beta$  release in response to NLRP3 activation by nigericin was substantially lower in PBMCs of patients with XLA compared with those of healthy donors ([Fig 3, E](#)), irrespective of whether priming conducted with R848 or ATP was used as an alternative NLRP3 trigger ([Fig 3, E](#)). Although differences in IL-1 $\beta$  levels in response to ATP were not statistically significant because of donor-to-donor variation, a clear trend toward lower IL-1 $\beta$  levels was clearly discernible. As expected, secreted mature caspase-1 and IL-1 $\beta$  levels were also reduced in PBMCs from patients with XLA compared with those from healthy donors ([Fig 3, F](#)), even though LPS-primed *IL1B* and *NLRP3* mRNA levels at the time of NLRP3 agonist addition were higher ([Fig 3, G](#)). Thus genetic ablation of BTK activity in both mice and human subjects impairs NLRP3 inflammasome activity and confirms a role for BTK in the NLRP3 inflammasome.

### BTK interacts directly with ASC and NLRP3 and promotes inflammasome formation

Given the early phosphorylation of BTK and its effect on downstream caspase-1 cleavage, we speculated whether BTK might directly interact with the core inflammasome components ASC and NLRP3. Indeed, when expressed in HEK293T cells, BTK interacted with both ASC ([Fig 4, A](#)) and NLRP3 ([Fig 4, B](#)) in co-immunoprecipitations. Additionally, overexpression-induced ASC speck formation, a surrogate visual readout for inflammasome formation,<sup>22</sup> in HEK293T cells transfected with ASC-green fluorescent protein (GFP) was significantly enhanced by BTK coexpression ([Fig 4, C](#); quantified in [Fig 4, D](#)). Interestingly, a spheroid ASC signal typical for ASC specks was surrounded by a spherical localization of BTK (see [Fig E2, A](#), in this article's Online Repository at [www.jacionline.org](http://www.jacionline.org)). In agreement with earlier experiments, ibrutinib ([Fig 4, E and F](#)) and CGI1746 (see [Fig E2, B](#)) reduced ASC speck formation in stably ASC-mCerulean-expressing murine macrophages<sup>22</sup> when treated with nigericin or the NLRP3 trigger Leu-Leu-OME, a lysosomal destabilizing agent.<sup>29</sup> Furthermore, the potential for ASC





cross-linking/oligomerization<sup>24</sup> in THP-1 cells stably expressing ASC-mCerulean was enhanced by nigericin stimulation but sensitive to ibrutinib (Fig 4, G). Collectively, BTK appears to directly influence inflammasome activation at the level of NLRP3 and ASC.

### BTK functionality is required for full *S aureus* toxin-elicited inflammasome activity

BTK-deficient patients with XLA experience recurrent bacterial infection with pathogens, including *S aureus*. Based on the observation that nigericin- and ATP-triggered IL-1 $\beta$  processing and secretion were impaired in patients with XLA (Fig 3), we wondered whether IL-1 $\beta$  release induced by the *S aureus* toxins, PVL, and LukAB, which both activate NLRP3 (Fig 5, A, and see Fig E3 in this article's Online Repository at [www.jacionline.org](http://www.jacionline.org)),<sup>30,31</sup> also required BTK. Indeed, BTK inhibition (Fig 5, B) and stable shRNA-mediated *BTK* knockdown (Fig 5, C) in THP-1 cells and ibrutinib treatment in primary MoMacs (Fig 5, D) strongly reduced IL-1 $\beta$  release in response to PVL and LukAB. Additionally, in LPS-primed PBMCs from patients with XLA, LukAB led to reduced IL-1 $\beta$  cleavage compared with that seen in healthy donors (Fig 5, E). Because LPS does not occur in gram-positive bacteria and *S aureus* instead activates TLR2,<sup>32</sup> the TLR2 agonist Pam<sub>3</sub>CSK<sub>4</sub> was also used for priming instead of LPS. Again, TLR2-primed PBMCs from patients with XLA showed reduced levels of cleaved IL-1 $\beta$  compared with those from healthy donors in response to LukAB (Fig 5, E). These genetic and pharmacologic *in vitro* results suggest that *in vivo* BTK might play a role in NLRP3 inflammasome/IL-1 $\beta$ -dependent host defense, as well as pathophysiological autoinflammation.

### BTK inhibition negatively affects IL-1 $\beta$ -dependent *S aureus* clearance *in vivo* and blocks IL-1 $\beta$ release in patients with MWS and ibrutinib-treated patients with cancer *ex vivo*

We next explored the possibility of whether BTK inhibition would affect the outcome of IL-1 $\beta$ -dependent infection in an *in vivo* setting. Murine experimental models of *S aureus* skin infection dependent on Nlrp3/ASC-inflammasome-dependent IL-1 $\beta$  for clearance.<sup>5,33</sup> Therefore we applied ibrutinib treatment to C57BL/6 mice intradermally infected with a bioluminescent community-acquired methicillin-resistant *S aureus* strain (USA300 LAC::*lux*).<sup>33</sup> Ibrutinib-treated mice showed increased bacterial burden, as measured based on *in vivo* bioluminescent signals (Fig 6, A and B) compared with vehicle-treated control mice. They also had larger skin lesions (Fig 6, C, and see Fig E4 in this article's Online Repository at [www.jacionline.org](http://www.jacionline.org)). Although additional *in vivo* effects of ibrutinib cannot be

ruled out, our data suggest a relevance for BTK in inflammasome-related host defense *in vivo*.

Our results thus far posed the question of whether BTK might be a plausible point of therapeutic intervention to target the many human inflammasome/IL-1 $\beta$ -related inflammatory processes or disorders.<sup>4</sup> MWS is an autoinflammatory disease caused by gain-of-function mutations in the NLRP3 gene *CIAS* and is characterized by excessive IL-1 $\beta$  release compared with that seen in healthy donors (see Fig E6 in this article's Online Repository at [www.jacionline.org](http://www.jacionline.org)).

To explore whether this phenotype could be ameliorated by BTK inhibition, we triggered IL-1 $\beta$  release by LPS (no second stimulus required because of NLRP3 autoactivation, see Prota et al<sup>34</sup>) in PBMCs from 4 patients with MWS in the absence or presence of ibrutinib. As shown in Fig 6, D, LPS-dependent IL-1 $\beta$  and caspase-1 release was strongly reduced for all assessed patients, and the level of inhibition corresponded to the dose of ibrutinib (Fig 6, E). General toxicity or anti-inflammatory effects were ruled out by using cytokine release and viability tests (data not shown). Thus pharmacologic BTK inhibition blocked excessive IL-1 $\beta$  release that characterizes the autoinflammatory MWS. To gain a first insight into whether application of ibrutinib in human patients would affect inflammasome activity *in vivo*, we stimulated PBMCs from male patients with cancer receiving ibrutinib daily *ex vivo* and compared their ability to process or release IL-1 $\beta$  or caspase-1 in response to the NLRP3 triggers nigericin, ATP, or both by means of immunoblotting or ELISA, respectively (Fig 6, G and F), whereas TNF release was comparable (Fig 6, H). Evidently, *in vivo* application of ibrutinib specifically correlated with reduced *ex vivo* IL-1 $\beta$  and caspase-1 processing and lower IL-1 $\beta$  release in these patients compared with subjects not receiving ibrutinib. Collectively, our data suggest that BTK inhibitors might block the NLRP3 inflammasome *in vivo* in patients.

## DISCUSSION

In the present work we show that BTK is a critical regulator of NLRP3 inflammasome activation in both human subjects and mice. This is illustrated by significant NLRP3 inflammasome loss-of-function phenotypes observed in functionally *BTK*-deficient cells from patients and mice and effects of pharmacologic inhibition of BTK in an *in vivo* *S aureus* infection model, which is congruent with inefficient bacterial control evidenced in human patients with XLA and *Xid* or *Nlrp3*<sup>-/-</sup> mice.<sup>12,33</sup> Additionally, our molecular analysis suggests that BTK regulates (and that consequently BTK inhibitors might act on) the inflammasome proximally to NLRP3 and ASC, as evidenced by interaction and colocalization of BTK with these inflammasome components. Furthermore, we



**FIG 3.** Genetic ablation of BTK in primary immune cells impairs NLRP3-mediated IL-1 $\beta$  release. **A**, IL-1 $\beta$  release from equal numbers of GM-CSF- or M-CSF-differentiated, LPS-primed, and nigericin-treated WT or *Btk* KO BMDMs (means + SEMs). **B**, quantitative RT-PCR (mean + SEM) before nigericin addition. **C**, IL-1 $\beta$  release from primed THP-1 cells expressing either a nontargeting (mock) or BTK shRNA. **D** and **E**, IL-1 $\beta$ , IL-2, and IFN- $\gamma$  release from LPS-primed PBMCs from male patients with XLA and age-matched male healthy donors (mean  $\pm$  SEM of biological replicates). Each symbol represents 1 donor. **F** and **G**, Supernatant immunoblot (Fig 3, F) or quantitative RT-PCR relative to *TBP* (mean + SD; Fig 3, G) of the stimulated PBMCs. Pooled data from 3 mice (biological replicates) per group (1 of 2 identical experiments) in Fig 3, A and B, and from 6 versus 3 donors (biological replicates; mean + SEM in gray) in Fig 3, D and E, are shown, respectively. In Fig 3, C, 1 representative of 2 experiments and in Fig 3, F and G, 2 versus 4 donors are shown, respectively. In Fig 3, A-C, G, and H, the Student *t* test and in Fig 3, D and E, a Mann-Whitney *U* test was used. \**P* < .05. N.D., Not detected; ns, not significant.

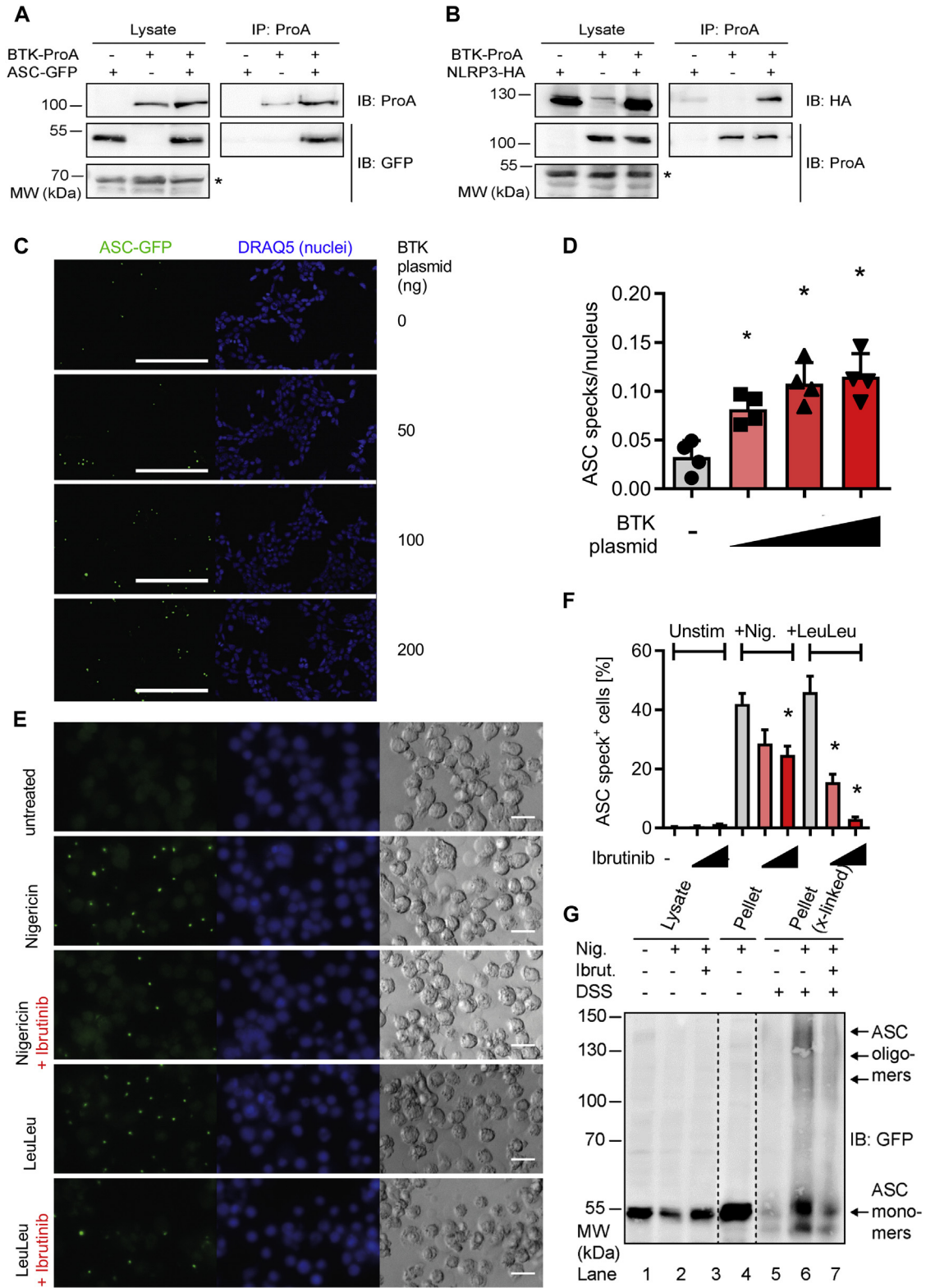


**FIG 4.** BTK directly interacts with ASC and NLRP3 and promotes inflammasome formation. **A** and **B**, Immunoblot (IB) of transfected HEK293T cells. \*Nonspecific loading control. **C** and **D**, Confocal microscopy of fixed and stained transfected HEK293T cells (scale bar = 200 μm; Fig 4, C) and quantification thereof (Fig 4, D). **E** and **F**, Representative fluorescence microscopy images of ASC specks (Fig 4, E) and quantification thereof (Fig 4, F) from immortalized *Nlrp3* KO macrophages overexpressing NLRP3-FLAG ASC-mCerulean. Scale bar = 20 μm. **G**, DSS cross-linking of ASCs from primed and nigericin-treated THP-1-ASC-mCerulean cells. In Fig 4, A-D, 1 of 2 and in Fig 4, E and G, 1 of 3 identical experiments is shown. Fig 4, F, shows the combined analysis of 3 experiments. In Fig 4, D and F, the Student *t* test was used. \**P* < .05.

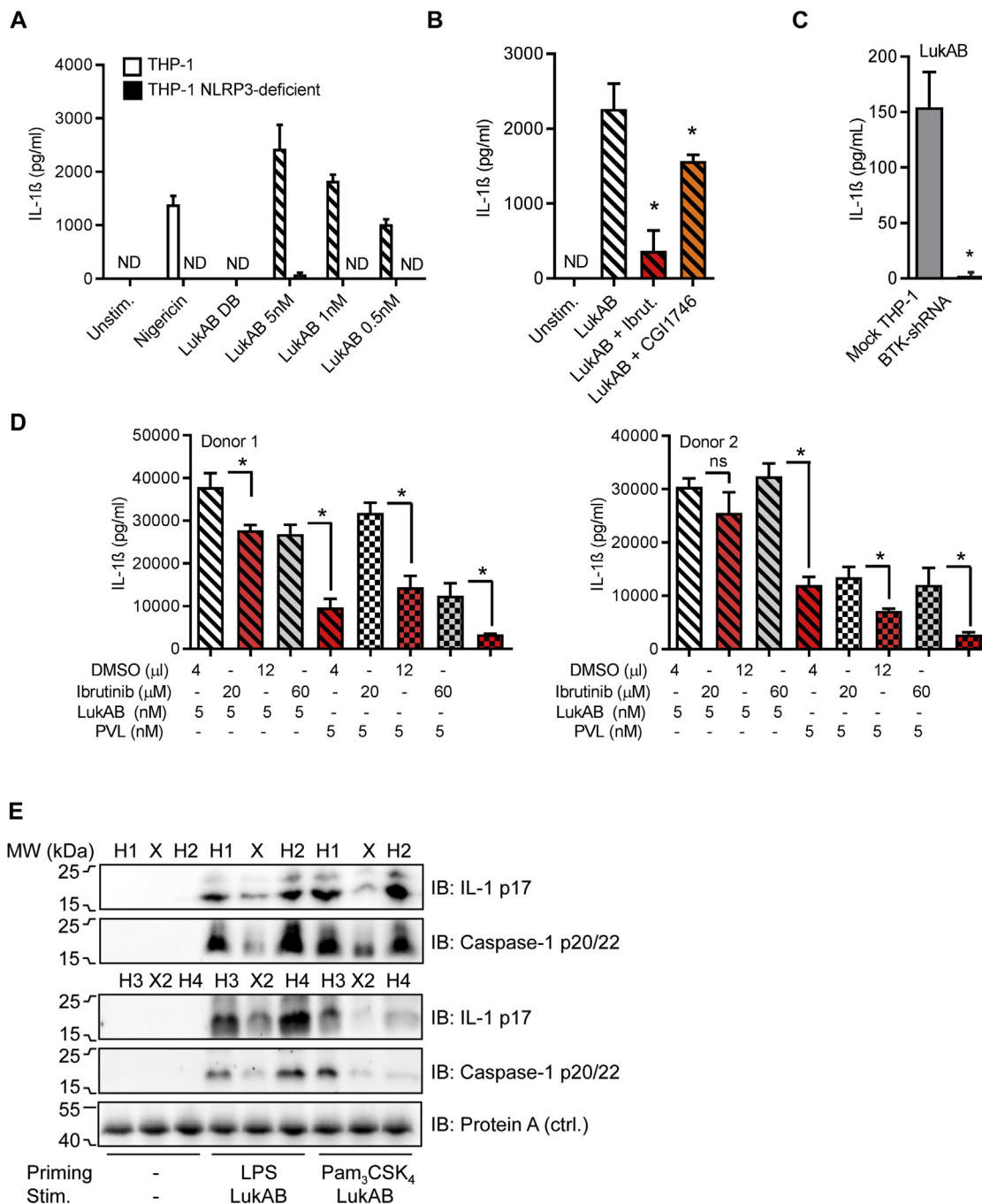


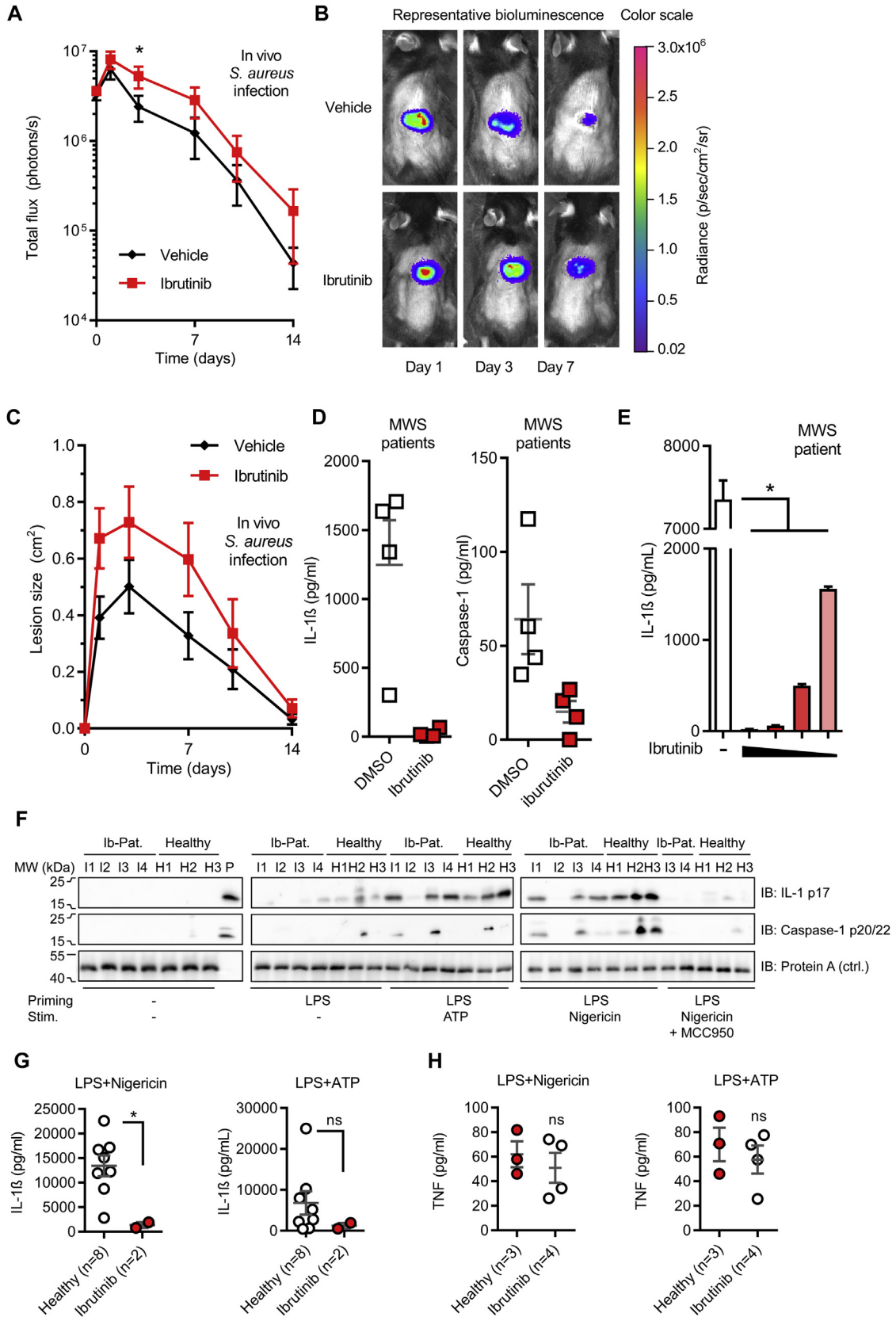
**FIG 5.** BTK functionality is required for full *S aureus* toxin-elicited inflammasome activity. **A** and **B**, IL-1 $\beta$  release from PMA-differentiated null (control; Fig 5, **A** and **B**) or NLRP3-deficient (Fig 5, **A**) THP-1 inhibitor-pretreated (Fig 5, **B**, only), with stimulation as indicated. **DB**, LukAB dialysis buffer. **C**, Primed THP-1 cells expressing either a nontargeting (mock) or BTK shRNA were stimulated as indicated. **D**, Primed human primary MoMacs analyzed as in Fig 2, **E** and **F**, but treated with LukAB or PVL. **E**, Supernatant immunoblot of LPS- or Pam<sub>3</sub>CSK<sub>4</sub>-primed PBMCs from male patients with XLA and age-matched male healthy donors. In Fig 5, **A-C**, 1 of 2 and in Fig 5, **D** and **E**, 2 of 2 identical experiments are shown. In all graphs means + SDs are shown, and the Student *t* test was used. \**P* < .05. *ND*, Not detectable; *ns*, not significant.

demonstrate that in human primary macrophages (as well as their murine counterparts), BTK inhibition impaired IL-1 $\beta$  processing and release. In blood samples from patients with MWS, BTK inhibition strongly reduced this pathologically relevant inflammatory event. Notably, reduced IL-1 $\beta$  secretion was also observed in PBMCs from patients receiving ibrutinib *in vivo*.

These findings represent considerable advances regarding our understanding of the NLRP3 inflammasome, its therapeutic tractability, and BTK-related immunodeficiency, which warrant further discussion.

First, our data significantly expand on the thus far known roles of BTK and highlight that BTK not only critically contributes to





adaptive immunity but is in fact also a key player in innate immunity. Although few reports described a role for BTK in TLR<sup>35,36</sup> and Fc receptor signaling,<sup>26</sup> recruitment,<sup>37</sup> and development<sup>13</sup> in myeloid cells, the abovementioned insights were almost exclusively gained for the murine system or human cell lines. Whether BTK played a prominent role in human innate immunity thus remained somewhat unaddressed. It is also for the murine system that Ito et al<sup>20</sup> recently provided a first glimpse into a possible role for BTK in inflammasome activation. In this study BTK loss or inhibition in murine cells reduced IL-1 $\beta$  release. Our study in primary cells from healthy volunteers, patients with XLA, patients with MWS, and ibrutinib-treated patients now provides evidence that BTK is indeed a key regulator of the NLRP3 inflammasome in human subjects. How the observed residual amounts of IL-1 $\beta$  released from PBMCs from patients with XLA (Fig 3, D and E) can be reduced further (Fig 6, F, and see Fig E5 in this article's Online Repository at [www.jacionline.org](http://www.jacionline.org)) by an NLRP3 inhibitor with unknown target, MCC950,<sup>38</sup> warrants further exploration. It seems plausible that the *BTK* mutations identified in the patients studied here (see the Methods section in this article's Online Repository) display low residual activity<sup>39</sup> or expression of BTK that is sufficient for low inflammasome activity but too low to support the development of B cells, thus leading to clinical XLA; alternatively, BTK might only be required for one of potentially several NLRP3 inflammasome pathways.<sup>40</sup>

Nevertheless, our study supports the notion that BTK is a master regulator of myeloid cell functions spanning the entire functional spectrum from development through initial pathogen recognition by TLRs to initiation of inflammation through the NLRP3 inflammasome to postadaptive functions involving the response to antibodies bound through Fc receptors. The versatility of BTK to participate in these diverse processes is staggering and clearly warrants further exploration, not least to investigate cross-talk between the different signaling pathways, as well as to closely define how pharmacologic inhibition of BTK affects these different BTK-dependent immune functions.

Indeed, this is necessary to explore potential therapeutic opportunities that could be deduced from the observation that BTK inhibitors reduce NLRP3-dependent IL-1 $\beta$  release. Human macrophages, which can be effectively blocked in their ability to release IL-1 $\beta$ , as shown here, have been seen as primary mediators in many inflammatory disorders. For example, in experimental mouse models for atherosclerosis, cholesterol crystals contribute to disease progression in a macrophage/IL-1-dependent manner.<sup>41</sup> Similarly, in Alzheimer models amyloid- $\beta$ -triggered neuroinflammation depends on NLRP3.<sup>42</sup> Targeting the IL-1 axis through BTK can have

considerable advantages over previously proposed strategies: for example, although proposed inhibitors, such as MCC950,<sup>38</sup> are highly effective, the precise mechanism of action and the actual molecular target seem unclear at current. Biological-based anti-IL-1 therapies, though proved and FDA approved, target inflammasome-distal events. Targeting the inflammasome through BTK might eventually overcome some of these disadvantages by focusing on a well-studied and well-defined molecular target, BTK, and an NLRP3 inflammasome (and thus caspase/IL-1 $\beta$ -processing) proximal event. Use of ibrutinib in treating human patients with MWS (Fig 6), acute stroke (as hinted to by Ito et al<sup>20</sup>), or atherosclerosis should be considered and is encouraged by the observed good tolerability and efficacy of BTK inhibitors in the cancer setting,<sup>10,11</sup> primary human immune cells (Figs 2-6), and even human platelets, as suggested by our most recent study.<sup>43</sup> The data shown in Fig 6, F and G, suggest that BTK inhibition can be considered for blocking inflammasome activity *in vivo*. Even if administration would have to be temporary (eg, to avoid adverse effects from infection, see below), a temporary blockade of the IL-1 axis might help break a vicious cycle of chronic inflammation.

For effective therapeutic exploitation, additional details need to be clarified. First, as with any pharmacologic inhibitor, off-target effects (ie, the possibility of other kinases apart from BTK being affected by ibrutinib or other "BTK" inhibitors) cannot be entirely ruled out and require further investigation. Second, although a direct interaction with NLRP3 and ASC has been demonstrated by us (Fig 4), it remains to be explored how exactly BTK participates in the inflammasome activation process. Ito et al<sup>20</sup> rule out an effect of Ca<sup>2+</sup> signaling, and by measuring additional cytokine or transcript levels, we can rule out that BTK ablation primarily affects caspase-1 or IL-1 $\beta$  cleavage or release through TLR-dependent priming, although this would have been conceivable because of the role of BTK in TLR signaling.<sup>35</sup> The SH2 and SH3 domains found in BTK are well-known motifs for protein-protein interactions, so that BTK might act as a scaffold protein for inflammasome nucleation or extension. However, because ibrutinib targets BTK kinase activity, it seems unlikely that BTK only acts as a molecular scaffold but rather participates as a kinase, possibly at the level of ASC phosphorylation.<sup>20</sup> The verification of ASC as a BTK interactor and substrate should be the subject of future studies.

Another important question to be addressed is what links the exposure of cells to upstream NLRP3 agonists with BTK activation. Studying the role of the pleckstrin homology domain, a common motif for receptor/membrane engagement, or different reported gain- or loss-of-function mutants, such as the *Xid* loss-of-function mutation (R28C), in the assays described here

**FIG 6.** BTK inhibition negatively affects IL-1 $\beta$ -dependent *S aureus* clearance *in vivo* and blocks excessive IL-1 $\beta$  release in patients with MWS *ex vivo*. **A** and **C**, Mean  $\pm$  SEM total flux (photons/s; Fig 6, A) and mean  $\pm$  SEM total lesion size (in square centimeters; Fig 6, C) from C57BL/6 mice (n = 10 per group) treated with vehicle or ibrutinib and inoculated intradermally with bioluminescent methicillin-resistant *S aureus* USA300 LAC::lux. **B**, Representative *in vivo* bioluminescent signals. **D**, LPS-induced IL-1 $\beta$  or caspase-1 release from LPS-stimulated PBMCs<sup>34</sup> from a patient with MWS. **E**, Ibrutinib was titrated from 60 to 30 to 15 to 7.5  $\mu$ mol/L for 2 patients with MWS; 1 patient is shown (mean  $\pm$  SD). **F-H**, IL-1 $\beta$ , caspase-1, TNF, and/or IL-6 cleavage and/or release (mean  $\pm$  SEM of biological replicates, each symbol represents 1 donor) from PBMCs from male patients with cancer receiving daily ibrutinib and male healthy donors. *P*, Blotting control. Pooled data from 4 versus 3 donors in Fig 6, F, and from 8 versus 2 donors in Fig 6, G, or 3 versus 4 donors in Fig 6, H, are shown (means  $\pm$  SEMs of biological replicates, each symbol represents 1 donor). In Fig 6, A, C, G, and H, the Mann-Whitney *U* test; in Fig 6, D, the Wilcoxon matched-pairs signed-rank test; and in Fig 6, E, the Student *t* test was used. \**P* < .05. ns, Not significant.

might shed light on these important mechanistic questions in the future.

BTK acting as a novel inflammasome component would make any genetic BTK insufficiency also a genetically determined functional NLRP3 inflammasome deficiency. Thus our work supports the notion that the BTK-mediated human XLA phenotype might represent the first reported genetic functional NLRP3 inflammasome deficiency in human subjects. Given that *S aureus* toxin-mediated release is BTK dependent (Fig 5) and that BTK-dependent IL-1 $\beta$  production is required for bacterial clearance in skin *S aureus* infection in mice (Fig 6, A-C),<sup>33</sup> human inflammasome-deficient patients would be expected to show a susceptibility to pyogenic bacteria, such as *S aureus*. This is indeed a clinical feature in patients with XLA.<sup>12,14</sup> It can be speculated whether high-dose IVIG and antibiotic therapy applied routinely to patients with XLA might mask a simultaneous NLRP3 inflammasome deficiency contributing to bacterial susceptibility in patients with XLA. Of note, a certain fraction of patients in ongoing clinical trials with ibrutinib show moderate-to-severe infections with the same pathogens frequently encountered in patients with XLA despite unaltered antibody levels (ie, a remaining adaptive/humoral defense component).<sup>10,11</sup> Potentially, this temporary bacterial susceptibility conferred by BTK inhibition might be significantly attributable to temporary inflammasome inhibition. Further studies should address this possibility in ongoing clinical trials with ibrutinib and explore the notion of a potential inflammasome deficiency to contribute to immunodeficiency in patients with XLA.

Collectively, unexpectedly, the data presented here imply that in human subjects and mice 2 protagonists of innate and adaptive immunity, NLRP3 and BTK, cooperate in activation of the inflammasome, an innate defense mechanism that is critical for activation of adaptive immunity. Our data in human primary cells provide a rationale for further investigations at the molecular level and for exploring therapeutic implications. Targeting the NLRP3 inflammasome at the level of BTK might bring inflammasome targeting unexpectedly within reach if larger clinical studies confirm the observed effects and FDA approval was extended beyond B-cell malignancies. Thus the growing number of BTK inhibitors developed for the treatment of hematologic malignancies might be interesting for clinicians working on the many reported IL-1 $\beta$ -driven inflammatory diseases to follow to glean insights into how to possibly apply BTK inhibition to their clinical settings.

We gratefully acknowledge T. Proikas-Cezanne and D. Bakula for assistance with confocal microscopy, I. Droste-Borel for help with mass spectrometry sample preparation, and M. Löffler and I. Schäfer for help with supplying samples from healthy donors and patients with MWS, respectively. We thank all study subjects and their families for participating in the study.

**Clinical implications:** Based on our results, it could be speculated that the NLRP3 inflammasome, which contributes to inflammatory pathologies in human subjects, could be targeted with BTK inhibitors.

## REFERENCES

- Kawai T, Akira S. Toll-like receptors and their crosstalk with other innate receptors in infection and immunity. *Immunity* 2011;34:637-50.
- McGettrick AF, O'Neill LA. NLRP3 and IL-1 $\beta$  in macrophages as critical regulators of metabolic diseases. *Diabetes Obes Metab* 2013;15(suppl 3):19-25.
- Chen GY, Nunez G. Sterile inflammation: sensing and reacting to damage. *Nat Rev Immunol* 2010;10:826-37.
- Broderick L, De Nardo D, Franklin BS, Hoffman HM, Latz E. The inflammasomes and autoinflammatory syndromes. *Annu Rev Pathol* 2015;10:395-424.
- Miller LS, Pietras EM, Uricchio LH, Hirano K, Rao S, Lin H, et al. Inflammasome-mediated production of IL-1 $\beta$  is required for neutrophil recruitment against *Staphylococcus aureus* in vivo. *J Immunol* 2007;179:6933-42.
- Hoffman HM, Mueller JL, Broide DH, Wanderer AA, Kolodner RD. Mutation of a new gene encoding a putative pyrin-like protein causes familial cold autoinflammatory syndrome and Muckle-Wells syndrome. *Nat Genet* 2001;29:301-5.
- Tsukada S, Saffran DC, Rawlings DJ, Parolini O, Allen RC, Klisak I, et al. Deficient expression of a B cell cytoplasmic tyrosine kinase in human X-linked agammaglobulinemia. *Cell* 1993;72:279-90.
- Bruton OC. Agammaglobulinemia. *Pediatrics* 1952;9:722-8.
- Hendriks RW. Drug discovery: new Btk inhibitor holds promise. *Nat Chem Biol* 2011;7:4-5.
- Burger JA, Keating MJ, Wierda WG, Hartmann E, Hoellenriegel J, Rosin NY, et al. Safety and activity of ibrutinib plus rituximab for patients with high-risk chronic lymphocytic leukaemia: a single-arm, phase 2 study. *Lancet Oncol* 2014;15:1090-9.
- Byrd JC, Furman RR, Coutre SE, Flinn IW, Burger JA, Blum KA, et al. Targeting BTK with ibrutinib in relapsed chronic lymphocytic leukemia. *N Engl J Med* 2013;369:32-42.
- Khan WN. Colonel Bruton's kinase defined the molecular basis of X-linked agammaglobulinemia, the first primary immunodeficiency. *J Immunol* 2012;188:2933-5.
- Fiedler K, Sindrilaru A, Terszowski G, Kokai E, Feyerabend TB, Bullinger L, et al. Neutrophil development and function critically depend on Bruton tyrosine kinase in a mouse model of X-linked agammaglobulinemia. *Blood* 2011;117:1329-39.
- Hendriks RW, Bredius RG, Pike-Overzet K, Staal FJ. Biology and novel treatment options for XLA, the most common monogenetic immunodeficiency in man. *Expert Opin Ther Targets* 2011;15:1003-21.
- Qiu Y, Kung HJ. Signaling network of the Btk family kinases. *Oncogene* 2000;19:5651-61.
- Peschel A, Hartl D. Anuclear neutrophils keep hunting. *Nat Med* 2012;18:1336-8.
- Miller LS, Cho JS. Immunity against *Staphylococcus aureus* cutaneous infections. *Nat Rev Immunol* 2011;11:505-18.
- Wang H, El Maadidi S, Fischer J, Grabski E, Dickhofer S, Klimosch S, et al. A frequent hypofunctional IRAK2 variant is associated with reduced spontaneous hepatitis C virus clearance. *Hepatology* 2015;62:1375-87.
- Bartok E, Bauernfeind F, Khaminets MG, Jakobs C, Monks B, Fitzgerald KA, et al. iGLuc: a luciferase-based inflammasome and protease activity reporter. *Nat Methods* 2013;10:147-54.
- Ito M, Shichita T, Okada M, Komine R, Noguchi Y, Yoshimura A, et al. Bruton's tyrosine kinase is essential for NLRP3 inflammasome activation and contributes to ischaemic brain injury. *Nat Commun* 2015;6:7360.
- Franklin BS, Bossaller L, De Nardo D, Ratter JM, Stutz A, Engels G, et al. The adaptor ASC has extracellular and 'prionoid' activities that propagate inflammation. *Nat Immunol* 2014;15:727-37.
- Stutz A, Horvath GL, Monks BG, Latz E. ASC speck formation as a readout for inflammasome activation. *Methods Mol Biol* 2013;1040:91-101.
- Khan WN, Alt FW, Gerstein RM, Malynn BA, Larsson I, Rathbun G, et al. Defective B cell development and function in Btk-deficient mice. *Immunity* 1995;3:283-99.
- de Almeida L, Khare S, Misharin AV, Patel R, Ratsimandresy RA, Wallin MC, et al. The PYRIN domain-only protein POP1 inhibits inflammasome assembly and ameliorates inflammatory disease. *Immunity* 2015;43:264-76.
- Pimienta G, Chaerkady R, Pandey A. SILAC for global phosphoproteomic analysis. *Methods Mol Biol* 2009;527:107-116.x.
- Di Paolo JA, Huang T, Balazs M, Barbosa J, Barck KH, Bravo BJ, et al. Specific Btk inhibition suppresses B cell- and myeloid cell-mediated arthritis. *Nat Chem Biol* 2011;7:41-50.
- Katsnelson MA, Rucker LG, Russo HM, DUBYAK GR. K+ efflux agonists induce NLRP3 inflammasome activation independently of Ca<sup>2+</sup> signaling. *J Immunol* 2015;194:3937-52.
- Tomlinson MG, Kane LP, Su J, Kadlecck TA, Mollenauer MN, Weiss A. Expression and function of Tec, Itk, and Btk in lymphocytes: evidence for a unique role for Tec. *Mol Cell Biol* 2004;24:2455-66.
- Hornung V, Bauernfeind F, Halle A, Samstad EO, Kono H, Rock KL, et al. Silica crystals and aluminum salts activate the NALP3 inflammasome through phagosomal destabilization. *Nat Immunol* 2008;9:847-56.

30. Holzinger D, Gieldon L, Mysore V, Nippe N, Taxman DJ, Duncan JA, et al. *Staphylococcus aureus* Panton-Valentine leukocidin induces an inflammatory response in human phagocytes via the NLRP3 inflammasome. *J Leukoc Biol* 2012;92:1069-81.
31. Melehani JH, James DB, DuMont AL, Torres VJ, Duncan JA. *Staphylococcus aureus* leukocidin A/B (LukAB) kills human monocytes via host NLRP3 and ASC when extracellular, but not intracellular. *PLoS Pathog* 2015;11:e1004970.
32. Takeuchi O, Hoshino K, Akira S. Cutting edge: TLR2-deficient and MyD88-deficient mice are highly susceptible to *Staphylococcus aureus* infection. *J Immunol* 2000;165:5392-6.
33. Cho JS, Guo Y, Ramos RI, Hebroni F, Plaisier SB, Xuan C, et al. Neutrophil-derived IL-1beta is sufficient for abscess formation in immunity against *Staphylococcus aureus* in mice. *PLoS Pathog* 2012;8:e1003047.
34. Rieber N, Gavrilov A, Hofer L, Singh A, Oz H, Endres T, et al. A functional inflammasome activation assay differentiates patients with pathogenic NLRP3 mutations and symptomatic patients with low penetrance variants. *Clin Immunol* 2015;157:56-64.
35. Jefferies CA, Doyle S, Brunner C, Dunne A, Brint E, Wietek C, et al. Bruton's tyrosine kinase is a Toll/interleukin-1 receptor domain-binding protein that participates in nuclear factor kappaB activation by Toll-like receptor 4. *J Biol Chem* 2003;278:26258-64.
36. Brunner C, Muller B, Wirth T. Bruton's tyrosine kinase is involved in innate and adaptive immunity. *Histol Histopathol* 2005;20:945-55.
37. Block H, Zarbock A. The role of the tec kinase Bruton's tyrosine kinase (Btk) in leukocyte recruitment. *Int Rev Immunol* 2012;31:104-18.
38. Coll RC, Robertson AA, Chae JJ, Higgins SC, Munoz-Planillo R, Inerra MC, et al. A small-molecule inhibitor of the NLRP3 inflammasome for the treatment of inflammatory diseases. *Nat Med* 2015;21:248-55.
39. Teocchi MA, Domingues Ramalho V, Abramczuk BM, D'Souza-Li L, Santos Vilela MM. BTK mutations selectively regulate BTK expression and upregulate monocyte XBPI mRNA in XLA patients. *Immun Inflamm Dis* 2015;3:171-81.
40. Gaidt MM, Ebert TS, Chauhan D, Schmidt T, Schmid-Burgk JL, Rapino F, et al. Human monocytes engage an alternative inflammasome pathway. *Immunity* 2016;44:833-46.
41. Diewell P, Kono H, Rayner KJ, Sirois CM, Vladimer G, Bauernfeind FG, et al. NLRP3 inflammasomes are required for atherogenesis and activated by cholesterol crystals. *Nature* 2010;464:1357-61.
42. Halle A, Hornung V, Petzold GC, Stewart CR, Monks BG, Reinheckel T, et al. The NALP3 inflammasome is involved in the innate immune response to amyloid-beta. *Nat Immunol* 2008;9:857-65.
43. Murthy P, Durco F, Miller-Ocuin JL, Takedai T, Shankar S, Liang X, et al. The NLRP3 inflammasome and Bruton's tyrosine kinase in platelets co-regulate platelet activation, aggregation, and in vitro thrombus formation. *Biochem Biophys Res Commun* 2017;483:230-6.



## METHODS

### Reagents

Nigericin, LPS, PMA, and ionomycin were from InvivoGen; ATP was from Sigma; ibrutinib and CG11746 were from Selleckchem; recombinant GM-CSF for monocyte differentiation was from PeproTech; Ficoll was from Merck Millipore; and anti-CD14-PE was from BD. Antibodies for immunoblots were as follows: caspase-1 (D7F10) antibodies were from Cell Signaling Technology (Danvers, Mass), ASC (F-9) was from Santa Cruz Biotechnology (Dallas, Tex), IL-1 $\beta$  was from R&D Systems (Minneapolis, Minn), and BTK was from BD Biosciences. For flow cytometry, anti-CD11b-APC and anti-CD14-PE were from ImmunoTools, anti-CD19-Pacific Blue was from BioLegend, and anti-CD3-FITC, anti-Btk (pY551)-PE, and anti-Btk (pY223)-Alexa Fluor 647 were from BD Biosciences. For co-immunoprecipitation experiments, all primary antibodies were purchased from Sigma-Aldrich: anti-HA (H9658) and anti-GFP (G1544) both used 1:5000 and anti-Protein A (P3775, dilution 1:62,500). Secondary horseradish peroxidase-coupled antibodies were anti-mouse (PA1-86015; Thermo Fisher Scientific) and anti-rabbit (5127; Cell Signaling Technology). Anti-ASC (Santa Cruz Biotechnology sc-271054) was used for DSS-crosslinking. Recombinant protein was from Thermo Fisher Scientific.

### Study subjects and sample acquisition

All human subjects provided written informed consent in accordance with the Declaration of Helsinki, and the study was approved by the local ethics committees. Buffy coats from healthy donors were provided by the Tübingen University Hospital Transfusion Medicine Department. Male patients with XLA with confirmed genetic and clinical BTK deficiency were recruited at the Center for Immunodeficiency at Freiburg University Hospital. Male healthy donors in a similar age range were recruited at the Department of Immunology, Tübingen, and blood was taken on the same day as that from patients with XLA. Samples were processed in the same way and measured together. Patients with MWS were recruited at the Pediatrics Department of the University Hospital Tübingen, as previously described.<sup>E1</sup> Patients are described in detail below.

### Isolation and stimulation of primary immune cells

PBMCs were isolated from whole blood or buffy coats by using Ficoll density gradient purification and washed 3 times with RPMI to remove residual platelets and then seeded in RPMI-1640 (Sigma), 10% FBS (GE Healthcare, Fairfield, Conn), 2 mmol/L L-glutamine (Life Technologies), and 1% Pen-Strep (Life Technologies). PBMCs were isolated from peripheral blood of 3 patients with XLA and 6 healthy donors. Cells were then treated with 10 ng/mL LPS for 3 hours and 15  $\mu$ mol/L nigericin for 1 hour or instead with 50 ng/mL PMA and 1  $\mu$ mol/L ionomycin for 4 hours. PBMCs from patients with MWS were seeded at a concentration of  $1 \times 10^6$  cells/mL in 24-well tissue culture plates. Cells were then treated with 10 ng/mL LPS, 1 mmol/L ATP concomitantly with 60  $\mu$ mol/L ibrutinib, or a DMSO control for 4 hours, and supernatants were collected for ELISA. For macrophage differentiation, monocytes were purified by means of positive selection from PBMCs with anti-CD14 magnetic beads (>90% purity assessed by using the anti-CD14-PE flow cytometry; Miltenyi Biotec) and seeded at a concentration of  $1 \times 10^6$  cells/mL in 96-well tissue-culture plates. Cells were differentiated into macrophages in the presence of 25 ng/mL recombinant human GM-CSF for 5 days.<sup>E2</sup> MoMacs were then primed with 300 ng/mL LPS for 3 hours and pretreated with ibrutinib at 20 or 60  $\mu$ mol/L for 10 minutes before stimulation with 15  $\mu$ mol/L nigericin or indicated amounts of LukAB or PVL for 1 hour. In all cases supernatants were then collected for ELISA.

### Plasmid constructs

ASC, NLRP3, and BTK coding sequences in pENTR clones were from the genomics core facility at DKFZ Heidelberg (Heidelberg, Germany). The inserts were transferred into pDEST plasmids containing N-terminal streptavidin-hemagglutinin (NLRP3; T. Bürckstümmer, CeMM, Vienna,

Austria, and M. Gstaiger, ETH Zurich, Zurich, Switzerland) and C-terminal Protein A (M. Kögl, DKFZ Heidelberg) or GFP tags (Stefan Pusch, Neuropathology, Heidelberg University) by LR Gateway cloning (Invitrogen, Carlsbad, Calif). Correct transfer was checked by means of restriction digest and DNA sequencing.

### Cell culture

HEK293T cells were cultured in Dulbecco modified Eagle medium supplemented with 10% FCS, L-glutamine (2 mmol/L), penicillin (100 U/mL), and streptomycin (100  $\mu$ g/mL; all from Life Technologies). THP-1 (ATCC) cells were cultured in RPMI 1640 supplemented with 10% FCS, L-glutamine (2 mmol/L), penicillin (100 U/mL), and streptomycin (100  $\mu$ g/mL; all from Life Technologies). THP-1-null (stably expressing a nontargeting shRNA) and NLRP3-deficient (stably expressing an NLRP3-targeting shRNA, both from InvivoGen) were cultured in RPMI 1640 supplemented with 10% FCS, L-glutamine (2 mmol/L), penicillin (100 U/mL), streptomycin (100  $\mu$ g/mL; all from Life Technologies), sodium pyruvate (1 mmol/L; from Invitrogen), HEPES buffer (10 mmol/L; from Sigma), Normocin (100  $\mu$ g/mL; from InvivoGen), and Hygromycin B (100  $\mu$ g/mL; from Invitrogen). iGluc THP-1 cells were a kind gift of V. Hornung, Institute of Molecular Medicine, Munich, Germany, and cultured as previously described.<sup>E3</sup> BTK-shRNA- and mock control-THP-1 cells were a kind gift of R. Morita, Keio University School of Medicine, Tokyo, Japan, and were cultured in RPMI 1640 supplemented with 10% FCS, L-glutamine (2 mmol/L), penicillin (100 U/mL), and streptomycin (100  $\mu$ g/mL; all from Life Technologies) in the presence of 1.5 and 2 mg/mL G418, respectively. ASC-mCerulean-expressing immortalized macrophages or THP-1 cells were described previously.<sup>E4,E5</sup> All cell lines and primary cells were cultured at 37°C and 5% CO<sub>2</sub>.

### Mice and generation of BMDM

Btk KO mice have been described previously.<sup>E6</sup> Btk KO and wild-type littermates (all C57BL/6 background) were used at an age of 8 to 12 weeks. In brief, bone marrow cells were isolated from femurs and tibiae by using standard procedures (details available on request) and  $3 \times 10^6$  cells/mL plated in 10-cm non-tissue culture-coated dishes in 10 mL of complete RPMI media containing 10% GM-CSF (M1 polarization)- or M-CSF (M2 polarization)-conditioned medium for 5 to 7 days. Cells were always counted and reseeded before *in vitro* assays to ensure equal cell numbers. *Ex vivo* animal experiments (Fig 3, A and B) were in accordance with institutional guidelines and German animal protection laws. *In vivo* infection experiments (Fig 6) were approved by the Johns Hopkins University Animal Care and Use Committee (ACUC protocol no. MO15M421). C57BL/6 female mice at 8 weeks of age were obtained from Jackson Laboratories (Bar Harbor, Me). All mouse colonies were maintained in specific pathogen-free conditions.

### Mass spectrometry

THP-1-null cells (Invitrogen) were grown in "light" (L-lysine/Lys0, L-arginine/Arg0), "medium-heavy" (D4-L-lysine/Lys4, <sup>13</sup>C6-L-arginine/Arg6), and "heavy" (<sup>13</sup>C<sub>6</sub><sup>15</sup>N<sub>2</sub>-L-lysine/Lys8, <sup>13</sup>C<sub>6</sub><sup>15</sup>N<sub>4</sub>-arginine/Arg10) SILAC medium for 3 passages. Incorporation of the labeled amino acids was in each case confirmed to be greater than 97%. For the experiment, cells were primed with 300 ng/mL PMA for 3 hours and left to rest overnight. The next day, the cells were detached and either left unstimulated (light) or stimulated with 15  $\mu$ mol/L nigericin for 5 (medium) or 10 (heavy) minutes. After washing with ice-cold PBS (containing phosphatase and protease inhibitors, Roche), cell pellets were snap-frozen and stored at -80°C before analysis. For phosphopeptide enrichment, cells were lysed in denaturation buffer (6 mol/L urea and 2 mol/L thiourea in 10 mmol/L Tris buffer, pH 8.0), and DNA was removed by means of addition of benzonase.

After determining the amount of protein in the lysates by using a Bradford assay, 3 mg of protein of each condition were pooled, and the mixture was digested in solution with trypsin. The resulting peptide mixture was subjected to phosphopeptide enrichment, as described previously,<sup>E7</sup> with minor

modifications: peptides were separated by using strong cation exchange (SCX) chromatography with a gradient of 0% to 35% SCX solvent B, resulting in 8 fractions that were subjected to phosphopeptide enrichment by titanium dioxide beads. Elution from the beads was performed 3 times with 100  $\mu$ L of 40% ammonia hydroxide solution in 60% acetonitrile (pH > 10.5). Peptide-rich fractions were subjected to titanium dioxide enrichment multiple times. Enrichment of phosphopeptides from the SCX flowthrough was done in 5 cycles. liquid chromatography–tandem mass spectrometry analyses were performed on an EasyLC nano-HPLC coupled to an LTQ Orbitrap XL (Thermo Scientific), as described previously.<sup>E8</sup> The peptide mixtures were injected onto the column in HPLC solvent A (0.5% acetic acid) at a flow rate of 500 nL/min and subsequently eluted with a 127-minute (phosphoproteome) segmented gradient of 5–33–90% HPLC solvent B (80% ACN in 0.5% acetic acid). During peptide elution the flow rate was kept constant at 200 nL/min. The 5 most intense precursor ions were fragmented by means of multistage activation of neutral loss ions at  $-98$ ,  $-49$ , and  $-32.6$  Th relative to the precursor ion.<sup>E9</sup> Sequenced precursor masses were excluded from further selection for 90 seconds. Full scans were acquired at resolution of 60,000 (Orbitrap XL, Thermo Fisher Scientific). The target values were set to 5000 charges for the LTQ (MS/MS) and  $10^6$  charges for the Orbitrap (MS), respectively; the maximum allowed fill times were 150 ms (LTQ) and 1000 ms (Orbitrap). The lock mass option was used for real-time recalibration of MS spectra.<sup>E7</sup>

MS data were processed by using default parameters of MaxQuant software (v1.2.2.9).<sup>E10</sup> Extracted peak lists were submitted to database search by using the Andromeda search engine<sup>E11</sup> to query a target-decoy<sup>E12</sup> database of *Homo sapiens* proteome (downloaded from Uniprot on December 25, 2012), containing also 248 commonly observed contaminants. In a database search full tryptic specificity was required, and up to 2 missed cleavages were allowed. Carbamidomethylation of cysteine was set as fixed modification; protein N-terminal acetylation, oxidation of methionine, and phosphorylation of serine, threonine, and tyrosine were set as variable modifications. Initial precursor mass tolerance was set to 6 ppm at the precursor ion and 0.5 Da at the fragment ion level. False discovery rates were set to 1% at the peptide, phosphorylation site, and protein group levels. Details regarding other phosphopeptides with nigericin-dependent are available on request.

## ELISA

IL-1 $\beta$ , IL-2, TNF, and IFN- $\gamma$  levels in supernatants were determined with half-area plates by ELISA (BioLegend) with triplicate points on a standard plate reader.

## Quantitative RT-PCR

mRNA was isolated with the RNeasy Mini Kit on a Qiacube robot (both from Qiagen) transcribed to cDNA (High Capacity RNA-to-cDNA Kit; Life Technologies), and *IL1b*, *Nlrp3*, *IL1*, and *NLRP3* mRNA expression was quantified relative to that of *TBP* by using TaqMan primers (Life Technologies) on a real-time cycler (7500 fast; Applied Biosystems), as described by Wang et al.<sup>E13</sup> Comparable cycle threshold values for *TBP* (data not shown) in all treatment groups confirmed equal cell numbers.

## ASC speck formation assay and confocal microscopy

HEK293T cells ( $4 \times 10^4$ ) were plated (24-well format; Greiner Bio-One, Monroe, NC) and transiently transfected as indicated. Forty-eight hours later, cells were fixed with 100% methanol, nucleic acids were stained with TO-PRO-3 (Thermo Fisher), and BTK-HA was stained with anti-HA–Alexa 594–conjugated antibodies. Samples were analyzed with a Zeiss LSM 510 confocal microscope (Zeiss, Oberkochen, Germany) under the  $\times 20$  objective. Excitation and emission wavelengths are available on request. Nuclei and ASC-GFP particle counting and analysis were performed with ImageJ software (National Institutes of Health, Bethesda, Md), with further details on request. Immortalized *Nlrp3* KO macrophages overexpressing NLRP3-FLAG and ASC-mCerulean were pretreated with ibrutinib or solvent

control for 10 minutes before stimulation (or with CGI1746 or solvent control) for 60 minutes before stimulation with either 5  $\mu$ mol/L nigericin (Life Technologies) or 1 mmol/L Leu-Leu-OMe-HCl (Chem-Impex) for 90 minutes. After stimulation, cells were fixed with 4% formaldehyde and nucleic acids were stained with DRAQ5 (eBioscience). Cells were imaged with a Zeiss Observer.Z1 epifluorescence microscope by using a  $\times 20$  objective, as previously described.<sup>E5</sup> Numbers of cells and specks were counted for 10 images per condition by using CellProfiler.<sup>E14</sup>

## Pro-IL-1 $\beta$ and caspase-1 cleavage

Equal numbers of cells were primed with PMA (100 ng/mL, InvivoGen) overnight or LPS (300 ng/mL, InvivoGen) for 3 hours and then stimulated with indicated stimuli in Opti-MEM (Gibco) to monitor caspase-1 and pro-IL-1 $\beta$  processing. Protein in supernatants was precipitated by using methanol (VWR International) and chloroform (Sigma). Where applicable, recombinant Protein A was added before precipitation as a control. Where applicable, cell fractions were lysed in RIPA buffer with protease inhibitors (Sigma). Fifteen percent and 12% SDS-PAGE gels were used for protein from supernatants and whole-cell lysates, respectively, and probed with the indicated antibodies.

## Co-immunoprecipitation

For co-immunoprecipitations,  $1.5 \times 10^6$  HEK293T cells were plated in 10-cm dishes (Greiner Bio-One) and 2 to 6 hours later were transfected with a calcium phosphate precipitation method with 5  $\mu$ g of appropriate plasmids. Cells were lysed 48 hours later in a buffer (50 mmol/L Tris [pH 8], 280 mmol/L NaCl, 0.5% NP-40, 0.2 mmol/L EDTA, 2 mmol/L EGTA, 10% glycerol, and 1 mmol/L dithiothreitol) with protease/phosphatase inhibitors (Roche). Cleared lysates were stored for immunoblot analysis. The remainder were subjected to immunoprecipitation of the BTK–Protein A fusion protein, 30  $\mu$ L of lysis buffer–equilibrated Dynabeads (M-280 Sheep Anti-Mouse IgG, Thermo Fisher Scientific) were incubated with lysates at 4°C for 3 hours. After washing of precipitated protein complexes 4 times, samples were boiled in Invitrogen’s NuPAGE 4 $\times$  LDS loading dye supplemented with 10 $\times$  Sample Reducing Agent and applied for SDS-PAGE and immunoblotting.

## Crosslinking of ASC oligomers

THP-1 null or ASC-mCerulean cells ( $2 \times 10^6$ ; Veit Hornung, Gene Center, Munich, Germany) were plated in a 6-well format (Greiner Bio-One), primed with 100 ng/mL PMA overnight or with 300 ng/mL LPS for 2 hours, respectively, and then treated with 60  $\mu$ mol/L ibrutinib for 1 hour and 15  $\mu$ mol/L nigericin for 1 hour, unless otherwise stated. After washing with PBS, cells were lysed at 4°C in 100  $\mu$ L of buffer<sup>E15</sup> containing 20 mmol/L HEPES (pH 7.4), 100 mmol/L NaCl, 1% NP-40, and 1 mmol/L sodium orthovanadate and supplemented with protease inhibitors (Roche) and Benzonase (Sigma-Aldrich). Lysates were cleared (16,000g at 4°C for 15 minutes) and used for immunoblot analysis. Pellets were resuspended in 250  $\mu$ L of PBS and subjected to 2 mmol/L DSS (Thermo Scientific) for 1 hour at room temperature. Crosslinked samples were spun (16,000g, at 4°C for 15 minutes), and the pelleted fraction was resuspended and boiled in Invitrogen’s NuPAGE LDS loading dye supplemented with Sample Reducing Agent and applied for immunoblotting.

## Flow cytometry and phospho-flow

For whole-blood analysis of healthy donors and patients with XLA, 200  $\mu$ L of whole blood from patients and healthy control subjects was stained with a mix of antibodies detecting cell surface antigens (anti-CD3–FITC, anti-CD19–Pacific Blue, anti-CD14–PE, and anti-CD11b–APC) for 30 minutes at room temperature in the dark. Samples were then fixed and permeabilized (Lyse/Fix Buffer, BD Biosciences) for 20 minutes, washed, and resuspended in 200  $\mu$ L of PBS 0.5% BSA for analysis (BD Fortessa). A standardized protocol and identical flow cytometer settings were used for all donors. Further settings are available on request. For phospho-flow analysis, the indicated primed cells were treated and then fixed (Lyse/Fix Buffer, BD

Biosciences). For phosflow analysis, the indicated primed cells were treated and then fixed (Lyse/Fix Buffer, BD Biosciences). LIVE/DEAD Fixable Aqua was used to stain dead cells (Life Technologies). Cells were permeabilized with 1 mL of cold methanol, Fc receptors were blocked (Human AB serum), and cells were stained with antibodies against anti-Btk (pY551) PE, anti-Btk (pY223) BV421, and anti-total BTK Alexa Fluor 647 (all from BD Biosciences). Corresponding isotype controls were from ImmunoTools.

### *S aureus* strains

For experiments in mice, a modified USA300 strain, LAC::lux,<sup>E16</sup> which possesses a modified *luxABCDE* operon from *Photobacterium luminescens* stably integrated into the bacterial chromosome that was transduced from bioluminescent strain Xen29 (PerkinElmer) was used. Live and metabolically active USA300 LAC::lux bacteria constitutively emit a blue-green light, which is present in all progeny. USA300 strain LAC::lux was streaked onto a tryptic soy agar plate (tryptic soy broth plus 1.5% bacto agar, BD Biosciences) and grown overnight at 37°C in a bacterial incubator. Single colonies were picked and placed into tryptic soy broth and grown overnight in shaking culture in a 37°C shaker at 240 rpm. After overnight culture (18 hours), a 1:50 subculture in tryptic soy broth was prepared for 2 hours at 37°C to achieve midlogarithmic phase bacteria. Bacteria were pelleted, resuspended in sterile PBS, and washed 3 times. Absorbance ( $A_{600}$ ) was measured to estimate the number of CFU, which was verified after overnight culture on tryptic soy agar plates.

### *In vivo* infection model

Ibrutinib (6 mg/kg, Selleckchem) in 3% DMSO (Sigma-Aldrich) and 5% corn oil (Sigma-Aldrich) in PBS or vehicle control was injected intravenously through the retro-orbital vein in anesthetized mice on days -1, 0, and 1. In addition, mice received 1 application of ibrutinib (6 mg/kg) in 10  $\mu$ L of DMSO or vehicle control on day 2. For infection, the dorsal backs of anesthetized mice (2% isoflurane) were shaved and injected intradermally with  $3 \times 10^7$  CFU of *S aureus* LAC::Lux: in 100  $\mu$ L of PBS by using a 29-gauge insulin syringe on day 0. Digital photographs were taken on days 1, 3, 7, 10, and 14, and total lesion size (in square centimeters) measurements were analyzed with Image J software (<http://imagej.nih.gov/ij/>) and a millimeter ruler as a reference.

### Quantification of *in vivo* *S aureus* bioluminescent imaging

Mice were anesthetized (2% isoflurane), *in vivo* bioluminescent imaging was performed (Lumina III IVIS, PerkinElmer), and total flux (photons/s) within a circular region of interest measuring  $1 \times 10^3$  pixels was measured by using Living Image software (PerkinElmer; limit of detection,  $2 \times 10^4$  photons/s).

### Purification of LukAB and PVL

The pQE30 vector (Qiagen) was used to produce recombinant His-tagged LukS-PV, LukF-PV, LukA and LukB (the 2 single components of PVL and LukAB, respectively) by using the following oligonucleotides: LukF (Bam-lukF forward: GGGGGGATCCTCCAATACACTTGATGCAGCT and PstlukF reverse: GCGCCTGCAGTCTATCTGTTAGCTCATAGGATT); LukS (BamHluk-S1: GGGGGGATCCAAAGCTGATAACAATATTGAGAA and Pstluk-S2: GGGGCTGCAGTCAATTATGTCCTTTTCATT); LukB (PstblhA forward: BCGCGCTGCAGGGCAACTTTTATTACTTATTTCTT and BamblhA reverse: CCCC GGATCCCCAGCTACTTTCATTTGCAAA GATT); and LukA (Pstblh-S1: CCCCTGCAGCGCCCTTTCAATATTA TCCT and BamHblh-S2: CCCC GGATCCAATTCAGCTCATAAGACTCT CAA). Primers were chosen to omit the region predicted to encode the signal peptide. PCR fragments were cloned into the *BamHI-PstI* cloning site of pQE30. Plasmids were transformed in *Escherichia coli* BL21 and verified by means of sequencing. LukS-PV, LukF-PV, and LukA proteins were purified by means of affinity chromatography on Ni-NTA columns (Qiagen) under native conditions according to the instructions of the manufacturer (Qiagen)

by using 50 mmol/L  $\text{NaH}_2\text{PO}_4$ , 300 mmol/L NaCl, 250 mmol/L imidazole, and 20% glycerol for elution. LukB was purified under denaturing conditions from inclusion bodies.

Briefly, inclusion bodies were resuspended in 6 mol/L guanidine HCl, 20 mmol/L Tris (pH 8.0), 500 mmol/L NaCl, and 20% glycerol and centrifuged, and the supernatant was packed with Ni-NTA on columns. Columns were washed (6 mol/L guanidine HCl, 20 mmol/L Tris [pH 8.0], 500 mmol/L NaCl, 20% glycerol, and 50 mmol/L imidazole), and LukB was eluted with 6 mol/L guanidine HCl, 20 mmol/L Tris (pH 8.0), 500 mmol/L NaCl, 20% glycerol, and 300 mmol/L imidazole. The fusion proteins were dialyzed against PBS/50% glycerol and stored at -20°C until use. Endotoxin contamination of the toxin stock solutions was excluded by using a limulus assay with a detection limit of 0.25 EU/mL (Lonza) and found to be negative. Single components were mixed in an equal molar ratio for use. IL-1 $\beta$  secretion was not detectable in stimulations using the single components (data not shown).

### Data analysis and statistics

Data were imported into and analyzed in GraphPad Prism version 5.0 by using 2-tailed Student *t* tests and nonparametric Mann-Whitney *U* or Wilcoxon matched-pairs signed-rank test unless stated otherwise. A *P* value of less than .05 was generally considered statistically significant and marked by an asterisk throughout the figure legends, even if considerably lower.

### Characteristics of patients with XLA

All patients were adult males and provided written informed consent for participation in the study.

Patient 1 (Fig 4, D and E) was given a diagnosis of XLA caused by agammaglobulinemia and absence of B cells after recurring bronchopulmonary infections. A *BTK* mutation mapping to a splicing site was confirmed by means of sequencing (g.IVS17+5G>A, c.1750+5G>A).

Patient 2 (Fig 4, D and E) was given a diagnosis of XLA because of the absence of all immunoglobulin subtypes and absence of B cells after recurring bronchopulmonary infections. A coding *BTK* mutation was confirmed by means of sequencing (c.1361A>T, p.454H>L). The patient has been receiving IVIG since 1984.

Patient 3 (Fig 4, D and E) was given a diagnosis of XLA caused by absence of all immunoglobulin subtypes and absence of B cells after recurring bronchopulmonary infections, episodes of pneumonia, otitis media and externa, and mild bronchiectasis. A *BTK* mutation mapping to a splicing site was confirmed by means of sequencing (Intron 7: 721+1 G-C). Drastically reduced but detectable *BTK* expression was seen.

Patient 4 (Figs 4, F and G, and 5, E) was given a diagnosis of Bruton agammaglobulinemia caused by IgG, IgA, and IgM levels of less than the detection limit and absence of peripheral B cells. The patient had recurring respiratory tract infections, including *Haemophilus influenzae*, and bronchiectasis. The patient also had an autoimmune enteropathy and ulcerating duodenitis treated with ileal resection.

### Characteristics of patients with MWS

All patients provided written informed consent for participation in the study. For further information, see to Rieber et al.<sup>E1</sup>

Patient 1 (Fig 6, D) was a 30-year-old woman with a confirmed p.E311K mutation. Complete response to anti-IL-1 therapy was seen.

Patient 2 (Fig 6, D) was a 54-year-old man with a confirmed p.E311K mutation. Complete response to anti-IL-1 therapy was seen.

Patient 3 (Fig 6, D) was a 54-year-old man with a confirmed p.E311K mutation. Complete response to anti-IL-1 therapy was seen.

Patient 4 (Fig 6, D) was a 5-year-old girl with a confirmed p.Q703K mutation who was currently not receiving anti-IL-1 therapy.

Patient 5 (Fig 6, E) was a 46-year-old man with a confirmed p.R260W mutation. Complete response to anti-IL-1 therapy was seen.

Patient 6 (Fig 6, E) was a 60-year-old man with a confirmed p.Val198Met mutation. Complete response to anti-IL-1 therapy was seen.

## Ibrutinib-treated patients

All patients provided written informed consent for participation in the study.

Patient 1 (Fig 6, G) was an 81-year-old man. Primary diagnosis/indication for ibrutinib treatment was mantle cell lymphoma (first diagnosed September 2006). Other secondary disorders were prostate cancer, hypertension, hyperthyroidism, and chronic kidney disease. Ibrutinib (Imbruvica) at a dosage of 560 mg/d was administered orally. Time of last administration before blood sampling (10 AM) was 8 AM.

Patient 2 (Fig 6, G) was an 80-year-old man. Primary diagnosis/indication for ibrutinib treatment was chronic lymphocytic leukemia (first diagnosed June 2008). Other secondary disorders were hypertension and hypogammaglobulinemia. Ibrutinib (Imbruvica) at a dosage of 420 mg/d was administered orally. Time of last administration before blood sampling (10 AM) was 8 AM.

Patient 3 (Fig 6, F) was an 86-year-old woman. Primary diagnosis/indication for ibrutinib treatment was chronic lymphocytic leukemia (first diagnosed May 2007). The other secondary disorders was atrial fibrillation. Ibrutinib (Imbruvica) at a dosage of 280 mg/d was administered orally. Time of last administration before blood sampling (10 AM) was 8 AM.

Patient 4 (Fig 6, F) was a 64-year-old man. Primary diagnosis/indication for ibrutinib treatment was mantle cell lymphoma (first diagnosed August 2008). Other secondary disorders were hypogammaglobulinemia, diabetes mellitus, and polymyalgia rheumatica. Ibrutinib (Imbruvica) at a dosage of 560 mg/d was administered orally. Time of last administration before blood sampling (10 AM) was 8 AM.

Patient 5 (Fig 6, F) was a 60-year-old man. Primary diagnosis/indication for ibrutinib treatment was chronic lymphatic leukemia (first diagnosed December 1999). Other secondary disorders were secondary antibody deficiency syndrome, history of autoimmune hemolysis with incomplete warm autoantibody, polyneuropathy in both feet, history of gram-negative sepsis at the time of colitis with thickening of cecum and colon ascendens, *E coli* detection (BK), history of septic pneumonia with detection of *E coli* (BK), and antibiotics with Tazobac Oesophageal varices of grade III fundus varices grade I. Ibrutinib (Imbruvica) at a dosage of 420 mg/d was administered orally. Time of last administration before blood sampling (10 AM) was between 6 and 9 AM.

Patient 6 (Fig 6, F) was an 87-year-old man. Primary diagnosis/indication for ibrutinib treatment was chronic lymphatic leukemia (first diagnosed February 1994). Other secondary disorders were pacemaker implantation, sick sinus syndrome, bradycardia, permanent atrial fibrillation, currently taking Apixaban, history of duodenal ulcer, Forrest III hemorrhage, cholelithiasis History of stent implantation, and postinterventional cholangiosepsis (*E coli* in pBK). Ibrutinib (Imbruvica) dosage of 420 mg/d was administered orally. Time of last administration before blood sampling (10 AM) was between 6 and 9 AM.

## REFERENCES

- E1. Rieber N, Gavrilov A, Hofer L, Singh A, Oz H, Endres T, et al. A functional inflammasome activation assay differentiates patients with pathogenic NLRP3 mutations and symptomatic patients with low penetrance variants. *Clin Immunol* 2015;157:56-64.
- E2. Verreck FA, de Boer T, Langenberg DM, Hoeve MA, Kramer M, Vaisberg E, et al. Human IL-23-producing type 1 macrophages promote but IL-10-producing type 2 macrophages subvert immunity to (myco)bacteria. *Proc Natl Acad Sci U S A* 2004;101:4560-5.
- E3. Bartok E, Bauernfeind F, Khaminets MG, Jakobs C, Monks B, Fitzgerald KA, et al. iGLuc: a luciferase-based inflammasome and protease activity reporter. *Nat Methods* 2013;10:147-54.
- E4. Franklin BS, Bossaller L, De Nardo D, Ratter JM, Stutz A, Engels G, et al. The adaptor ASC has extracellular and 'prionoid' activities that propagate inflammation. *Nat Immunol* 2014;15:727-37.
- E5. Stutz A, Horvath GL, Monks BG, Latz E. ASC speck formation as a readout for inflammasome activation. *Methods Mol Biol* 2013;1040:91-101.
- E6. Khan WN, Alt FW, Gerstein RM, Malynn BA, Larsson I, Rathbun G, et al. Defective B cell development and function in Btk-deficient mice. *Immunity* 1995;3:283-99.
- E7. Olsen JV, Macek B. High accuracy mass spectrometry in large-scale analysis of protein phosphorylation. *Methods Mol Biol* 2009;492:131-42.
- E8. Koch A, Krug K, Pengelley S, Macek B, Hauf S. Mitotic substrates of the kinase aurora with roles in chromatin regulation identified through quantitative phosphoproteomics of fission yeast. *Sci Signal* 2011;4:rs6.
- E9. Schroeder MJ, Shabanowitz J, Schwartz JC, Hunt DF, Coon JJ. A neutral loss activation method for improved phosphopeptide sequence analysis by quadrupole ion trap mass spectrometry. *Anal Chem* 2004;76:3590-8.
- E10. Cox J, Mann M. MaxQuant enables high peptide identification rates, individualized p.p.b.-range mass accuracies and proteome-wide protein quantification. *Nat Biotechnol* 2008;26:1367-72.
- E11. Cox J, Neuhauser N, Michalski A, Scheltema RA, Olsen JV, Mann M. Andromeda: a peptide search engine integrated into the MaxQuant environment. *J Proteome Res* 2011;10:1794-805.
- E12. Elias JE, Gygi SP. Target-decoy search strategy for increased confidence in large-scale protein identifications by mass spectrometry. *Nat Methods* 2007;4:207-14.
- E13. Wang H, El Maadidi S, Fischer J, Grabski E, Dickhofer S, Klimosch S, et al. A frequent hypofunctional IRAK2 variant is associated with reduced spontaneous hepatitis C virus clearance. *Hepatology* 2015;62:1375-87.
- E14. Carpenter AE, Jones TR, Lamprecht MR, Clarke C, Kang IH, Friman O, et al. CellProfiler: image analysis software for identifying and quantifying cell phenotypes. *Genome Biol* 2006;7:R100.
- E15. de Almeida L, Khare S, Misharin AV, Patel R, Ratsimandresy RA, Wallin MC, et al. The PYRIN domain-only protein POPI inhibits inflammasome assembly and ameliorates inflammatory disease. *Immunity* 2015;43:264-76.
- E16. Thurlow LR, Hanke ML, Fritz T, Angle A, Aldrich A, Williams SH, et al. *Staphylococcus aureus* biofilms prevent macrophage phagocytosis and attenuate inflammation in vivo. *J Immunol* 2011;186:6585-96.



Accepted publication 3

**Cyanobacterial antimetabolite 7-deoxysedoheptulose blocks the shikimate pathway to inhibit the growth of prototrophic organisms**

Klaus Brilisauer, Johanna Rapp, Pascal Rath, Anna Schöllhorn, Lisa Bleul, Elisabeth Weiß, Mark Stahl, Stephanie Grond & Karl Forchhammer





**Nature Communications (2019) Feb 1;10(1): 545**

ARTICLE

<https://doi.org/10.1038/s41467-019-08476-8>

OPEN

# Cyanobacterial antimetabolite 7-deoxy-sedoheptulose blocks the shikimate pathway to inhibit the growth of prototrophic organisms

Klaus Brilisauer <sup>1,2</sup>, Johanna Rapp <sup>2</sup>, Pascal Rath<sup>1</sup>, Anna Schöllhorn <sup>2</sup>, Lisa Bleul<sup>3</sup>, Elisabeth Weiß<sup>3</sup>, Mark Stahl<sup>4</sup>, Stephanie Grond<sup>1</sup> & Karl Forchhammer <sup>2</sup>

Antimetabolites are small molecules that inhibit enzymes by mimicking physiological substrates. We report the discovery and structural elucidation of the antimetabolite 7-deoxy-sedoheptulose (7dSh). This unusual sugar inhibits the growth of various prototrophic organisms, including species of cyanobacteria, *Saccharomyces*, and *Arabidopsis*. We isolate bioactive 7dSh from culture supernatants of the cyanobacterium *Synechococcus elongatus*. A chemoenzymatic synthesis of 7dSh using *S. elongatus* transketolase as catalyst and 5-deoxy-D-ribose as substrate allows antimicrobial and herbicidal bioprofiling. Organisms treated with 7dSh accumulate 3-deoxy-D-arabino-heptulosonate 7-phosphate, which indicates that the molecular target is 3-dehydroquinate synthase, a key enzyme of the shikimate pathway, which is absent in humans and animals. The herbicidal activity of 7dSh is in the low micromolar range. No cytotoxic effects on mammalian cells have been observed. We propose that the in vivo inhibition of the shikimate pathway makes 7dSh a natural antimicrobial and herbicidal agent.

<sup>1</sup>Institute of Organic Chemistry, Eberhard Karls Universität Tübingen, Auf der Morgenstelle 18, 72076 Tübingen, Germany. <sup>2</sup>Microbiology, Organismic Interactions, Eberhard Karls Universität Tübingen, Auf der Morgenstelle 28, 72076 Tübingen, Germany. <sup>3</sup>Interfaculty Institute of Microbiology and Infection Medicine Tübingen (IMIT), Eberhard Karls Universität Tübingen, Eugenstraße 6, 72076 Tübingen, Germany. <sup>4</sup>Center for Plant Molecular Biology, Eberhard Karls Universität Tübingen, Auf der Morgenstelle 32, 72076 Tübingen, Germany. Correspondence and requests for materials should be addressed to S.G. (email: [biomolchemie@orgchem.uni-tuebingen.de](mailto:biomolchemie@orgchem.uni-tuebingen.de)) or to K.F. (email: [biomolchemie@orgchem.uni-tuebingen.de](mailto:biomolchemie@orgchem.uni-tuebingen.de))

Cyanobacteria—the dominating photoautotrophic, oxygen-producing microbes on earth—have gained increasing attention in natural product research in recent years. Their omnipresence in the light-exposed biosphere is based on a large repertoire of survival strategies for withstanding challenging environmental conditions and protecting their niches against competitors. To this end, cyanobacteria produce a wide range of secondary metabolites, often with a unique composition and specialized functions, which mediate manifold processes, such as chemical defense<sup>1</sup>, preservation<sup>2</sup>, and quorum sensing<sup>3</sup>. Some of the known cyanobacterial metabolites exhibit antiviral<sup>4</sup>, antibacterial<sup>5</sup>, antifungal<sup>6</sup>, or herbicidal<sup>7</sup> activities, with promising possible applications in human health, agriculture, or industry<sup>8</sup>.

Although cyanobacteria produce a broad range of bioactive compounds in terms of structure and targets, only few are described as classical antimetabolites. Antimetabolites are chemical analogs of the natural substrates of enzymes, where they bind to the active site but are not converted to the functional product. In this way, antimetabolites block a biological process, such as a biosynthetic pathway. One of the best-studied cyanobacterial antimetabolites is the non-proteinogenic amino acid  $\beta$ -methylamino-L-alanine (BMAA), which was initially isolated from cultures of species of *Nostoc*<sup>9</sup>. BMAA can be mistakenly incorporated into nascent proteins in place of L-serine, which possibly causes protein misfolding and aggregation<sup>10</sup>.

Antimetabolites are useful for controlling the growth of microorganisms, fungi, and plants. To avoid harmful side effects, these compounds should target biological processes that do not occur in animals, especially mammals. One such process involves the enzymes of the shikimate pathway, in which seven enzymes catalyze the sequential conversion of erythrose 4-phosphate and phosphoenolpyruvate (PEP) via shikimate to chorismate<sup>11</sup>, the essential precursor of the aromatic amino acids phenylalanine, tyrosine, and tryptophan. Each enzyme of the shikimate pathway catalyzes an essential reaction in chorismate biosynthesis that cannot be bypassed by an alternative enzyme. The inhibition of any enzyme of this pathway, therefore, leads to impairment of the entire cell metabolism and results in arrested growth or even cell death<sup>12</sup>. Chemical compounds that interfere specifically with any enzyme activity in this pathway are considered harmless for humans and other mammals when handled at reasonable concentrations<sup>13</sup>. Therefore, the enzymes of the shikimate pathway are attractive potential targets for the development of novel antimetabolites.

One of the most prominent antimetabolites that targets the shikimate pathway is the synthetic herbicide glyphosate [N-(phosphonomethyl)glycine]<sup>14</sup>, whose use is intensely discussed, most recently due to its perturbation of the gut microbiota of honey bees<sup>15</sup>. Since its initial commercialization in 1974, glyphosate has become the main component of various total herbicides applied in agriculture, industry and private households, today in amounts of >800,000 tons per year<sup>16</sup>. Glyphosate is a potent inhibitor of the 5-enolpyruvylshikimate 3-phosphate (EPSP) synthase, which converts PEP and shikimate 3-phosphate to EPSP. As a transition state analog of PEP, glyphosate leads to the accumulation of shikimate 3-phosphate<sup>17</sup>. This blocking of the synthesis of the end products of the aromatic pathway results in perturbation of metabolic homeostasis and eventually leads to cell death. To our knowledge, glyphosate is the only bioactive compound with a potent in vivo inhibitory effect on the shikimate pathway that has been described to date. Another target of antimetabolites is the first enzyme in branched-chain amino acid synthesis, acetohydroxyacid synthase (AHAS, E.C. 2.2.1.6). Like the shikimate pathway, the branched-chain amino acid synthesis pathway is only found in plants, bacteria and fungi and therefore,

compounds inhibiting the AHAS are highly successful commercial herbicides<sup>18,19</sup>.

Allelochemicals, bioactive compounds for the inhibition of rival organisms, play a major role in cyanobacterial niche competition. Both filamentous and colonial cyanobacteria are known to be potent producers of a wide variety of allelochemicals and other secondary metabolites<sup>20,21</sup>. By contrast, little is known about the synthesis of such metabolites by simple unicellular cyanobacteria like *Synechococcus* and *Prochlorococcus* species. Indeed, for a long time it was not even anticipated that these cyanobacteria produce bioactive metabolites because of their small, stream-lined genomes and lack of non-ribosomal peptide synthase gene clusters<sup>22</sup>. However, newer findings suggest an extensive ability of simple unicellular cyanobacteria for the production of secondary metabolites, which is mainly based on catalytic promiscuity<sup>23</sup>.

*Synechococcus elongatus* PCC 7942 is one of the most commonly used model organisms for molecular genetic studies in cyanobacteria<sup>24</sup>. Its circular chromosome (ca. 2.7 Mb, GenBank accession no. CP000100) and plasmids (GenBank accession nos. AF441790 and S89470) lack apparent gene clusters for the synthesis of complex secondary metabolites<sup>25</sup>. However, it has been reported that collapsing aged cultures of *S. elongatus* secrete a non-identified hydrophobic metabolite that inhibits the growth of a large variety of photosynthetic organisms<sup>26</sup>.

In this work, we identify an anti-cyanobacterial bioactivity in supernatants of stationary *S. elongatus* cultures. We assign this bioactivity to a hydrophilic compound that therefore differs from the metabolite cited above. Subsequent bioactivity-guided isolation, structural elucidation, and characterization of the mode of action reveal the first identified natural antimetabolite that targets the shikimate pathway in vivo.

## Results

**Isolation of the bioactive metabolite.** Supernatants of stationary cultures of *S. elongatus* inhibited the growth of *Anabaena variabilis*. The inhibitory activity could be extracted from lyophilized culture supernatants with the polar solvent methanol, but not with chloroform, acetone, or ethyl acetate as visualized by agar-diffusion plate assays (Fig. 1a). The producer strain was not affected by these extracts. Significant production of the inhibitor required CO<sub>2</sub> supplementation of liquid cultures and was dependent on the cell density of the producer strain. Inhibitor content apparently peaked after about 2 weeks of growth of *S. elongatus* cultivated in batch cultures in BG11 medium (Fig. 1b).

The chemical characterization of the bioactive compound indicated high polarity and absence of UV absorption. The low levels produced demanded an optimized bioactivity-guided isolation protocol with several enrichment and purification steps. A chromatographically pure compound was obtained via successive size-exclusion chromatography, medium-pressure liquid chromatography (MPLC) on normal phase, and ligand/ion-exchange high-performance liquid chromatography (HPLC) coupled to evaporative light-scattering detection (ELSD) (Supplementary Fig. 1). The molecular formula of the bioactive molecule was determined by electrospray ionization high-resolution mass spectrometry (ESI-HRMS) to be C<sub>7</sub>H<sub>14</sub>O<sub>6</sub> (M<sub>R</sub> = 194.18 Da from  $m/z$  = 217.0675 [M+Na]<sup>+</sup>) (Supplementary Fig. 2).

We elucidated the structure of the chromatographically pure compound using nuclear magnetic resonance (<sup>1</sup>H-NMR, <sup>13</sup>C-NMR, and two-dimensional spectra; Supplementary Table 1, Supplementary Figs. 12–16). The signals were assigned to the constitution of a 7-deoxyheptulose and indicated the relative

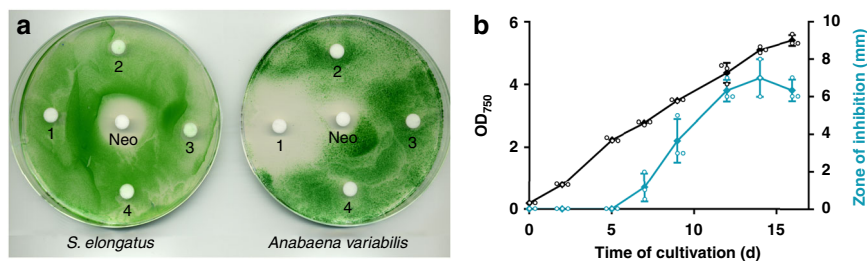


**Fig. 1** Extracts of supernatant of *Synechococcus elongatus* inhibits growth of *Anabaena variabilis*. **a** Agar-diffusion plate assay with the effect of organic extracts (1, methanol; 2, chloroform; 3, acetone, and 4, ethyl acetate) of lyophilized supernatant of stationary-phase *S. elongatus* cultures on the growth of the producer strain and *A. variabilis*. Neomycin (Neo, 20  $\mu$ g) served as positive control. **b** Optical density of producer strain *S. elongatus* (black) and zone of *A. variabilis* growth inhibition (diameter) of methanol extracts of *S. elongatus* supernatant on agar diffusion plates (turquoise). Values represent the mean values of three biological replicates; standard deviations are indicated. Dots indicate data distribution. Source data are provided as a Source Data file

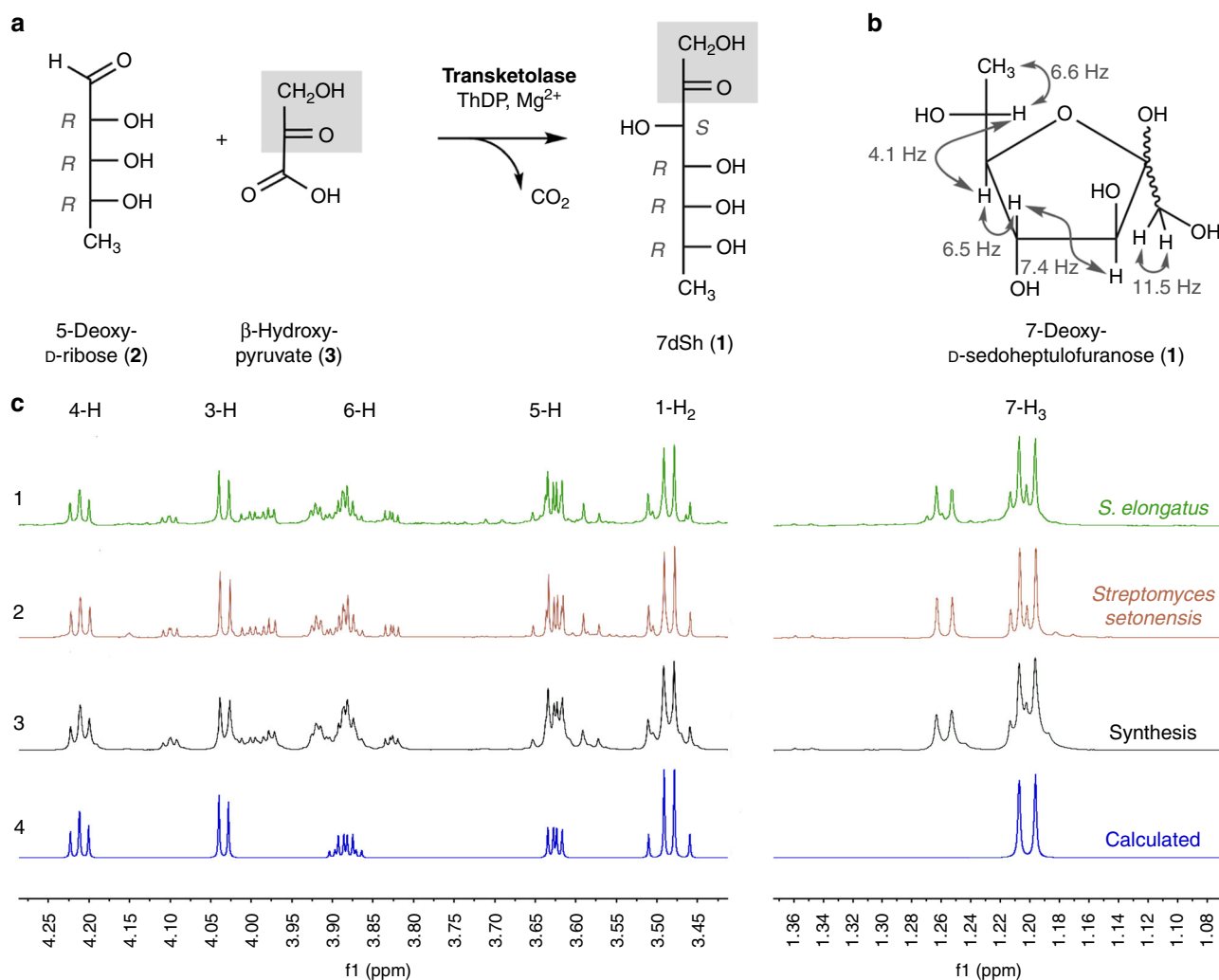


**Fig. 2** Structure and chemoenzymatic synthesis of 7-deoxy-sedoheptulose (7dSh, **1**). **a** Chemoenzymatic synthesis of 7-deoxy-sedoheptulose (7dSh). Absolute configurations of stereo-centers are indicated. **b** Chemical structure of 7dSh in the furanose form with given assignments of coupling constants (gray). **c** ( $^1\text{H}$  NMR spectra of 7dSh ( $\text{CD}_3\text{OD}$ , 600 MHz) chromatographically purified from supernatants of stationary phase cultures of *S. elongatus* (1, green), of the purified 7dSh from the supernatants of *Streptomyces setonensis* as control (2, red), and of enzymatically synthesized 7dSh (3, black). Predicted from assigned NMR-data (4, blue) of 7dSh in the 7-deoxy-D-*altro*-heptulofuranose form (Bruker, TopSpin software). Additional proton NMR signals in 1-3 give evidence for the dynamic forms of 7dSh in solution (open chain tautomers, ring conformers)

configuration mainly present in the furanose form (Fig. 2b, c). In marked contrast to six-membered sugar rings (pyranoses), the five-membered furanoses exhibit complex ring conformations, and the coupling pattern only allows a suggested

relative configuration<sup>27</sup>. The occurrence of pyranose and furanose forms of D-2-heptuloses are known for D-*altro*-2-heptulose, D-*manno*-2-heptulose, D-*galacto*-2-heptulose, and D-*gluco*-2-heptulose<sup>28</sup>. The only D-2-heptulose existing mainly in furanose form



corresponds to the *altro* configuration, which rendered this configuration most probable for the inhibitor isolated from culture supernatants of *S. elongatus*.

**Chemoenzymatic synthesis of 7-deoxy-sedoheptulose.** To unambiguously prove the chemical structure of the 7-deoxyheptulose from *S. elongatus* culture supernatants, we established the chemoenzymatic synthesis of 7-deoxy-D-*altro*-2-heptulose (**1**) (7-deoxy-sedoheptulose, 7dSh). C<sub>7</sub>-carbohydrate intermediates occur in the pentose phosphate pathway and can be biosynthesized by the transfer of a C<sub>2</sub>-unit onto a C<sub>5</sub>-precursor using the enzyme transketolase. Transketolase (EC 2.2.1.1) stereospecifically adds the nucleophile to the *re*-face of the D-enantiomers of 2-hydroxyaldehydes (aldoses) and controls the stereochemistry of the reaction to result in (3*S*, 4*R*)-configured ketoses<sup>29</sup>. We cloned the gene encoding the *S. elongatus* transketolase (Synpcc7942\_0538) in an *Escherichia coli* His-tag (pET15b) overexpression vector and purified the recombinant protein by affinity chromatography (see Methods). In the enzymatic synthesis of 7dSh, recombinant *S. elongatus* transketolase transfers the C1–C2 ketol unit of β-hydroxyypyruvate (**3**) to 5-deoxy-D-ribose (**2**) in the presence of thiamine diphosphate and divalent cations (Mg<sup>2+</sup>)<sup>30</sup> (Fig. 2a). Release of CO<sub>2</sub> from β-hydroxyypyruvate during the transketolase reaction prevents the back-reaction and enables a one-way synthesis of 7-deoxy-D-*altro*-2-heptulose (**1**), which is the only product according to NMR and MS data.

Transketolases efficiently react with phosphorylated sugars, but reactions with dephosphorylated sugars result in low yields<sup>31</sup>. In agreement, the chemoenzymatic synthesis of 7dSh from 5-deoxy-D-ribose gave yields of about 20%. We purified chemoenzymatically synthesized 7dSh following the same protocol used for purifying 7dSh from culture supernatants (Supplementary Fig. 1), except that size-exclusion chromatography on Sephadex LH20 could be omitted.

The <sup>1</sup>H-NMR spectrum of chemoenzymatically synthesized 7dSh (**1**) was identical to that of the compound isolated from *S. elongatus* culture supernatant. The chemical structure of 7dSh was reported in 1970 as the metabolite SF-666B from *Streptomyces setonensis* nav. sp. by Ezaki, Tsuruoka<sup>32</sup>. SF-666B was described to show exclusive activity against *Gluconobacter oxydans* subsp. *suboxydans* at low micromolar concentrations (0.8 μg mL<sup>-1</sup>)<sup>33</sup>. Therefore, we isolated SF-666B from culture supernatants of the *Streptomyces setonensis* production strain

following our purification protocol (Supplementary Fig. 1). NMR spectroscopy revealed that SF-666B is indeed identical to 7dSh isolated from *S. elongatus* culture supernatants and to chemoenzymatically synthesized 7dSh (Fig. 2c).

**Activity of 7dSh against cyanobacterial strains.** With the assigned structure of 7dSh (**1**) and milligram amounts of pure compound at hand, we aimed for detailed biological profiling of the compound. In contrast to the previously reported activity of SF-666B, none of the 7dSh preparations (chemoenzymatically synthesized, purified from culture supernatants of *S. elongatus* or *Streptomyces setonensis*) showed any activity against *Gluconobacter oxydans* under the previously described assay conditions<sup>33</sup> and under various other tested conditions (not shown). By contrast, all 7dSh preparations inhibited the growth of the filamentous cyanobacterium *A. variabilis*. To clarify the biological activity of 7dSh and its biological mode of action, we first analyzed the effects of 7dSh on cyanobacteria in more detail (Fig. 3).

The effect of 7dSh (**1**) on *A. variabilis* depended on the ratio between the 7dSh concentration and the cell density of the cultures (determined as optical density at 750 nm, OD<sub>750</sub>; Fig. 3a). Cultures with an initial OD<sub>750</sub> of 0.5 were hardly affected by 7dSh concentrations up to 5 μg mL<sup>-1</sup> (ca. 25 μM). When the cell density of *A. variabilis* was lowered to an OD<sub>750</sub> of 0.2, 7dSh had a dose-dependent effect. At a concentration of 2.5 μg mL<sup>-1</sup> (ca. 13 μM), 7dSh showed a cytostatic effect. A further increase of 7dSh to 5 μg mL<sup>-1</sup> resulted in lysis of the cells. With even lower initial cell densities (initial OD<sub>750</sub> < 0.05), the effect of 7dSh was even more pronounced; already 2.5 μg mL<sup>-1</sup> 7dSh had a bactericidal effect. Therefore, the effect of 7dSh on *A. variabilis* can be either bacteriostatic or bactericidal, depending on the amount of 7dSh available per cell. This result indicated a cellular binding site for 7dSh that reduces the titer of the compound in solution or a metabolic alteration of 7dSh.

We subsequently used bactericidal concentrations of 7dSh (**1**) for bioprofiling to obtain unambiguous results. Since 7dSh was active against a cyanobacterium but not against *Gluconobacter oxydans*, we speculated that 7dSh might target the photosynthetic apparatus. Treatment of *A. variabilis* with 7dSh (ca. 50 μM) led to a slow decrease in photosynthetic oxygen formation over a period of 24 h (Fig. 3b). This effect is in contrast to that of specific inhibitors of photosynthesis, such as 3-(3,4-dichlorophenyl)-1,1-dimethylurea, which act almost immediately. The slow decrease resembled the effect of the protein synthesis inhibitor

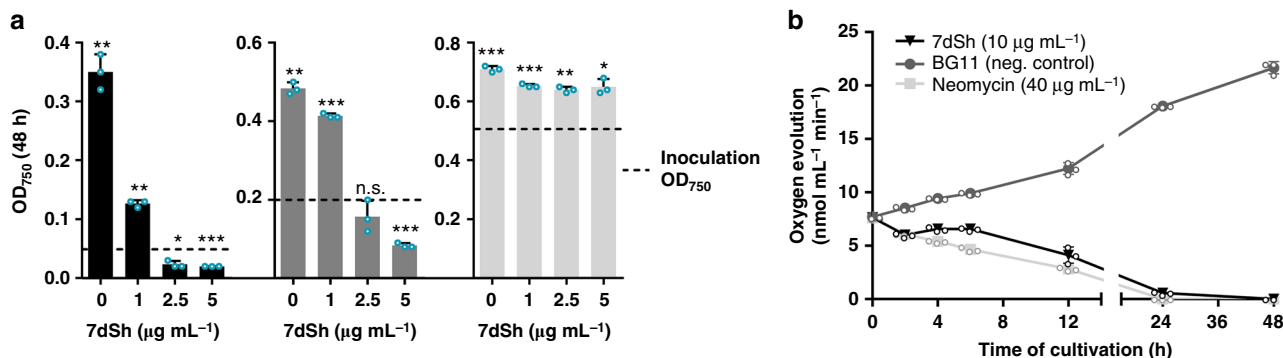


**Fig. 3** Effect of 7dSh (**1**) on the growth and photosynthetic oxygen evolution of *A. variabilis* cultures. **a** Growth of *A. variabilis* (OD<sub>750</sub>) at different concentrations of 7dSh after 48 h of incubation. Cultures were inoculated to an OD<sub>750</sub> of 0.05, 0.2, or 0.5 (marked by dashed lines). 7dSh in aqueous solution was added at time 0. Significant differences between adjusted initial OD<sub>750</sub> and OD<sub>750</sub> after 48 h were analyzed in a one sample *t*-test (\**p*-value < 0.05; \*\**p*-value < 0.01; \*\*\**p*-value < 0.001; n.s., not significant). **b** Photosynthetic oxygen evolution by *A. variabilis* (initial OD<sub>750</sub> = 0.3) in the presence of 7dSh or neomycin (positive control) or without supplementation (BG11, negative control). 7dSh (ca. 50 μM) and neomycin (ca. 65 μM) were added as aqueous solution. Values in both graphs represent the mean values of three biological replicates; standard deviations are indicated. Dots indicate data distribution. Source data are provided as a Source Data file

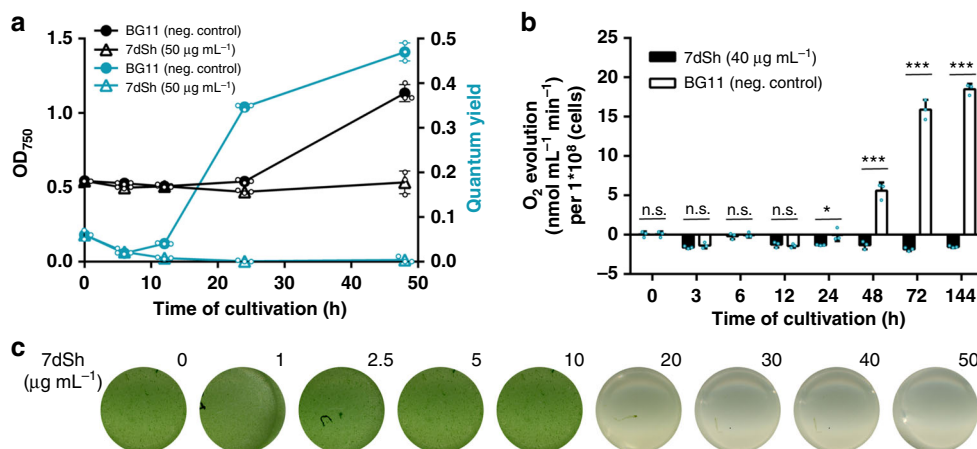


**Fig. 4** 7dSh (**1**) prevents regeneration of resuscitating *Synechocystis*. **a** Optical density (black) and PSII quantum yield (turquoise) of chlorotic *Synechocystis* cultures (initial  $OD_{750} = 0.5$ ) regenerating in the absence or presence of 7dSh.  $NaNO_3$  (17.3 mM) and 7dSh (ca. 260  $\mu M$ ) were added in aqueous solution at 0 h. Values represent the mean values of three biological replicates; standard deviations are indicated. Dots indicate data distribution. **b** Oxygen evolution of resuscitating *Synechocystis* cultures (initial  $OD_{750} = 0.5$ ) upon addition of nitrate ( $NaNO_3$ , 17.3 mM) in the presence or absence of 7dSh (ca. 206  $\mu M$ ). Significant differences between 7dSh treatment and untreated control for each timepoint were analyzed in an unpaired t-test (\* $p$ -value < 0.05; \*\* $p$ -value < 0.01; \*\*\*  $p$ -value < 0.001; n.s., not significant). Values represent the mean values of three biological replicates; standard deviations are indicated. Dots indicate data distribution. **c** Cultures of chlorotic *Synechocystis* (initial  $OD_{750} = 0.5$ ) 48 h after addition of nitrate ( $NaNO_3$ , 17.3 mM) and 7dSh. Numbers indicate concentration ( $\mu g mL^{-1}$ ) of 7dSh added to the culture. Source data are provided as a Source Data file

neomycin, which slowly decreases photosynthetic oxygen evolution by inhibiting the PSII repair cycle. This similarity suggested an indirect effect of 7dSh on photosynthesis, ultimately mediated by the inability to maintain the PSII repair cycle.

To narrow down the cellular processes targeted by 7dSh (**1**), we made use of the unique properties of the recovery of nitrogen-starved chlorotic cells as an experimental system, where different metabolic activities are activated in a sequential order<sup>34</sup>. Here, long-term nitrogen-starved *Synechocystis* sp. cells were allowed to resuscitate from chlorosis by adding nitrate. In a typical experiment, the cells return to vegetative growth within 48 h in a highly coordinated process. Almost immediately after nitrate addition, dormant cells switch on metabolism and re-establish the basic enzymatic machinery. After approximately 16 h, photosynthesis and  $CO_2$  fixation are turned on, and at the end of recovery, cells divide again. To reveal whether and at which stage resuscitation is blocked by 7dSh, chlorotic *Synechocystis* sp. cells were treated with 7dSh immediately before nitrate was added to initiate resuscitation. Following the addition of nitrate, control cultures showed the expected re-greening and return of photosynthetic activity<sup>34</sup>. The presence of 7dSh prevented resuscitation and re-greening in a dose-dependent manner (Fig. 4c). Measurement of oxygen exchange (Fig. 4b) and of PSII activity through pulse amplitude modulation (PAM) fluorometry<sup>35</sup> (Fig. 4a) showed that 7dSh-treated cells initially started respiratory glycogen consumption but then were unable to proceed further in the recovery and to restore their photosynthetic machinery. This clearly indicated that 7dSh affected metabolism at an early stage of resuscitation that is mainly characterized by anabolic reactions such as de novo amino acid synthesis<sup>34</sup>.

**Inhibition of 3-dehydroquinase synthase by 7dSh.** To elucidate the mechanism of action, the effect of 7dSh (**1**) on the metabolic pattern of resuscitating *Synechocystis* sp. and exponentially growing *A. variabilis* was analyzed. Liquid cultures of the respective cyanobacteria were incubated in the absence or presence of 7dSh. At different time points, cells were collected and

extracted with an acidic methanol/water solution (see Methods) for molecular analysis by LC-HRMS. Software-based subtraction (MetaboliteDetect 2.1, Bruker Daltonics) of the standardized MS chromatograms facilitated the detection of metabolic differences between cell samples of untreated and 7dSh-treated cultures. This analysis revealed a fast and massive accumulation of a metabolite with the sum formula of  $C_7H_{13}O_{10}P$  ( $M_R = 288.14$  Da from  $m/z = 289.0325$   $[M+H]^+$  and  $287.0171$   $[M-H]^-$ ) in 7dSh-treated cells. Within 1 h after 7dSh (**1**) addition to *A. variabilis* cultures, the concentration of the respective compound increased more than fifteen fold as compared to initial concentration of untreated control cultures ( $t = 0$  h) (Supplementary Fig. 3a, b). The accumulation of the respective compound further increased over time, reaching the 72-fold concentration (about 1.1  $\mu M$ ) as compared to untreated control cultures (about 16 nM) after 4 h. The sum formula ( $C_7H_{13}O_{10}P$ ) and comparison of the MS/MS fragmentation pattern (Supplementary Fig. 3c) with MetFrag insilico fragmentation<sup>36</sup> and data in the literature<sup>37</sup> revealed that the accumulated compound was 3-deoxy-D-arabino-heptulosonate 7-phosphate (DAHP) (**4**, Supplementary Fig. 4). DAHP is the substrate of 3-dehydroquinase (DHQ) synthase, one of the first enzymes in the shikimate pathway, which converts DAHP to DHQ. This essential reaction in shikimate biosynthesis cannot be bypassed by alternative enzymes. The accumulation of DAHP is in accordance with DHQ synthase being the biological target of 7dSh<sup>38</sup>. Within the five-step reaction mechanism for conversion of DAHP to DHQ by DHQ synthase<sup>39</sup>, the second step represents the  $\beta$ -elimination of the phosphate group of DAHP (Supplementary Fig. 4). We propose that 7dSh (**1**) mimics DAHP (**4**), the natural substrate of DHQ synthase. The C-7-methyl group of 7dSh, which is absent in DAHP, would impede the  $\beta$ -elimination in step 2, thereby leading to an inhibition of DHQ synthase and consequently the accumulation of DAHP.

Inhibition of the shikimate pathway triggers a metabolic perturbation that leads to decreased pools of aromatic amino acids, and, as a result of perturbed protein synthesis, also to the accumulation of non-aromatic amino acids such as leucine, valine, and arginine<sup>40</sup>. Thus, to confirm our hypothesis, we analyzed the levels of aromatic and selected non-aromatic amino

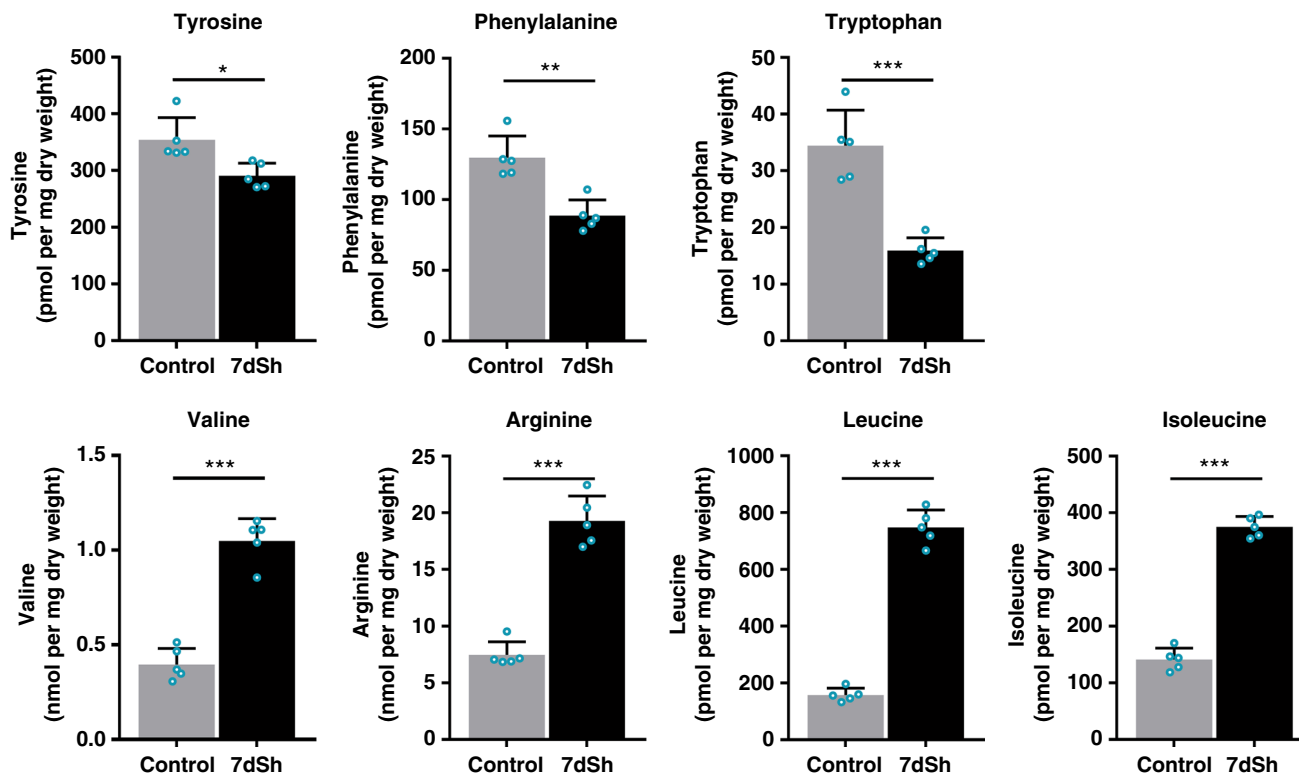


**Fig. 5** Effects of 7dSh (**1**) on amino acid levels in *A. variabilis* cells. Levels of selected amino acids in *A. variabilis* (initial  $OD_{750} = 0.5$ ) treated with 7dSh ( $260 \mu\text{M}$ ) for 4 h and respective untreated control cultures. Significant differences between 7dSh treatment and untreated control were analyzed in an unpaired *t*-test (\**p*-value < 0.05; \*\**p*-value < 0.01; \*\*\**p*-value < 0.001; n.s., not significant). Values represent the mean values of five biological replicates; standard deviations are indicated. Dots indicate data distribution. Source data are provided as a Source Data file

acids in 7dSh-treated and untreated *A. variabilis* cultures by LC-HRMS (Fig. 5). 7dSh (**1**) induced a significant accumulation of the non-aromatic amino acids leucine, isoleucine, valine and arginine. Within 4 h, the levels of isoleucine, arginine and valine increased almost threefold, and that of leucine about fivefold. By contrast, the levels of all aromatic amino acids significantly decreased in comparison to untreated control cultures (about 55% for tryptophan, 30% for phenylalanine and 20% for tyrosine).

The significant accumulation of DAHP (**4**) and changes in amino acid levels were also detected in cultures of nitrogen-starved *Synechocystis* sp. that were resuscitating from chlorosis in the presence of 7dSh (**1**) (Supplementary Fig. 5). Because of the lower metabolic activity of chlorotic cultures, DAHP accumulation was delayed but comparable to 7dSh-treated *A. variabilis* cultures.

We obtained further evidence that 7dSh (**1**) is an inhibitor of the shikimate pathway in an amino acid feeding experiment. The uptake of aromatic metabolites should mitigate the effects induced by 7dSh. PAM fluorometry of *A. variabilis* cultures revealed a 7dSh-induced decrease in the PSII quantum yield to about 10% of that of untreated control cultures (Supplementary Fig. 6). This effect was alleviated by supplementation with a mixture of aromatic amino acids. By contrast, supplementation of untreated control cultures with the aromatic amino acid mixture did not affect their PSII quantum yield. Supplementation with aromatic amino acids similarly alleviates the effects of glyphosate on other cyanobacteria<sup>41</sup>.

**Antifungal and herbicidal effects of 7dSh.** As the shikimate pathway occurs in other bacteria and in fungi and plants, we

decided to investigate the effects of 7dSh (**1**) on organisms other than cyanobacteria. We chose the yeast model organism *Saccharomyces cerevisiae* as the fungal representative. When *S. cerevisiae* was cultivated in YPD complex medium, 7dSh did not affect growth. By contrast, when the yeast was grown in YNB minimal medium with defined carbon and nitrogen sources, 7dSh ( $10 \mu\text{g mL}^{-1}$ , ca.  $50 \mu\text{M}$ ) inhibited growth (Supplementary Fig. 7), with a lower growth rate and a significantly lowered final optical density ( $OD_{600}$  of about 0.5) compared to growth in the absence of 7dSh (final  $OD_{600}$  of about 0.95). Glyphosate ( $100 \mu\text{g mL}^{-1}$ , ca.  $590 \mu\text{M}$ ) had to be applied at more than tenfold higher concentration to achieve a similar effect. A similar decreased growth rate instead of complete growth inhibition of microbes has earlier been described for glyphosate<sup>42</sup>. If an antimetabolite binds reversibly to the targeted enzyme, it will be replaced by the accumulating natural substrate. Therefore, a high intracellular concentration of the antimetabolite and low abundance of target enzyme favor inhibition of the targeted reaction. The observed residual growth of *S. cerevisiae* is consistent with a putative reversible binding of 7dSh.

As the representative for testing the effects of 7dSh (**1**) on plants, we chose the model organism *Arabidopsis thaliana*. Seedlings of *A. thaliana* germinated in mineral salt medium were significantly affected by micromolar concentrations of 7dSh. After 7 days, seedlings of the untreated control formed distinct roots with numerous root hairs and green cotyledons (Fig. 6a). The control seedlings showed gravitropism, and the distance between the shoot and root apical meristem was about 6 mm (Fig. 6b). Even a low concentration of 7dSh ( $5 \mu\text{g mL}^{-1}$ , ca.  $25 \mu\text{M}$ ) significantly affected the size of the seedlings. At concentrations of 25 or  $50 \mu\text{M}$ , the growth inhibition effects of 7dSh were similar to those of glyphosate at the same concentrations.

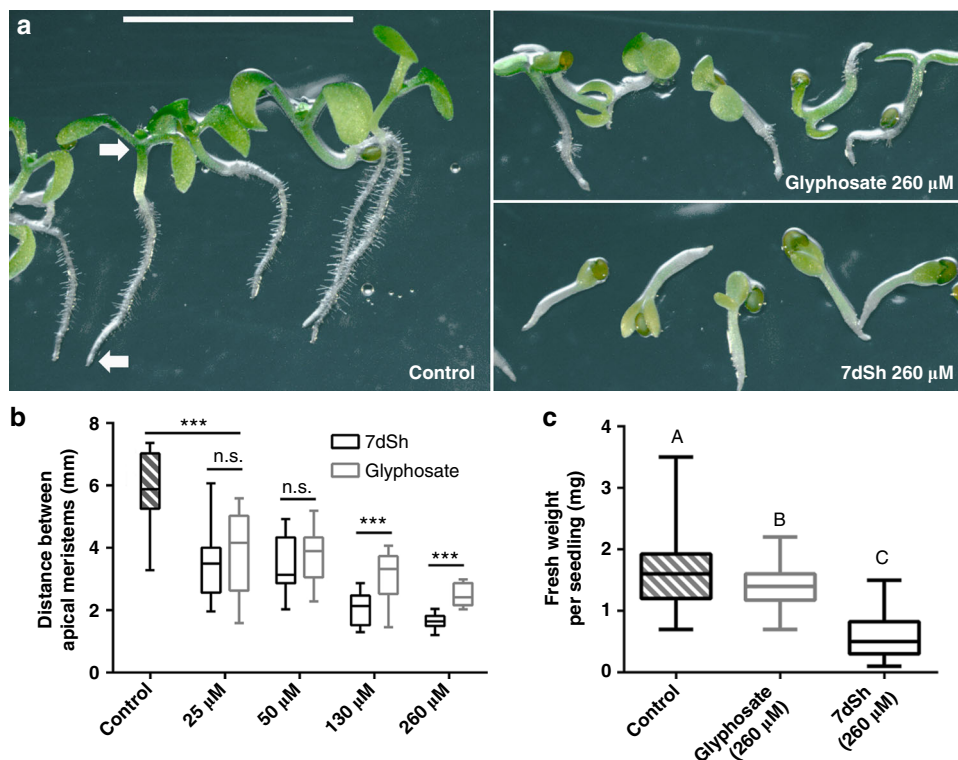


**Fig. 6** 7dSh (**1**) reduces the growth of *A. thaliana* seedlings. **a** Morphological appearance of autotrophically grown *Arabidopsis thaliana* seedlings 7 days after induction of germination. Seedlings were grown in constant light on agar plates without an antimetabolite (control) or in the presence of 7dSh or glyphosate. Plates were mounted vertically and illuminated from above. White arrows mark the root and shoot apical meristem. Scale bar (5 mm) applies to all images. **b** Measurement of the distance between root and shoot apical meristem. Significant differences between seedling sizes were analyzed in an unpaired *t*-test (\**p*-value < 0.05; \*\* *p*-value < 0.01; \*\*\* *p*-value < 0.001; n.s., not significant). Box-and-whisker plots represent the values of at least 16 seedlings. **c** Effect of 7dSh and glyphosate (each 260 μM) on the growth of *A. thaliana* on soil after 18 days in a day/night cycle. Statistical analysis was performed by using a one-way ANOVA. Tukey's multiple comparison test was used as the post-hoc test. Means that were significantly different (*p*-value < 0.05) are marked with different capital letters in the diagram. Box-and-whisker plots represent the values of at least 58 *A. thaliana* seedlings. For **b, c**: Error bars indicate range, box bounds indicate second and third quartiles, center lines indicate median. Source data are provided as a Source Data file

At concentrations of 130 and 260 μM, the inhibitory effect of 7dSh significantly surpassed that of glyphosate at the same concentrations, both in terms of seedling size (Fig. 6b) and morphological appearance (Fig. 6a). Impaired growth and aberrant morphology of the seedlings were particularly evident at higher concentrations of 7dSh (260 μM). In this case, the seedling growth was arrested within the first days. Only minor root and cotyledon formation was observed, and gravitropism was impaired (Fig. 6a and b). In comparison, *A. thaliana* seedlings that had been treated with higher concentration of glyphosate (260 μM) were less affected. They developed further, formed roots with small root hairs and bigger cotyledons. In the following days (day 7 to 14), no further plant growth or morphological change was observed in the presence of the inhibitors.

LC-HRMS analysis of whole plant extracts of the *A. thaliana* seedlings revealed a 7dSh-induced accumulation of DAHP, which was not detectable for the control or glyphosate-treated seedlings (Supplementary Fig. 8). As a proof of principle the accumulation of shikimate 3-phosphate was detectable in glyphosate-treated seedlings but not detectable in control or 7dSh-treated plants.

In order to evaluate the herbicidal activity of 7dSh (**1**) in more natural conditions, growth of *A. thaliana* in presence of the inhibitor was investigated in soil in a day/night cycle (Fig. 6c). After 18 days, seedlings were harvested and weighted. The weight

of the seedlings was significantly reduced in 7dSh and glyphosate treatment as compared to untreated control. Furthermore, the inhibitory effect of 7dSh significantly surpassed that of glyphosate as the weight of the 7dSh-treated seedlings was less than half as much as that of the glyphosate-treated seedlings.

Early germination events are characterized by the efficient reactivation of metabolic pathways<sup>43</sup>. Metabolites required for the induction of germination are stored in the seeds. Once these reserve materials are depleted, the proliferation of the seedlings relies on de novo synthesis of intermediates and growth factors. Glyphosate- or 7dSh-induced inhibition of the shikimate pathway therefore leads to an effective arrest of the seedling growth.

**Cytotoxicity of 7dSh on mammalian cells.** To determine whether 7dSh (**1**) affects mammalian metabolism, we tested various human cell lines (THP-1 macrophages, A549 human lung epithelial cells, HepG2 human liver epithelial-like cells, 293 human embryonal kidney cells) and primary human neutrophils in cytotoxicity assays. 7dSh did not show any cytotoxic effects on tested human cell lines and primary cells (Supplementary Fig. 9a), even at 5 mM, a concentration that is two orders of magnitude higher than that required for its herbicidal effect. Neither 7dSh nor glyphosate at 5 mM lysed cells, as measured by the release of lactate dehydrogenase. Further, the morphological appearance



of 7dSh-treated macrophages did not differ from that of the untreated control (Supplementary Fig. 9b,c).

**The biology of 7dSh for the producer strain.** It is surprising to us that 7dSh (1), which has never before been described in cyanobacteria, was isolated from the unicellular cyanobacterium *S. elongatus*. *S. elongatus* is a common laboratory strain but has never been described as a producer of hydrophilic secondary metabolites. The role of 7dSh in metabolism and for the physiology of the producer strain yet remains enigmatic. Due to the streamlined genome, which lacks classical secondary metabolite gene clusters<sup>25</sup>, the biosynthesis of 7dSh is not yet clear. However, to the best of our knowledge, a specific biosynthetic gene cluster or pathway may not be necessary for the biosynthesis of 7dSh. It has been shown for another cyanobacterial strain with a small genome, that enzymatic promiscuity enables the production of a large variety of secondary metabolites without the need of specific enzymes<sup>23</sup>. One of the enzymes known for enzymatic promiscuity is the transketolase, the enzyme we used for chemoenzymatic synthesis of 7dSh. The transketolase plays a fundamental role in cyanobacterial metabolism, e.g., in the Calvin cycle, and exhibits a wide substrate specificity. To shed light on the biosynthesis of 7dSh, we screened *S. elongatus* cultures for the presence of a potential 7dSh precursor. The screening resulted in the isolation of the monosaccharide 5-deoxy-D-ribose (2), a metabolite never isolated from nature before (Supplementary Fig. 10a, b, Supplementary Fig. 17–21).

The effective *in vitro* conversion of 5-deoxy-D-ribose (2) to 7dSh (1), carried out by the *S. elongatus* transketolase in our chemoenzymatic synthesis, suggests this reaction is the final step in the biosynthesis of 7dSh. The affinity of the cyanobacterial transketolase to 5-deoxy-D-ribose was about 100-fold lower than the affinity to the natural transketolase substrate D-ribose 5-phosphate (Supplementary Fig. 10c, d), enough to explain the minute levels of 7dSh produced by *S. elongatus* in later stages of growth, where CO<sub>2</sub> fixation and consequently D-ribose 5-phosphate levels decrease. Nevertheless, the synthesis of the assumed precursor 5-deoxy-D-ribose remains enigmatic. Future studies shall clarify whether this compound is a side product of a primary metabolic pathway or whether yet unidentified enzymes are involved.

The biological role of 7dSh (1) for the producer strain remains obscure. Since 7dSh shows allelochemical characteristics and is excreted to the medium, its production could also be a strategy of *S. elongatus* to protect its niches against other competitors. Even though the low production level of 7dSh in laboratory test conditions questions this hypothesis, the 7dSh concentration could be higher under certain natural conditions, such as in biofilms. Although *S. elongatus* laboratory strains usually grow planktonically, the re-isolated wild-type grows in a biofilm<sup>44</sup>. When growing in a biofilm or a microbial mat, the concentration of 7dSh could increase to a level sufficient to provide physiological effects such as controlling the surrounding microbial community.

## Discussion

This paper reports the first natural compound—the rare sugar 7-deoxy-sedoheptulose (7dSh; 1)—that acts as an *in vivo* inhibitor of the DHQ synthase as part of the shikimate pathway. Even though various inhibitors of DHQ synthase have been described in the literature<sup>38,45–47</sup> (Supplementary Fig. 11), none of these metabolites were reported to show strong *in vivo* activity against microbes or plants. Furthermore, in contrast to the known DHQ synthase inhibitors, 7dSh is comparatively simple to synthesize and production could be easily scaled up. Notably, 7dSh shows

*in vivo* activity, especially against autotrophically growing organisms. We expect that 7dSh would also inhibit the growth of microorganisms in habitats with minimal nutrient concentrations. In nutrient-saturated habitats, microorganisms can take up aromatic metabolites from their environment and thereby mitigate the effect of 7dSh. The promising *in vivo* activity confers 7dSh antibacterial, antifungal, and herbicidal characteristics, which could enable its deployment as an agent in agriculture, water management, veterinary medicine, and even human medicine. Additional studies are needed to determine the medical and economic potential of 7dSh.

## Methods

**Strains and culture conditions.** Cyanobacterial strains (*Synechococcus elongatus* PCC 7942, *Anabaena variabilis* ATCC 29413, and *Synechocystis* sp. PCC 6803) were routinely cultivated under photoautotrophic conditions with continuous illumination at 30–60  $\mu$ E (Lumilux de Lux, Daylight, Osram) at 27 °C. Cells were cultivated in flasks with shaking at 120–130 rpm. Unless indicated otherwise, cells were cultivated in BG11 medium<sup>48</sup> supplemented with 5 mM NaHCO<sub>3</sub>. For BG11 solid medium, 15 g L<sup>-1</sup> Bacto agar (Difco) was autoclaved separately and combined with BG11 liquid medium.

Large-scale batch cultures of *S. elongatus* were cultivated in 1 L flasks containing 700 mL BG11 medium for 14 days under illumination at 55  $\mu$ E. The cultures were gassed with air supplemented with 2% CO<sub>2</sub>. Batch cultures were inoculated with densely grown pre-cultures to an OD<sub>750</sub> of 0.2.

For cultivation of nitrogen-starved *Synechocystis* sp., NaNO<sub>3</sub> was omitted from BG11 medium as previously described<sup>34</sup>. Nitrogen starvation was initiated by centrifugation of the cells at room temperature at less than 3500  $\times$ g (Hereaus Megafuge 1.0 R). Cell pellets were washed, resuspended (desired OD<sub>750</sub> = 0.4) and cultivated in BG11 without NaNO<sub>3</sub> for two weeks (shaken in 500 mL Erlenmeyer flasks). Resuscitation of chlorotic cells was initialized by the centrifugation of the cells at less than 3500  $\times$ g (Hereaus Megafuge 1.0 R) followed by the resuspension of the cell pellets in BG11.

*Streptomyces setonensis* SF666 (NBRC No. 13797) and *Gluconobacter oxydans* subsp. *suboxydans* (VTT E-97003) were cultivated as previously described<sup>35</sup>. Briefly, *S. setonensis* was grown in complex media containing 2.5% (w/v) glucose, 3.5% (w/v) soy flour (soybean meal), 0.5% (w/v) soluble vegetable protein and 0.25% (w/v) NaCl at pH 7.0 and 28 °C for 7 days. Cultures were grown under constant shaking (250 rpm) in 500 mL Erlenmeyer flasks covered by foam caps. *G. oxydans* was grown in complex media containing 0.2% (w/v) Na-glutamate, 0.2% (w/v) K<sub>2</sub>HPO<sub>4</sub>, 2% (w/v) sucrose, 0.2% (w/v) peptone, 0.5% (w/v) yeast extract, 0.01% (w/v) MgCl<sub>2</sub>, 0.001% (w/v) FeSO<sub>4</sub> and 0.001% (w/v) MnSO<sub>4</sub> at pH 6.8 and 30 °C. Cultures were tested for their sensitivity against 7dSh on agar plates (1.5% (w/v) agar) and in liquid media in 96 well plates. 96 well plates were analyzed by a microplate reader (Tecan Spark®10 M) at a wavelength of 600 nm.

*Saccharomyces cerevisiae* was grown in yeast extract-peptone-dextrose (YPD)<sup>49</sup> medium or yeast nitrogen base (YNB) without amino acids (Sigma-Aldrich) medium supplemented with 0.5 g L<sup>-1</sup> fructose and 1 g L<sup>-1</sup> casamino acids with continuous shaking at 30 °C.

For agar plate experiments seeds of *Arabidopsis thaliana* accession Col-0 were germinated in half-strength Murashige and Skoog (MS) salts basal medium (Sigma Aldrich) agar plates (1.5%, w/v, Bacto agar) under constant illumination (60  $\mu$ E) at 24 °C. For simultaneous growth of seedlings, seeds were stored at 4 °C overnight prior to initiation of germination. Subsequent, seedlings were grown for 7 days. To achieve growth of seedlings along the agar, plates were mounted vertically and illuminated from above.

For *Arabidopsis thaliana* experiments in soil, 24-well plates (three plates for each condition) were filled half with autoclaved and dried GS90 standard soil (Patzter GmbH, Germany) and vermiculite. Subsequently, wells were filled with 750  $\mu$ L water (control), 7dSh or glyphosate (each 260  $\mu$ M in aqueous solution, for glyphosate pH 7 was adjusted with NaOH). Each well was planted with a single seed of *A. thaliana* and the plate was incubated at 4 °C in the dark for five days to ensure a simultaneous growth of the seedlings. After that the seedlings were transferred to a growth chamber (air humidity 40%) with a 16 h day (20 °C) and 8 h night (18 °C) cycle with a light intensity of 85  $\mu$ E. After 18 days the seedlings were harvested and weighted.

**Extraction of *S. elongatus* culture lyophilisates.** For lyophilisate extraction, 100 mL of *S. elongatus* batch cultures (grown for 14 days) were lyophilized. Lyophilisate was solved in 1 mL methanol, chloroform, acetone, or ethyl acetate. A 10  $\mu$ L aliquot of each extract was applied to agar diffusion plates spread with *A. variabilis*.

**Correlation of OD<sub>750</sub> and inhibitor production level.** At each time point, 25 mL of each *S. elongatus* batch culture was centrifuged at room temperature at 4500  $\times$ g for 5 min. The supernatant was evaporated to dryness, and the residue was dissolved in 80  $\mu$ L methanol. A 40  $\mu$ L aliquot of each extract was applied to agar diffusion plates spread with *A. variabilis*.

**A. variabilis growth inhibition assays.** The inhibition of the growth of *A. variabilis* by *S. elongatus* extracts was assayed in BG11 liquid medium and on BG11 solid medium. In agar diffusion tests, paper discs containing dried samples of *S. elongatus* extracts were applied to agar plates freshly inoculated with *A. variabilis*. Agar plates were incubated under constant illumination at 40  $\mu\text{E}$  and 27 °C for 5–6 days.

For growth inhibition assays in liquid medium, *A. variabilis* was grown in 24-well plates in 1 mL BG11 (initial OD = 0.05, unless stated otherwise). Test samples and controls were applied in water. The cultures were shaken at 100 rpm and 27 °C for 2–3 days under constant illumination at 40  $\mu\text{E}$ .

**Summary of 7dSh purification from *S. elongatus*.** Culture supernatants were adjusted to pH 4 with 0.5 M HCl and then lyophilized. The lyophilisate was extracted with methanol and concentrated in vacuo. The methanol extract was applied to a gel filtration/size-exclusion column (Sephadex LH20, 1.6  $\times$  80 cm, flow rate 0.5 mL min<sup>-1</sup>, in methanol). The active fractions ( $t_{\text{R}}$  ca. 8 h) were pooled, evaporated to dryness and loaded in silica gel onto a Si 35, SF10–4g cartridge for separation of metabolites by normal phase medium-pressure liquid chromatography (MPLC) at a flow rate of 10 mL min<sup>-1</sup> with a chloroform (solvent A) /methanol (solvent B) gradient as follows: 100% A, then solvent B in solvent A increased by 10% every 5 min to a total of 40% B in 25 min. The active fractions (elution after about  $t_{\text{R}}$  = 18–21 min) were pooled, evaporated to dryness, re-dissolved in water and loaded onto a ligand/ion-exchange high-performance liquid chromatography (HPLC) column (HiPlex Ca, 300 mm  $\times$  7.7 mm, Agilent). HPLC with isocratic water elution (flow 0.5 mL min<sup>-1</sup>, temperature column oven: 85 °C) for 20 min led to the chromatographically pure 7dSh (1) ( $t_{\text{R}}$  = 15 min).

**Physicochemical characterization of 7dSh from *S. elongatus*.** For high-resolution mass spectrometry (HR-MS) data, purified 7dSh (1) was applied to a HiPlex Ca column of a Dionex Ultimate 3000 HPLC system (Thermo Fisher Scientific) coupled to a maXis 4 G ESI-QTOF mass spectrometer (Bruker Daltonics). 7dSh was eluted isocratically with water (flow rate 0.5 mL min<sup>-1</sup>, temperature column oven: 85 °C) for 20 min. The ESI source was operated at a nebulizer pressure of 2.0 bar, and dry gas was set to 8.0 L min<sup>-1</sup> at 200 °C. MS/MS spectra were recorded in auto MS/MS mode with collision energy stepping enabled. The scan rates for full scan and MS/MS spectra were set to 1 Hz and 7 Hz, respectively. Sodium formate was used as internal calibrant in each analysis. The molecular formula was calculated from monoisotopic masses using the SmartFormula function of DataAnalysis (Bruker Daltonics).

NMR measurements were recorded on a Bruker AMX600-, Avance III HDX700-, and AVI400 instruments. Deuterated methanol or water was used as solvent and internal standard. All spectra were recorded at room temperature. Chemical shifts are reported as  $\delta$  values relative to the respective solvent as an internal reference. Coupling constants ( $J$ ) were reported in Hertz (Hz). Abbreviations of multiplicity: *s* = singlet, *d* = doublet, *dd* = doublet of doublet, *m* = multiplet. Optical rotations were measured with a Perkin–Elmer 241. *R<sub>f</sub>* values on TLC were determined on silica gel 60 F254 plates (Merck, 0.2 mm). Compounds were detected with orcinol staining reagent (10 mL sulfuric acid containing 0.1 g Fe (III)-chloride and 1 mL orcinol solution (in 6% ethanol)).

**Cloning and purification of *S. elongatus* transketolase.** The ORF *Synpcc7942\_0538* of *Synechococcus elongatus* PCC 7942 was PCR amplified using the primer combination 5'-CATCACAGCAGCGGCTGGTGCCGCGCGGCAGCCATATGCTCG AGATGGTTGTTGCGGCTCAATC-3' and 5'-AGCAGCCA ACTCAGCTTCCTTTCG GGCTTTGTTA GCAGCCGATCCTAGCCGATCA CTGCTTTCG-3'. After restriction of the pET15b vector with *Bam*HI, the fragment was fused with the vector backbone using Gibson assembly<sup>50</sup>. The final construct was introduced into *E. coli* BL21 (DE3) cells by transformation. Overexpression of *Synpcc7942\_0538* was induced by addition of 0.5 mM IPTG. After 12 h of induction at 37 °C, cells were harvested by centrifugation. All subsequent steps were carried out at 0–4 °C. The pellet was resuspended in 10 mL of lysis buffer (50 mM Tris-HCl, 300 mM NaCl, 10 mM imidazole, pH 7.5, protease inhibitor (complete ULTRA tablets, Roche), lysozyme, and DNase), and cells were lysed by sonification. Cell debris and insoluble material were removed by centrifugation (25 min at 4 °C and 35,000  $\times$  g). The cleared cell lysate was applied to a HisTrap HP column (GE Healthcare Life Science). After column washing, the bound proteins were eluted in fractions with 10 mL elution buffer (50 mM Tris-HCl, 300 mM NaCl, 500 mM imidazole, pH 7.5). Transketolase-containing fractions were combined, dialyzed in dialysis buffer (50 mM Tris-HCl pH 8.0, 100 mM NaCl, 5 mM MgCl<sub>2</sub>, 1 mM DTT, 0.5 mM EDTA, 50% glycerol) and stored at –20 °C.

**Chemoenzymatic synthesis of 7-deoxy-D-altrio-2-heptulose.** The synthesis of 7dSh (1) was inspired by the chemoenzymatic synthesis of sedoheptulose 7-phosphate<sup>51</sup>. 5-Deoxy-D-ribose (2) (Glentham Life Sciences) (50 mg, 250  $\mu\text{M}$ ) was dissolved in 1.5 mL HEPES buffer (100 mM, pH 7.5) containing thiamine pyrophosphate (1.3 mg, 2 mM) and MgCl<sub>2</sub> (0.4 mg, 3 mM).  $\beta$ -Hydroxypropionate (3) as its lithium salt hydrate (54 mg, 285 mM) was added, and the pH was adjusted to 7.5. The reaction was initiated by addition of 4 mg transketolase (EC 2.2.1.1), and the mixture was shaken at 400 rpm and 30 °C for 24 h (Thriller<sup>®</sup>, Peqlab). The

reaction was stopped by the addition of 6 mL methanol, followed by centrifugation (2500  $\times$  g, 10 min). The supernatant was evaporated to dryness, and 7dSh was purified as described in our purification protocol for extraction of 7dSh from *S. elongatus* cultures, except that size-exclusion chromatography on Sephadex LH20 was omitted.

**Photosynthetic oxygen evolution and PAM fluorometry.** Photosynthetic oxygen evolution was determined in vivo using a Clark-type oxygen electrode (Hansatech Instruments RS232, Norfolk, UK). Two milliliters of treated or untreated cultures were transferred to the measurement chamber. Oxygen formation was measured for 10 min at room temperature under illumination at 50  $\mu\text{E}$ . PSII activity was analyzed in vivo with a WATER- pulse amplitude modulation (PAM) chlorophyll fluorometer (Walz GmbH, Efeltrich, Germany). All samples were dark-adapted for 5 min before measurement. Measurement of the PSII quantum yield ( $F_v/F_m$ ) was performed at room temperature with WinControl Data Acquisition software.

**Analysis of cyanobacterial and herbal metabolite patterns.** Aliquots (2 mL) of cyanobacterial cultures were centrifuged (30 s, 20,817  $\times$  g), and the pellets were immediately frozen in liquid nitrogen. *A. thaliana* plants were crushed in a mortar under liquid nitrogen cooling. The pellets or plant materials were extracted with 600  $\mu\text{L}$  methanol, followed by a second extraction of the material with 600  $\mu\text{L}$  20% methanol containing 0.1% formic acid. Both supernatants of each material extraction were combined and lyophilized, and the residue was dissolved in 100  $\mu\text{L}$  20% methanol containing 0.1% formic acid. Extracts (10  $\mu\text{L}$ ) were examined by LC-HRMS (Dionex Ultimate 3000 HPLC system from Thermo Fisher Scientific, coupled to a maXis 4 G ESI-QTOF mass spectrometer from Bruker Daltonics). LC-HRMS settings were adopted from<sup>52</sup>. Obtained mass spectra were compared and processed using MetaboliteDetect (Bruker Daltonics). Molecular formulas were calculated from monoisotopic masses using the SmartFormula function of DataAnalysis (Bruker Daltonics).

**Quantification of amino acids and DAHP in *A. variabilis*.** For the quantification of amino acids (Trp, Tyr, Phe, Val, Arg, Leu, and Ile) and DAHP the freeze dried sample material (10 mL, OD<sub>750</sub> = 0.5) was homogenized with a Retsch ball mill (two cycles, 30 s each). Extraction was done with 400  $\mu\text{L}$  80% methanol containing 0.1% formic acid followed by a second extraction step with 400  $\mu\text{L}$  20% methanol also containing 0.1% formic acid. Both supernatants were combined and brought to dryness in a vacuum concentrator. The dried samples were redissolved in 150  $\mu\text{L}$  0.1 M hydrochloric acid for analyses.

Amino acid analyses were done with a Water UPLC-SynaptG2 LC-MS system. Chromatography was carried out on a 2.1  $\times$  100 mm Waters Acquity HSST3 column. For separation a 10 min gradient from 99% water to 99% methanol (both solvents with 0.1% formic acid) was used. The mass spectrometer was operated in ESI positive mode and scanned from 50 to 2000 *m/z* with a scan rate of 0.5 s. For quantification extracted ion chromatograms were generated and integrated. An external calibration function was used for the calculation of absolute amounts.

DAHP analyses were done on a Thermo Scientific/Dionex ICS 5000 system. Chromatography was carried out on a 3.0  $\times$  150 mm CarboPac PA 20 column. For separation a 32 min gradient from 75 mM sodium hydroxide to a 75 mM sodium hydroxide/500 mM sodium acetate mixture was used. Quantification was done by integration of the signal and absolute amounts were calculated with an external calibration function.

**Supplementation with aromatic amino acids.** *A. variabilis* in BG11 liquid medium (initial OD<sub>750</sub> = 0.2) was supplemented with aromatic amino acids to a final concentration of 1 mM tryptophan, 1 mM tyrosine, 1 mM phenylalanine, 1  $\mu\text{g}$  mL<sup>-1</sup> *p*-aminobenzoate, or 1  $\mu\text{g}$  mL<sup>-1</sup> *p*-hydroxybenzoate.

**Cytotoxicity of 7dSh on mammalian cells.** Human THP1 cells (DSMZ, ACC 16) were grown in RPMI 1640 medium with 2 mM glutamine, 10% heat-inactivated FBS, 2% HEPES, 1% penicillin-streptomycin (10000 U mL<sup>-1</sup>, Gibco) and 1 mM sodium pyruvate. To induce differentiation, cells were seeded in RPMI medium containing 1% penicillin-streptomycin and treated with 160 nM phorbol-12-myristate-13-acetate for 24 h. A546 cells, HepG2 cells, and HEK 293 cells were grown in Dulbecco's Modified Eagle's Medium (DMEM) with 10% Fetal Bovine Serum (FCS) and 1% penicillin-streptomycin. Human neutrophils were isolated from healthy blood donors by biocoll/histopaque density gradient centrifugation and resuspended in RPMI + 2% human serum albumin (HSA) + 2 mM sodium pyruvate + 10 mM HEPES. THP1 cells ( $1 \times 10^5$  or  $3 \times 10^5$ ) were seeded in 96-well cell culture plates in a final volume of 100  $\mu\text{L}$  or in 8-well  $\mu$ -slides in a final volume of 300  $\mu\text{L}$ , respectively. After differentiation, the cells adhered to the culture dishes. A546 (ATCC CCL-185) cells, HepG2 (ATCC HB-8065) cells, HEK 293 (InvivoGen 293-null) cells ( $0.5 \times 10^5$ ) and human neutrophils ( $1 \times 10^6$ ) were seeded in 96-well cell culture plates in a final volume of 200  $\mu\text{L}$ .

To evaluate the cytotoxic potential of 7dSh (1) and glyphosate, human THP1 macrophages were treated with 5 mM of the respective compounds in RPMI medium with 1% penicillin-streptomycin for 24 h. A546 cells, HepG2 cells, and HEK 293 cells were treated with 5 mM of the respective compounds for 24 h in DMEM medium (without phenol red) + 10% FCS + 1% penicillin-streptomycin.

Human neutrophils were treated in RPMI + 2% HSA + 2 mM sodium pyruvate + 10 mM HEPES for 5 h. Cells in medium were used as negative control, and cells treated with 1% Triton X-100 were used as positive control (100% cytotoxicity). After the indicated time points the cytotoxic potential of the compounds was determined according to the release of lactate dehydrogenase into the supernatant using the Cytotoxicity Detection Kit (Roche) following instructions of the manufacturer. The data represent the mean of three independent experiments.

For microscopic analysis, THP1 macrophages in 8-well  $\mu$ -slides were treated with 5 mM 7dSh in RPMI medium with 1% penicillin-streptomycin or were untreated for 24 h. Cells were fixed with 150  $\mu$ l icecold PBS containing 3.7% formaldehyde for 30 min. Wells were washed three times with HBSS, and incubated with 2.5  $\mu$ l Alexa Fluor 647 Phalloidin (Thermo Fisher) in 100  $\mu$ l PBS containing 1% BSA for 30 min. Cells were stained with one drop of NucBlue® Fixed Cell ReadyProbes® reagent (DAPI, Thermo Fisher) and mounted using fluorescence mounting medium (DAKO). Image acquisition was performed in the confocal mode of an inverted Zeiss LSM 710 NLO microscope employing Zeiss Plan-Apochromat  $\times$ 63/1.40 oil DIC M27 objective with the following excitation wavelengths: DAPI: 405 nm; Phalloidin: 633 nm. Images were exported in overlays as 16-bit tagged image files for further analysis. Overlays were batch processed for intensity and color balance.

**Isolation and structural elucidation of 5-deoxy-D-ribose.** 5-Deoxy-D-ribose (2) was isolated from cultures of *S. elongatus* as described for the isolation of 7dSh (1) from *S. elongatus* except that pooling of the fractions from chromatography was adapted to 5-deoxy-D-ribose. On Sephadex LH20, 5-deoxy-D-ribose co-eluted with 7dSh. On MPLC, 5-deoxy-D-ribose eluted after 14–15 min. On HPLC with a HiPlex Ca column, the compound showed a retention time of 25.5 min. The isolated compound and commercially available 5-deoxy-D-ribose (Glentham Life Sciences) were analyzed by NMR spectroscopy and mass spectrometry as described for 7dSh.

**Kinetic characterization of the *S. elongatus* transketolase.** The kinetics of the *S. elongatus* transketolase were characterized for D-ribose 5-phosphate (Sigma Aldrich) or 5-deoxy-D-ribose (2) (Glentham Life Sciences) as acceptors of the transferred C1-C2 ketol unit. Reaction mix contained 0.1 mM glycylglycine buffer pH 7.5, 3 mM MgCl<sub>2</sub>, 2 mM thiamine pyrophosphate (TPP), 0.5 mM NADH, 100 mM-D-erythrose, 10 units yeast ADH and 5.75  $\mu$ g mL<sup>-1</sup> *S. elongatus* transketolase. For determination of  $K_M$  and  $V_{max}$ , the substrate concentrations were varied: D-ribose 5 phosphate (0.1 mM to 2.0 mM) or 5-deoxy-D-ribose (75 mM to 600 mM). Absorption at 340 nm was recorded. The reaction was performed in a final volume of 200  $\mu$ l or 400  $\mu$ l. Michaelis–Menten kinetic profiles were determined using GraphPad prism.

**Reporting summary.** Further information on experimental design is available in the Nature Research Reporting Summary linked to this article.

## Data availability

Data supporting the findings of this work are available within the paper and its Supplementary Information files and from the corresponding authors upon reasonable request. The source data underlying Figs. 1, 3–6 and Supplementary Figs 3, 5, 6, 7, 9, and 10 are provided in Source Data file.

Received: 10 July 2018 Accepted: 9 January 2019

Published online: 01 February 2019

## References

- Nagle, D. G. & Paul, V. J. Chemical defense of a marine cyanobacterial bloom. *J. Exp. Mar. Bio. Ecol.* **225**, 29–38 (1998).
- Leão, P. N., Engene, N., Antunes, A., Gerwick, W. H. & Vasconcelos, V. The chemical ecology of cyanobacteria. *Nat. Prod. Rep.* **29**, 372–391 (2012).
- Sharif, D. I., Gallon, J., Smith, C. J. & Dudley, E. Quorum sensing in Cyanobacteria: N-octanoyl-homoserine lactone release and response, by the epilithic colonial cyanobacterium Gloeotheca PCC6909. *ISME J.* **2**, 1171–1182 (2008).
- Schaeffer, D. J. & Krylov, V. S. Anti-HIV activity of extracts and compounds from Algae and Cyanobacteria. *Ecotoxicol. Environ. Saf.* **45**, 208–227 (2000).
- Singh, R. K., Tiwari, S. P., Rai, A. K. & Mohapatra, T. M. Cyanobacteria: an emerging source for drug discovery. *J. Antibiot.* **64**, 401–412 (2011).
- Singh, I. P., Milligan, K. E. & Gerwick, W. H. Tanikolide, a Toxic and Antifungal Lactone from the Marine Cyanobacterium *Lyngbya majuscula*. *J. Nat. Prod.* **62**, 1333–1335 (1999).
- Berry, J. P., Gantar, M., Perez, M. H., Berry, G. & Noriega, F. G. Cyanobacterial toxins as allelochemicals with potential applications as algacides, herbicides and insecticides. *Mar. Drugs* **6**, 117–146 (2008).
- Rastogi, R. P. & Sinha, R. P. Biotechnological and industrial significance of cyanobacterial secondary metabolites. *Biotechnol. Adv.* **27**, 521–539 (2009).
- Cox, P. A., Banack, S. A. & Murch, S. J. Biomagnification of cyanobacterial neurotoxins and neurodegenerative disease among the Chamorro people of Guam. *Proc. Natl Acad. Sci.* **100**, 13380–13383 (2003).
- Dunlop, R. A., Cox, P. A., Banack, S. A. & Rodgers, K. J. The non-protein amino acid BMAA Is Misincorporated into Human Proteins in Place of L-Serine Causing Protein Misfolding and Aggregation. *PLoS One* **8**, e75376 (2013).
- Bentley, R. & Haslam, E. The shikimate pathway—a metabolic tree with many branches. *Crit. Rev. Biochem. Mol. Biol.* **25**, 307–384 (1990).
- Ducati, R., Basso, L. & Santos, D. Mycobacterial shikimate pathway enzymes as targets for drug design. *Curr. Drug. Targets* **8**, 423–435 (2007).
- Herrmann, K. M. & Weaver, L. M. The shikimate pathway. *Annu. Rev. Plant. Physiol. Plant. Mol. Biol.* **50**, 473–503 (1999).
- Duke, S. O. & Powles, S. B. Glyphosate: a once-in-a-century herbicide. *Pest. Manag. Sci.* **64**, 319–325 (2008).
- Motta, E. V. S., Raymann, K., Moran, N. A. Glyphosate perturbs the gut microbiota of honey bees. *Proc. Natl Acad. Sci.* **115**, 10305–10310 (2018).
- Benbrook, C. M. Trends in glyphosate herbicide use in the United States and globally. *Environ. Sci. Eur.* **28**, 3 (2016).
- Steinrücken, H. C. & Amrhein, N. The herbicide glyphosate is a potent inhibitor of 5-enolpyruvylshikimic acid-3-phosphate synthase. *Biochem. Biophys. Res. Commun.* **94**, 1207–1212 (1980).
- Lonhienne, T. et al. Structural insights into the mechanism of inhibition of AHAS by herbicides. *Proc. Natl Acad. Sci.* **115**, E1945–E1954 (2018).
- Daniel, G. M., Jian-Guo, W., Thierry, L. & William, G. L. Crystal structure of plant acetohydroxyacid synthase, the target for several commercial herbicides. *FEBS J.* **284**, 2037–2051 (2017).
- Leão, P. N. et al. Synergistic allelochemicals from a freshwater cyanobacterium. *Proc. Natl Acad. Sci.* **107**, 11183–11188 (2010).
- Paul, D. G. N. & Valerie, J. Production of secondary metabolites by filamentous tropical marine cyanobacteria: ecological functions of the compounds. *J. Phycol.* **35**, 1412–1421 (1999).
- Shih, P. M. et al. Improving the coverage of the cyanobacterial phylum using diversity-driven genome sequencing. *Proc. Natl Acad. Sci.* **110**, 1053–1058 (2013).
- Li, B. et al. Catalytic promiscuity in the biosynthesis of cyclic peptide secondary metabolites in planktonic marine cyanobacteria. *Proc. Natl Acad. Sci.* **107**, 10430–10435 (2010).
- Golden, S. S., Brusslan, J. & Haselkorn, R. Genetic engineering of the cyanobacterial chromosome. *Methods Enzymol.* **153**, 215–231 (1987).
- Copeland, A. et al. Complete sequence of chromosome 1 of *Synechococcus elongatus* PCC 7942 (2014).
- Cohen, A., Sendersky, E., Carmeli, S. & Schwarz, R. Collapsing Aged Culture of the Cyanobacterium *Synechococcus elongatus* Produces Compound(s) Toxic to Photosynthetic Organisms. *PLoS One* **9**, e100747 (2014).
- Wang, X. & Woods, R. J. Insights into furanose solution conformations: beyond the two-state model. *J. Biomol. NMR* **64**, 291–305 (2016).
- Collins, P. Ch. 8-H. *Dictionary of Carbohydrates*. (Chapman and Hall/CRC, 2005).
- Turner, N. J. Applications of transketolases in organic synthesis. *Curr. Opin. Biotechnol.* **11**, 527–531 (2000).
- Kobori, Y., Myles, D. & Whitesides, G. Substrate specificity and carbohydrate synthesis using transketolase. *J. Org. Chem.* **57**, 5899–5907 (1992).
- Sprenger, G. A., Schorken, U., Sprenger, G. & Sahn, H. Transketolase A of *Escherichia coli* K12. Purification and properties of the enzyme from recombinant strains. *Eur. J. Biochem.* **230**, 525–532 (1995).
- Ezaki, N., Tsuruoka, T., Ito, T. & Niida, T. Studies on new antibiotics, SF-666 A and B. I. Isolation and characterization of SF-666 A and B. *Sci. Rept Meiji Seika Kaisha* **11**, 15–20 (1970).
- Shomura, T. et al. Studies on new antibiotics, SF-666 A and B. II. Some biological characteristics of SF-666 A and B. *Sci. Rept Meiji Seika Kaisha* **11**, 21–25 (1970).
- Klotz, A. et al. Awakening of a Dormant Cyanobacterium from Nitrogen Chlorosis Reveals a Genetically Determined Program. *Curr. Biol.* **26**, 2862–2872 (2016).
- Schreiber, U., Bilger, W., Neubauer, C. Chlorophyll fluorescence as a noninvasive indicator for rapid assessment of in vivo photosynthesis. In: *Ecophysiology of Photosynthesis* (eds. Schulze E. -D., Caldwell M. M.) (Springer Berlin Heidelberg, 1995).
- Wolf, S., Schmidt, S., Müller-Hannemann, M. & Neumann, S. In silico fragmentation for computer assisted identification of metabolite mass spectra. *BMC Bioinforma.* **11**, 148 (2010).
- Oldiges, M. *Metabolomanalyse zur Untersuchung der Dynamik im Aromatenbiosyntheseweg in L-Phenylalanin Produzenten von Escherichia coli* (2005).
- Montchamp, J. L., Piehler, L. T. & Frost, J. W. Diastereoselection and in vivo inhibition of 3-dehydroquinate synthase. *J. Am. Chem. Soc.* **114**, 4453–4459 (1992).



39. Carpenter, E. P., Hawkins, A. R., Frost, J. W. & Brown, K. A. Structure of dehydroquinase reveals an active site capable of multistep catalysis. *Nature* **394**, 299–302 (1998).
40. Vivancos, P. D. et al. Perturbations of Amino Acid Metabolism Associated with Glyphosate-Dependent Inhibition of Shikimic Acid Metabolism Affect Cellular Redox Homeostasis and Alter the Abundance of Proteins Involved in Photosynthesis and Photorespiration. *Plant Physiol.* **157**, 256–268 (2011).
41. Powell, H. A., Kerby, N. W. & Rowell, P. Natural tolerance of cyanobacteria to the herbicide glyphosate. *New Phytol.* **119**, 421–426 (1991).
42. Fischer, R. S., Berry, A., Gaines, C. G. & Jensen, R. A. Comparative action of glyphosate as a trigger of energy drain in eubacteria. *J. Bacteriol.* **168**, 1147–1154 (1986).
43. Fait, A. et al. Arabidopsis seed development and germination is associated with temporally distinct metabolic switches. *Plant Physiol.* **142**, 839–854 (2006).
44. Parnasa, R. et al. Small secreted proteins enable biofilm development in the cyanobacterium *Synechococcus elongatus*. *Sci. Rep.* **6**, 32209 (2016).
45. Liu, J. S., Cheng, W. C., Wang, H. J., Chen, Y. C. & Wang, W. C. Structure-based inhibitor discovery of *Helicobacter pylori* dehydroquinase synthetase. *Biochem. Biophys. Res. Commun.* **373**, 1–7 (2008).
46. Le Marechal, P., Froussios, C., Level, M. & Azerad, R. The interaction of phosphonate and homophosphonate analogues of 3-deoxy-D-arabino heptulosonate 7-phosphate with 3-dehydroquinase synthetase from *Escherichia coli*. *Biochem. Biophys. Res. Commun.* **92**, 1104–1109 (1980).
47. Tian, F., Montchamp, J.-L. & Frost, J. W. Inhibitor Ionization as a Determinant of Binding to 3-Dehydroquinase Synthetase. *J. Org. Chem.* **61**, 7373–7381 (1996).
48. Rippka, R., Deruelles, J., Waterbury, J. B., Herdman, M. & Stanier, R. Y. Generic Assignments, Strain Histories and Properties of Pure Cultures of Cyanobacteria. *Microbiology* **111**, 1–61 (1979).
49. Yeast Extract–Peptone–Dextrose (YPD) Medium (Liquid or Solid). *Cold Spring Harbor Protocols* 2017, pdb.rec090563 (2017).
50. Gibson, D. G. et al. Enzymatic assembly of DNA molecules up to several hundred kilobases. *Nat. Methods* **6**, 343 (2009).
51. Charmantray, F., Helaine, V., Legeret, B. & Hecquet, L. Preparative scale enzymatic synthesis of D-sedoheptulose-7-phosphate from beta-hydroxyppyruvate and D-ribose-5-phosphate. *J. Mol. Catal. B-Enzym* **57**, 6–9 (2009).
52. Zettler, J., Zubeil, F., Kulik, A., Grond, S. & Kayser, L. Epoxomicin and Eponemycin Biosynthesis Involves gem-Dimethylation and an Acyl-CoA Dehydrogenase-Like Enzyme. *Chembiochem* **17**, 792–798 (2016).

## Acknowledgements

Work of the authors is supported and funded by the RTG 1708 “Molecular principles of bacterial survival strategies”, the Institutional Strategy of the University of Tübingen (Deutsche Forschungsgemeinschaft, ZUK 63) and the “Glycobiotechnology” initiative (Ministry for Science, Research and Arts Baden-Württemberg). We thank Dr. Klaus Eichele, Anorganic Chemistry, University of Tübingen for NMR-predictions. Thanks to Dr. Sandra Richter, ZMBP University of Tübingen, Dr. Dorothee Wistuba, University of Tübingen and Dr. Timo Niedermeyer, University of Halle and Dr. Christiane Wolz,

IMTT Tübingen for helpful discussions. We are indebted to Karen Brune for critically reading the manuscript.

## Author contributions

K.B. performed culture cultivation, isolated 7dSh (1) and 5-deoxy-D-ribose (2), designed and performed synthesis of 7dSh and HPLC-MS experiments of the metabolite pattern and the biological test systems, wrote manuscript with input from all authors. J.R. designed and performed plant assays on soil and performed statistical analysis. P.R. performed NMR analysis and interpreted NMR data. A.S. designed and performed cloning, purification and kinetic characterization of transketolase. L.B. and E.W. designed and performed cytotoxicity studies on mammalian cells. M.S. designed and performed DAHP and amino acid quantification. S.G. designed and interpreted chemical experiments, edited manuscript. K.F. designed and interpreted biological experiments, edited manuscript.

## Additional information

**Supplementary Information** accompanies this paper at <https://doi.org/10.1038/s41467-019-08476-8>.

**Competing interests:** University of Tübingen has filed a patent application that covers 7dSh, 7dSh analogs and their use (EKUT-0365, German patent application number DE10 2017 01 898.1, International patent application number PCT/EP2018/082440). The remaining authors declare no competing interests.

**Reprints and permission** information is available online at <http://npg.nature.com/reprintsandpermissions/>

**Journal peer review information:** *Nature Communications* thanks William Dyer, William Gerwick, and the other anonymous reviewer(s) for their contribution to the peer review of this work. Peer reviewer reports are available.

**Publisher's note:** Springer Nature remains neutral with regard to jurisdictional claims in published maps and institutional affiliations.



**Open Access** This article is licensed under a Creative Commons Attribution 4.0 International License, which permits use, sharing, adaptation, distribution and reproduction in any medium or format, as long as you give appropriate credit to the original author(s) and the source, provide a link to the Creative Commons license, and indicate if changes were made. The images or other third party material in this article are included in the article's Creative Commons license, unless indicated otherwise in a credit line to the material. If material is not included in the article's Creative Commons license and your intended use is not permitted by statutory regulation or exceeds the permitted use, you will need to obtain permission directly from the copyright holder. To view a copy of this license, visit <http://creativecommons.org/licenses/by/4.0/>.

© The Author(s) 2019



Manuscript ready for submission 2

**Strain dependent activation of the sensor kinase SaeS of *Staphylococcus aureus* by human neutrophil peptides 1-3 (HNP 1-3) is influenced by the D-alanylation of wall teichoic acids**

Lisa Bleul, Jana-Julia Götz, Jessica Ziemann, Andres Lamsfus-Calle, Hubert Kalbacher and Christiane Wolz

Manuscript ready for submission

Strain dependent activation of the sensor kinase SaeS of *Staphylococcus aureus* by human neutrophil peptides 1-3 (HNP 1-3) is influenced by the D-alanylation of wall teichoic acids

Lisa Bleul<sup>1</sup>, Jana-Julia Götz<sup>1,3</sup>, Jessica Ziemann<sup>1</sup>, Andres Lamsfus-Calle<sup>1</sup>, Hubert Kalbacher<sup>2</sup> and Christiane Wolz<sup>1\*</sup>

<sup>1</sup>Interfaculty Institute of Microbiology and Infection Medicine, University of Tuebingen, Tuebingen, Germany

<sup>2</sup>Interfaculty Institute of biochemistry, University of Tuebingen, Tuebingen, Germany

<sup>3</sup>present address: Centre for Biomedicine and Medical Technology, Heidelberg University, Medical Faculty Mannheim, Mannheim, Germany

Key words: Human neutrophil peptides, SaeS, *Staphylococcus aureus*, Wall teichoic acids, D-alanylation

For correspondence: Christiane Wolz, Elfriede-Aulhorn-Strasse 6, 72076 Tübingen, Germany, E-Mail address: [christiane.wolz@med.uni-tuebingen.de](mailto:christiane.wolz@med.uni-tuebingen.de); Phone: 49-7071-2980187. Fax: 49-7071-295165

## Abstract

The SaeRS two-component system of *Staphylococcus aureus* controls the expression of various secreted and cell bound virulence factors, which are important for the interaction with phagocytes. The histidine-kinase SaeS is activated by phagocytosis related signals like human neutrophil peptides (HNP1-3). However, some strains do not respond to HNP1-3 despite sequence identity in the *saePQRS* operon. This indicates that other factors are involved in the HNP1-3 dependent activation of SaeS. Interestingly, sensing of sodium hypochlorite was found independent of strain background, indicating different mechanisms. Our results show, that D-alanylation of wall-teichoic acids influences HNP1-3 dependent activation of SaeS. However, analyses of the *dltABCD* operon sequence and its expression as well as comparison of HNP1 sensitivity did not explain the different responsiveness. Strain dependent SaeS activation is likely due to subtle changes in cell-envelope properties.

## Introduction

*Staphylococcus aureus* is a major human pathogen that causes a variety of human diseases such as skin infections, sepsis, endocarditis, pneumonia and toxic shock syndrome (Gajdacs, 2019, Turner *et al.*, 2019). Professional phagocytes rapidly engulf and eradicate invading bacteria. However, *S. aureus* has developed a variety of immune evasion strategies (de Jong *et al.*, 2019, Moldovan & Fraunholz, 2019). Several toxins and immune-modulatory molecules are involved in these processes. The expression of these factors is driven by a complex interactive regulatory network. The SaePQRS system controls the expression of many important virulence genes thereby displaying a central regulator upon phagocytosis (Voyich *et al.*, 2005, Flack *et al.*, 2014, Cho *et al.*, 2015, Liu *et al.*, 2016). The *saePQRS* operon consists of four ORFs, of which *saeR* and *saeS* show strong sequence homology to response regulators (RRs) and histidine kinases (HKs) of bacterial two-component systems, respectively. The auxiliary proteins SaeP (lipoprotein) and SaeQ (membrane protein) were shown to form a protein complex with SaeS thereby activating SaeS phosphatase activity (Jeong *et al.*, 2012), indicating that they are required to return the system to the pre-activation state. The *saePQRS* operon (Fig. 1A) is transcribed from two promoters (P1 and P3) and a total of four overlapping RNAs (T1–T4) are detectable. The mature T1 transcript is transcribed from the auto-activated P1

promoter. The most abundant and stable T2 RNA is generated by RNaseY-dependent endoribonucleolytic cleavage of T1 between *saeP* and *saeQ* (Marincola *et al.*, 2012). T3 is transcribed from the constitutive P3 promoter to ensure a basal level of *saeRS* expression (Li & Cheung, 2008, Jeong *et al.*, 2011). The sensor kinase SaeS was classified as intramembrane-sensing histidine kinase (IM-HK) (Mascher, 2006). IM-HK's have short input domains consisting of two transmembrane regions and are missing an extracellular sensing domain making it likely that sensing occurs at the membrane interface. The N-terminal sensory domain of SaeS consists of two transmembrane regions with a short external linker region. A single amino acid substitution in the first transmembrane helix (L18P) in strain Newman renders the system hyperactive (Mainiero *et al.*, 2010). SaeS phosphorylation and thus activation of the system was shown to be mediated by phagocytosis related signals (Voyich *et al.*, 2009) such as human neutrophil peptides (HNP1-3), H<sub>2</sub>O<sub>2</sub> (Geiger *et al.*, 2008), sodium hypochlorite (NaOCl) (Loi *et al.*, 2018) or calprotectin via ion sequestering (Cho *et al.*, 2015). In several studies a very specific activation of SaeS by sub-inhibitory concentrations of HNP1-3 was confirmed for strains of the USA300 lineage (Flack *et al.*, 2014, Zurek *et al.*, 2014, Liu *et al.*, 2015). Other strains were rarely analysed concerning sensory mechanisms. However, the widely used strains 8325 or Col were found non-responsive to HNP1-3 sensing (Geiger *et al.*, 2008). The molecular mechanism by which the SaeS receives and processes cognate signals is not understood. For HNP1-3 mediated SaeS activation, residues of the linker domain as well as the first transmembrane region were found to be important (Flack *et al.*, 2014, Liu *et al.*, 2015). Nevertheless, SaeS activation and subsequent SaeR phosphorylation leads to regulation of at least 20 virulence genes containing a conserved SaeR binding motif (Mainiero *et al.*, 2010, Nygaard *et al.*, 2010, Sun *et al.*, 2010, Liu *et al.*, 2016). Two different classes of the Sae target promoters were identified. The class I (or low affinity) targets (e.g. *coa*, *eap*, and P1 promoter of *saePQRS*) require SaeS activation by a cognate signal and are highly expressed in the hyperactive strain Newman. Class II (or high affinity) targets (*hla* and *hlb*) are insensitive to the SaeS signalling or SaeS polymorphism (Mainiero *et al.*, 2010). Thus, only transcription of class I target genes are informative for SaeS activity. Here we analysed factors required for HNP1-3 dependent SaeS activation. Expression of *eap* was validated and used a read-out for SaeS activity. We show that D-alanylation of the wall-teichoic acid (WTA) is required for signal transduction. Strain

specific differences of HNP1-3 mediated SaeS activation are likely due to the different make-up of the cell envelope. However, SaeS activation through NaOCl likely occurs via a distinct mechanism which is independent of the strain background.

## Results

### *Strain-specific activation of SaeS by HNP1-3*

To confirm that the response to HNP1-3 is dependent on the strain background we analysed transcription of *saePQRS* and its canonical target gene *eap* in different strains. Addition of HNP1-3 resulted in induction of *sae* and *eap* in strain USA300, whereas in strain HG001 and Col the system was non-responsive (Fig. 1B). Strain Newman is known to be constitutive active due to mutation in SaeS (Mainiero *et al.*, 2010). We analysed whether the strain can respond to HNP1-3 when SaeS<sup>P</sup> is replaced by SaeS<sup>L</sup>. Indeed, strain Newman HG with chromosomally repaired SaeS (Mainiero *et al.*, 2010) was rendered HNP1-3 responsive similar to strain USA300. Thus, USA300 and Newman HG are representatives of HNP1-3 responder strains whereas strains HG001 and Col represent non-responder strains. Sequence comparison of these strains revealed no difference in *saePQRS* operon. This indicates that other strain features interfere with the SaeS signalling cascade.

### *Auto activation, SaePQ proteins or SaeS stability do not influence HNP1-3 signalling*

Sae P1 promotor fusions and transcriptional analysis of the *saePQRS* operon or *hla* are often used as read-out for Sae activity (Novick & Jiang, 2003, Bischoff *et al.*, 2004, Li & Cheung, 2008, Johnson *et al.*, 2011, Parsons *et al.*, 2014). However, from these analyses it remains unclear whether these factors interfere with P1 promoter activity (transcriptional regulation) or via SaeS activation (phosphorylation). One can assume that differences in transcriptional regulation are in part responsible for the observed strain specific gene expression of the *saePQRS* operon. Therefore, we unlinked SaeS activation by HNP1-3 from transcriptional regulation. We integrated the plasmids harbouring *saePQRS*<sup>L</sup>, *saeRS*<sup>L</sup> (native SaeS) or *saeRS*<sup>P</sup> (SaeS with L18P) into the *sae* mutant of USA300. In these constructs SaeS was fused with C-terminal 3x-FLAG. Full-length complementation resulted in *sae* and *eap* expression comparable to wild type strain with slight increase of the size of *sae* specific transcripts due to 3x-FLAG-fusion. Complementation with the short constructs (pRS<sup>L</sup> or pRS<sup>P</sup>) (missing *saeQ*, *saeP* and the autoregulatory P1 promoter) resulted in very

weak *saeRS* expression driven only by the internal P3 promoter (Fig. 1C). However, even under these conditions HNP1-3 resulted in strong *eap* activation similar to the full length, high *saePQRS* expressing construct. Thus, SaeS activation is largely independent of auto-regulation and factors influencing P1 promoter activity. This also indicates that strain specificity is not due to differential transcriptional regulation.

Thus, factors interfering with SaeS on the protein level are likely involved in the different responsiveness. In other two-component systems auxiliary proteins were shown to interfere with histidine kinases to modulate signal perception. However, we could exclude that the auxiliary proteins SaeP or SaeQ are involved in HNP1-3 sensing, because they are not present in the fully responsive short SaeRS constructs (Fig. 1C).

Previously, it was shown that SaeS<sup>P</sup> is less stable than SaeS<sup>L</sup> due to proteolytic cleavage by FtsH (Jeong *et al.*, 2011, Liu *et al.*, 2017). We hypothesised that activation of SaeS by HNP1-3 also renders the SaeS protein susceptible to FtsH cleavage. Therefore, we analysed SaeS protein abundance and localisation upon HNP1-3 challenge. We analysed USA300 and HG001 *sae* mutants complemented with the SaeRS-3xFlag fusions. SaeS was detected using anti-Flag antibodies. Consistent with previous results SaeS<sup>P</sup> was less abundant compared to SaeS<sup>L</sup> (Fig. 1D), likely due to proteolytic cleavage. However, HNP1-3 treatment had no impact on SaeS abundance indicating that HNP1-3 does not alter FtsH susceptibility. Moreover, SaeS abundance and localisation was not different between USA300 and HG001 and thus SaeS processing is not informative concerning strain difference in HNP1-3 dependent SaeS activation.

#### *Activation of SaeS by sodium hypochlorite and HNP1-3 is not correlated*

SaeS activation may be influenced by other factors, which might give a hint on the sensing mechanism through their mode of action (e.g. involvement of physiological parameters such as membrane charge or fluidity). We first tested other antimicrobial peptides for their ability to activate Sae. We chose melittin, the main component of the honeybee venom because it is structurally similar to HNP1-3, and the antimicrobial peptide LL-37 because it is also produced in human granulocytes. Melittin as well as LL-37 did not result in SaeS activation (Fig. 2A) emphasising the high specificity of HNP1-3. The Rho-inhibiting antibiotic Bicyclomycin (BCM) (Nagel

*et al.*, 2018), the proton ionophor CCCP (Muthaiyan *et al.*, 2008) and sodium hypochlorite (NaOCl) stress (Loi *et al.*, 2018) were recently shown to up-regulate genes of the SaeR regulon whereas fatty acids (Neumann *et al.*, 2015) were inhibitory. Under our conditions only the activating effect of NaOCl could be confirmed. Other substances showed only very weak or no effect on Sae activation (Fig. 2B). To test if NaOCl activates the Sae system also in a strain specific manner we analysed responder and non-responder strains upon NaOCl treatment. NaOCl led to SaeS activation in all analysed strains (Fig. 2C). However, now the HNP1-3 non-responder strains HG001 and Col showed higher SaeS activating capacity. This indicates that HNP1-3 and NaOCl signalling involve different mechanisms.

#### *D-Alanylation of the WTA influences HNP1-3 dependent SaeS activation*

Changes in the cell surface charge present a natural defence mechanism against cationic antimicrobial peptides such as HNP1-3 and might interfere with SaeS sensing. Surface charge is mainly influenced by lysinylation of phosphatidylglycerol via MprF (Oku *et al.*, 2004, Staubitz *et al.*, 2004) and D-alanylation of teichoic acids via the *dltABCD* operon (Peschel *et al.*, 1999). The GraRS two-component system responds to different CAMPs by activating the expression of *mrpF* and *dltABCD* (Li *et al.*, 2007) and thus a *graRS* mutant has a lower surface charge and is more susceptible to HNP1 (Yang *et al.*, 2012).

A *graRS* mutant was indeed impaired in HNP1-3 dependent SaeS activation (Fig. 3A). We next analysed whether lysinylation of phosphatidylglycerol and/or alanylation of teichoic acids mediate the effect. An *mrpF* mutant was only slightly impaired in SaeS activation. We next constructed a strain with IPTG inducible *dltABCD* operon. Of note, strains with full deletions of *dltABCD* were found to accumulate second side mutation. Under non-inducing conditions, the *dltABCD* mutant was impaired in SaeS activation similar to a *graRS* mutant (Fig. 3BC). *DltABCD* leads to D-alanylation of LTA and WTA. We thus analysed whether deletion of the substrate of D-alanylation also affects SaeS sensing. WTAs are glycopolymers with multiple functions (Weidenmaier & Lee, 2016) including resistance towards antimicrobial molecules (Peschel *et al.*, 1999, Peschel *et al.*, 2000, Brown *et al.*, 2012), antimicrobial fatty acids (Kohler *et al.*, 2009) and lysozyme (Bera *et al.*, 2007). Some mechanisms require glycosylation or D-alanylation of WTA. Deletion of *tagO*, the first gene of the WTA biosynthesis gene cluster, also resulted in inhibition of

HNP1-3 signalling (Fig. 3BC). To verify that indeed the lack of D-alanylation is the reason for abrogated sensing of a *tagO* mutant, we also included a *tarS/tarM* double mutant, which is deficient in glycosylation of the WTA. Glycosylation of WTA does not influence HNP1-3 dependent SaeS activation (Fig. 3B). The phenotype of the *tagO* as well as the mutation in the *dltABCD* operon could be successfully complemented (Fig. 3DE). Thus, D-alanylation of WTA is required for HNP1-3 dependent SaeS activation.

*Single-nucleotide polymorphism in dltD does not influence HNP1-3 dependent SaeS activation*

To gain insights into the strain specificity we compared *dltABCD* operon sequence of USA300 and HG001. There was one amino acid difference in *dltD* gene between both strains. We performed mutagenesis to exchange the *dltD* allele of USA300 with *dltD* of HG001 and vice versa. Inserting the *dltD* gene of USA300 in HG001 could not restore the ability to sense HNP1-3 and the *dltD* of HG001 in USA300 does not abrogate HNP1-3 dependent SaeS activation (Fig. 4A). Thus, the single amino acid substitution in *dltD* is not the responsible for the strain specific SaeS sensing mechanism.

*Strain specific SaeS activation does not correlate with dltABCD expression or defensive sensitivity*

D-alanylation of teichoic acids is a defence mechanism against CAMPs and one may assume that strain differences in the expression of the *dltABCD* operon might be the reason for strain specific sensing of HNP1-3. We therefore analysed expression of *dltA* in responder and non-responder strains. Without the addition of HNP1-3 there were no significant differences in *dltA* expression between the strains (Fig. 4B). Interestingly only the responder strains showed a trend (not significant) to elevated levels of *dltA* transcripts after addition of HNP1-3. We also tested if the strains show differences in the sensitivity against HNP1. Strains USA300 and HG001 seem to be slightly more sensitive but this does not correlate with HNP1-3 responsiveness (Fig. 4C).



## Discussion

The SaePQRS System of *S. aureus* is a major virulence regulator important for the interaction with professional phagocytes (Voyich *et al.*, 2005, Voyich *et al.*, 2009, Munzenmayer *et al.*, 2016) and responds to phagocytosis related signals such as HNP1-3 and NaOCl. Here we show that D-alanylation of the WTA influence the HNP1-3 dependent SaeS activation. We hypothesise that strain specific alterations of the cell-envelope are likely to influence this mechanism.

### *Role of WTA D-alanylation for SaeS sensing*

Mutations in either *tagO* or *dltABCD* resulted in severe inhibition of SaeS activation as shown by lack of *eap* induction upon HNP1-3 treatment. *Eap* expression was used as read-out for SaeS activation/phosphorylation. We show that *eap* induction is independent of transcriptional regulation of the *saePQRS* operon or the auxiliary proteins SaeP or SaeQ and is highly correlated to SaeS activation either by HNP1-3 treatment or by the constitutive active SaeS<sup>P</sup> allele as present in strain Newman. D-alanylation of WTA probably enables HNP1-3 to access SaeS or more likely another putative SaeS interaction partner finally resulting in SaeS conformational changes. The N-terminal sensory domain of SaeS was predicted to contain a nine amino acid long linker peptide located between two transmembrane helices (Liu *et al.*, 2015). It was proposed that the overall conformation of the SaeS transmembrane domains, not single residues in the extracellular loops is critical for the SaeS's kinase activity (Liu *et al.*, 2015, Liu *et al.*, 2016). This is consistent with the suggestion that the N-terminal region of intramembrane-sensing histidine kinases transduces external signals to the kinase domain via interaction with a "true sensor" (Mascher, 2014). Our results indicate that D-alanylation of WTA somehow supports the interaction of HNP1-3 with the proposed "true sensor". WTA is localised within the peptidoglycan and thus physical contact with SaeS is unlikely. We speculate a proposed "true sensor" may bridge the gap. Nevertheless, our data indicate that HNP1-3 dependent SaeS activation is highly specific and independent on HNP1-3 antimicrobial activity. This is based on our findings that i.) SaeS activation in responder and non-responder strains does not correlate with antimicrobial sensitivity of the strains; ii.) loss of D-alanylation results in higher antimicrobial activity but less SaeS activation imposed by HNP1-3; iii.) other cationic peptides with similar structure and antimicrobial property such as melittin or LL37 are not acting as signal for SaeS activation; iv.) membrane

perturbations imposed by the ionophor CCCP showed no effect on SaeS activation; v.) deletion of *mprF* did not abrogate HNP1-3 sensing.

### *Strain specificity*

We show that SaeS activation is highly strain specific despite identical *saePQRS* sequence. We compared SaeS activating ability of HNP1-3 and NaOCl. In contrast to HNP1-3, all investigated strains showed a response to NaOCl. Interestingly, the HNP1-3 responder strains USA300 and Newman HG were less responsive towards NaOCl indicating different underlying mechanisms for SaeS activation. HNP1-3 sensing requires D-alanylation of WTA. Thus, one may assume that difference in cell-envelope composition or properties account for the degree of responsiveness in different strains. WTA content and modification is probably variable in response to different environmental cues, different regulatory mechanisms and differs between strains (Schade & Weidenmaier, 2016, Wanner *et al.*, 2017). WTA content and modification was found to be modulated by the quorum sensing Agr system (Wanner *et al.*, 2017). One may speculate that the observed influence of Agr on Sae activation (Novick & Jiang, 2003, Geiger *et al.*, 2008) may be linked to altered cell-envelope in *agr* mutants. Any even subtle difference in the cell envelope including sequestering of ions (Koprivnjak *et al.*, 2006) might influence strain dependency of SaeS activation. It was recently shown that SaeS activity is repressed by Cu, Fe, and Zn and that the Zn bound-form of calprotectin relieves this repression (Cho *et al.*, 2015). However, our data indicate that there is no difference in *dltA* expression between responder and non-responder, which might explain the different responsiveness. We see a slight (not significant) induction of *dltA* upon HNP1-3 treatment, only in the responder strains. Nevertheless, we believe that upregulation of *dltA* cannot be the primary cause for the strain specific SaeS response due to the following reasons i.) other antimicrobial peptides (e.g. Melittin, LL37) also result in *dltABCD* upregulation but do not activate SaeS (Li *et al.*, 2007); ii.) the induction of *dltABCD* from the IPTG inducible promoter, renders *dltABCD* expression HNP1-3 insensitive, however SaeS is still responsive; iii.) *dltABCD* expression without HNP1-3 is strain dependent but does not correlate with SaeS activation. Furthermore, we aimed to mimic D-alanylation present in strain USA300, by exchanging the single amino acid substitution in the *dltD* gene of strain HG001. Unfortunately, we could not restore sensing through this approach. Therefore, strain specific differences remain

unsolved. Alternatively, expression or sequence of the proposed “true HNP1-3 sensor” might be different between strains. The elucidation of such factors/conditions might not be trivial due to the complex composition of the cell-envelope.

## Experimental procedures

### *Bacterial strains and growth conditions*

*S. aureus* strains (Suppl. Table S1) were grown in tryptic soy broth (TSB). For strains carrying resistance genes, antibiotics were used only in pre-cultures (5 µg/ml tetracycline, 10 µg/ml erythromycin or chloramphenicol). For experiments with antimicrobial peptides, a modified lysogeny broth (LB50, half yeast extract [2.5g/liter] and half tryptone [5g/liter], no NaCl, LB50) was used, as described elsewhere (Peschel *et al.*, 1999). The overnight cultures were washed with LB50 and diluted to an initial OD<sub>600</sub> of 0.1 in fresh LB50 medium without antibiotics. For the conditional *dlt* knockout strain (USA300 pCG477) IPTG (0.75 mM) was added in all pre-cultures and on agar plates. For analysis of *dltABCD* knockdown the strain was grown without IPTG. Strains were grown at 37°C with constant shaking to OD<sub>600</sub> of 1 and then aliquots were treated with human neutrophil peptides (5 µg/ml HNP1-3), synthetic HNP1 (5µg/ml, Peptanova), Melittin (0.05µM, Sigma), LL-37 (5µM and 10µM), Bicyclomycin (BCM, 80µg/ml, Santa Cruz Biotechnology), Carbonyl cyanide 3-chlorophenylhydrazone (CCCP, 0.1 and 0.5 µM, Sigma), Sodium hypochlorite (NaOCl, 1mM and 2mM, Morphisto), Oleic acid (10µM and 100µM, Sigma). Cultures were further incubated for 1 h at 37°C with constant shaking and harvested for Northern and Western Blot analysis.

### *Isolation of HNP1-3 from human neutrophils*

Neutrophils were isolated from peripheral blood by gradient centrifugation (Geiger *et al.*, 2012) and human neutrophil peptides HNP1–3 were isolated as described previously (Harwig *et al.*, 1994). The lyophilized samples were dissolved in 0.01% acetic acid at a concentration of 1 mg/ml. Purities of all three defensin variants HNP1, HNP2, and HNP3, purity and quality was confirmed by ESI-MS with the expected masses.

### *Generation of mutants and construction of plasmids*

The markerless *tagO* deletion mutant was obtained using the mutagenesis vector pBASE6 (Geiger *et al.*, 2012). Flanking regions were amplified, and cloned into pBASE6 by using Gibson assembly (Oligonucleotides listed in Table S2). The resulting plasmid pCG472 was transformed into RN4220 followed by transduction into *S. aureus* strain USA300. The markerless *saePQRS* deletion mutant in HG001 was obtained by transforming RN4220 with the mutagenesis vector pCG335 (Munzenmayer *et al.*, 2016) followed by transduction of the plasmid into *S. aureus* strain HG001. Mutageneses were performed as described (Bae and Schneewind, 2006). Mutations were verified by PCR using oligonucleotides in the mutated gene, phenotypically on blood agar plates to confirm the expected haemolytic pattern and with coagulase to test for Sae functionality. For Sae complementation plasmids *saeRS* or *saePQRS* including P1 Promotor were amplified and cloned into the SAPI integration vector pJL42 using the SphI/Ascl restriction sites. The resulting Plasmids for SaeRS (pCG421) and SaePQRS (pCG422) served as backbone for the construction of the SaeS-3xFlag fusion Plasmids. 3x-Flag and Terminator were amplified from pMIB5892 and cloned into pCG421 and pCG422 using Gibson assembly resulting in pCG667 and pCG555, respectively. SaeS-3xFlag fusion Plasmid with the Newman L18P substitution in SaeS was obtained with site-directed-mutagenesis of pCG667 resulting in pCG668. To obtain a conditional *dltABCD* knockout mutant part of the *dltABCD* operon was cloned behind a IPTG-inducible Pspac promoter in the vector pMUTIN4 using the EcoRI/BamHI restriction sites. The resulting plasmid pCG477 was integrated into RN4220 followed by transduction into *S. aureus* strain USA300. Single mutants of other genes in strain USA300 were obtained by transduction using donor strains listed in Table S1. All mutants were verified by PCR and phenotypically on blood agar plates to confirm the expected haemolytic pattern.

### *Western Blot analysis*

Equal amounts of bacteria were washed with 1x TE buffer and incubated 10 min on ice in 1x TE with Protease inhibitor cocktail (EDTA-free mini tablets, Roche). Cells were lysed with 0.5 ml of zirconia-silica beads (0.1 mm diameter) in a high-speed homogenizer and spun down at 13000 rpm for 30min to clarify the lysate. Membranes were pelleted by ultracentrifugation for 1h at 55,000 rpm and 4°C

(Beckman TLA-55 rotor). RunBlue LDS sample buffer (Expedeon) containing additional 100mM DTT for reducing conditions was added to the supernatant (referred to as cytoplasm) and to the pellets (referred to as membrane) and then heated for 10 min at 95°C. Run blue dual color prestained SDS-marker (Expedeon) and samples were loaded onto 12% SDS-PAGE gel (Expedeon) for electrophoresis and either stained with Comassie or transferred to polyvinylidene difluoride (PVDF) membrane (Biorad) by wet transfer in Tris-Glycine-SDS buffer (TGS buffer, Expedeon). Membranes were blocked with 5% non-fat dried milk powder in 1x Tris-buffered saline containing 0.05% Tween20 for 1 h and then incubated with primary mouse anti-Flag antibody (Sigma Aldrich) followed by goat anti-mouse HRP-conjugated secondary antibody. Membrane blot was developed using Pierce ECL Western Blotting Substrate (Thermo Scientific).

#### *RNA isolation, Northern Blot analysis and quantitative reverse transcription PCR (qRT PCR)*

RNA was isolated as described (Geiger et al., 2012). Briefly, bacteria were lysed in 1 ml of Trizol reagent (Invitrogen Life Technologies) with 0.5 ml zirconia-silica beads (0.1 mm-diameter) in a high-speed homogenizer (Fastprep-24, MP). RNA was isolated as described in the manufacturer instructions of Trizol. DNA was removed using DNase I (recombinant, Roche) when qRT PCR was performed after. Northern Blot analysis was performed as described previously (Goerke *et al.*, 2000). Digoxigenin-labeled probes were generated according to the digoxigenin labelling PCR Kit (Roche) with oligonucleotides described. qRT PCR was performed as described (Munzenmayer *et al.*, 2016) and relative quantification of the genes of interest was expressed in relation to the expression of the constitutive reference gene *gyrB* ( $\Delta\Delta C_t$  method).

#### *Susceptibility of S. aureus to HNP1*

HNP1 susceptibility assay was performed as described (Xiong *et al.*, 1999) with HNP1 concentrations ranging from 0.39 to 6.25  $\mu\text{g/ml}$  (in a final volume of 100 $\mu\text{l}$ ). Briefly peptide and logarithmic phase *S. aureus* cells (final inoculum  $10^5$  CFU/ml) were added in a 96 well low binding microtiter plate and incubated 2h at 37°C. After

incubation appropriate dilutions were plated on tryptic soy agar plates and incubated at 37°C for the enumeration of colony forming units (cfu) on the following day.

*Ethics*

Blood was taken from healthy donors in strict accordance with the institutional guidelines, according to Declaration of Helsinki principles. The protocol was approved by the Institutional Review Board of the University of Tübingen. Written informed consent was received from all participants.

The work was supported by grants from the Deutsche Forschungsgemeinschaft (TR156, project A2) to CW and LB, the Landesgraduiertenförderung BW to LB. We thank Natalya Korn and Vittoria Bisanzio for excellent technical assistance.

### Legends to the Figures

Figure 1: *HNP1-3 dependent SaeS activation*. (A) SaePQRS operon architecture indicating the transcriptional units (T1-T4) starting from promoter P1 or P3 respectively and the RNase Y cleavage site. (B and C) *S. aureus* strains were grown to OD<sub>600</sub> of 1 and aliquots treated without or with human neutrophil peptides (5 µg/ml HNP1-3) for 1 h. 2µg of total RNA was hybridized with DIG-labeled probes for detection of *sae* and *eap* transcripts. 16S rRNA was used as loading control. T1, T2 and T3 indicate the different *sae* transcripts. (D) *S. aureus* strains were grown as described above and harvested for Western Blot analyses. SaeS was detected using anti-Flag antibody. (C and D) pPQRS<sup>L</sup>: integrative *sae* full-length complementation, pRS<sup>L</sup>: integrative complementation with *saeRS<sup>L</sup>* (native SaeS), pRS<sup>P</sup>: integrative complementation with *saeRS<sup>P</sup>* (SaeS with L18P).

Figure 2: *Sodium Hypochlorite dependent SaeS activation*. (A and B) *S. aureus* strain USA300 was treated with HNP1-3 (5µg/ml), Melittin (0.05µM), LL-37 (5µM and 10µM) (A), synthetic HNP1 (5µg/ml), Bicyclomycin (BCM, 80µg/ml), Carbonyl cyanide 3-chlorophenylhydrazone (CCCP, 0.1 and 0.5 µM), sodium hypochlorite (NaOCl, 1mM and 2mM) or oleic acid (10µM and 100µM) (B) and strains USA300, HG001, Newman HG and Col were treated with 2mM NaOCl (C) for 1 h. Northern Blot analyses was performed as described above.

Figure 3: *D-Alanylation of the WTA influences HNP1-3 dependent SaeS activation*. *S. aureus* strains were grown with HNP1-3 (5µg/ml) for 1h. Northern Blot analyses (A,B,D and E) was performed as described above (C) qRT-PCR with RNA of USA300 and its isogenic *dlt* and *tagO* mutant. Relative quantification of the *sae* was expressed in relation to the expression of the constitutive reference gene *gyrB*. Significance was determined by one-way analysis of variance with Tukey's multiple comparison post-test. The data represent the mean of three independent experiments. \*\*P < 0.01, ns, not significant.

Figure 4: *dltA expression and sensitivity towards HNP1-3*

*S. aureus* strains were grown with HNP1-3 (5µg/ml) for 1h. (A) Northern Blot analyses was performed as described above (B) qRT-PCR with RNA of strains USA300, HG001, Newman HG and Col. Relative quantification of *sae* was expressed

in relation to the expression of the constitutive reference gene *gyrB*. (C) *S. aureus* strains USA300, HG001, NewmanHG and Col were incubated with HNP1 concentrations ranging from 0.39 to 6.25 µg/ml (in a final volume of 100µl) for 2h at 37°C and colony counts enumerated. Bacterial counts after HNP1 treatment are expressed in relation to untreated control.



Figure 1

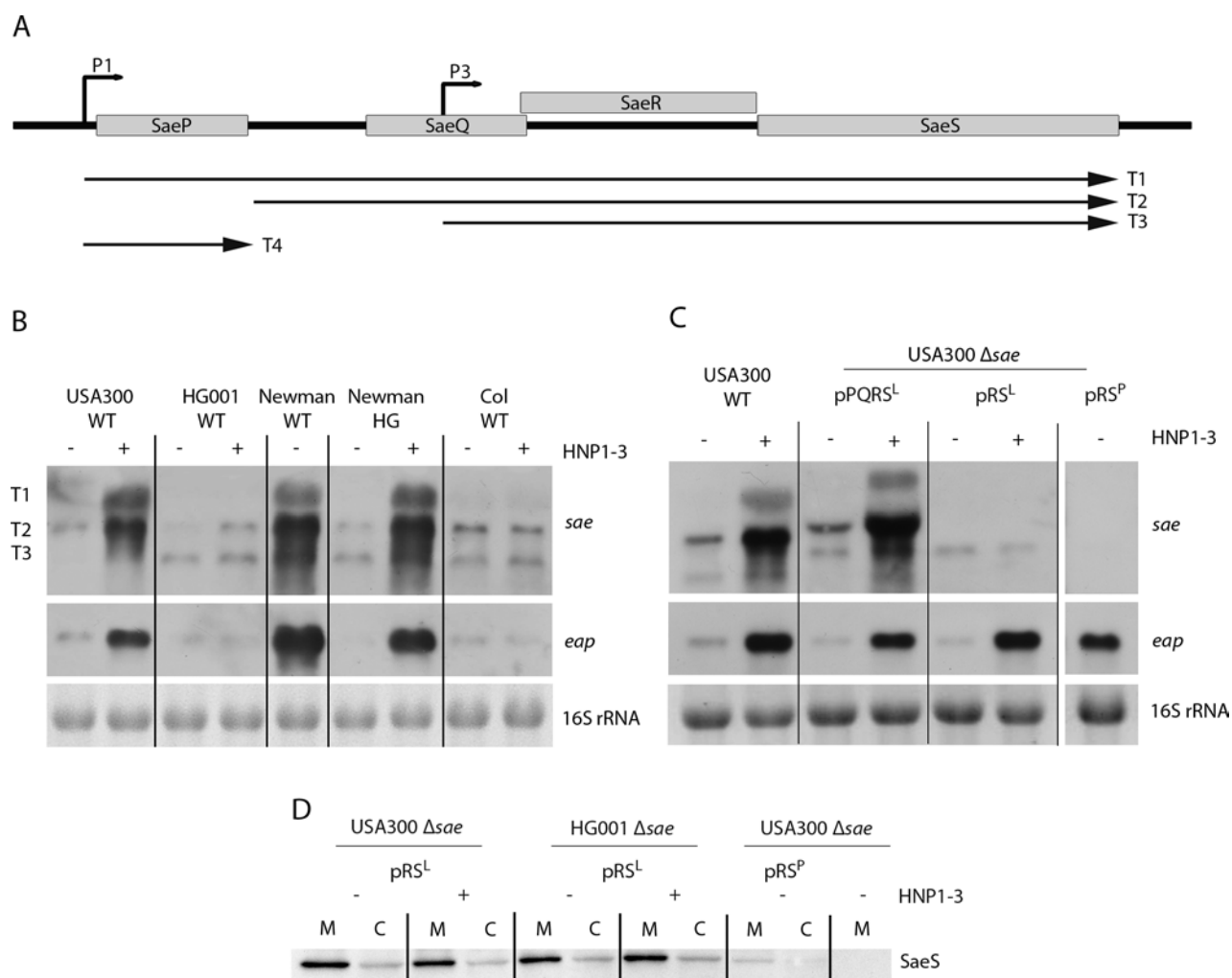


Figure 2

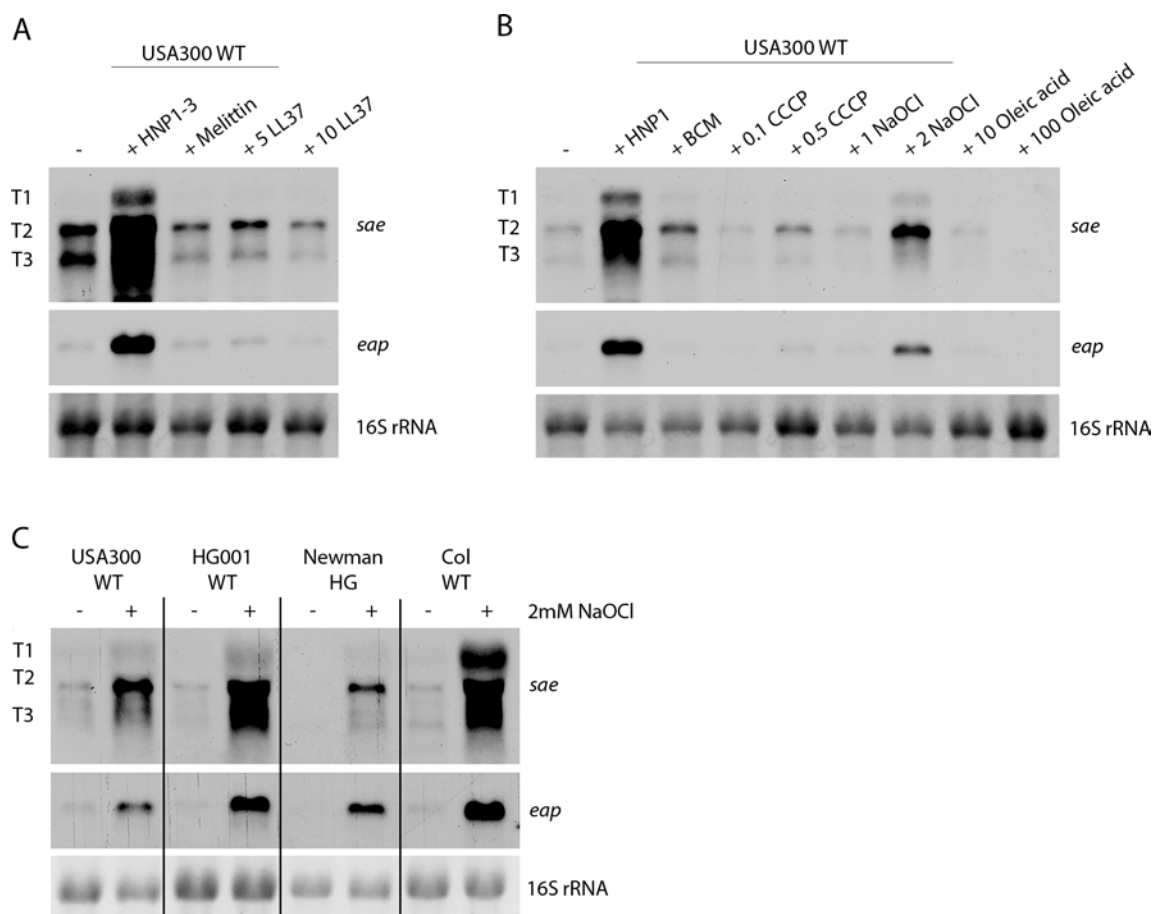


Figure 3

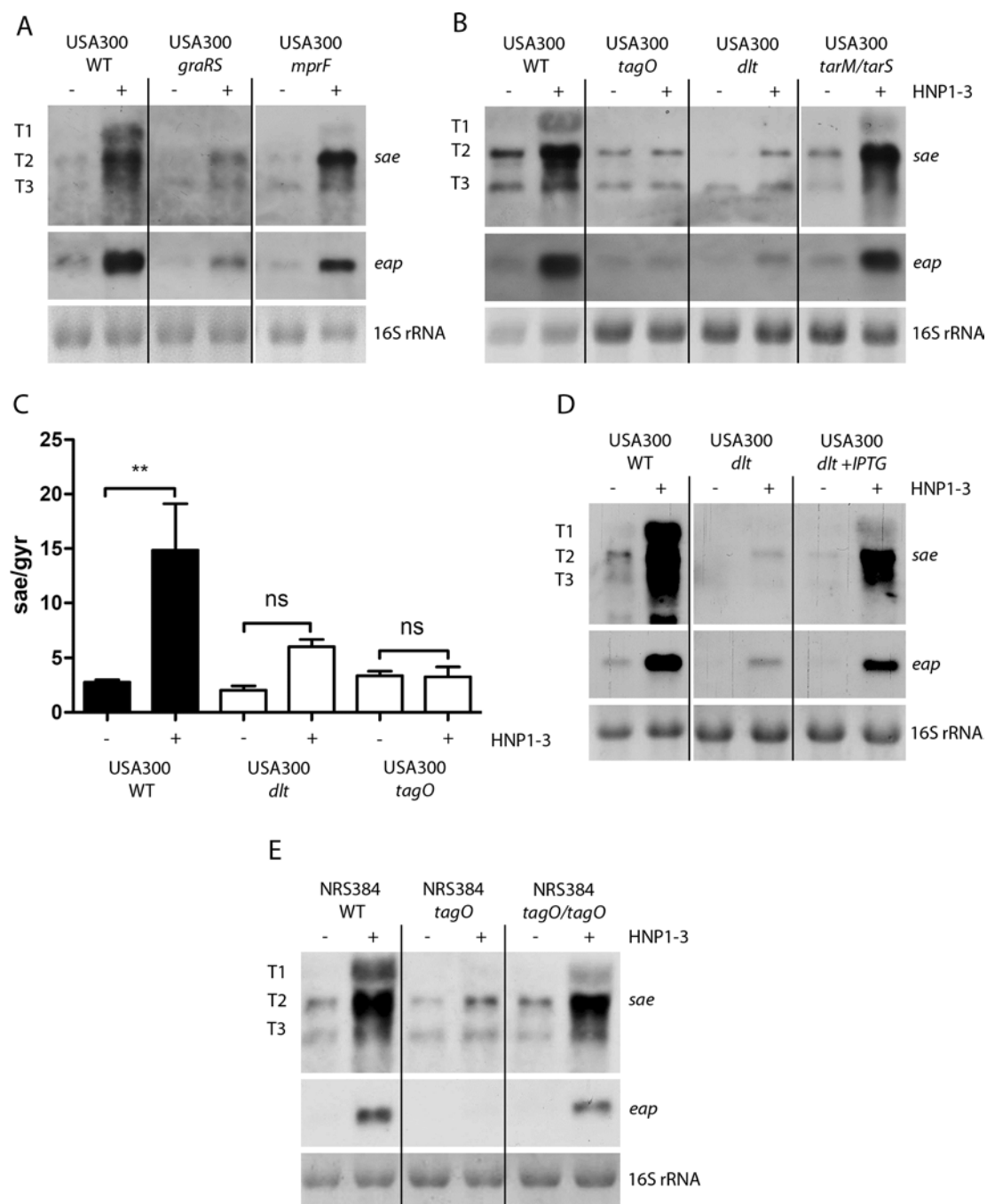
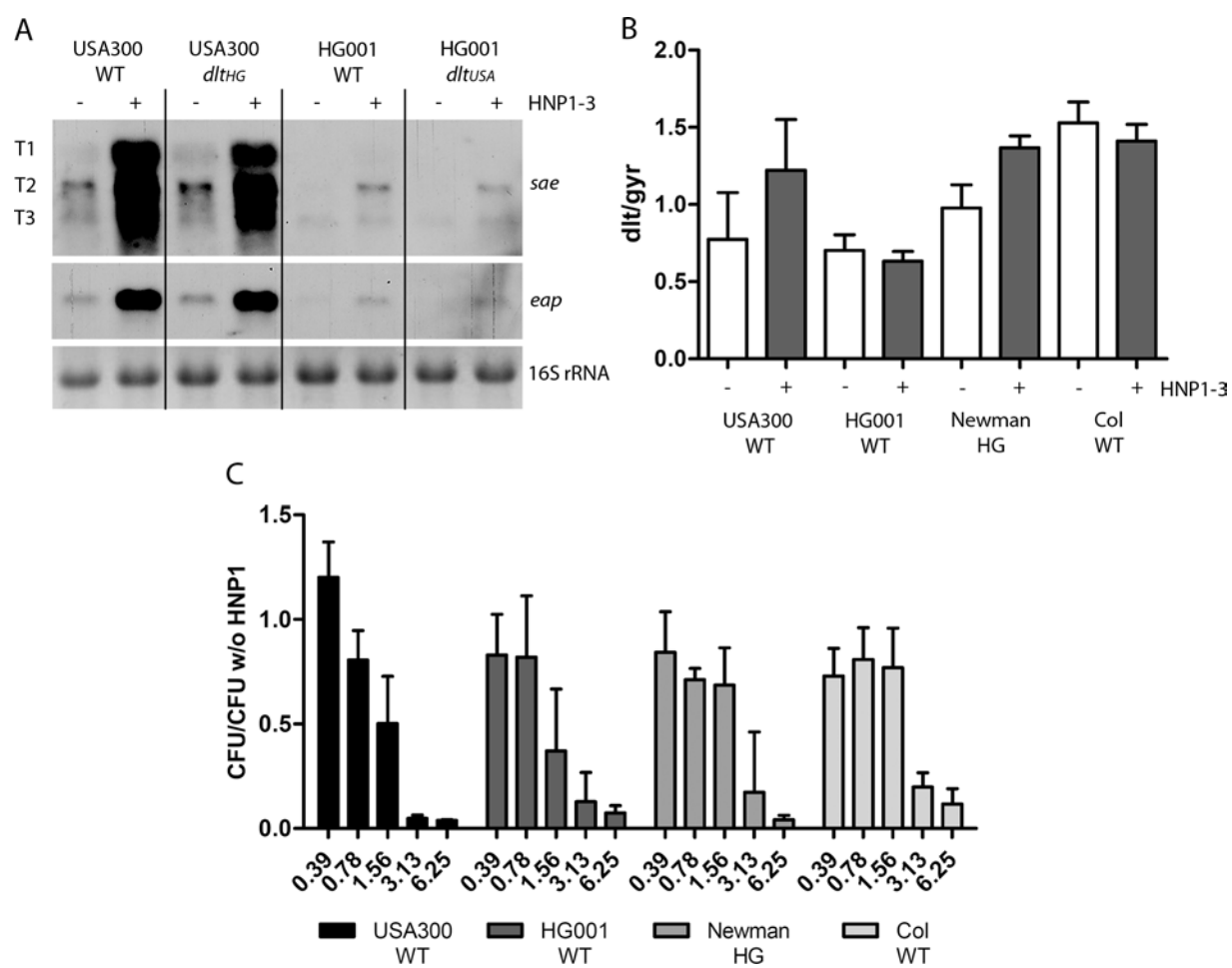


Figure 4



References

- Bera A, Biswas R, Herbert S, Kulauzovic E, Weidenmaier C, Peschel A & Gotz F (2007) Influence of wall teichoic acid on lysozyme resistance in *Staphylococcus aureus*. *J Bacteriol* **189**: 280-283.
- Bischoff M, Dunman P, Kormanec J, Macapagal D, Murphy E, Mounts W, Berger-Bachi B & Projan S (2004) Microarray-based analysis of the *Staphylococcus aureus* sigmaB regulon. *J Bacteriol* **186**: 4085-4099.
- Brown S, Xia G, Luhachack LG, *et al.* (2012) Methicillin resistance in *Staphylococcus aureus* requires glycosylated wall teichoic acids. *Proc Natl Acad Sci U S A* **109**: 18909-18914.
- Cho H, Jeong DW, Liu Q, Yeo WS, Vogl T, Skaar EP, Chazin WJ & Bae T (2015) Calprotectin Increases the Activity of the SaeRS Two Component System and Murine Mortality during *Staphylococcus aureus* Infections. *PLoS pathogens* **11**: e1005026.
- de Jong NWM, van Kessel KPM & van Strijp JAG (2019) Immune Evasion by *Staphylococcus aureus*. *Microbiology spectrum* **7**.
- Flack CE, Zurek OW, Meishery DD, Pallister KB, Malone CL, Horswill AR & Voyich JM (2014) Differential regulation of staphylococcal virulence by the sensor kinase SaeS in response to neutrophil-derived stimuli. *Proc Natl Acad Sci U S A* **111**: E2037-2045.
- Gajdacs M (2019) The Continuing Threat of Methicillin-Resistant *Staphylococcus aureus*. *Antibiotics (Basel, Switzerland)* **8**.
- Geiger T, Goerke C, Mainiero M, Kraus D & Wolz C (2008) The virulence regulator Sae of *Staphylococcus aureus*: promoter activities and response to phagocytosis-related signals. *J Bacteriol* **190**: 3419-3428.
- Geiger T, Francois P, Liebeke M, Fraunholz M, Goerke C, Krismer B, Schrenzel J, Lalk M & Wolz C (2012) The stringent response of *Staphylococcus aureus* and its impact on survival after phagocytosis through the induction of intracellular PSMs expression. *PLoS Pathog* **8**: e1003016.
- Goerke C, Campana S, Bayer MG, Doring G, Botzenhart K & Wolz C (2000) Direct quantitative transcript analysis of the agr regulon of *Staphylococcus aureus* during human infection in comparison to the expression profile in vitro. *Infection and immunity* **68**: 1304-1311.
- Harwig SS, Ganz T & Lehrer RI (1994) Neutrophil defensins: purification, characterization, and antimicrobial testing. *Methods Enzymol* **236**: 160-172.
- Jeong DW, Cho H, Lee H, Li C, Garza J, Fried M & Bae T (2011) Identification of the P3 promoter and distinct roles of the two promoters of the SaeRS two-component system in *Staphylococcus aureus*. *J Bacteriol* **193**: 4672-4684.
- Johnson M, Sengupta M, Purves J, *et al.* (2011) Fur is required for the activation of virulence gene expression through the induction of the sae regulatory system in *Staphylococcus aureus*. *Int J Med Microbiol* **301**: 44-52.

Kohler T, Weidenmaier C & Peschel A (2009) Wall teichoic acid protects *Staphylococcus aureus* against antimicrobial fatty acids from human skin. *J Bacteriol* **191**: 4482-4484.

Koprivnjak T, Mlakar V, Swanson L, Fournier B, Peschel A & Weiss JP (2006) Cation-induced transcriptional regulation of the *dlt* operon of *Staphylococcus aureus*. *J Bacteriol* **188**: 3622-3630.

Li D & Cheung A (2008) Repression of *hla* by *rot* is dependent on *sae* in *Staphylococcus aureus*. *Infect Immun* **76**: 1068-1075.

Li M, Cha DJ, Lai Y, Villaruz AE, Sturdevant DE & Otto M (2007) The antimicrobial peptide-sensing system *aps* of *Staphylococcus aureus*. *Mol Microbiol* **66**: 1136-1147.

Liu Q, Yeo WS & Bae T (2016) The SaeRS Two-Component System of *Staphylococcus aureus*. *Genes (Basel)* **7**.

Liu Q, Cho H, Yeo WS & Bae T (2015) The extracytoplasmic linker peptide of the sensor protein SaeS tunes the kinase activity required for staphylococcal virulence in response to host signals. *PLoS Pathog* **11**: e1004799.

Liu Q, Hu M, Yeo WS, He L, Li T, Zhu Y, Meng H, Wang Y, Lee H & Liu X (2017) Rewiring of the FtsH regulatory network by a single nucleotide change in *saeS* of *Staphylococcus aureus*. **7**: 8456.

Loi VV, Busche T, Tedin K, *et al.* (2018) Redox-Sensing Under Hypochlorite Stress and Infection Conditions by the Rrf2-Family Repressor HypR in *Staphylococcus aureus*. *Antioxid Redox Signal* **29**: 615-636.

Mainiero M, Goerke C, Geiger T, Gonser C, Herbert S & Wolz C (2010) Differential target gene activation by the *Staphylococcus aureus* two-component system *saeRS*. *J Bacteriol* **192**: 613-623.

Marincola G, Schafer T, Behler J, Bernhardt J, Ohlsen K, Goerke C & Wolz C (2012) RNase Y of *Staphylococcus aureus* and its role in the activation of virulence genes. *Mol Microbiol* **85**: 817-832.

Mascher T (2006) Intramembrane-sensing histidine kinases: a new family of cell envelope stress sensors in Firmicutes bacteria. *FEMS Microbiol Lett* **264**: 133-144.

Mascher T (2014) Bacterial (intramembrane-sensing) histidine kinases: signal transfer rather than stimulus perception. *Trends Microbiol* **22**: 559-565.

Moldovan A & Fraunholz MJ (2019) In or out: Phagosomal escape of *Staphylococcus aureus*. **21**: e12997.

Munzenmayer L, Geiger T, Daiber E, Schulte B, Autenrieth SE, Fraunholz M & Wolz C (2016) Influence of Sae-regulated and Agr-regulated factors on the escape of *Staphylococcus aureus* from human macrophages. *Cell Microbiol* **18**: 1172-1183.

Muthaiyan A, Silverman JA, Jayaswal RK & Wilkinson BJ (2008) Transcriptional profiling reveals that daptomycin induces the *Staphylococcus aureus* cell wall stress stimulon and genes responsive to membrane depolarization. *Antimicrob Agents Chemother* **52**: 980-990.

Nagel A, Michalik S, Debarbouille M, *et al.* (2018) Inhibition of Rho Activity Increases Expression of SaeRS-Dependent Virulence Factor Genes in *Staphylococcus aureus*, Showing a Link between Transcription Termination, Antibiotic Action, and Virulence. **9**.

Neumann Y, Ohlsen K, Donat S, Engelmann S, Kusch H, Albrecht D, Cartron M, Hurd A & Foster SJ (2015) The effect of skin fatty acids on *Staphylococcus aureus*. *Arch Microbiol* **197**: 245-267.

Novick RP & Jiang D (2003) The staphylococcal *saeRS* system coordinates environmental signals with quorum sensing. *Microbiology* **149**: 2709-2717.

Novick RP & Jiang D (2003) The staphylococcal *saeRS* system coordinates environmental signals with *agr* quorum sensing. *Microbiology* **149**: 2709-2717.

Nygaard TK, Pallister KB, Ruzevich P, Griffith S, Vuong C & Voyich JM (2010) SaeR binds a consensus sequence within virulence gene promoters to advance USA300 pathogenesis. *J Infect Dis* **201**: 241-254.

Oku Y, Kurokawa K, Ichihashi N & Sekimizu K (2004) Characterization of the *Staphylococcus aureus* *mprF* gene, involved in lysinylation of phosphatidylglycerol. *Microbiology* **150**: 45-51.

Parsons JB, Broussard TC, Bose JL, Rosch JW, Jackson P, Subramanian C & Rock CO (2014) Identification of a two-component fatty acid kinase responsible for host fatty acid incorporation by *Staphylococcus aureus*. *Proc Natl Acad Sci U S A* **111**: 10532-10537.

Peschel A, Vuong C, Otto M & Gotz F (2000) The D-alanine residues of *Staphylococcus aureus* teichoic acids alter the susceptibility to vancomycin and the activity of autolytic enzymes. *Antimicrob Agents Chemother* **44**: 2845-2847.

Peschel A, Otto M, Jack RW, Kalbacher H, Jung G & Gotz F (1999) Inactivation of the *dlt* operon in *Staphylococcus aureus* confers sensitivity to defensins, protegrins, and other antimicrobial peptides. *J Biol Chem* **274**: 8405-8410.

Schade J & Weidenmaier C (2016) Cell wall glycopolymers of Firmicutes and their role as nonprotein adhesins. *FEBS letters* **590**: 3758-3771.

Staubitz P, Neumann H, Schneider T, Wiedemann I & Peschel A (2004) MprF-mediated biosynthesis of lysylphosphatidylglycerol, an important determinant in staphylococcal defensin resistance. *FEMS Microbiol Lett* **231**: 67-71.

Sun F, Li C, Jeong D, Sohn C, He C & Bae T (2010) In the *Staphylococcus aureus* two-component system *sae*, the response regulator SaeR binds to a direct repeat sequence and DNA binding requires phosphorylation by the sensor kinase SaeS. *J Bacteriol* **192**: 2111-2127.

Turner NA, Sharma-Kuinkel BK, Maskarinec SA, Eichenberger EM, Shah PP, Carugati M, Holland TL & Fowler VG, Jr. (2019) Methicillin-resistant *Staphylococcus aureus*: an overview of basic and clinical research. *Nature reviews Microbiology* **17**: 203-218.

Voyich JM, Braughton KR, Sturdevant DE, *et al.* (2005) Insights into mechanisms used by *Staphylococcus aureus* to avoid destruction by human neutrophils. *J Immunol* **175**: 3907-3919.

Voyich JM, Vuong C, DeWald M, *et al.* (2009) The SaeR/S gene regulatory system is essential for innate immune evasion by *Staphylococcus aureus*. *J Infect Dis* **199**: 1698-1706.

Wanner S, Schade J, Keinhorster D, *et al.* (2017) Wall teichoic acids mediate increased virulence in *Staphylococcus aureus*. *Nat Microbiol* **2**: 16257.

Weidenmaier C & Lee JC (2016) Structure and Function of Surface Polysaccharides of *Staphylococcus aureus*. *Curr Top Microbiol Immunol*.

Xiong YQ, Yeaman MR & Bayer AS (1999) In vitro antibacterial activities of platelet microbicidal protein and neutrophil defensin against *Staphylococcus aureus* are influenced by antibiotics differing in mechanism of action. *Antimicrob Agents Chemother* **43**: 1111-1117.

Yang SJ, Bayer AS, Mishra NN, Meehl M, Ledala N, Yeaman MR, Xiong YQ & Cheung AL (2012) The *Staphylococcus aureus* two-component regulatory system, GraRS, senses and confers resistance to selected cationic antimicrobial peptides. *Infect Immun* **80**: 74-81.

Zurek OW, Nygaard TK, Watkins RL, Pallister KB, Torres VJ, Horswill AR & Voyich JM (2014) The role of innate immunity in promoting SaeR/S-mediated virulence in *Staphylococcus aureus*. *J Innate Immun* **6**: 21-30.



### Eidesstattliche Erklärung

Ich erkläre hiermit, dass ich die zur Promotion eingereichte Arbeit mit dem Titel:

**„The Sae two-component system of *Staphylococcus aureus*: sensing mechanism and impact on bacteria-phagocyte interaction”**

selbständig verfasst, nur die angegebenen Quellen und Hilfsmittel benutzt und wörtlich oder inhaltlich übernommene Stellen als solche gekennzeichnet habe. Ich erkläre, dass die Richtlinien zur Sicherung guter wissenschaftlicher Praxis der Universität Tübingen beachtet wurden. Ich versichere an Eides statt, dass diese Angaben wahr sind und dass ich nichts verschwiegen habe. Meine eigenen Beiträge zu Gemeinschaftsarbeiten habe ich in der „declaration of author contribution“ dargestellt.

Tübingen, den

## Curriculum vitae

### Persönliche Informationen

---

**Lisa Bleul** geb. Münzenmayer  
Geboren am 29.11.1989 in Ostfildern-Ruit

Wallmerstr. 6  
70327 Stuttgart

Tel.: 01724055424  
E-Mail: lisa.sabrina@gmx.de

### Akademische Ausbildung

---

- Seit 10/2014            **Promotion** am Interfakultären Institut für Mikrobiologie und Infektionsmedizin Tübingen (IMIT) bei PD Dr. Christiane Wolz
- 10/2012-09/2014       **Studium** der Biologie an der Eberhard-Karls-Universität Tübingen, Masterstudium Schwerpunkt Mikrobiologie
- 10/2009-09/2012       **Studium** der Biologie an der Eberhard-Karls-Universität Tübingen, Bachelorstudium

### Schulische Ausbildung

---

- 09/2000-06/2008        Württemberg-Gymnasium, Stuttgart-Untertürkheim  
Allgemeine Hochschulreife

### Stipendium

---

- 04/2015-03/2017       **Promotionsstipendium** nach dem Landesgraduiertenförderungsgesetz (LGFG)

### Weiterbildungen

---

- 10/2018                EBC\*L Stufe A: Internationales Zertifikat für Wirtschaftskompetenz
- 11/2017                Projektmanagement Workshop

### Acknowledgements

Zunächst möchte ich mich ganz herzlich bei meiner Betreuerin Prof. Dr. Christiane Wolz bedanken. Danke Christiane, für die wundervolle Zeit in deiner Arbeitsgruppe, für deine immer offene Tür, deine großartige Unterstützung, deine Anregungen und vor allem den Freiraum für eigene Ideen und „geheim“-Experimente. Du bist wirklich eine tolle Chefin und ich bin froh, dass ich die Chance hatte meine Doktorandenzeit in deiner Arbeitsgruppe zu verbringen. Vielen Dank für deine Unterstützung bei meinen zukünftigen Plänen, auch wenn ich mich schlussendlich nicht für die Forschung entschieden habe.

Prof. Dr. Fritz Götz möchte ich für das Erstellen des Zweitgutachtens danken.

Weiterhin möchte ich mich bei meiner Arbeitsgruppe bedanken. Mädels, Ihr seid einfach die Besten und ich werde die Zeit mit euch sehr vermissen. Vor allem unsere Cooking- Days und die tolle Atmosphäre im Labor werden mir fehlen. Mein Dank geht an Shilpa, Dani, Petra, Carina, Esther, Andrea, Janina, Isa, Vitty und alle ehemaligen Mitarbeiter und Studenten der AG Wolz (Besonders Andres, Jana und Jessy für Ihre tolle Arbeit). Denkt immer daran: Science is fun! Besonders danken möchte ich Naty und ihren magischen Händen, für die großartige Unterstützung bei meinen Experimenten (besonders die Pflege unserer Zellen und die unendlichen CFU Versuche).

Dr. Hubert Kalbacher möchte ich für die Aufreinigung der Defensine danken, ohne die meine Versuche nicht möglich gewesen wären.

Besonderer Dank gilt meiner Familie. Meinen Eltern, die mich von Anfang an, vor allem auch finanziell, unterstützt haben, wo sie nur konnten und mich immer bestärkt haben diesen Weg zu gehen. Meinen Großeltern und meinem Bruder Florian für ihre Unterstützung (Meiner Oma, besonders fürs aufmerksame und geduldige Zuhören beim Üben meiner Präsentationen). Meinem Mann Basti danke ich für die Motivation, wann immer ich sie gebraucht habe um durchzuhalten. Danke, dass du immer für mich da bist.